Objective and Subjective Evaluation of Reflecting and Diffusing Surfaces in Auditoria

by

Trevor John Cox

This thesis was submitted for the degree of Doctor of Philosophy in the Department of Applied Acoustics, University of Salford.

Submitted March 1992.

Contents

Chapter 3. The Theoretical Prediction of Scattering from Reflectors and Diffusers

Chapter 4. Theoretical Predictions and Measurements of the Scattering from Thin Rigid Plane Panels

Chapter 5. Theoretical Predictions and Measurements of the Scattering from Curved Panels

Chapter 6. Theoretical Predictions and Measurements of the Scattering from Quadratic Residue Diffusors

Chapter 7. The Relative Performance of Diffusing and Reflecting Surfaces

Chapter 8. The Subjective Measurement System

Chapter 9. The Difference Limen for Spatial Impression

Chapter 10. The Difference Limen of Clarity

Chapter 11. The Perception of Diffuse Reflections in the Sound Field

Chapter 12. The Initial Time Delay Gap

Chapter 13. Conclusions

Chapter 14. Further Work

Table of Illustrations

Acknowledgements

I would like to thank the following people: Dr R.J. Orlowski; Dr Y.W. Lam; the staff and fellow postgraduates in the Acoustics Department; Dr M. Barron; Dr J-D. Polack; Dr G. Dodd; and the technicians in the Civil Engineering Department. I am grateful to Dr R. J. M. Craik and colleagues at the Department of Building, Heriot-Watt University for their support during the subjective measurements at Heriot-Watt University. Especially for the subsequent loan of the subjective measurement equipment. Thanks go to The Acoustics Laboratory, Technical University of Denmark and The Acoustics Laboratory, University of Trondheim, Norway, who allowed me to use their room acoustic computer prediction programs. Finally, I would like to thank the people who participated in the subjective tests, who must have nightmares about being locked in an anechoic chamber and being forced to listen to Handel's water music.

Abstract

The performance of reflectors and diffusers used in auditoria have been evaluated both objectively and subjectively.

Two accurate systems have been developed to measure the scattering from surfaces via the cross correlation function. These have been used to measure the scattering from plane panels, curved panels and quadratic residue diffusers (QRDs). The scattering measurements have been used to test theoretical prediction methods based on the Helmholtz-Kirchhoff integral equation. Accurate prediction methods were found for all surfaces tested. The limitations of the more approximate methods have been defined. The assumptions behind Schroeder's design of the QRD have been tested and the local reacting admittance assumption found to be valid over a wide frequency range. It was found that the QRD only produces uniform scattering at low frequencies. For an on-axis source the scattering from a curved panel was as good as from a QRD. For an oblique source the QRD produced much more uniform scattering than the curved panel.

The subjective measurements evaluated the smallest perceivable change in the early sound field, the part most influenced by reflectors and diffusers. A natural sounding simulation of a concert hall field within an anechoic chamber was used. Standard objective parameters were reasonable values when compared to values found in real halls and subjective preference measurements. A difference limen was measured for early lateral energy fraction (.048 ± .005); inter aural cross correlation (.075 ± .008); clarity index (.67 ± .13 dB); and centre time (8.6 ± 1.6ms). It was found that; (i) when changes are made to diffusers and reflectors, changes in spatial impression will usually be larger than those in clarity; and (ii) acousticians can gain most by paying attention to lateral sound in auditoria. It was also found that: (i) diffuse reflections in the early sound field are not perceived differently from specular reflections; and (ii) the initial time delay gap is not significant to listener preference.

Glossary of Symbols

a	Half panel width
c	Speed of sound
C_{80}	Clarity index
$C(\sigma)$	Cosine part of Fresnel integral
C_{xy}	Real part of cross spectrum
C'_{xy} or $C'(\omega)$	Real part of processed cross spectrum
C_{xy1} or $C_1(\omega)$	Real part of cross spectrum for measurement with the diffuser
C_{xy2} or $C_2(\omega)$	Real part of cross spectrum for measurement without diffuser
d	Difference between minimum and maximum path lengths from panel to receiver
d_1	Source distance to point of reflection (Figure 4.15)
d_2	Receiver distance to point of reflection (Figure 4.15)
d_{max}	Maximum depth of quadratic residue diffuser
d^*	Characteristic distance
D	Deutlichkeit
E(t)	Exponential energy decay
$E_0(t)$	Initial energy of exponential decay
EDT	Early decay time
ELEF	Early lateral energy fraction
f	Frequency
FT	Fourier transform
G	Green's function
h	Half panel height
h(t)	Impulse response of panel
$H(\omega)$	Measured transfer function for two microphone measurement
$H_2(\omega)$	Measured transfer function for single microphone measurement
$H_{mic}(\omega)$	Transfer function between two microphones
i	$\sqrt{-1}$
IACC	Inter aural cross correlation coefficient
k	(i) Wavenumber (ii) Positive integer (including zero)

$k(t)$	Cross correlation coefficient between the signals at the two ears
l	Half the largest panel dimension
L	Sound pressure level
L_0	Fixed sound pressure level, taken to be 70 dBA
m	Air absorption coefficient
MOD	Modulus
n	(i) Quadratic residue sequence number sequence
	(ii) Number of averages
n_{max}	Maximum number in quadratic residue sequence
N	Prime number for generation of QRD
	Integration limit for discretized impulse response
$\underline{n}_r$	Unit vector at receiver in the direction of $\underline{r}$ (Figure 3.1)
$\underline{n}_s$	Normal to surface, pointing away from surface (Figure 3.1)
$p(t)$ or $p(f)$	[1]Pressure
p_0	[1]Magnitude of point source
$p_8(t)$	[1]Pressure measured using figure of eight microphone
$p_i(t)$	[1]Incident pressure
$p_l(f,\theta)$	[1]Full length diffuser pressure prediction
$p_{l/2}(f,\theta)$	[1]Half length diffuser pressure prediction
$p'_l(f,0^-)$	[1]Full length plane panel pressure prediction for infinitely wide panel
$p'_{l/2}(f,0^-)$	[1]Half length plane panel pressure prediction for infinitely wide panel
$p_l(t)$	[1]Pressure at left ear
p_n	[1]Discretized impulse response components
$p_r(t)$	[1]Pressure at right ear
$p_s(f)$	[1]Scattered pressure
$p_t(f)$	[1]Total pressure
$Q_{xy}(\omega)$	Imaginary part of cross spectrum
Q'_{xy2} or $Q'(\omega)$	Imaginary part of processed cross spectrum
Q_{xy1} or $Q_1(\omega)$	Imaginary part of cross spectrum for measurement with the diffuser

[1]Case non-specific

Q_{xy2} or $Q_2(\omega)$	Imaginary part of cross spectrum for measurement without the diffuser
$\underline{r}$	Vector from origin to receiver (Figures 3.1 and 3.3)
$\underline{r}_0$	Vector from origin to source (Figures 3.1 and 3.3)
$\underline{r}_2$	Vector from a point on the surface to receiver (Figure 3.1)
$\underline{r}_s$	Vector from origin to a point on the surface (Figure 3.1)
R	(i) Reverberant to early energy ratio (ii) Reflection factor
$R_{xy}(\omega)$	Cross correlation function
$R'_{xy}(\omega)$	Processed cross correlation function
s	Surface area of room
S	Surface of integration
$S(\sigma)$	Sine part of Fresnel integral
SI	Subjective degree of spatial impression
SINC(x)	SIN(x)/x
S_{xy1} or $S_1(\omega)$	Cross spectrum for the measurement with the diffuser
S_{xy2} or $S_2(\omega)$	Cross spectrum for the measurement without the diffuser
S'_{xy} or $S'(\omega)$	Processed cross spectrum
$S_{xx}(\omega)$	Auto spectrum of loudspeaker microphone signal for measurement without diffuser present
$S_{yy}(\omega)$	Auto spectrum of diffuser microphone signal
t	Time
T	Time interval for correlation integrals
T_{60}	Reverberation time
T_c	Centre time
v	Room volume
w	Well width
x	x coordinate of receiver (Figure 3.3)
x(t)	Loudspeaker microphone signal
y(t)	Diffuser microphone signal
α	(i) Integration variable for cross correlation functions (ii) Surface absorption coefficient

	(iii) Angle of incidence
β	(i) Admittance
	(ii) Angle of incidence and reflection (Figure 4.15)
β_x	Variable used in Fresnel solution (Equation 3.18)
γ	Variable used in Fresnel solution (Equation 3.17)
γ^2	Coherence function
ϵ	Variable used in formulation of Helmholtz-Kirchhoff integral equation (Equation 3.1)
θ	(i) Angle of reflection (Figures 3.1 and 3.3)
	(ii) Angle of incidence relative to an axis drawn through the ears of the listener
λ	Wavelength
λ_{max}	Maximum wavelength for which QRD produces 'optimum' diffusion
λ_{min}	Minimum wavelength for which QRD produces 'optimum' diffusion
Φ_{ll}	Auto correlation coefficient for left ear
Φ_{lr}	Cross correlation coefficient between left and right ear
Φ_{rr}	Auto correlation coefficient for right ear
σ^2	Variance
$\sigma_{\pm a,z}$	Variables used in Fresnel integrals (Equations 3.19 and 3.20)
$[\psi]$	Time dependant velocity potential
τ	Time delay
τ_x	Time delay between loudspeaker and diffuser microphones
τ_y	Time delay between diffuser microphone and panel
τ_d	Time delay between loudspeaker microphone and panel
τ_r	Time delay between loudspeaker microphone and diffuser microphone involving reflection off the panel (Figure 2.5)
τ_0	Time delay between loudspeaker and loudspeaker microphone
ω	Angular frequency
φ	Velocity potential
*	Convolution.

Chapter 1

Introduction

1.1 Introduction

Auditorium acoustics is a combination of objective and subjective effects. Even if the sound field within an auditorium is well defined, this still has to be related to the perception of the listeners. Modern auditorium acoustics is based on objective parameters. There are many such parameters [Cremer 1982, Kuttruff 1991a], an example is early lateral energy fraction. These parameters are known to be related to certain preferred subjective responses. By 'optimizing' the objective parameters, the preference of the audience will also be 'optimized'. For the example of early lateral energy fraction, the subjective feeling is one of being enveloped in a broad sound field; the jargon for this is spatial impression [Barron 1974].

This research project has investigated both objective and subjective effects. In particular, it has assessed the performance of finite sized surfaces such as reflectors and diffusers. The project has involved:

1. Development of systems to measure the scattering from finite sized surfaces.

2. Development of methods to predict the scattering from finite sized surfaces.
3. Subject tests to find out how small a change can be perceived in the early sound field. The early sound field is the part of the impulse response most influenced by reflectors and diffusers.

1.2 Objective Measurements

The sound field within an auditorium can be defined by it's pressure impulse response. When designing an auditorium, an acoustician has two main methods for predicting such an impulse response: either physical scale modelling or computer modelling. Physical scale modelling is a well known and long established technique in room acoustics [Barron 1983b, 1987]. An accurate scale model of the auditorium is built, nowadays 1:50 scale is usually used. Then by working with frequencies 50 times the audible range, the performance of the auditorium can be judged. The models allow the acoustician to get a reasonable idea of how the auditorium will perform before the hall is built, so avoiding expensive mistakes in the real hall. Unfortunately, building models is time consuming and expensive. So in recent years there has been much interest in computer modelling.

The two main algorithms for computer modelling of sound propagation in enclosed spaces have existed for sometime. They are the image source

method, and the ray tracing method; details of both methods can be found in Kuttruff [1991a Pages 282-287] or Stephenson [1990]. It is only in recent years, however, that there has been sufficient computing power to allow these methods to evaluate auditoria on desktop computers. Now many acoustic consultancies use computer modelling. Unfortunately, present day computer models have a major flaw, they can not properly predict the scattering from finite sized surfaces. One objective of this project was to improve understanding of these scattering processes. This was done through our theoretical predictions and measurements of the scattering from diffusing and reflecting surfaces. This will help scattering to be incorporated into computer models. An example of how predictions or measurements of the scattering from finite sized surfaces, can be incorporated into ray tracing models, is given in the next paragraph.

A ray tracing model literally traces rays around the auditorium, bouncing them off surfaces using Snell's law - i.e. angle of incidence equals angle of reflection. The sound rays are attenuated after each reflection according to the absorption coefficient of the surface. A popular approach to model scattering is to introduce a probability distribution function for the scattering direction after the ray reflects from the surface [Kuttruff 1991b]. To do this, the scattering properties of the surface needs to be known. It must either be measured or theoretically predicted.

Two cross correlation methods for the measurement of the scattering off surfaces were developed during this project. Both methods were accurate. The

method which used a pseudo-random white noise source signal was also very fast. Details of the measurement methods can be found in Chapter 2, along with a brief review of other possible systems.

A range of prediction methods have been tested, from the simple and fast, to the more rigorous and slow. For all surfaces tested, accurate prediction methods were found. As the more rigorous methods take a long time to compute, they may not be of practical use to acousticians and may be too slow for incorporation into ray tracing models. Consequently simple prediction methods were also looked at. These might have taken a matter of minutes or seconds to compute, where the more rigorous methods might have taken hours. With the more approximate methods, their limitations have been defined, in terms of the frequency ranges and receiver positions over which they work, and also the accuracy achieved.

Three types of surfaces commonly found in auditoria have been tested: plane surfaces; curved surfaces; and quadratic residue diffusers. The results are also applicable to other situations such as studio monitor rooms and even scattering from industrial machinery. Once the sound from these three types of surfaces can be predicted, the performance of most other surfaces occurring in auditoria can also be predicted, as many tend to be hybrids and variants of the three types of surfaces tested here.

Chapter 3 gives details of the theoretical prediction methods used. In Chapters 4 to 6 details of the comparisons between theoretical predictions and measurements for the scattering from the surfaces are given. Here the success, or otherwise, of each theory is considered.

Predicting the performance of diffusers is not just important to allow more accurate predictions of the sound field through computer modelling. Good concert hall design requires knowledge of the scattering performance of diffusers. Of the three types of panels tested, the most interesting were the quadratic residue diffusers (QRDs). A QRD consists of a series of wells of equal width but different depth, and was designed by Schroeder to give uniform scattering [Schroeder 1979]. Photographs of the QRDs used in a recently built concert hall can be seen in Plates 1.1 and 1.2. There have been comparatively few measurements to test the actual performance of QRDs [D'Antonio 1985, Strube 1980a-b 1981, Polack 1988]. Consequently, there are many questions still to be answered about the scattering performance. This investigation tested the approximations behind Schroeder's design. Of most importance, it tested the assumption of the local reacting admittances used to model the QRD. It was also possible to compare the QRDs scattering performance with 'optimum diffusion', as well as with the scattering from plane panels and curved panels. The discussions of the scattering performance of the reflectors and diffusers can be found in Chapter 8.

Plate 1.1 Quadratic residue diffusers in situ in a recently built concert hall.

Plate 1.2 End view of a quadratic residue diffuser used in a recently built concert hall.

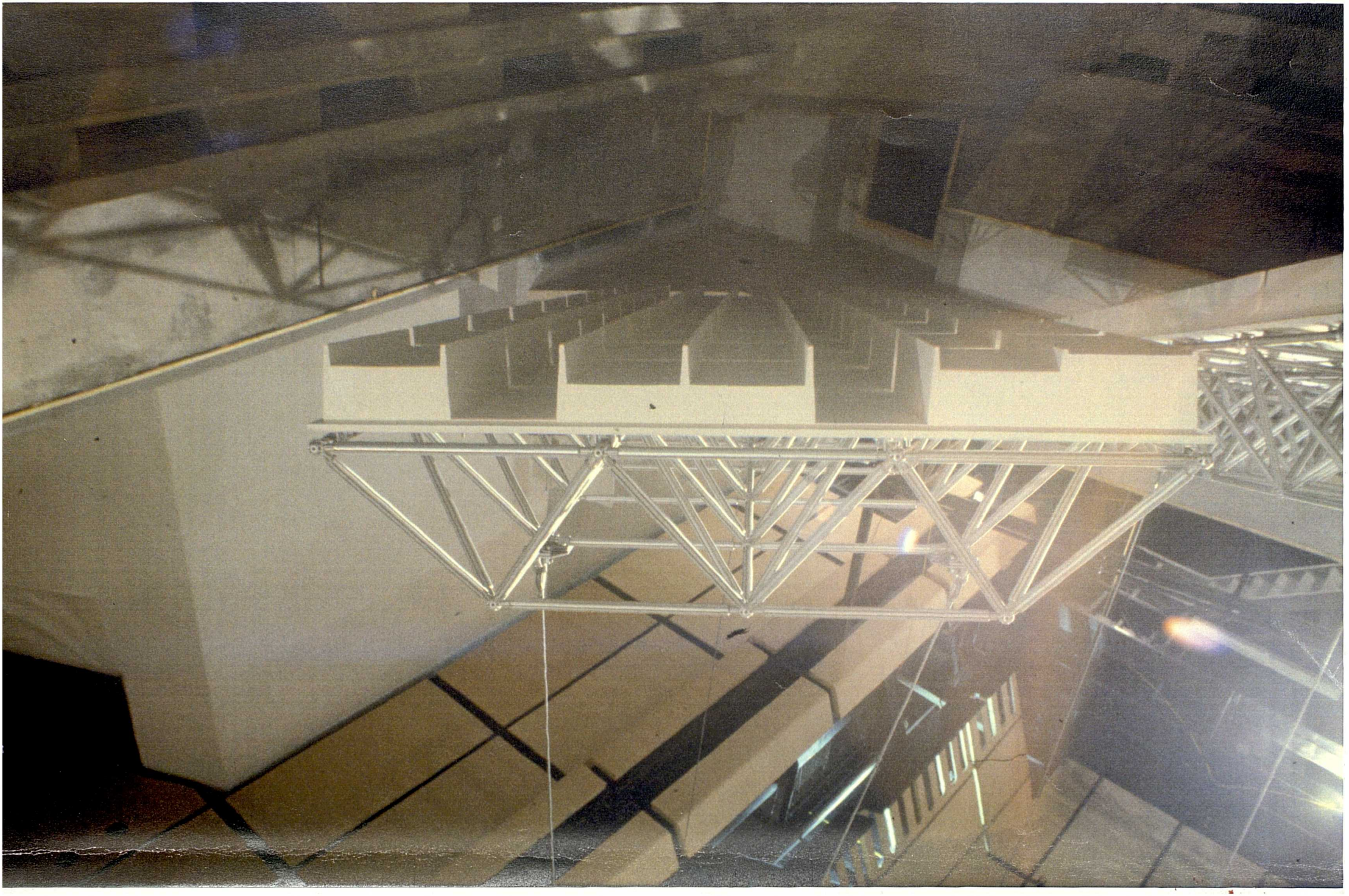

1.3 Subjective Measurements

Although most of the current objective parameters which can be used to characterize a concert hall have been known for many decades, their use is not that widespread. The only exception is reverberation time, where measurement is simple and standardized. There are a number of different reasons for the objective parameters not being used: (i) there are many different parameters, many duplicating the same subjective effect; (ii) the measurements need equipment different from standard reverberation time measurements; and (iii) a consensus is only slowly emerging from the scientific literature. All these factors have resulted in a certain inertia in acousticians using the objective parameters. Their use, however, may well become more widespread with the increase in the use of computer modelling. Most computer models automatically produce a full range of the objective parameters.

In the assessment of some of the newer objective parameters, there appears to be a lack of knowledge about the size of changes that people can perceive. It is well established that measuring the reverberation time to the nearest tenth of a second is the accuracy required. Smaller changes can not be perceived by the majority of the listeners [Cremer 1982 pages 505-507]. But what about the newer criteria such as early lateral energy fraction? So our subjective measurements have concentrated on assessing how small a change people can perceive in an auditorium's impulse response. As this project has been concerned with the performance of reflectors and diffusers, we have concentrated on

changes to the early sound field. The first few reflections arriving at the listeners can be greatly influenced by the position, orientation and type of diffuser. This lead us to measure difference limen for early lateral energy fraction, inter aural cross correlation, centre time and clarity index. The results of these measurements are given in Chapters 9 and 10. The tests were done using an artificial sound field created in an anechoic chamber. The simulation system sounded natural subjectively. Also the key objective parameters - reverberation time, early decay time, clarity index, early lateral energy fraction and overall A-weighted sound pressure level - were all reasonable values when compared to values measured in real halls and preferred values measured in other subjective measurements. A description of the simulation system can be found in Chapter 8 along with details of the test method.

The results for the difference limens can be used in many ways: (i) they give guide lines as to how accurately the objective parameters should be measured; (ii) they stipulate to what accuracy computer models need to be able to predict the objective parameters; and (iii) they also tell acousticians whether changes to the positions and orientations of reflectors and diffusers will actually be heard by the audience.

Experiments on the importance of diffusion in the early sound field were also carried out. We wished to test whether the treatment of surfaces with diffusing elements changed the preference of listeners. In the reverberant sound field, there are such a large number of different reflections, coming from so

many different surfaces, that the influence of diffuse reflections will be masked. In the early sound field, however, much fewer reflections arrive, and so listeners might be able to perceive a difference when the reflections are made more diffuse. Our interest was raised by Le Quartz in Brest, France. This is a theatre where the side walls have been lined with quadratic residue diffusers. Details of the measurements can be found in Chapter 11.

The final subjective tests concerned the initial time delay gap. This is the time difference between the arrival of the direct sound and the first reflection. The initial time delay gap has been used by some as an objective parameters [Beranek 1962, Ando 1977 1979], but is not well established. If the initial time delay gap was important to preference it would have important implications to the positions and orientations of reflectors and diffusers. It would be particularly important to auditoria which have subdivided audiences. Here a larger than usual number of listeners are near to walls, and so have a relatively short initial time delay gap. (The idea of subdividing the audience was suggested by Cremer [1975] as increasing the amount of lateral sound increases the degree of spatial impression). Therefore, experiments were carried out to assess the importance of the initial time delay gap, as detailed in Chapter 12.

Chapter 2

The Measurement of Scattering from Finite Sized Surfaces

2.1 Introduction

Before constructing a system to measure the scattering from surfaces, a survey of possible methods was done. This chapter begins with a brief overview of the methods available, including a discussion of their various merits. It was decided to develop a new measurement system based on the cross correlation function. Originally a two microphone method was used with white noise as a source. Unfortunately, although this method was accurate it was slow. Consequently, this was later superseded by a system using a pseudo-random white noise source, providing both fast and accurate measurements. This chapter gives full descriptions of the two methods. They had much in common, and are presented in historical order.

2.2 Possible Methods to Measure Sound Scattering.

The various systems available to measure the scattering from surfaces have their methods dominated by the need to separate the incident and reflected sound. For reasons discussed below in Section 2.5, both the scattered and total

field were required. If just the total field was needed, a simple single microphone measurement would have sufficed.

There are a number of methods available to measure the scattering from finite sized surfaces of the dimensions of surfaces typically found in auditoria. The main options are:

1. Directional microphone method.
2. Impulse source method.
3. Time delay spectroscopy.
4. Doublet source method.
5. Two microphone cross correlation method using a white noise source.
6. One microphone cross correlation method using a pseudo-random white noise source.

2.2.1 Directional microphone method

The directional microphone method is the simplest technique. A continuous sound source, probably white noise, is used along with a highly directional microphone. The direct sound and reflected sound are then separated by the fact that they subtend different angles at the microphone, and the microphone has a highly directional response. The method is reliant on a sharp cut-off in the response of the microphone with angle, and this factor determines the accuracy of the measurement. The method may be reasonable for a receiver

normal to the panel ($\theta=0°$, θ being the receiver angle), but as the scattering angle increases ($\theta \rightarrow 90°$) the results will get more and more inaccurate as more and more of the direct sound is picked up by the microphone. Another criticism is that the method prevents the extraction of the total sound field, this would have to be measured separately.

2.2.2 Impulse source system

Using an impulse source is a common technique in acoustics [Barron 1984, Aoshima 1981, Ortega 1991]. For our measurements, once the time signal is captured the impulse response would be similar to Figure 2.1, consisting of an incident sound peak and reflected sound peak separated in time. (The impulse response in Figure 2.1 was measured by the single microphone cross correlation technique. Details of that measurement system is given in Section 2.4). Separation of the reflected sound and incident sound is then possible by consideration of arrival times. So it is simple to obtain both the scattered and total field from the results. The main problems for an impulse measurement is that loudspeakers can not produce sharp impulses with high power. This results in low levels at the microphone, and decreased signal to noise ratio. There are several solutions to this problem:

(i) Use the highest possible level into the loudspeaker and average the response many times.

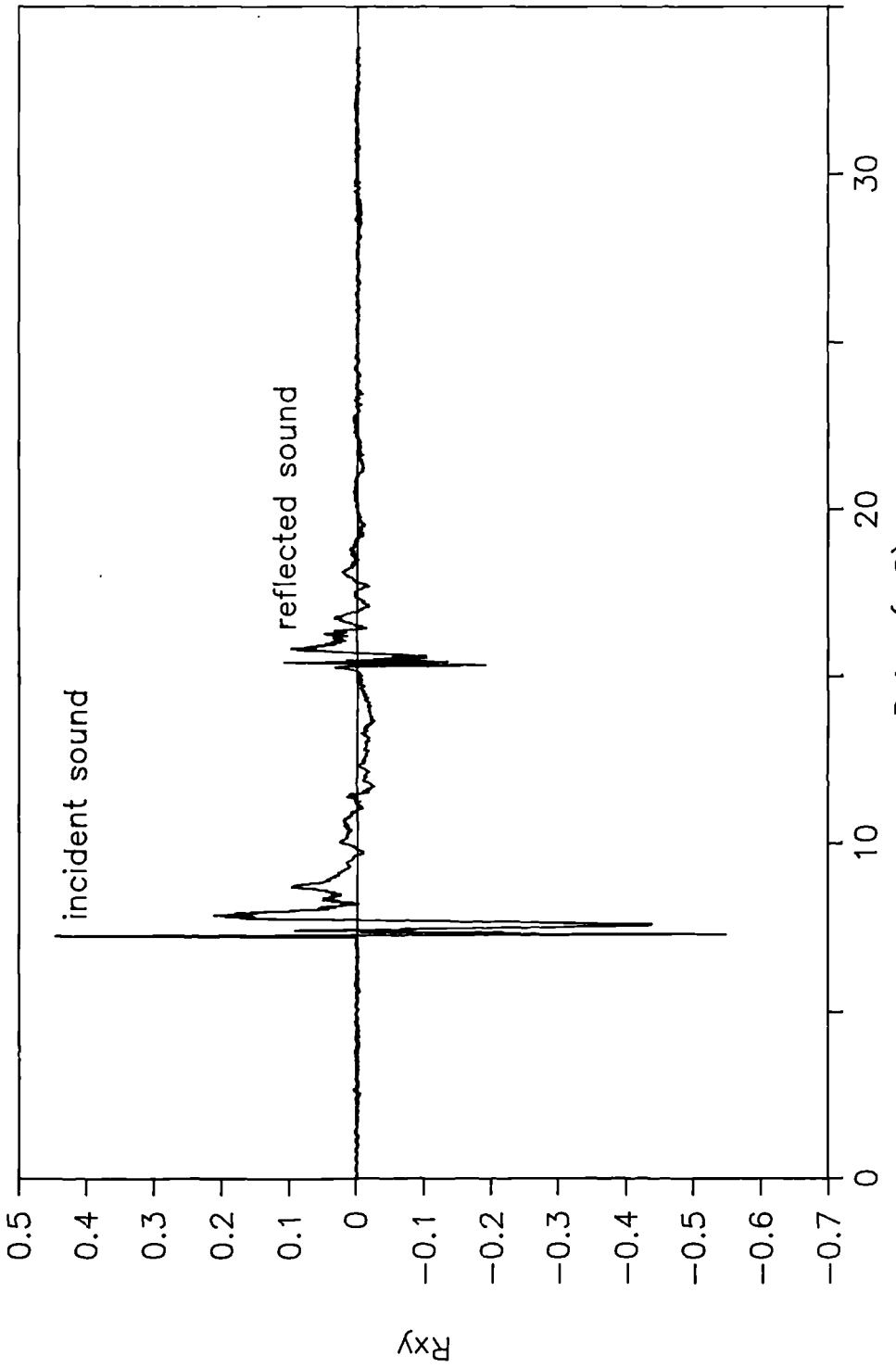

Figure 2.1 Impulse response for diffuser measurement.

(ii) Use half a period of a sinusoidal wave as a source. This allows more power to be fed into the loudspeaker and so reduces the number of averages [Barron 1984]. Unfortunately, the frequency response of the impulse created by part of a sinusoid is band limited, and so measurements have to be done several times to cover the full bandwidth required.

(iii) Use computer generated impulses based on the inverse of the loudspeaker's response [Aoshima 1981]. This can be used to maximise power output while producing a sharp impulse response.

Even when using the last two techniques, averaging is needed, and the measurement technique is slow.

2.2.3 Time delay Spectroscopy

Time Delay Spectroscopy (TDS) [Heyser 1988, Vanderkooy 1989, Cable 1980] is a standard technique usually used to measure loudspeaker responses. It has been used by others to measure the response of quadratic residue diffusers [D'Antonio 1985]. In this system the source is a narrow band swept sinusoid. The signal collected by the microphone goes through a narrow band filter, the microphone filter, which can also be swept. By simultaneously sweeping the frequency of the source and the microphone filter with a set frequency difference, it is possible to pick out sound with a particular amount of time delay. The system is effectively a gating system working in the time domain.

There is a problem in that the reaction of the panel to a swept signal is unknown. The source is not similar to a music source.

2.2.4 Doublet source method

A Doublet source can be used to measure the scattering from surfaces [Dodd 1988]. If two identical sources of opposite phase are set radiating, the well known doublet source radiation pattern is created. There exists a line of cancellation along which a microphone can be traversed. This is illustrated in Figure 2.2. Along this line of cancellation the microphone picks up none of the incident sound, and measures the reflected sound only.

The system is limited by how accurately the two opposite phase sources can be produced, and also how accurately the microphone is positioned relative to the sources. The largest disadvantage of the system is that it does not allow full radial plots to be done as the microphone is constrained to a straight line. With the size of anechoic chamber which was available, this would have severely restricted the range of scattering angles which could have been measured.

2.2.5 Cross correlation methods

The cross correlation methods allow the measurement of the scattering with a continuous source, while producing the impulse response via the cross correlation function. They allow the separation of the direct and reflected sound

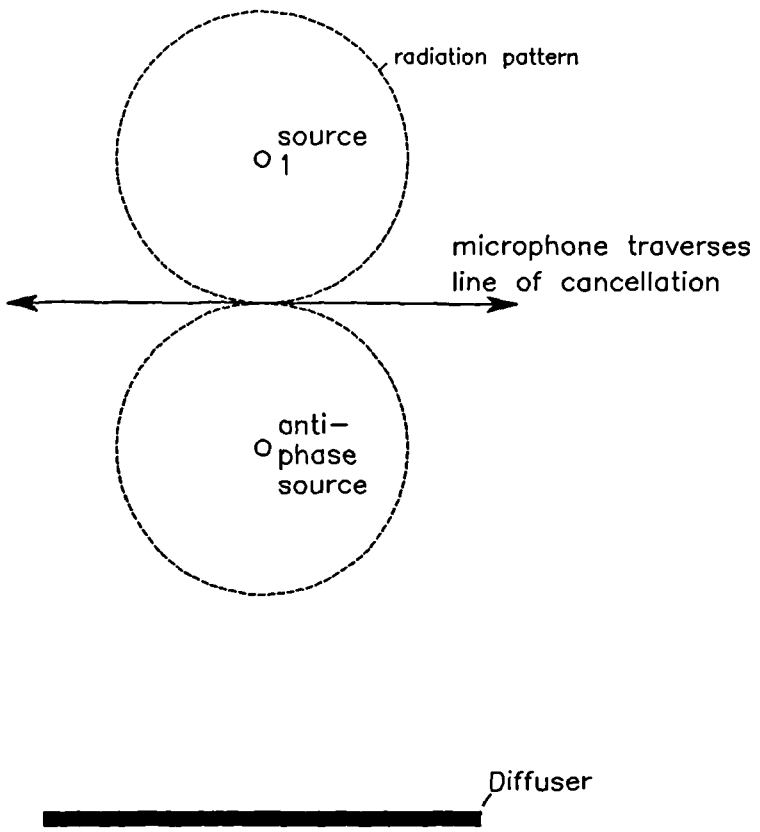

Figure 2.2. Set up for doublet source measurement system.

by subtraction and time gating. Unfortunately, using a white noise source means that the measurement is slow, but this can be overcome by using a pseudo-random noise signal. More details of these systems are given in Sections 2.3 and 2.4.

2.2.6 Summary of methods available

In Table 2.1 a summary of the possible measurement methods are given. The directional microphone response system was considered inaccurate. The doublet source method would not allow radial plots and so was also not

considered. The impulse source method, time delay spectroscopy and cross correlation techniques all provided possible ways to measure the scattering from the surfaces accurately. It was decided to develop the cross correlation technique, which to our knowledge had not been used before.

Table 2.1. Summary of possible methods for the measurement of scattering from diffusing and reflecting surfaces.

Measurement system.	Advantages.	Disadvantages.
Directional microphone.	Simple, quick.	Inaccurate, particularly at large scattering angles.
Impulse source.	Well known technique, accurate.	Difficult to obtain enough source power, slow.
Time delay spectroscopy.	Ready made systems available, accurate.	Response of panels to swept sinusoid unknown? Needs specialized equipment.
Doublet source.	Simple	Does not allow radial plots. Accuracy of source calculation and measurement unknown.
Two microphone, cross correlation white noise source.	Accurate. Only needs standard microphones and frequency analysis equipment.	Slow.
Single microphone cross correlation pseudo-random white noise source.	Very accurate and quick.	Needs specialized equipment.

2.3 The Two Microphone, White Noise Source, Cross Correlation System

2.3.1 General principle of measurement system

The experimental set up for the two microphone cross correlation system is shown in Figure 2.3. A loudspeaker radiated white noise from one end of the anechoic chamber, the reflecting panel was placed at the opposite end. The pressure was measured by two microphones. The loudspeaker microphone was not far from the loudspeaker. The diffuser microphone was nearer the diffuser, and was rotated to allow the scattering from the panel to be measured as a function of scattering angle.

A cross correlation was calculated between the two microphones using a dual channel FFT analyzer. The pressures at the two microphones will be represented by x(t) and y(t) for the loudspeaker and diffuser microphones respectively. Then the two sided cross correlation function, $R_{xy}(\tau)$, is given by [Bendat 1986 1980]:

$$R_{xy}(\tau) = \lim_{T\to\infty}[\frac{1}{T}\int_{-T}^{T} x(t)y(t+\tau)dt] \qquad 2.1$$

The cross correlation function is a standard method for comparing two signals. Figure 2.4 illustrates a very simple example. Consider the case where the two microphone signals, x(t) and y(t), are identical except for a time delay between them. White noise is random and any time segment is unique. When the

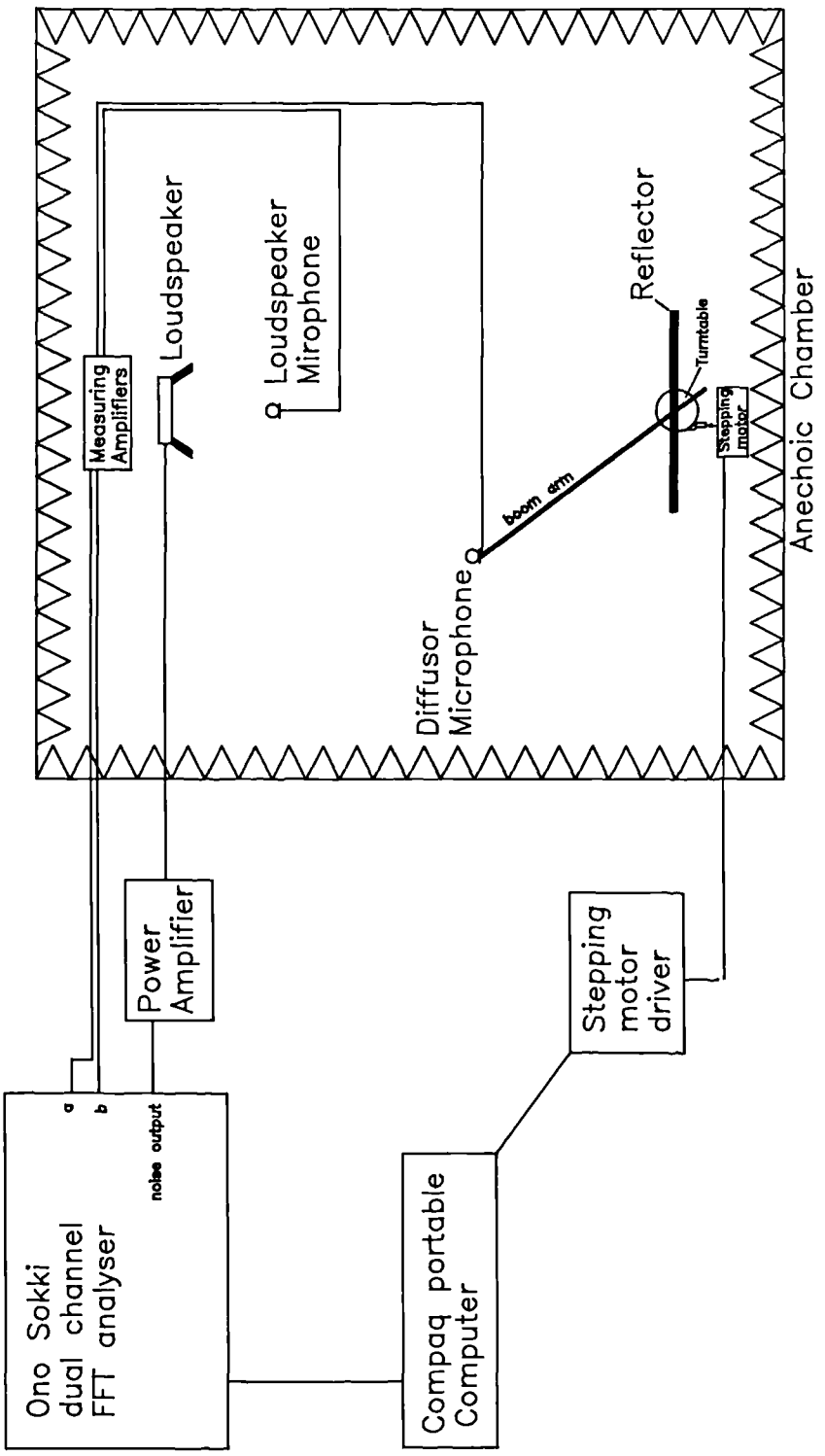

Figure 2.3. Experimental set-up for two microphone cross correlation measurement.

microphone signals x(t) and y(t) are compared, only when a certain time delay, τ_1, is added to the microphone response x(t), will the two signals be identical. When such a time delay results in the two microphone signals being the same, the cross correlation function is large and finite[1], at other delays the two signals are dissimilar and the cross correlation is zero.

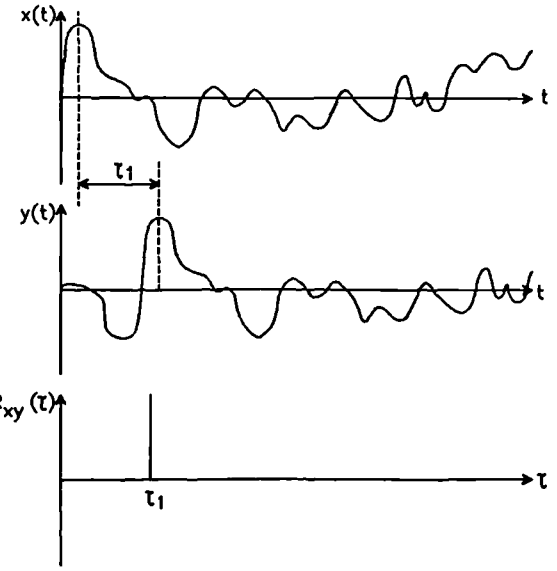

Figure 2.4. Demonstration of the cross correlation process. In this case $y(t)=x(t-\tau)$.

For the actual measurement with the diffuser, one such delay, τ_x, was equal to the time taken for the sound to travel direct from one microphone to another. Another delay, τ_r, was the time taken for the sound to travel from one microphone to another reflecting off the panel. Figure 2.5 illustrates the definitions of these time delays. In this case the two microphone signals were not simply related by a time delay. However, the cross correlation function worked provided that the two signals are linearly related. So the various sound paths between the microphones had to be linear, including the reflection from the panel.

[1]The definition of the cross correlation gives infinity for identical signals. In reality, however, an infinite time segment can never be taken, and so the cross correlation always remains finite.

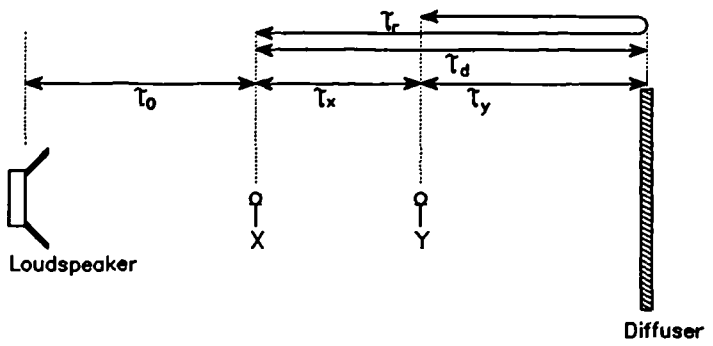

Figure 2.5. Definitions of delays used in developing the theory of the cross correlation method.

An example of the measured cross correlation function is given in Figure 2.6. The incident sound and reflected sound can clearly be seen. There are two other 'secondary' peaks both at negative time delays (the second of the secondary peaks is to the left of the graph at too large a delay to be seen). The secondary peaks occur because the sound reflecting from the panel was picked up by the loudspeaker microphone. From the cross correlation definition, Equation 2.1, when there are two time delays at each microphone when the signals are similar, there are four correlation peaks. The secondary peaks are well separated in time from the incident and reflected sound, and so could easily be removed by time gating.

It can be seen from the cross correlation function, Figure 2.6, that the incident and reflected sound could be separated in the time domain. This process will be discussed in Section 2.3.3. A Fourier transform could then be taken of just the reflected sound to produce the processed cross spectrum. To remove the response of the white noise generator, power amplifier, and loudspeaker systems, the processed cross spectrum was divided by the auto spectrum of the

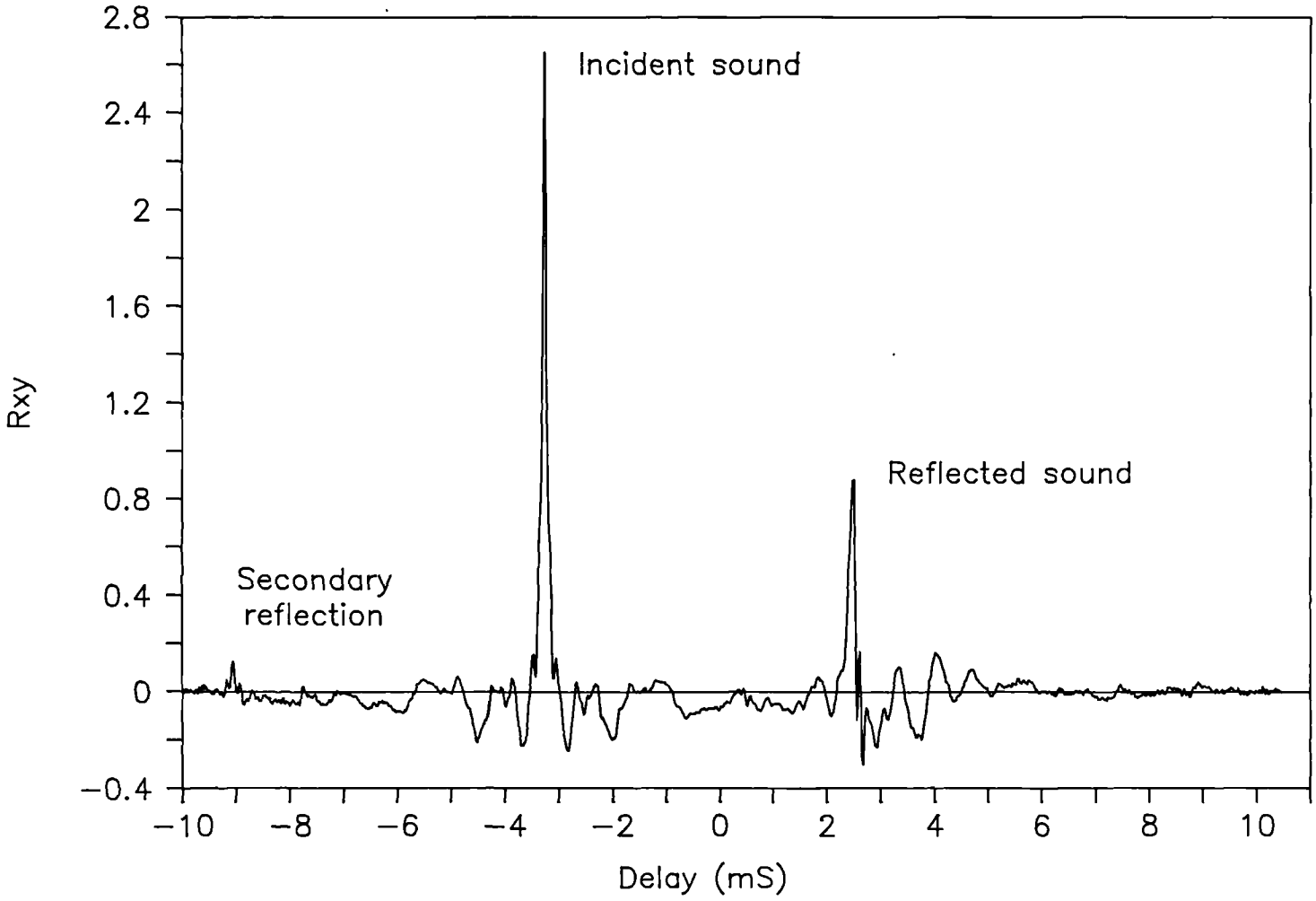

Figure 2.6. Example of measured cross correlation function for the with diffuser measurement

loudspeaker microphone measured with no diffuser present. The difference in the responses of the microphones also had to be allowed for, this was represented by the transfer function between the two microphones, $H_{mic}(\omega)$.

The resulting transfer function measured, $H(\omega)$, represents the change in the sound wave of a continuous white noise source, travelling from the loudspeaker microphone to the diffuser microphone reflecting off the panel. This is given by:

$$H(\omega) = \frac{S'_{xy}(\omega)}{H_{mic}(\omega)S_{xx}(\omega)} \qquad 2.2$$

where $S'_{xy}(\omega)$ is the processed cross spectrum, $S_{xx}(\omega)$ the auto spectrum of the loudspeaker microphone for the measurement without the panel present. A full derivation of Equation 2.2 is given in Section 2.3.2.

Analysis of the total sound field was identical except that the processed cross spectrum used in Equation 2.2 was calculated from the complete cross correlation function minus the secondary reflections.

2.3.2 The theoretical basis for the cross correlation method

Consider the experimental set up shown in Figure 2.5. The signal received at the microphone y is a combination of the sound direct from the loudspeaker and the same signal convolved with the impulse response of the panel and further delayed, i.e:

$$y(t) = p(t-\tau_x) + \int_{-\infty}^{\infty} h(\alpha)p(t-\tau_r-\alpha)d\alpha \qquad 2.3$$

where h(α) is the impulse response of the panel, and p(t) is the signal from the loudspeaker as it passes the loudspeaker microphone.

The loudspeaker microphone response is similarly:

$$x(t) = p(t) + \int_{-\infty}^{\infty} h(\alpha)p(t-2\tau_d-\alpha)d\alpha \qquad 2.4$$

The instantaneous cross correlation between the two microphones is [x(t).y(t)], and is given by:

$$[p(t)+\int_{-\infty}^{\infty} h(\alpha)p(t-2\tau_d-\alpha)d\alpha]\cdot[p(t-\tau_x)+\int_{-\infty}^{\infty} h(\alpha)p(t-\tau_r-\alpha)d\alpha] \qquad 2.5$$

This can be expanded to:

$$\begin{aligned}&[p(t)p(t-\tau_x)]\\ &+[\int_{-\infty}^{\infty} h(\alpha)p(t)p(t-\tau_r-\alpha)d\alpha]\\ &+[\int_{-\infty}^{\infty} h(\alpha)p(t-2\tau_d-\alpha)p(t-\tau_x)d\alpha]\\ &+[\int_{-\infty}^{\infty} h(\alpha)p(t-2\tau_d-\alpha)d\alpha\cdot\int_{-\infty}^{\infty} h(\alpha)p(t-\tau_r-\alpha)d\alpha]\end{aligned} \qquad 2.6$$

The four terms resulting in the four cross correlation peaks can be seen in this formulation. The first term is the direct sound, the last two terms are the secondary reflections. The unwanted sound - i.e. the direct sound and secondary

reflections - can now be eliminated. This leaves just the reflected sound. The instantaneous processed cross correlation product is then:

$$[x(t)\cdot y(t+\tau)]' = \int_{-\infty}^{\infty} h(\alpha)p(t)p(t-\tau_r-\alpha)d\alpha \qquad 2.7$$

An estimate of the full processed cross correlation, $R'_{xy}(\tau)$, is then derived from Equation 2.7 by applying the cross correlation definition shown in Equation 2.1:

$$R'_{xy}(\tau) = \int_{-T}^{T} [x(t)y(t+\tau)]'dt \qquad 2.8$$

Using Equations 2.7 and 2.8, and the fact that the auto correlation function is the cross correlation of a function with itself, it can be shown that:

$$R'_{xy}(\tau) = \int_{-T}^{T} h(\alpha)R_{xx}(\tau-\tau_r-\alpha)d\alpha \qquad 2.9$$

Finally, taking the Fourier transform of Equation 2.9 and rearranging gives:

$$H(\omega) = \frac{S'_{xy}(\omega)}{S_{xx}(\omega)} \qquad 2.10$$

$$with \quad H(\omega) = FT[h(\alpha)]e^{-\tau_r}$$

where $S'_{xy}(\omega)$ is the processed cross spectrum; $S_{xx}(\omega)$ is the auto spectrum of the loudspeaker microphone for the measurement without the diffuser; FT denotes a fourier transform; and $H(\omega)$ is the required transfer function. For the definition of the transfer function see discussions about Equation 2.2.

To get the full measurement Equation 2.2, an extra transfer function is included to allow for the different microphone responses. The effect is that the instantaneous cross correlation is in reality convolved with the transfer function between the two microphones. So in Equation 2.8 $[x(t).y(t)]'$ should be replaced by $H_{mic}*[x(t).y(t)]'$ (* denotes a convolution). The microphone transfer function then appears on the denominator as a simple multiplier when the Fourier transform is taken. For further details on cross correlation measurement systems see Bendat and Piersol [Bendat 1980].

2.3.3 Separation of incident sound and reflected sound

For the scattered field to be found the direct sound had to be eliminated from the cross correlation. This was done by two process, subtraction and time gating. Figure 2.7 illustrates the processes. The tail of the incident sound peak overlaps with that of the reflected sound peak, this means simple time gating would not be sufficient. Consequently, the system was measured twice, once with the diffuser present and once without. The two results were subtracted. The result is shown in Figure 2.7c. This eliminated a large amount of the incident sound peak and so allowed separation of the reflected sound from the residual of the direct sound peak by simple time gating. The subtraction process had the added advantage of eliminating any unwanted reflections from the apparatus like the turntable support and boom arm. All equipment was covered in large quantities of foam to minimize unwanted reflections.

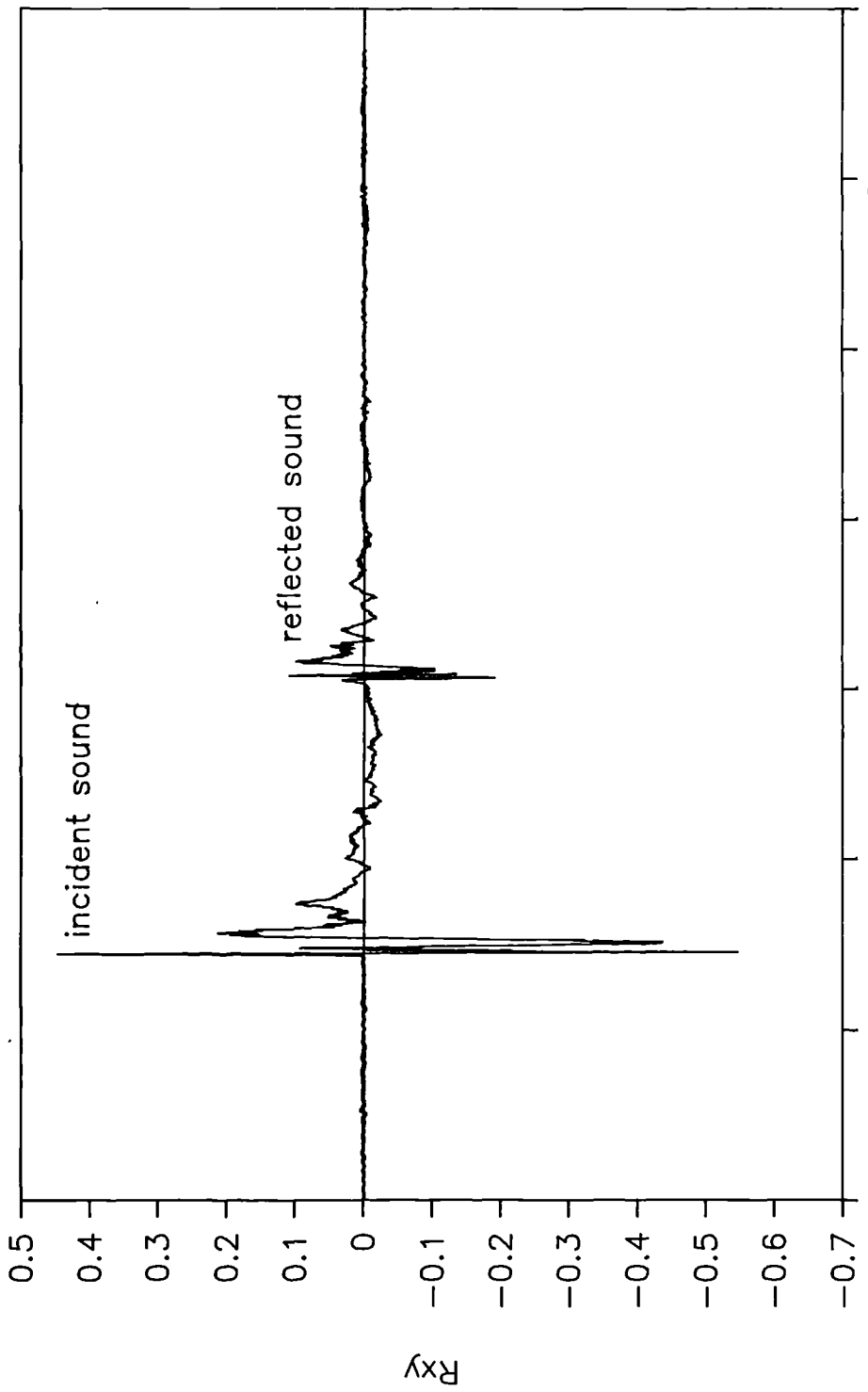

Figure 2.7a. Cross correlation function for the measurement with the diffuser present.

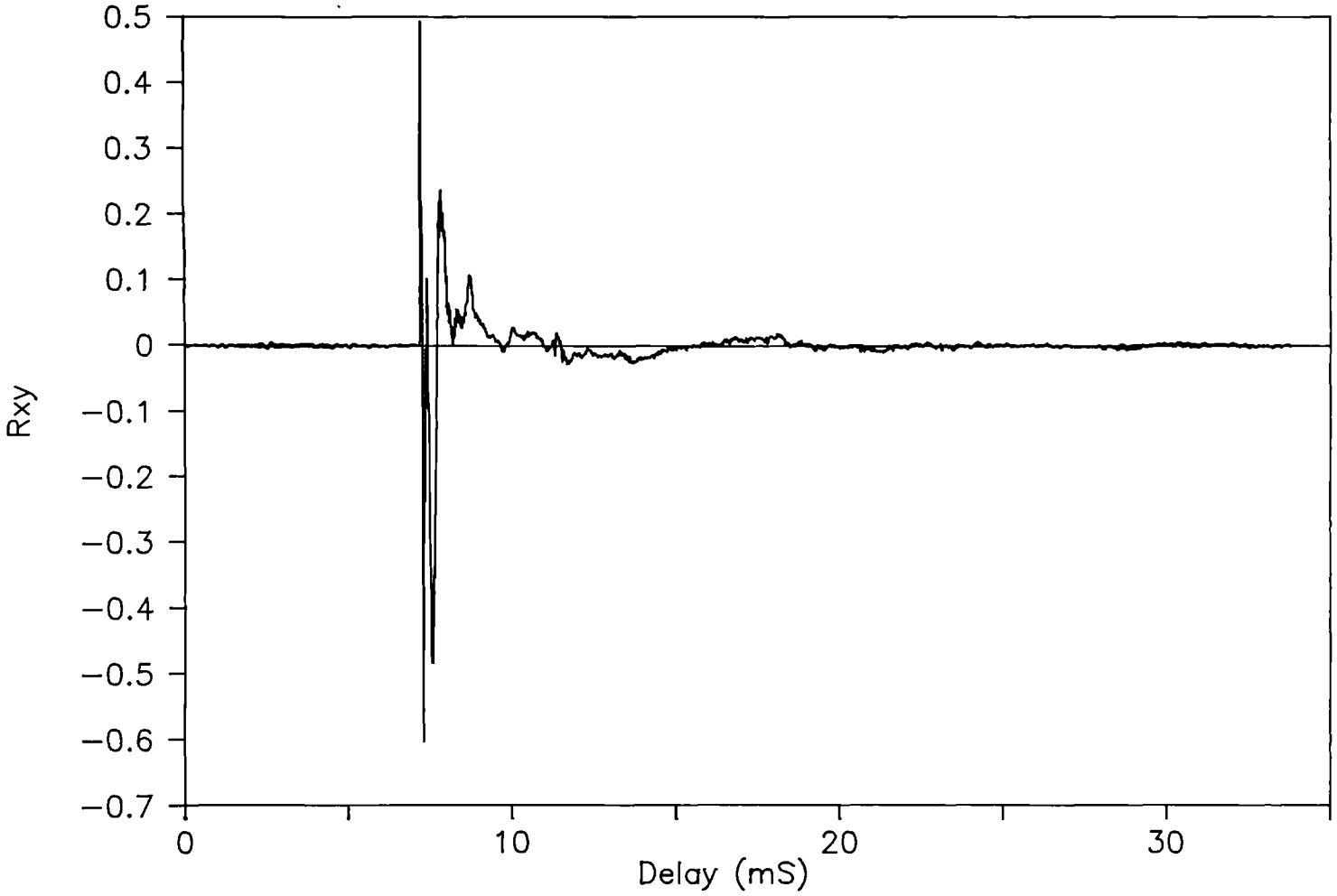

Figure 2.7b. Measured cross correlation function for the measurement without the diffuser present.

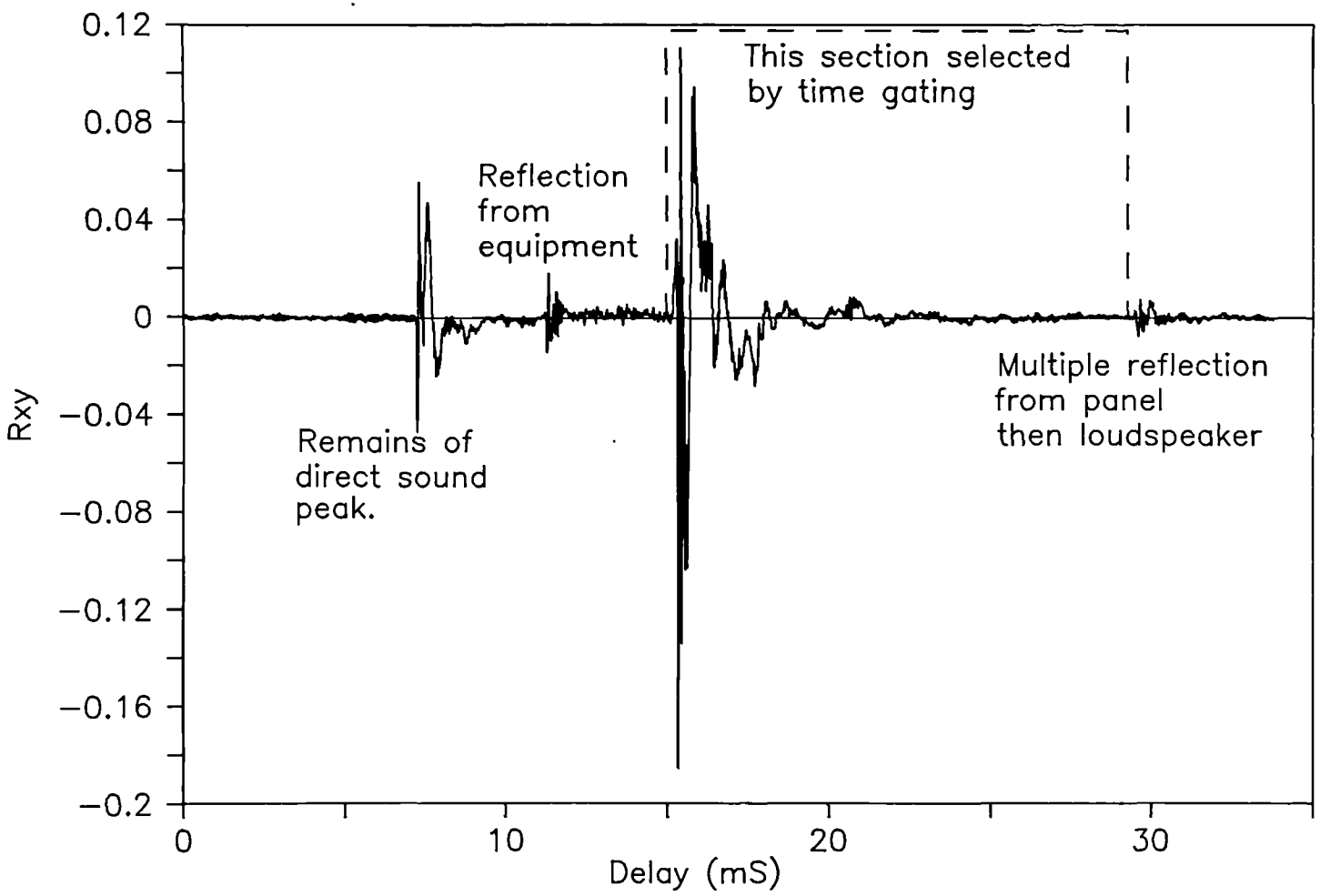

Figure 2.7c. Example of cross correlation function after subtracting cross correlations for the with diffuser measurement and the without diffuser measurement.

2.3.4 Microphone calibration

A pair of matched Brüel and Kjær microphones (4183) were used for the measurements. The use of matched microphones increases the coherence between the microphone signals and so improved the accuracy of the measurement. Despite the microphones being matched, the responses were slightly different and so a calibration was necessary. To do this the microphones were placed a few centimetres apart at one end of the anechoic chamber, equidistant from the loudspeaker, which was at the other end radiating white noise. The Ono Sokki dual channel FFT analyzer then allowed the transfer function to be directly measured via the standard cross spectrum method [Bendat 1986 1980].

2.3.5 Movement of the diffuser microphone.

To allow transfer functions to be calculated as a function of scattering angle, a boom arm and stepping motor was used. This system allowed the boom to be moved and stopped at the appropriate angle while the measurement was taken. It also allowed accurate reproduction of the microphone positions for the measurements without diffuser when compared to the measurements with diffuser. This was necessary to allow subtraction of the two cross correlations. The experimental set up in the anechoic chamber is shown in Plate 2.1.

Plate 2.1 The set up within the anechoic chamber for the measurement of scattering from diffusers and reflectors.

2.3.6 Assessment of measurement accuracy

Many measurements using white noise use the coherence function as a test for accuracy. The coherence function for two pressure signals x(t) and y(t) is defined as [Bendat 1986 1980]:

$$\gamma_{xy}^2(\omega) = \frac{|S_{xy}(\omega)|^2}{S_{xx}(\omega)S_{yy}(\omega)} \qquad 2.11$$

where $S_{xy}(\omega)$ is the cross spectrum of the two signals and $S_{xx}(\omega)$ and $S_{yy}(\omega)$ represent their respective auto spectra. It can be shown that $0 \leq \gamma^2_{xy}(\omega) \leq 1$.

If x(t) and y(t) are related by a single linear transfer function h(t) so that y(t)=h(t)*x(t), then the coherence function is one (* denoting convolution). Imperfect systems such as those with an amount of coherent background noise in either of the signals, produce a coherence of less than 1. So the coherence gives a measure of how much noise there is in a system.

Unfortunately, in our system the coherence function was complicated by the presence of more than one main correlation peak. This lead to the coherence function having a comb filter type response. An example is shown in Figure 2.8. This was exacerbated by the presence of the secondary reflections. These reduce the coherence, yet do not decrease the accuracy of the measurement as they were easily eliminated by time gating. Consequently, the coherence function was not a good measure for testing the accuracy of this system. Therefore direct evaluation of the variance of the system was used.

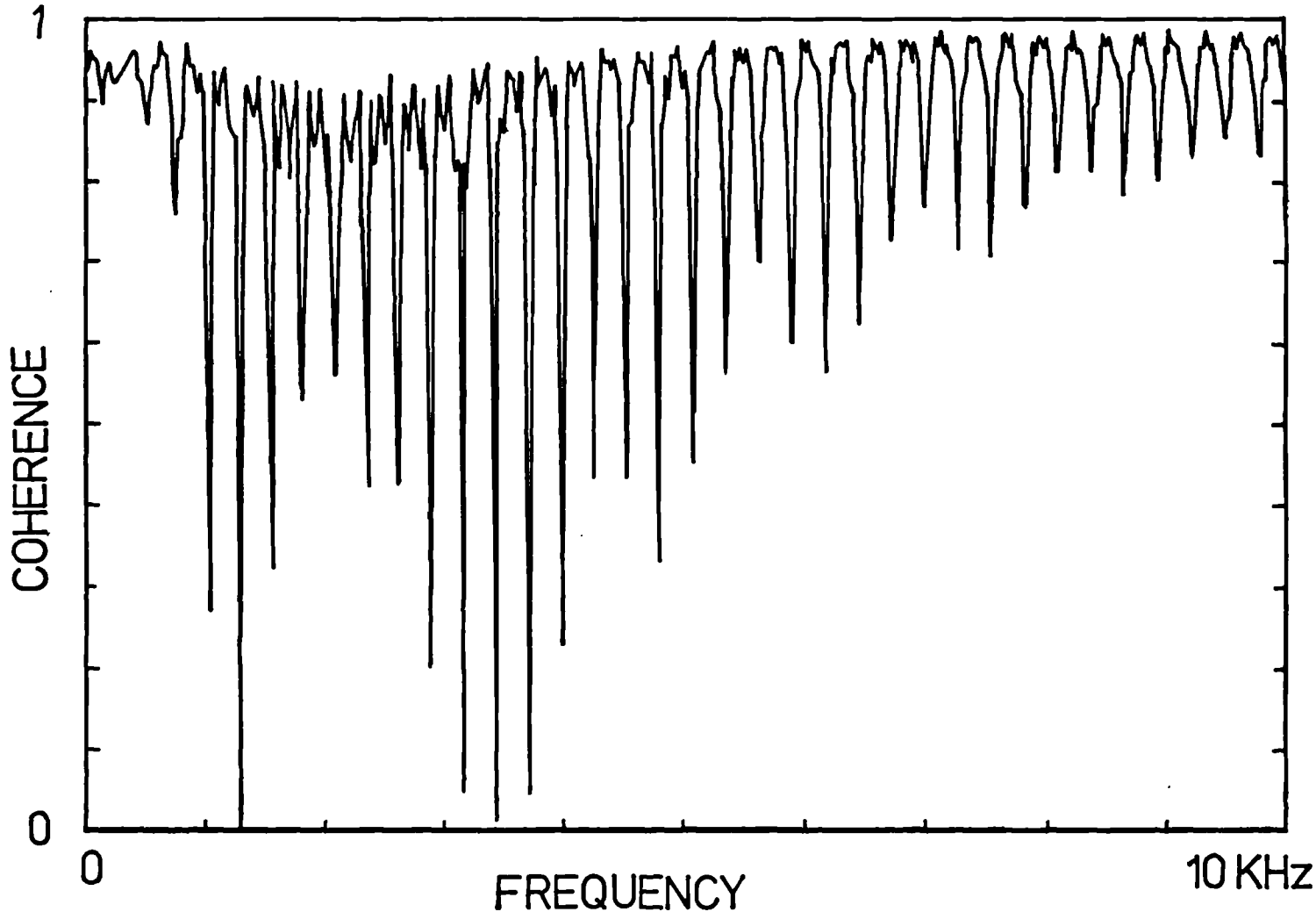

Figure 2.8 Coherence function.

White noise is a random signal, and so it requires averaging to get an accurate estimate of functions such as the cross correlation function. It was necessary to assess how many averages would be needed to get a certain accuracy. The error formula was derived by combining the error formulations for cross spectra and auto spectra given in Bendat and Piersol [Bendat 1980]. The derivation can be found in Appendix 1. It shows that the variance of the resulting transfer function is:

$$\sigma^2|H(\omega)| = \left[\frac{|S'_{xy}(\omega)|^2}{|H^2_{mic}(\omega)|^2|S_{xx}(\omega)|^2}\right]\left[\frac{\sigma^2|S'_{xy}(\omega)|}{|S'_{xy}(\omega)|^2} + \frac{\sigma^2|S_{xx}(\omega)|}{|S_{xx}(\omega)|^2}\right] \qquad 2.12$$

where σ^2 denotes variance; $S'_{xy}(\omega)$ the processed cross spectrum; $S_{xx}(\omega)$ the auto spectrum of the loudspeaker microphone for the without diffuser measurement; and $H_{mic}(\omega)$ the transfer function between the two the microphones.

The derivation assumed that:

1. The signals were noise free. Reasonable in laboratory conditions.
2. The error in the microphone calibration was small. As the microphones are very close together in the calibration, the coherence between them was one. As the calibration was only done once in each session, it could be done with a very large number of averages to eliminate random errors. Both these conditions made the error assumption reasonable.
3. The random error of the auto spectrum and cross spectrum were independent of each other. This could not have been completely true as these two spectra were either completely or partially derived from the

loudspeaker microphone signal with no diffuser present. This assumption was tested as detailed in the following paragraphs.

The theoretical error formula was tested against measurement. To do this twenty identical measurements of the transfer function of a simple plane panel were made and the random error calculated. Standard statistical formulations were used [Bendat 1980]. In Figure 2.9 the experimentally derived percentage random error and theoretically expected values are shown for 128 averages. It can be seen that there was good agreement between the experimental and theoretical random errors in the locations of the minima and maxima. In general the theoretically predicted variance was greater than the experiment, due to the fact that the processed cross spectrum and auto spectrum for the measurement without the diffuser were not truly independent. This lead to some errors being counted more than once. So assumption 3 above was good except that it lead to an over estimation of roughly 2% in the random error.

The graph of variance verses frequency shows a large number of minima and maxima. The cause of the comb filter effect was interference between the direct and reflected sound. When the frequency was such that the distance from diffuser microphone to the panel was an integer number, N, of quarter wavelengths, destructive or constructive interference occurred between the incident and reflected sound. When N was odd, destructive interference occurred. This resulted in a decreased sound pressure level at the diffuser

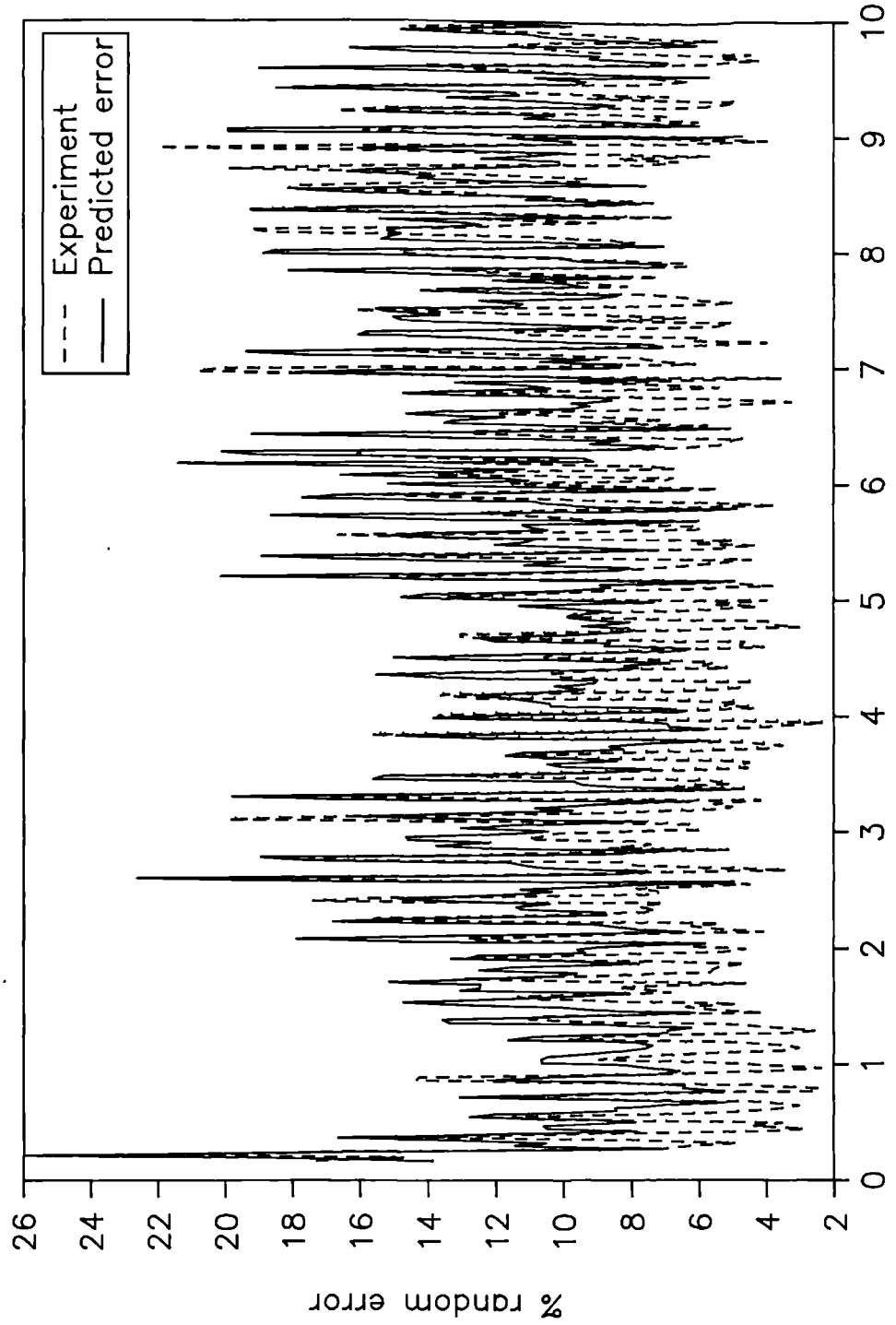

Figure 2.9. Error in transfer function for two microphone measurement system.

microphone, a reduction in the signal to noise ratio, and consequently a reduction in accuracy.

For the experiments, 1024 averages were used to get an average 3.5% accuracy for the transfer function. The formulation 2.12 above, allows the calculation of the errors for other number of averages. The error value of 3.5% is for the random error and does not include bias errors. Bias errors could have been caused by such effects as: unwanted reflections off equipment; bad construction of the panels; and misalignment of equipment.

2.3.7 The problem with using white noise

Unfortunately, there was a major drawback in using white noise as a source, the averaging required to obtain a reasonable estimate of the transfer function was very time consuming. To measure the scattering from a single panel to a 3.5% accuracy required 1024 averages for each receiver position and took 24 hours. Consequently, a much faster maximum length sequence, pseudo-random noise source measurement system was used instead.

2.4 One Microphone, Pseudo-Random Noise Source, Cross Correlation Method

To reduce the time required for measurement a pseudo-random noise source which uses a maximum length sequence, was used. A maximum length

sequence is a set of pulses of different widths but equal magnitudes, the width of the pulses are determined by the maximum length number sequence [Rife 1989, Herbert 1983]. An example is shown in Figure 2.10 for a short sequence based on N=15. Over the length of the signal the order of the impulses is unique, so in a similar way to white noise, cross correlations and similar functions can be calculated. Yet the maximum length sequence is a deterministic signal, which means that for relatively noise free microphone signals, only a single cross correlation measurement is needed. So the time consuming averaging process used with a white noise source is no longer needed. Accurate

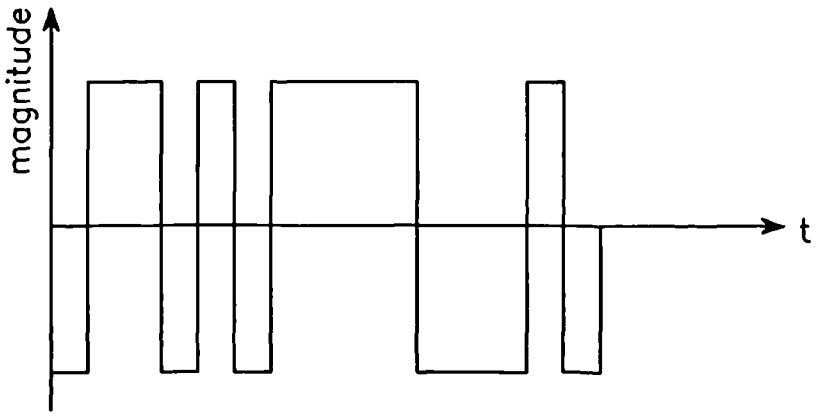

Figure 2.10. A maximum length sequence based on N=15.

measurements of cross correlations can be obtained in seconds, where using white noise would take minutes.

We could also measure to a higher accuracy with the maximum-length sequence. The accuracy of the maximum length sequence source system was tested by making identical experiments and calculating the variance. It was found

that a simple cross spectrum calculated in the anechoic chamber was accurate to .02% with no averages.

The actual technique for measurement was nearly identical to the two microphone cross correlation method. The major difference was that the reference against which the cross correlation was calculated was no longer the loudspeaker microphone but the maximum length sequence source signal generated by the computerized measurement system. This provided a noise free input source for the cross correlation function, which was necessary to exploit the deterministic nature of the pseudo-random sequence. This meant that there was no need for a relative calibration of the microphone pair. A calibration was still needed of the responses of the loudspeaker and other equipment. The new experimental set up is shown in Figure 2.11.

With this system, the transfer function measured was not exactly the same as for the white noise measurement system detailed in Section 2.3. In the white noise measurement system normalization was done with the incident sound at the loudspeaker microphone's position. In the maximum length sequence measurement system, no such microphone exists, so normalization was done at the single microphone's position. The new transfer function will be denoted $H_2(\omega)$. At any one microphone position the transfer function was the scattering from the panel normalized to the incident sound field at that position. The measurement equation then was:

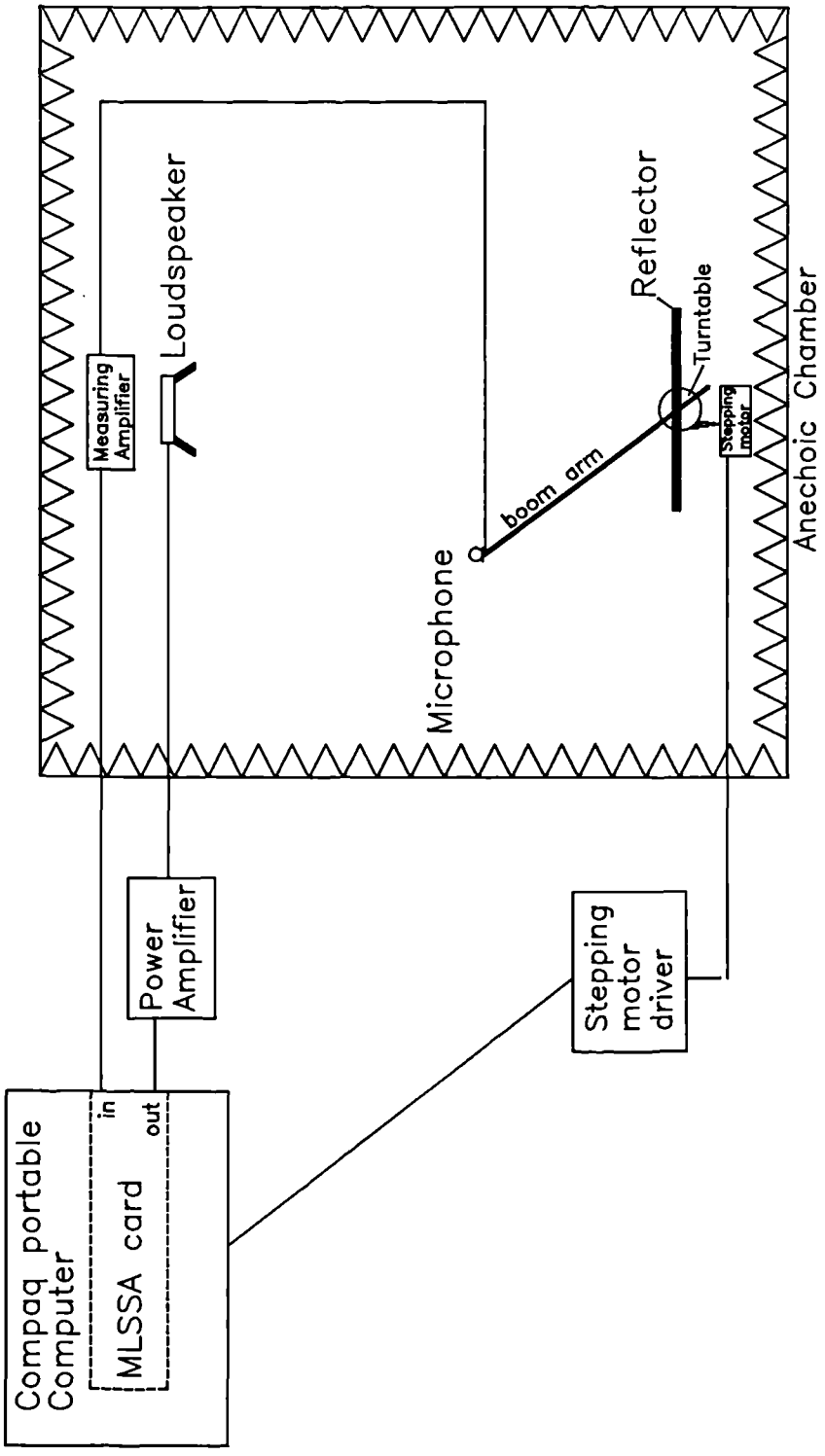

Figure 2.11. Set-up for measurement using single microphone, cross correlation technique.

$$H_2(\omega) = \frac{S'_{xy}(\omega)}{S_{yy}(\omega)} \qquad 2.13$$

where $S_{xy}(\omega)$ is the processed cross spectrum, and $S_{yy}(\omega)$ the auto spectrum of the microphone signal with no diffuser present. A similar analysis to that given in Section 2.3.2 can be used to derive this formulation.

A commercial implementation of the maximum length sequence technique on a portable personal computer was used. This was the MLSSA package. All other equipment, like the microphone control system were the same as for the two microphone method. The need to control the microphone position from the computer, meant the author had to develop customized computer programs using the device drivers provided, to supplement the measurement system.

2.5 Reasons for Measuring the Scattered and Total Field.

When measuring the performance of diffusers at low frequency both the scattered and total sound fields were checked against theoretical predictions. In the actual auditorium it is only the total field that is heard by the audience, and so interest in the scattered field could be questioned. However, there were several reasons for needing to look at the scattered field:

(i) At low frequency the total field was a simple picture, having a few minima and maxima which are well separated. This made comparison between theory and experiment easy. At high frequency, however, the interference pattern in the

total field became extremely complicated and vast varying. A small change in receiver or panel position resulted in a large change in the measured field. It was no longer simple to compare total fields, and so the scattered fields had to be used.

(ii) The performance of the quadratic residue diffuser is defined in the scattered field. It is claimed that it produces 'optimum' diffusion - i.e. uniform scattering of sound to all angles. This could only be tested in the scattered field.

(iii) When the results of scattering measurements are incorporated into ray tracing models, a simple probability distribution of the ray angle at each reflection is used [Kuttruff 1991b]. This distribution is determined from the scattered field.

2.6 Displaying of Results

For the figures of scattered field and total field shown in this thesis, the pressures have been normalized to the incident sound pressure at the microphone. This will be labelled on the Y-axis as Ps/Pi, Pt/Pi or P/Pi; the value given is in dB. The only exception is Chapter 7 where the performance of the diffusers are being considered. Here the pressure is normalized to a single fixed microphone position, this will be labelled on the Y-axis as P (dB).

2.7. Conclusions

Systems have been developed to allow the measurement of the scattering from finite sized reflectors and diffusers. The first system, based on a white noise source was accurate but slow. It requires little specialized equipment. It took 24 hours to produce an random error of 3.5% in the scattered sound field. The second system, based on a maximum length system, was both more accurate and much faster. Measurements could be done in a couple of hours, most of this time being taken up with moving the microphone.

Chapter 3

The Theoretical Prediction of Scattering from Reflectors and Diffusers

3.1 Introduction

Many wave phenomena have been solved via the Helmholtz-Kirchhoff integral equation, whether these be electromagnetic or acoustic waves, radiation or scattering. This investigation have concentrated on the application of various solutions of the integral equation to predict the scattering from reflectors and diffusers commonly found in auditoria. The prediction methods had varying degrees of simplicity, computation time and accuracy.

3.2 The Helmholtz-Kirchhoff Integral Equation

3.2.1 Definition of the Helmholtz-Kirchhoff Integral Equation

The Helmholtz-Kirchhoff integral equation formulates the pressure at a point, as a combination of the pressure direct from the sources, and a surface integral of the pressure and it's derivative over the reflecting surfaces. In this

project the constant frequency form of the theorem was used. This gives the pressure p(r) for one point source as [Pierce 1981 pages 180-182]:

$$p(\underline{r}) = \frac{1}{4\pi\epsilon}\iint_s (-G(\underline{r}-\underline{r}_s)\nabla p(\underline{r}_s) + p(\underline{r}_s)\nabla G(\underline{r}-\underline{r}_s)).\underline{n}_s \, dS + p_i(\underline{r}-\underline{r}_0) \qquad 3.1$$

where $p_i(\underline{r}-\underline{r}_0)$ is the sound pressure direct from the source; $G(\underline{r}-\underline{r}_s)$ the appropriate free field Green's function; and $\underline{n}_s$ the unit vector normal to the surface, pointing out of the surface. ϵ can have values of 0,½ or 1 depending respectively on whether the point $\underline{r}$ lies within the reflecting object, on the surface of the reflecting object, or external to the reflecting object. Figure 3.1 shows the definition of the vectors used.

The derivation of Equation 3.1 is a well known problem and can be found in many standard texts [Pierce 1981 pages 182-, Ghatak 1979, Burton 1973], and so shall not be discussed here. Only the application of the equation will be discussed.

The Green's function is taken to be the standard form for free space. In our sign convention, where the time dependence is assumed to be e^{iwt} and $\sqrt{-1}$ is i, G is given by:

$$G(\underline{r}-\underline{r}_s) = \frac{e^{-ik|\underline{r}-\underline{r}_s|}}{|\underline{r}-\underline{r}_s|} \qquad 3.2$$

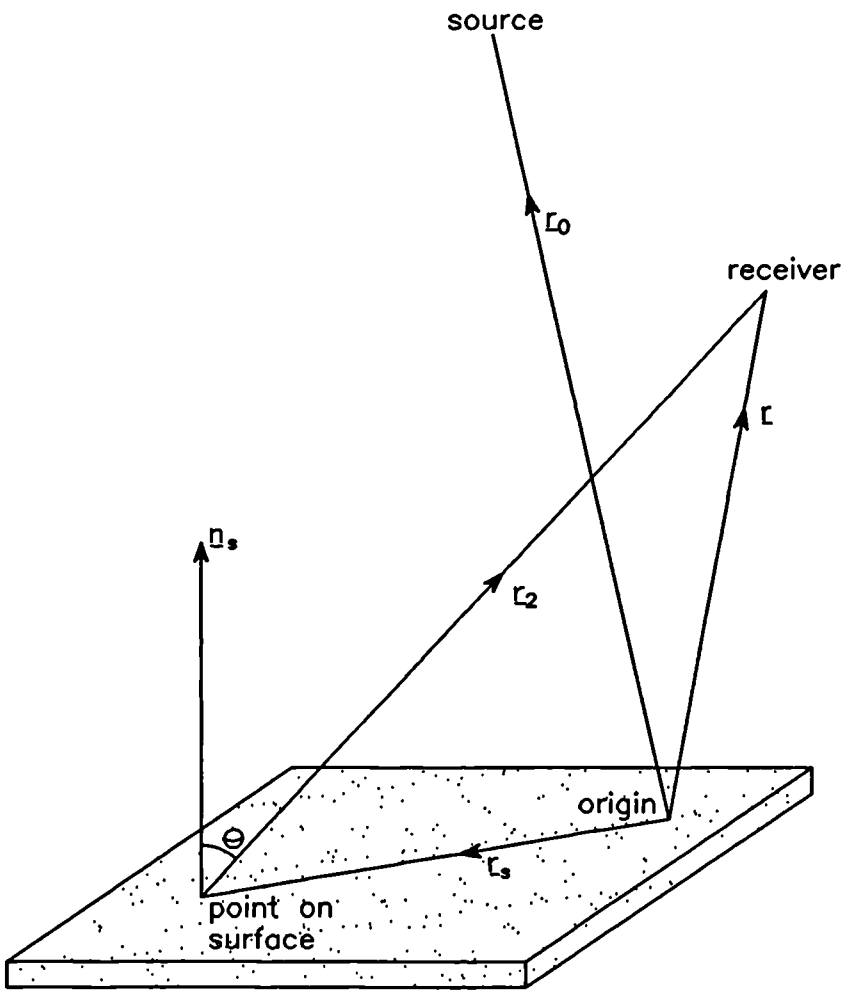

Figure 3.1. Definitions of vectors used in theoretical prediction methods.

3.2.2 Local reacting admittance assumption

If a surface is taken to be local reacting, the derivative of the surface pressure at any point will simply be related to the surface velocity at that point. The ratio of surface velocity to pressure being a fixed surface admittance. This assumption of local reaction enables the Helmholtz-Kirchhoff integral equation to be solved readily. For the hard rigid panels this assumption is exact. In the

Helmholtz-Kirchhoff integral equation, Equation 3.1, the term in $G\nabla P.\underline{n}_s$ vanishes for a rigid surface as the velocity normal to the surface is zero. Consequently, there are no problems in defining an exact admittance which is also zero.

For surfaces with non zero admittance, the assumption of the local reaction needs to be justified. In most of the theoretical prediction methods used in this work, the complex shape of the quadratic residue diffuser (QRD) was approximately represented by a simple box with a variable admittance on the surface. Consequently, tests were necessary to examine the validity of the local reaction admittance assumption for the QRD. The representation of the QRD in the theoretical prediction methods is detailed in Chapter 6, along with the tests of the validity of the local reacting admittance assumption.

3.3 General solution method

The solution of the Helmholtz-Kirchhoff integral equation for scattering involves applying Equation 3.1 twice. First the surface pressures and velocities on the scattering surface have to be found. Second the integral is carried out over the sources and scattering surface to determine the pressures at the external receiver positions. It can be seen from the Equation 3.1, that once the surface pressures and velocities are known, the solution of the external point pressure is a simple numerical integration. The difficulties in solving the Helmholtz-Kirchhoff integral equation centre around the first part of the process, obtaining

the surface pressures and velocities. The problem is that the surface pressure and velocities depend not only on the sources, but also on the surface pressures and velocities themselves. In the past, approximations for the surface pressure were commonly used, one such example is the Kirchhoff approximation. In more recent decades the increase in computing power available has meant that a rigorous numerical solution taking into account of the mutual surface interactions is possible. These methods are outlined in more detail in Sections 3.4 to 3.6.

All surfaces tested allowed exploitation of symmetry to greatly reduce computation time. Symmetry was exploited in all the theoretical prediction methods.

3.4 3D Boundary Integral Method

This method is a rigorous numerical solution of the Helmholtz-Kirchhoff integral equation, the values of the surfaces pressures being obtained via simultaneous equations. The method is as follows. The scattering surface is discretized into a number of surface elements across which it is approximated that the pressure, velocity and admittance are constant - the admittance being known. The elements must have dimensions sufficiently small to prevent errors in representing the pressure variation on the surface. To allow the pressure to be taken as uniform across the element, a upper limit of one quarter of a wavelength is usually taken for the element's dimensions [Lam 1990].

Once the surface has been discretized, a set of simultaneous equations can be set up for the surface pressure using Equations 3.1 and 3.2, with $\underline{r}$ being taken as positions on the surface. Each equation gives the pressure on a particular surface element, as a sum of the contributions from the sources, and a sum of the contributions from all elements. The simultaneous equations are solved via the CHIEF method [Schenck 1968], giving values for the surface pressures on each of the elements.

If the set of simultaneous equations were solved alone, it would be possible to get non-unique solutions at certain frequencies. These equate to eigensolutions of the physical body dimensions. To obtain the correct unique solutions, the fact that the pressure is zero inside the surface is used as a constraint. Formulations of Equation 3.1 with $\underline{r}$ chosen at interior points are added to the matrix to form an over determined system. The number of interior points is increased until convergence of the solution is achieved [Schenck 1968]. In general one interior point was sufficient to ensure convergence of the surface pressures and velocities. However, it is possible that the single interior point could equate to a node of the eigensolution of the physical body dimensions, and so the interior point would still fail to ensure a unique solution. Therefore, using two interior points was preferred.

As stated in Section 3.3, once the surface pressures are known, a simple surface integration of Equation 3.1 yields the external point pressure. Lam's

computer program implementation of the method was used in this work [Lam 1990].

3.5 Solution of the Helmholtz-Kirchhoff Integral Equation in the Thin Panel Limit.

Consider a rectangular panel represented in the 3D boundary integral method by a set of surface elements covering all sides of the body. When the panel becomes extremely thin, the 3D boundary integral method breaks down because there is a discontinuity in the pressure across the surface. Terai has given a solution for a perfectly rigid panel in the limit when the panel becomes infinitely thin [Terai 1980].

The derivation requires not only the Helmholtz-Kirchhoff integral equation given in Equation 3.1, but also the first order derivative form. For $\underline{r}$ on the surface, Equation 3.1 and it's first order derivative are given by:

$$P(\underline{r}) = \frac{1}{2\pi}\iint_S -G(\underline{r}-\underline{r}_s)\frac{\partial}{\partial \underline{n}_s}p(\underline{r}_s) + p(\underline{r}_s)\frac{\partial}{\partial \underline{n}_s}G(\underline{r}-\underline{r}_s)dS + 2P_i(\underline{r}-\underline{r}_0) \qquad 3.3$$

$$\frac{\partial P(\underline{r})}{\partial \underline{n}_r} = \frac{1}{2\pi}\iint_S -\frac{\partial}{\partial \underline{n}_r}G(\underline{r}-\underline{r}_s)\frac{\partial}{\partial \underline{n}_s}p(\underline{r}_s) + p(\underline{r}_s)\frac{\partial^2}{\partial \underline{n}_r \partial \underline{n}_s}G(\underline{r}-\underline{r}_s)dS + 2\frac{\partial P_i(\underline{r}-\underline{r}_0)}{\partial \underline{n}_r} \qquad 3.4$$

where $\underline{n}_r$ is the normal to the surface at $\underline{r}$.

Consider the situation when a rigid panel reduces in thickness to a infinitely thin body. This is illustrated in Figure 3.2. In that case if $\underline{n}_{s1}$ is written as $\underline{n}$, it can be shown that Equations 3.3 and 3.4 become:

$$p(\underline{r}_1)+p(\underline{r}_2) = \frac{1}{2\pi}\iint_S \{-G(\underline{r}-\underline{r}_s)\left(\frac{\partial p(\underline{r}_{s1})}{\partial \underline{n}}-\frac{\partial p(\underline{r}_{s2})}{\partial \underline{n}}\right) + [p(\underline{r}_{s1})-p(\underline{r}_{s2})]\frac{\partial}{\partial \underline{n}}G(\underline{r}-\underline{r}_s)\}\, dS + 2P_i(\underline{r}-\underline{r}_0) \qquad 3.5$$

$$\left(\frac{\partial P(\underline{r}_1)}{\partial \underline{n}_r}+\frac{\partial P(\underline{r}_2)}{\partial \underline{n}_r}\right) = \frac{1}{2\pi}\iint_S \{-\frac{\partial}{\partial \underline{n}_r}G(\underline{r}-\underline{r}_s)\frac{\partial}{\partial \underline{n}}[p(\underline{r}_{s1})-p(\underline{r}_{s2})] + [p(\underline{r}_{s1})-p(\underline{r}_{s2})]\frac{\partial^2}{\partial \underline{n}_r \partial \underline{n}}G(\underline{r}-\underline{r}_s)\}\, dS + 2\frac{\partial P_i(\underline{r}-\underline{r}_0)}{\partial \underline{n}_r} \qquad 3.6$$

This method has been applied to rigid panels only, and so Equations 3.5 and 3.6 can be simplified further. The velocity terms of the two equations must be zero as the velocities must be equal and opposite on either side of the panel. This then leads to:

$$p(\underline{r}_1)+p(\underline{r}_2) = \frac{1}{2\pi}\int_S\int [p(\underline{r}_{s1})-p(\underline{r}_{s2})]\frac{\partial}{\partial n}G(\underline{r}-\underline{r}_s)dS + 2p_i(\underline{r}-\underline{r}_0) \qquad 3.7$$

$$0 = \frac{1}{2\pi}\int_S\int [p(\underline{r}_{s1})-p(\underline{r}_{s2})]\frac{\partial^2}{\partial n_r \partial n}G(\underline{r}-\underline{r}_s)dS + 2\frac{\partial p_i(\underline{r}-\underline{r}_0)}{\partial n_r} \qquad 3.8$$

The solution method for the thin panel integral Equations 3.7 and 3.8 is similar to the 3D boundary integral method. Again the surface is discretized, but this time on one side only. So this method just over halves the number of elements needed to represent a thin panel when compared to the 3D boundary integral method. The surface pressures and velocities are again assumed constant across each element. A set of simultaneous equations are constructed and solved in terms of the pressure difference across the panel using Equation 3.8. Once the surface pressure differences are known a simple numerical integration of the following equation, derived from Equation 3.1, gives the external pressure:

$$P(\underline{r}) = \frac{1}{4\pi}\int_S\int [p(\underline{r}_{s1})-p(\underline{r}_{s2})]\frac{\partial}{\partial n}G(\underline{r}-\underline{r}_s)dS + P_i(\underline{r}-\underline{r}_0) \qquad 3.9$$

If the surface pressures are needed these can be obtained from the values for the surface pressure differences and from Equation 3.7.

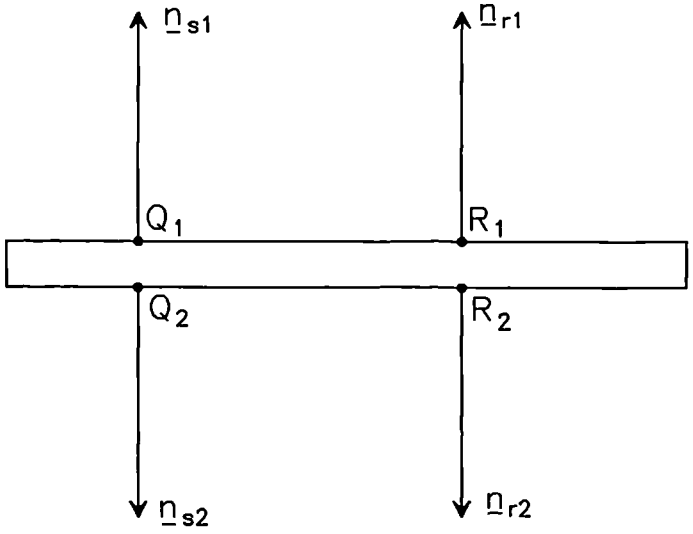

The points Q1 and Q2 are points on either side of the surface at $\underline{r}_{s1}$ and $\underline{r}_{s2}$ respectively.

The points R1 and R2 are receiver points on opposite sides of the surface at $\underline{r}_1$ and $\underline{r}_2$ respectively.

Figure 3.2. Definitions of vectors and positions used in thin panel limit solution.

As this method has been solved using the derivative of the Helmholtz-Kirchhoff integral equation the solutions are unique [Burton 1973]. There is no need to form an over determined system as there was with the 3D boundary integral method where internal points were used. In our implementation of this theory, the simultaneous equations were solved in a similar way to the 3D boundary integral method, except in the element containing the receiver point itself. Here, to obtain more rapid convergence of the surface integral, Terai's numerical solution for the integral was applied explicitly [Terai 1980].

3.6 Transient Model

It is possible to use the full time dependant form of the Helmholtz-Kirchhoff integral equation, instead of the constant frequency version, to derive the surface pressures. This is given by [Kawai 1990]:

$$\psi(r,t) = \frac{1}{4\pi e}\iint_S \{[\psi]\frac{\partial}{\partial n_s}(\frac{1}{r-r_s}) - \frac{1}{c}[\frac{\partial \psi}{\partial t}](\frac{1}{r-r_s})\frac{\partial r-r_s}{\partial n_s} - [\frac{\partial \psi}{\partial n_s}](\frac{1}{r-r_s})\} dS + \psi_i(r-r_0,t) \qquad 3.10$$

where $[\psi]=\varphi(\underline{r}_s,t-(\underline{r}-\underline{r}_s)/c)$ and is the full time dependant form of the velocity potential, and c the speed of sound.

To solve the time dependant form the surface is again discretized. It can be shown from the integral equation [Kawai 1990, Mitzner 1967, Friedman 1962] that the velocity potential and it's derivative on the surface can then be represented by the incident velocity potential from the source plus contributions from the other elements at previous times. This is an exact solution and not an iterative method. Problems arise because the convergence of the surface velocity potentials can be very slow. When choosing the elements it is necessary to satisfy the quarter wavelength condition so that the pressure variation is well represented. It is also necessary that any variation within any time step is restricted to one element. This leads to a very small time step, and hence slow convergence.

The method has advantages over the constant frequency methods in that once the impulse response has been calculated, the full frequency response can easily be obtained by a Fourier transform. However, the model needs further development, particularly for non-rigid bodies as the formulation of admittance in the time domain is unclear. Unfortunately, time did not allow development of the model in this project. It does offer an alternative solution method to the more standard constant frequency methods.

3.7 Kirchhoff Approximate Solution

The well known Kirchhoff approximation for optics, is that the wave function and it's derivative across an aperture are unaltered from the incident wave, and that away from the aperture both are zero (the source being on the opposite side of the aperture to the receiver) [Ghatak 1979]. Adapted for scattering in acoustics, it can be used to obtain the surface pressures and velocities. The approximation gives the surface pressures (velocities) as a scalar (vector) sum of the incident wave and reflected wave at that point. This is applied to the front of the surface only. On the back, sides, and away from the panel the pressure contribution to the integral is taken to be zero. For a perfectly rigid body this leads to a surface pressure on the front of twice the incident pressure and a surface velocity of zero. For a surface with a non-zero local reacting admittance the pressure and it's derivative are given by:

$$p(r) = p_i(r)(1+R) \qquad 3.11$$

$$\nabla P(r_s).n_s = -i\beta kP(r_s) \qquad 3.12$$

where ß is the normalized locally reacting admittance; R the local reflection factor; P_i the incident sound pressure on the surface; and k the wavenumber. For plane wave reflections, these are related by:

$$\beta = \frac{(1-R)}{(1+R)}COS(\alpha) \qquad 3.13$$

where α is the angle of incidence.

This approximation alone allows much faster predictions as it eliminates the need to solve the matrix of simultaneous equations for the surface pressures. A simple numerical integration of Equation 3.1, using the Green's function of Equation 3.2, and the boundary conditions of Equations 3.11 to 3.13, yields the external point pressure.

3.8 Fresnel and Fraunhofer Approximate Solutions

Once the Kirchhoff approximation for the surface pressures has been taken, it is possible to solve the resulting integral by the well known Fresnel and Fraunhofer solution methods. The later method is the far field solution, the

former method is a solution nearer the panel and requires the use of the standard Fresnel integrals.

The approximations involved for both solutions are similar, except that the Fraunhofer solution is more stringent about how close to the panel predictions can be done. For the Fraunhofer solution the receiver must be in the far field. The true far field pressure distribution is only achieved when the receiver distance is much larger than l and kl^2, l being half the largest panel dimension [Pierce 1981 page 217, Kinsler 1982 pages 187-188]. The other approximations required for both prediction methods are:

(1) The source is many wavelengths from the panel $r_0 \gg \lambda$.

(2) The receiver is many wavelengths from the panel $r \gg \lambda$.

(3) For a particular source and receiver position, over the range of the integration the angles subtended by the source and receiver to a normal to the panel do not vary significantly.

(4) Over the range of the integration, the variation in the source to panel, and source to receiver distances are small.

The methods of Polack and Dodd [Polack 1988] and Skudrzyk [Skudrzyk 1971] will be followed. A diagram showing the definitions of distances can be seen in Figure 3.1.

To begin with, the Green's function and Kirchhoff's approximation for the surface pressure must be incorporated into the Helmholtz-Kirchhoff integral equation. This involves the combination of Equations 3.1, 3.2, 3.11, 3.12 and 3.13 to produce the following expression:

$$p_s(r) \approx \frac{ikp_0}{4\pi}\int_s\int [\frac{e^{-ik(r_2+r_0)}}{r_2 r_0}[(R(r_s)-1)+(1+R(r_s))COS(\theta)]dS \qquad 3.14$$

The source is a point source of strength p_0 normal to the surface, and θ is the receiver angle. For simplicity only the scattered field expression is shown. The incident sound field contribution seen in Equation 3.1 can be added in to Equation 3.14 to obtain the total field, if required. The analysis now differs depending on the reflector being modelled.

3.8.1 Solution for rigid plane panels

For the rigid plane panel, R = 1, the standard Fresnel-Kirchhoff diffraction formula results [Ghatak 1979]. From this the formulations for Fresnel and Fraunhofer diffraction can be derived. The derivations will not be repeated here. (Although as we are dealing with off-axis receivers as well as on-axis receivers, the solution slightly differs from the more usual form given in Ghatak. Another derivation of the Fresnel solution can be found in [Leizer 1966]). It can be shown that in the far field the Fraunhofer solution is a SINC function - i.e. SIN(x)/x. The Fresnel solution results in the Fresnel integrals, the numerical solutions of which can be found in standard texts [Abramowitz 1965 pages 295-].

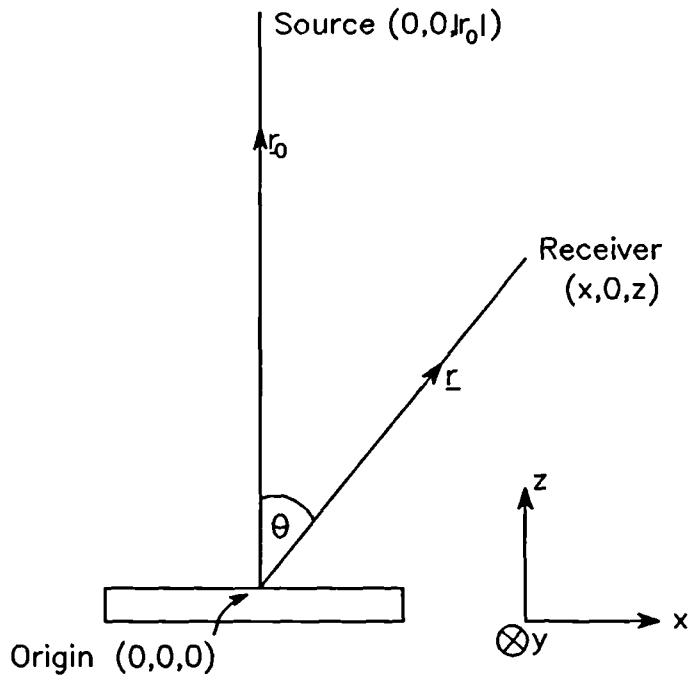

Figure 3.3. Definitions of vectors and distances.

Figure 3.3 shows the definitions of panel, receiver and source positions used in these two solutions. The panel front is taken to be on the z=0 plane; the source lies on the panel normal, drawn through the panel centre. The receiver and source are on the y=0 plane. In this case the Fraunhofer solution for the scattered pressure is

$$p_s(r) \approx \frac{-4ihap_0 SINC(\frac{kxa}{r})COS(\theta)e^{-ik(r_0+r)}}{\lambda r_0 r} \qquad 3.15$$

where a and h are half the width and height of the panel; θ the receiver angle; r and r_0 the receiver and source distances to the centre of the panel; and x the displacement of the receiver in the x direction.

The Fresnel solution for the rigid plane panel is:

$$p_s(r) \approx \frac{-ip_0 COS(\theta) e^{-ik(r+r_0)+\frac{i}{4\gamma}(\beta_x^2)}}{(r+r_0)} \{[C(\sigma_a)-C(\sigma_{-a})]-i[S(\sigma_a)-S(\sigma_{-a})]\} \times\{[C(\sigma_z)-iS(\sigma_z)]\} \quad 3.16$$

$$\gamma = \frac{k}{2}\left(\frac{1}{r}+\frac{1}{r_0}\right) \quad 3.17$$

$$\beta_x = k\left(\frac{x}{r}\right) \quad 3.18$$

$$\sigma_{\pm a} = \sqrt{\frac{2\gamma}{\pi}}\left(\pm a - \frac{\beta_x}{2\gamma}\right) \quad 3.19$$

$$\sigma_z = h\sqrt{\frac{2\gamma}{\pi}} \quad 3.20$$

where C(σ) and S(σ) are the standard Fresnel integrals [Abramowitz 1965].

3.8.2 Solution for non-rigid surface

The case for a non-rigid surface will now be considered. The first step to derive the Fraunhofer solution from Equation 3.14 is to make further approximations for the source and receiver distances from the panel. It is assumed that the receiver is in the far field. Then it can be shown that:

$$\frac{e^{-ikr_2}}{r_2} \approx \frac{e^{-ik(r+r_s SIN(\theta))}}{r} \quad 3.21$$

Definitions of the vectors can be found in Figures 3.1 and 3.3. Applying Equation 3.21 to Equation 3.14, and also assuming a far field source yields:

$$p_s(r) \approx \frac{-ikp_0 e^{-ik(r+r_0)}}{4\pi r r_0} \times [(COS(\theta)-1)\iint_s e^{-ikr_s SIN(\theta)} ds + (COS(\theta)+1)\iint_s R(r_s) e^{-ikr_s SIN(\theta)} ds] \quad 3.22$$

The first term in this expression is always zero. Consequently, Equation 3.22 reduces to:

$$P_s(r) \approx \frac{-ikP_0}{4\pi} \frac{e^{-ik(r+r_0)}}{rr_0} (COS(\theta)+1)\iint_s R(r_s) e^{-ikr_s SIN(\theta)} ds \quad 3.23$$

Equation 3.23 gives the diffraction from the surface as a Fourier transform of the surface reflection coefficients, this is analogous to Fourier optics.

For the quadratic residue diffuser, a further approximation is taken that the diffraction in the x and y direction are orthogonal. This allows much faster one dimensional integration to be used. This will be referred to as the simple Fraunhofer theory.

3.9 Geometric Approximation to Curved Panel Scattering

A simple method to solve the scattering from a curved surface is to break the problem into separate components: one for the effect of the finite sized panel, and another for the scattering caused by the curvature [Rindel 1985]. The finite sized panel effects can be predicted by the Fresnel solution method shown in Equations 3.16 to 3.20. The effects of the curved surface can be solved using

geometric scattering theory. In geometric scattering theory, it is assumed that the wavelength of the sound is small compared to the panel's curvature. Then the effects of curvature can be accounted for by the variation in the direction of the local normal to the panel surface. The energy in the sound beam is taken to be proportional to the width of the ray tube. The curvature causes the beam to spread after reflection and so reduces the energy at any one point. It can then be shown that the attenuation due to the curvature spreading the source beam for plane waves is given by [Rindel 1985]:

$$attenuation \approx \left|1+\frac{d^*}{R_c COS(\beta)}\right| \qquad 3.24$$

$$d^* = \frac{2rr_o}{r+r_o} \qquad 3.25$$

where R_c is the radius of the curved panel, ß is the angle of incidence and reflection; r is the receiver distance; and r_0 the source distance.

Pierce [1981 pages 413-417] gives a formulation applicable for incident spherical waves. The reflected wave amplitude is defined by the ratio of the pressure at the receiver, $P(\underline{r})$ to the surface pressure, $P_s(\underline{r}_s)$. This is given by:

$$\frac{P(\underline{r})}{P_s(\underline{r}_s)} \approx (1 + \frac{r}{r_0})(1 + \frac{r}{r_0} + \frac{2r}{R_c COS(\theta)}) \qquad 3.26$$

3.10 Conclusions

Various theoretical prediction methods based on the Helmholtz-Kirchhoff integral equation have been given. The methods cover a range of

approximations. As shall be shown in the following chapters, the methods also span a range of accuracies and computation times. The success or otherwise of the theoretical prediction methods will be discussed in Chapters 4 to 6.

Chapter 4

Theoretical Predictions and Measurements of the Scattering from Thin Rigid Plane Panels

4.1 Introduction

As a starting point for our investigation into predictions from reflectors and diffusers, a rigid thin plane panel was tested. Plane surfaces commonly occur in auditoria. They can cause echo problems, however, as they tend to create strong specular reflections, particularly at high frequencies.

This chapter discusses the performance of the theoretical prediction methods given in Chapter 3. They have varying degrees of approximation, accuracy, and computation time. The predictions were compared with experimental results. The use of a cut-off frequency [Rindel 1986] to describe the scattering from plane panels will also be discussed. This is a concept used by acousticians when designing reflectors. Discussions of the merits of the plane panel as a reflector in auditoria, and comparison with other reflectors and diffusers are given later in Chapter 7.

4.2 The Panels Tested and the Measurement Systems Used

4.2.1 The panel measured

The rectangular plane panel was made of lead clad plywood of dimensions 1.918 x .302 x .01 metres. The lead was 1.5 mm thick and on the front face only. Using lead on the front surface ensured surface vibrations were not a problem. This was checked by vibration measurements using an accelerometer. The panel was roughly a fifth of the size of reflectors typically used in auditoria.

4.2.2 Measurement system used

The experimental results quoted were done using the single microphone cross correlation method. Details of this method can be found in Chapter 2. The source was central to the panel at a normal distance of 3.96m. The pressure field was measured at a radius of 1.178m, centred around the panel centre. The temperature at the time of measurement was 25.5°c.

4.2.3 Other panel tested

Once it was found that the 3D boundary integral method gave accurate predictions of the scattering, the analysis continued by prediction only. A shorter panel was used so that computations could be carried our faster. The panel had

dimensions .412 x .24 x .01 metres. The source was at 5m centred normal to the panel. The receiver radius was 2m. The panel is roughly a fifth of the size of reflectors typically used in auditoria.

4.3 Theoretical Prediction Methods

Five different theoretical prediction methods were tested as described in Chapter 3. All methods involved solving the Helmholtz-Kirchhoff integral equation with varying degrees of approximation. In descending order of approximation they are:

1. 3D boundary integral method.
2. Thin panel limit solution.
3. Kirchhoff approximate solution.
4. Fresnel solution.
5. Fraunhofer far field solution.

4.4 Results and Discussions

4.4.1 3D Boundary integral method

The rigorous numerical solution of the Helmholtz-Kirchhoff integral equation produced accurate predictions of both the total and the scattered field. In Figures 4.1 and 4.2 examples are given at 3 KHz. Good accuracy was achieved

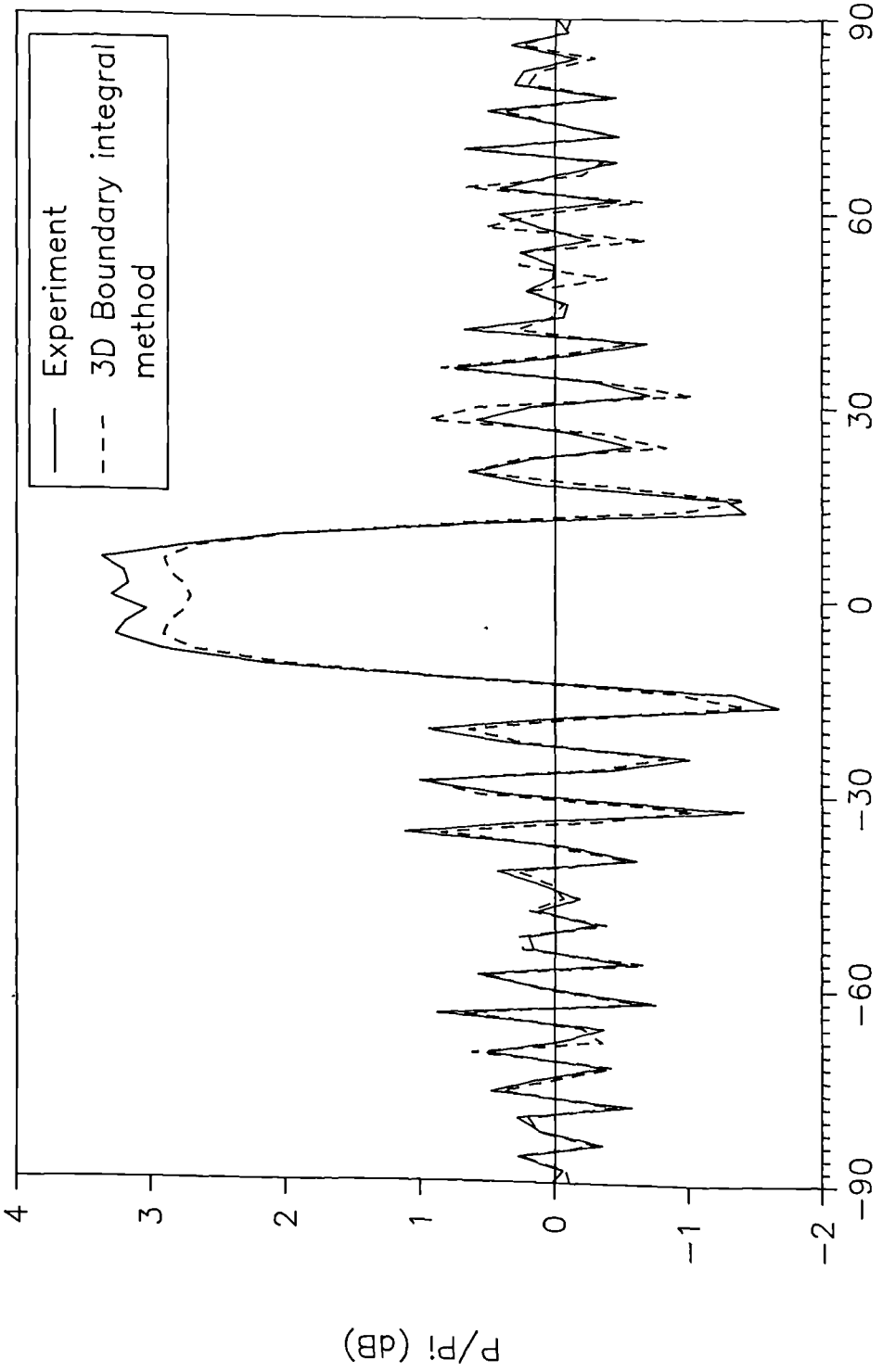

Figure 4.1 Comparison of 3D boundary integral method solution with experiment for plane panel. Total field at 2989 Hz.

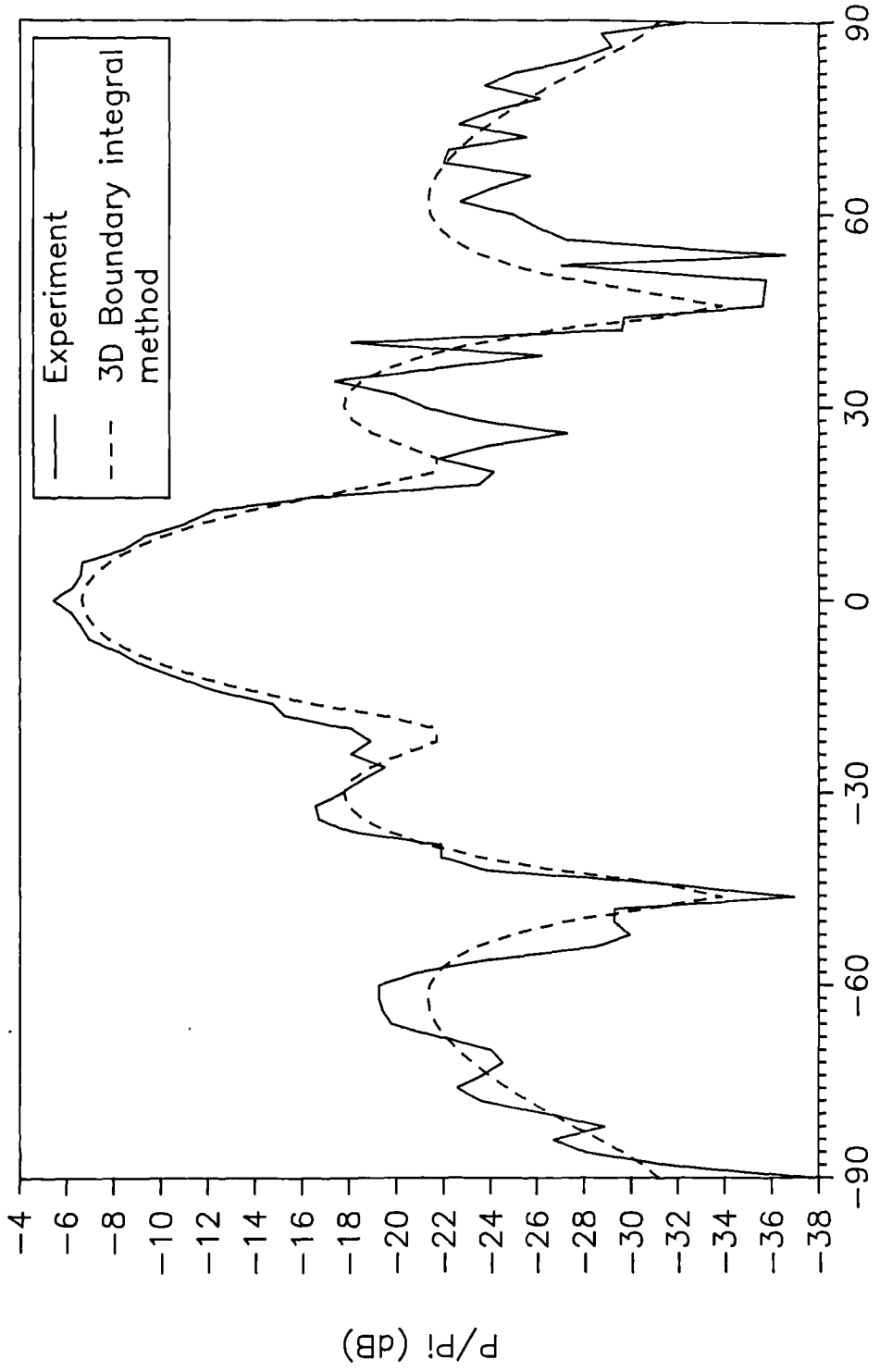

Figure 4.2. 3D boundary integral method prediction compared with experiment for plane panel. Scattered field at 2989 Hz.

over all scattering angles, -90° to 90°, and for all frequencies up to 6 KHz. The worst deviation in the total field at any frequency was 1 dB. Such deviations compare favourably with the findings of Terai [Terai 1980]. It was not possible to test the theory above 6 KHz because of computational limitations. The high degree of success of this theory below 6 KHz gives no reason to doubt its accuracy at higher frequencies.

4.4.2 Thin panel limit solution

The solution of the Helmholtz-Kirchhoff integral equation in the thin panel limit produces very similar results to the 3D boundary integral method and experiment. Examples are shown in Figures 4.3 to 4.5 at 1 KHz, 2 KHz and 4 KHz respectively. The pressures predicted by the thin panel limit model are accurate for nearly all scattering angles. The predictions only deviate significantly at large scattering angles and high frequencies. Below about 3 KHz the thin panel limit solution gives slightly different results than for the 3D boundary integral method at large scattering angles. Only at higher frequencies, however, are the deviations large enough to confirm that the 3D boundary integral method is giving better agreement with experiment.

In general, at large scattering angles, the thin panel limit solution gives a lower scattered pressure level than the 3D boundary integral method. Deviations are due to the thin panel method not representing the finite sized edge of the panel. This can be shown by comparing the thin panel limit solution,

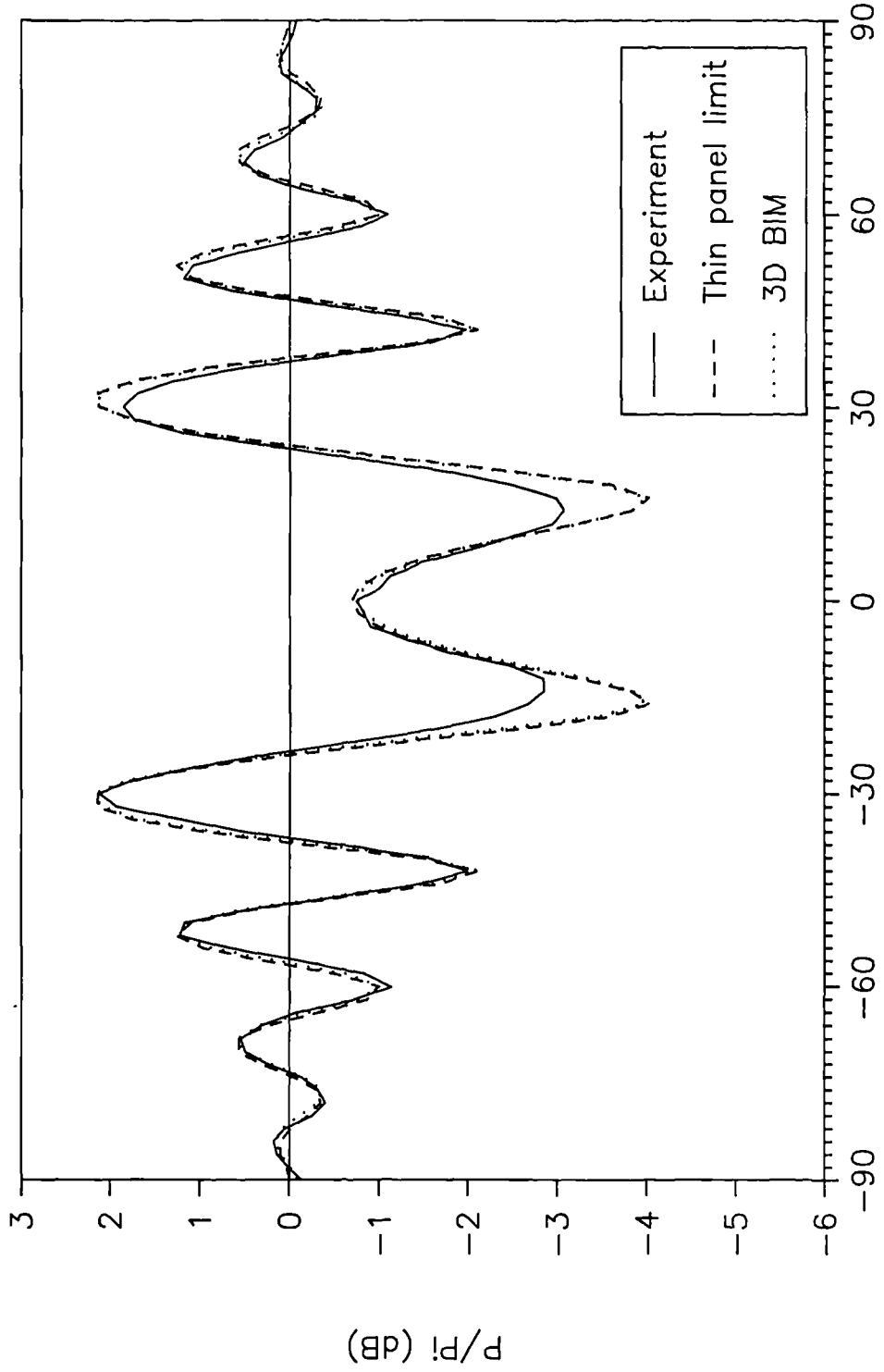

Figure 4.3. Comparison of thin panel limit solution with experiment and 3D boundary integral method solution. Total field 1006 Hz.

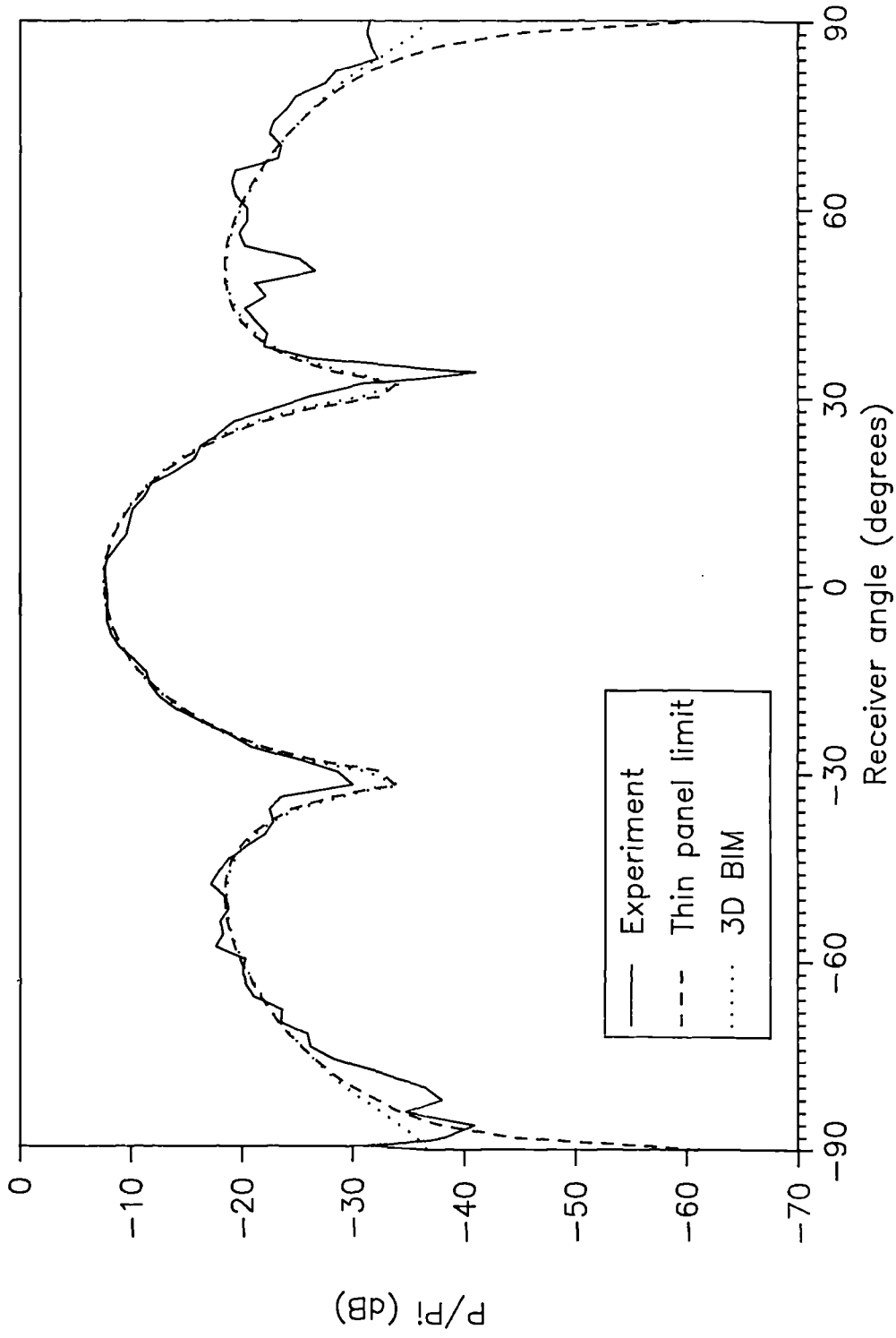

Figure 4.4. Comparison of thin panel limit solution, experiment and 3D boundary integral method solution. Scattered field at 2012 Hz.

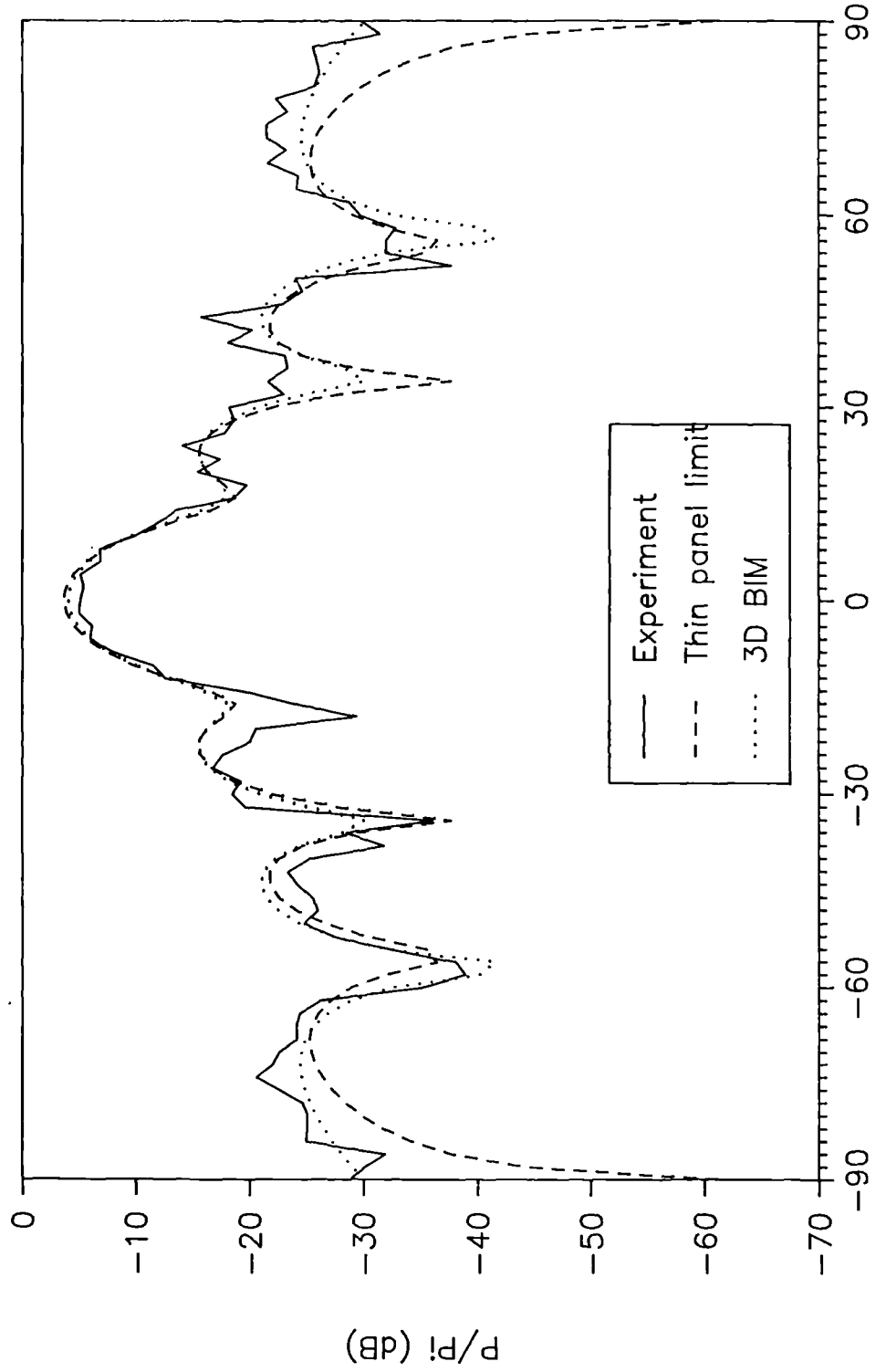

Figure 4.5. Comparison of thin panel limit solution, experiment and 3D boundary integral method prediction. Scattered field at 3995 Hz.

with a surface integration over the predicted surface pressures from the 3D boundary integral method, with the edge elements omitted. It is found that the two results are very similar. The remaining error produced, is mainly due to representing the finite distance between the pressure distribution on the front and the back of the panel as being infinitely small. This becomes more significant at higher frequencies.

4.4.3 Kirchhoff approximate solution

The solution of the Helmholtz-Kirchhoff integral equation using Kirchhoff's approximation for the surface pressures gives surprisingly accurate results near the specular reflection angle. Examples are shown in Figures 4.6 and 4.7 for the total and scattered field at 4 KHz and 3.5 KHz.

The Kirchhoff approximation assumes the surface pressure to be two times the incident pressure on the front of the panel, and the pressures on the back and the edges to be zero. An example of the pressures on the surface of the plane panel is shown in Figure 4.8. The pressures are shown across the width of the panel at 3995 Hz. The figure compares the Kirchhoff approximate pressures to the accurate 3D boundary integral method predictions. It can be seen that the pressure across the panel front is roughly twice the incident pressure and the pressure on the back is relatively small. This explains the success of the Kirchhoff theory.

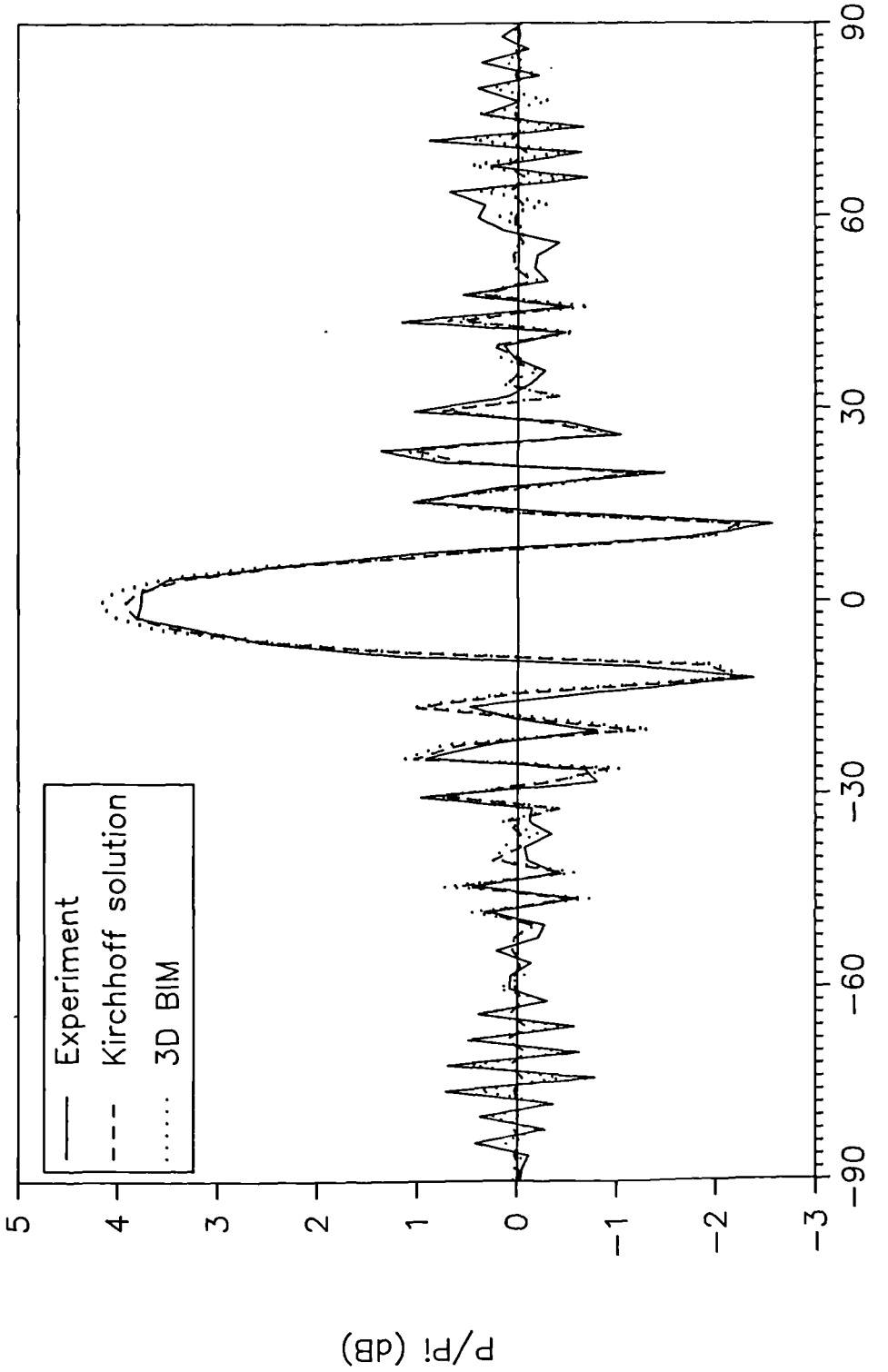

Figure 4.6. Comparison of Kirchhoff solution, experiment and 3D boundary integral method prediction. Total field at 3995 Hz.

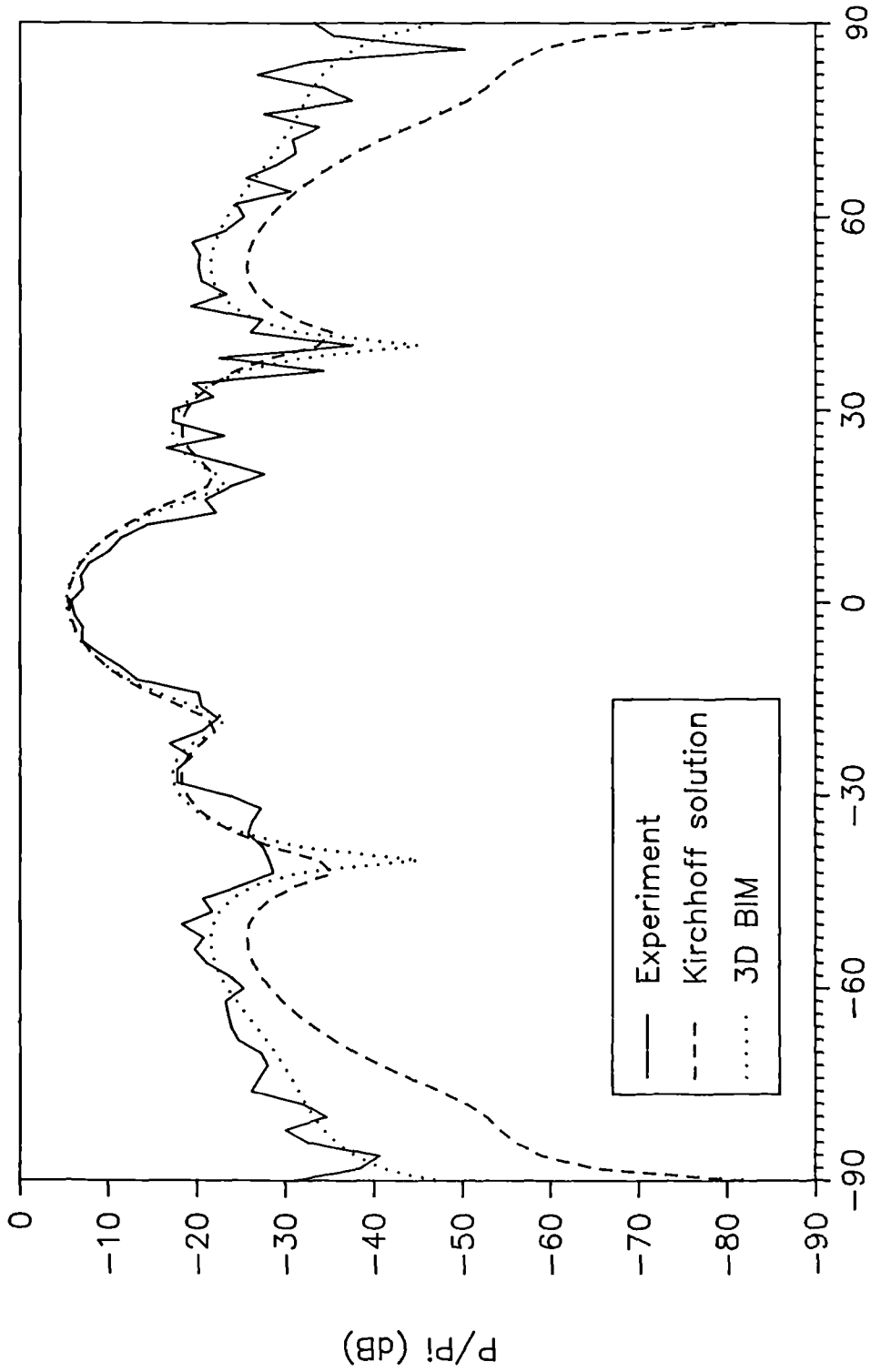

Figure 4.7. Comparison of Kirchhoff solution, experiment and 3D boundary integral method solution. Scattered field at 3492 Hz.

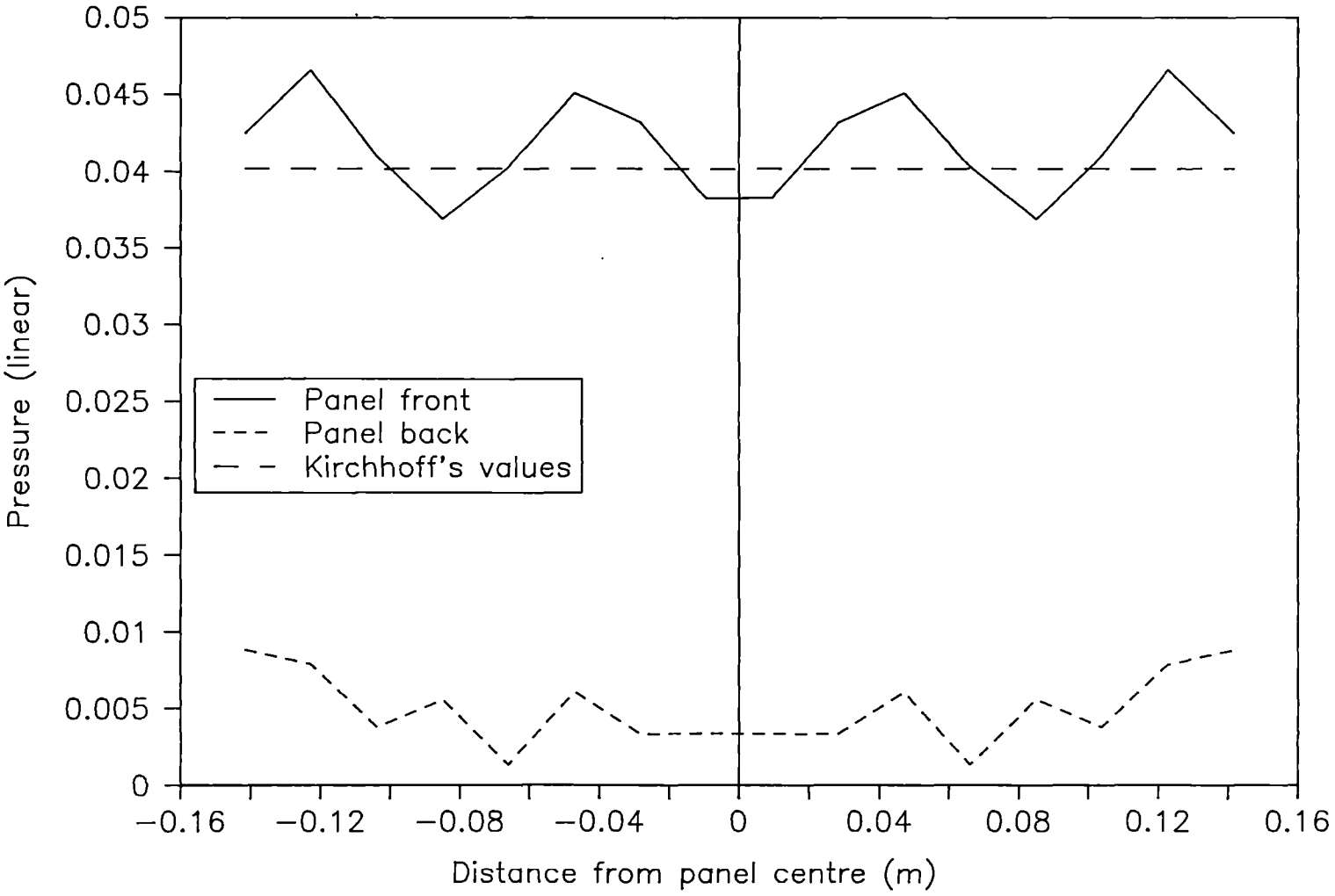

Figure 4.8. Predicted surface pressures across width of plane panel. Comparison of 3D boundary integral method values with Kirchhoff's approximate values for pressure on front.

As stated above, the Kirchhoff approximate solutions become inaccurate for large scattering angles. There are two sources of error:

(i) As with the thin panel limit solution, there is an inaccuracy associated with not representing the finite sized edges of the panel. This is more important at high frequencies where the edge is of significant size when compared to the wavelength of the sound.

(ii) Approximating the surface pressure distribution to be uniform and the pressure on the front face to be two times the incident pressure. The 'average' pressure on the front of the panel is roughly two times the incident sound as illustrated in Figure 4.8. Consequently, it is assuming the uniform pressure distribution which is the more significant error.

For near on-axis pressures, the deviation between the Kirchhoff approximate solution and the 3D boundary integral method solution decreases as the frequency of the prediction increases. This is to be expected as the accuracy of the Kirchhoff approximation improves for small wavelengths where mutual interactions on the surface are less significant.

4.4.4 Fresnel solution

The Fresnel solution method also gives surprisingly good predictions considering the extent of the approximations. Examples of the total and scattered

field are shown in Figures 4.9 and 4.10 at 2.5 KHz and 2 KHz respectively. The results are very similar to that given by the Kirchhoff approximate solution. The general pattern of minima and maxima are the same as for the Kirchhoff approximate solution, only the relative magnitudes of each peak varies, and then only by a small amount. The Fresnel solution method works best for a near normal receiver, becoming less accurate as the scattering angles increases. The accuracy of the on-axis predictions increases with frequency. The failure of the Fresnel solution is mainly due to the inaccuracies of the Kirchhoff approximate pressures. Details of this have been given in Section 4.4.3.

4.4.5 The Fraunhofer solution

The Fraunhofer solution is an approximate solution for receivers in the far field. The long length of the plane panel measured, 1.92m, meant that for all frequencies tested the receiver was effectively in the near field. This meant that the Fraunhofer predictions were inaccurate and unsatisfactory for this combination of panel size, receiver distance, and frequency range.

To further test the Fraunhofer solution the shorter panel detailed in Section 4.2.3 was used. In Figures 4.11 and 4.12, examples of the predicted scattered field are shown at 2 KHz and 8 KHz respectively. The predictions are compared to the accurate 3D boundary integral method solutions and the Kirchhoff approximate solutions.

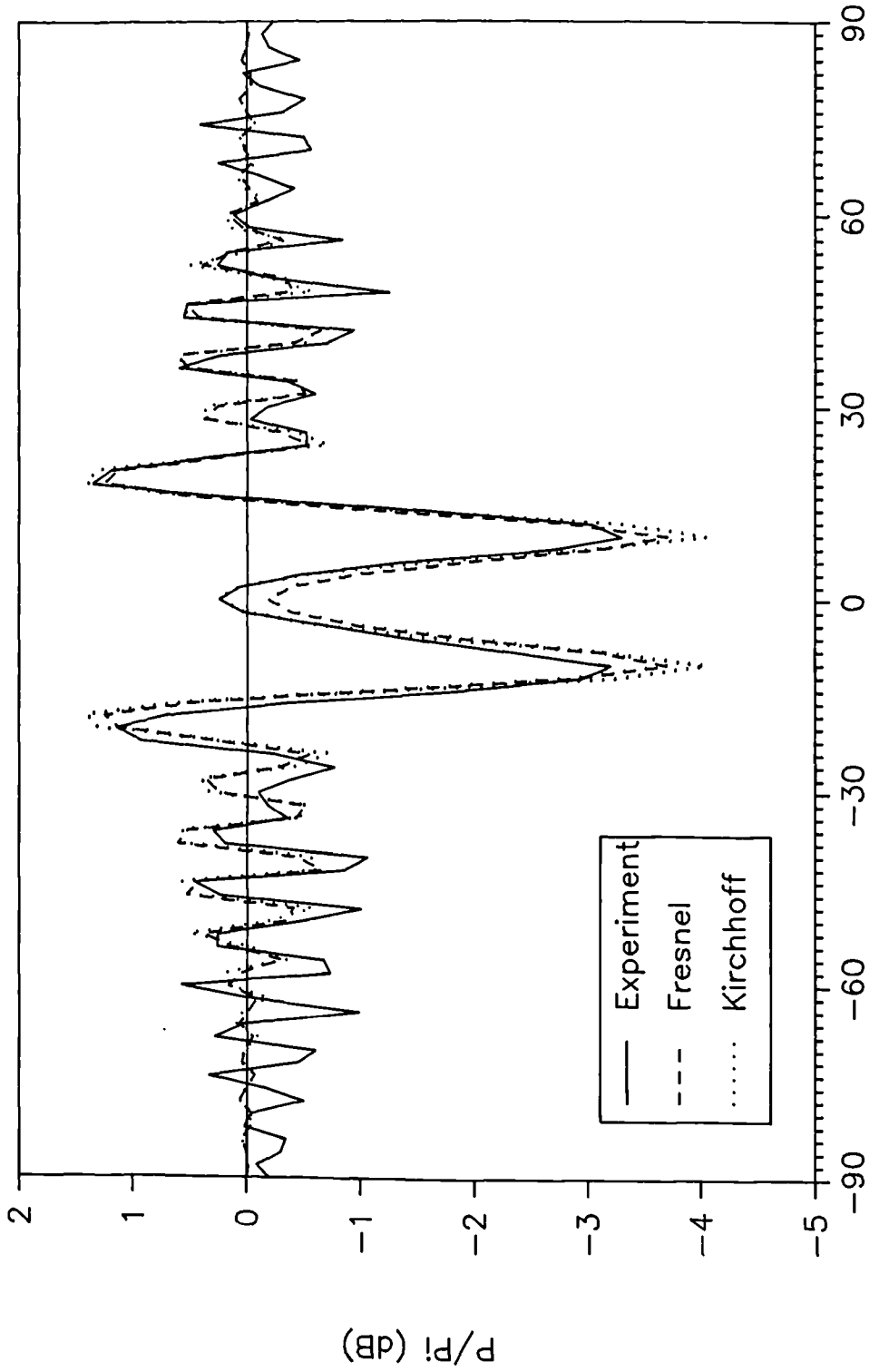

Figure 4.9. Comparison of Fresnel solution with experiment and Kirchhoff solution. Total field at 2486 Hz.

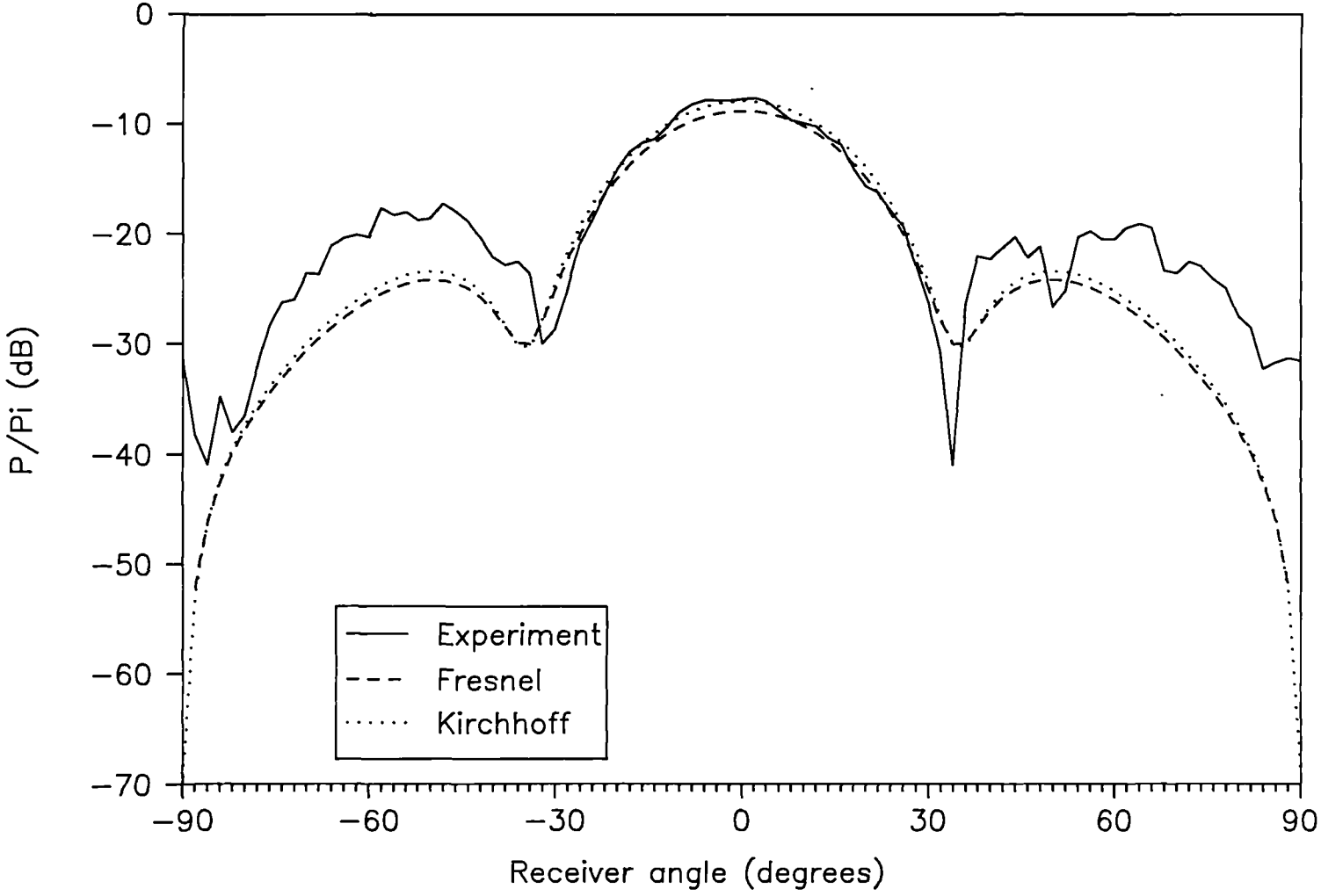

Figure 4.10. Comparison of Fresnel solution with experiment and Kirchhoff solution. Scattered field at 2012 Hz.

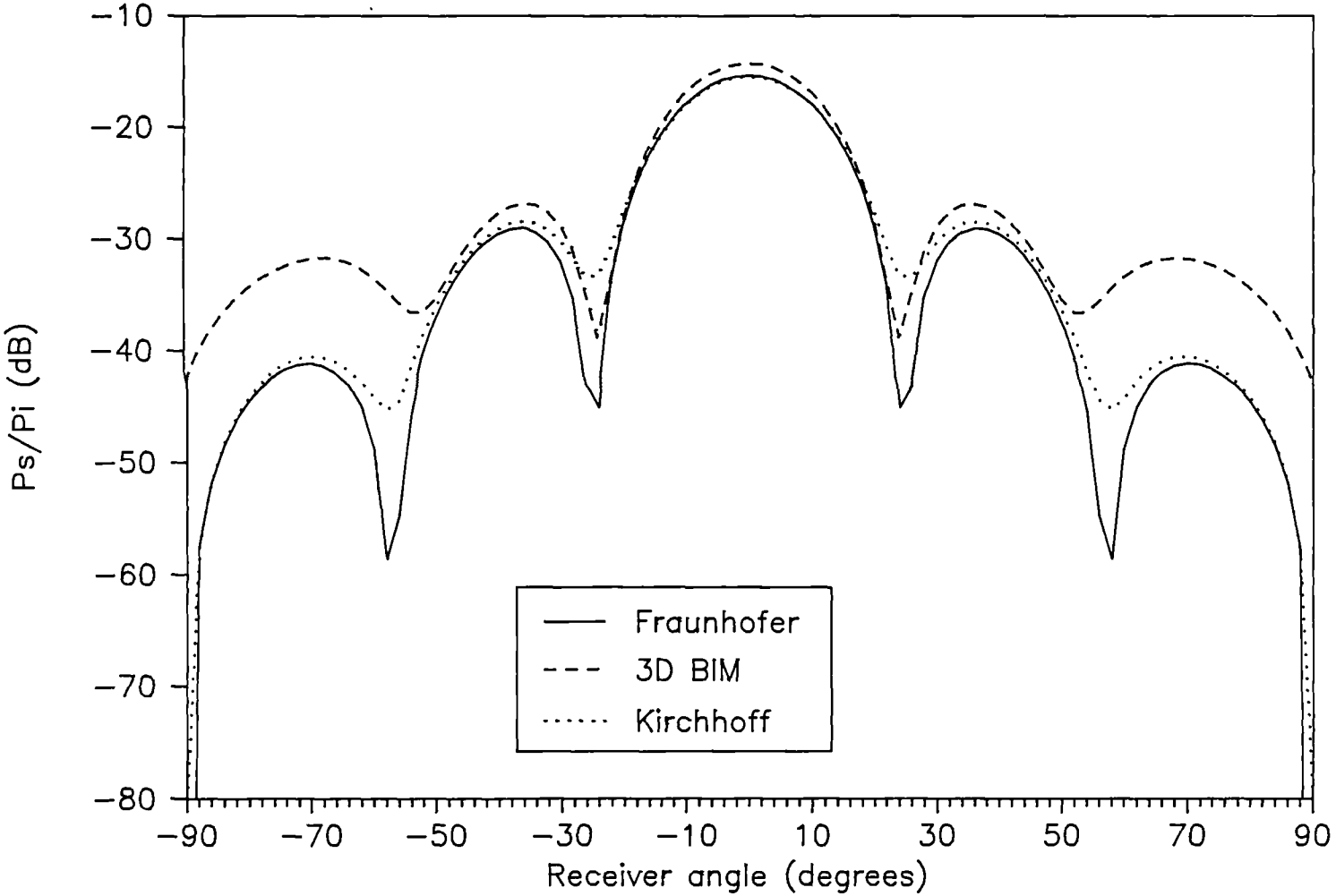

Figure 4.11. Comparison of Fraunhofer solution with 3D boundary integral method solution and Kirchhoff solution. Short simulated plane panel. Scattered field at 2KHz.

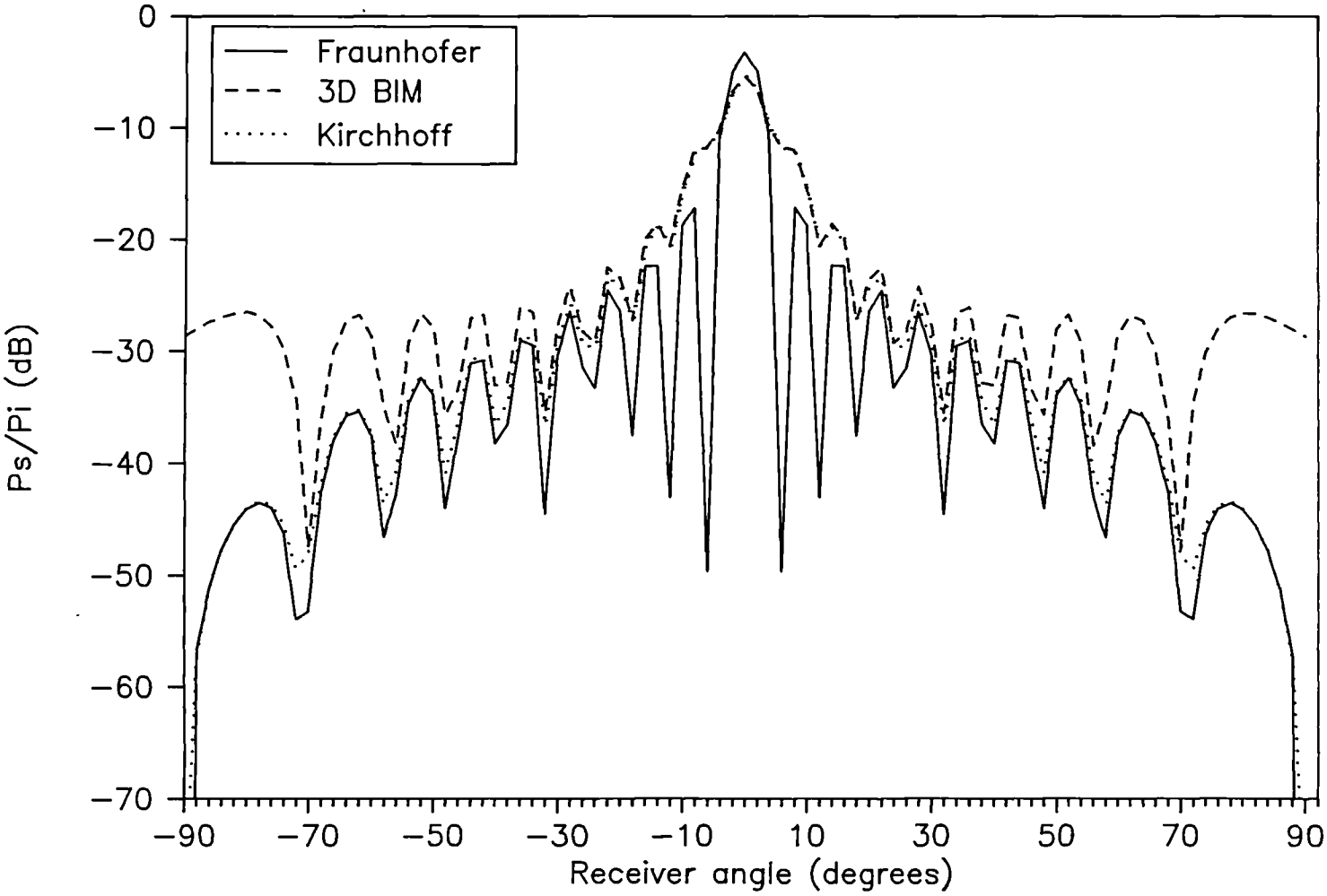

Figure 4.12 Comparison of Fraunhofer solution with 3D boundary integral method solution and Kirchhoff solution. Scattered field from short simulated plane panel at 7990 Hz.

The accuracy of the Fraunhofer solutions are limited by the accuracy of the Kirchhoff approximate surface pressures. At low frequencies the Fraunhofer predictions are nearly as accurate as the Kirchhoff approximate solutions, although at large scattering angles it tends to over estimate the depth of the minima. At higher frequencies, deviations between the Kirchhoff approximate solutions and the Fraunhofer solutions can be seen for all scattering angles.

There are two sources of error in the Fraunhofer solutions. A large amount of the errors is due to the inaccuracies of the Kirchhoff's approximate surface pressures - details of this have been given in Section 4.4.3. The remaining errors are due to the Fraunhofer solution method, in particular the fact that the receiver is not in the far field.

The far field is defined as the region where the difference in the maximum and minimum path length from the panel to the receiver, is small compared to wavelength. In this region, all points on the panel are effectively at the same distance from the receiver [Kinsler 1982 pages 187-188]. An illustration of this is shown in Figure 4.13. The path difference from the nearest and furthest part of the panels is smaller for an on-axis receiver than for an off-axis receiver. Therefore for a particular receiver radius, the on-axis receiver is in the far field for a larger range of frequencies. Hence why the deviation between the Fraunhofer solution and Kirchhoff solutions occur at lower frequencies for larger scattering angles. It can be confirmed that the far field approximation is the source of the error between the Fraunhofer and Kirchhoff solutions, by doing

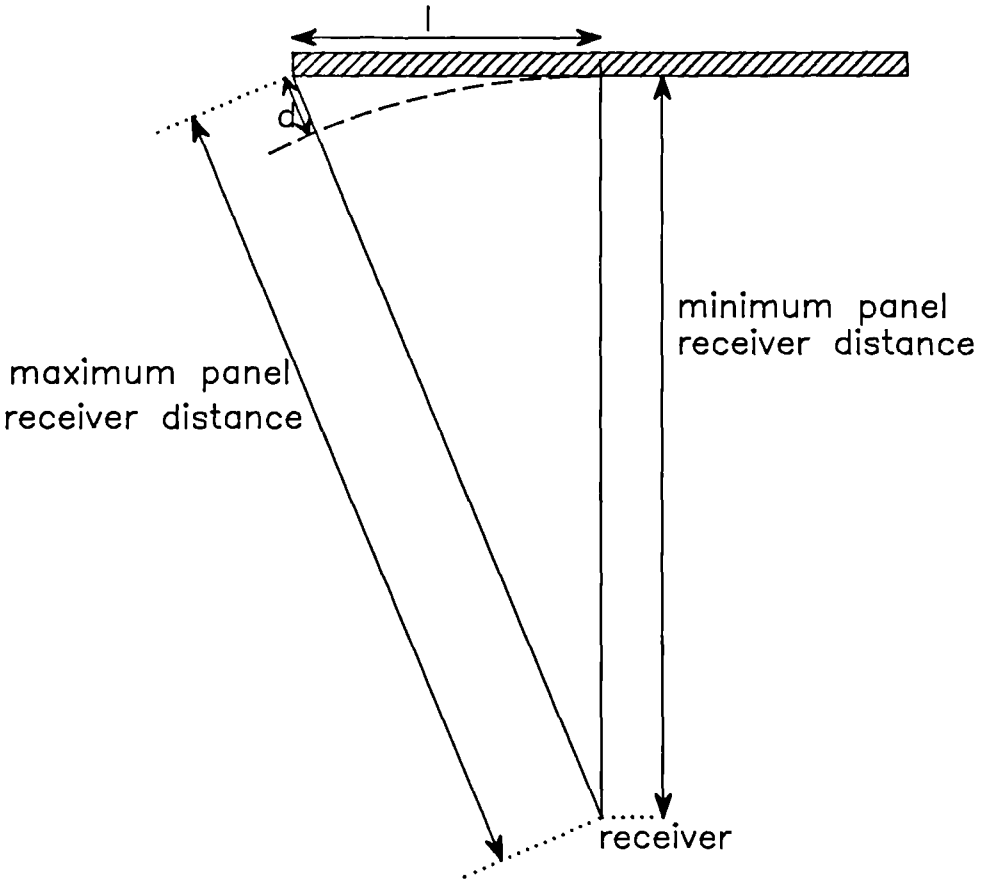

Figure 4.13. Explanation of far field location. The receiver is in the far field provided d is much smaller than the wavelength.

predictions for receiver positions a long way from the panel. There the Kirchhoff and Fraunhofer solutions converge for all angles and frequencies tested.

The extent of the near field is for receiver distances less than about l or kl^2 where l is half the largest panel dimension [Pierce 1981 page 225]. For the shorter simulated panel being tested here, the kl^2 constraint is the limiting factor. From our results, it is found that the deviation between the Kirchhoff theory and Fraunhofer theory is significant for near on-axis receivers only at frequencies above 6 KHz. This corresponds to $.4kl^2$ for the on-axis receiver distance - i.e. the geometric scattering angle. Although deviations are seen at lower frequencies and larger scattering angles, these are not particularly large. Also, for a plane panel, the scattered energy is concentrated around the geometric scattering angle, and so this is the region of most interest. Therefore, the useful limits of the Fraunhofer theory was found to be for receiver distances greater than $.4kl^2$.

4.5 The Cut-off Frequency for Plane Reflectors

There has been discussions in the acoustic literature about the cut-off frequency of plane reflectors [Cremer 1989 1990, Rindel 1985 1986]. The assumption is that there is a limiting frequency above which diffraction does not greatly affect the scattered field. This gives acousticians a rough guide to the frequency below which the panel most effectively scatters sound in all directions, and above which the panel produces specular type reflections.

An example is given in Figure 4.14 for the on-axis scattered pressure field verses frequency for the measured plane panel for normal incidence. It can be seen that there is a transition frequency above which the on-axis pressure does remain roughly constant. Superimposed is the approximate solution following the method of Rindel [1986]. Rindel's method uses the Fresnel solution method, with the Fresnel integrals approximated by simple mathematical functions. Using this solution method, Rindel found a transition frequency above which the Fresnel integrals remain roughly constant, this point is defined as the cut-off frequency. For a plane panel it is given as:

$$f \approx \frac{cd^*}{2(2aCOS(\beta))^2} \qquad 4.1$$

$$d^* = \frac{2d_1d_2}{(d_1+d_2)} \qquad 4.2$$

where d_1 and d_2 are the source and receiver distances from the point of reflection; a half the width of the panel; and ß the angle of incidence and reflection. Figure 4.15 shows definitions of the distances.

As Figure 4.14 illustrated, the simple theory of Rindel describes the overall scattered pressure distribution quite well. It does not, however, model the local minima and maxima. It can be seen that the cut-off frequency suggested by Rindel (3.5 KHz) coincides roughly with the -2.5 dB point for the panel acting as a high pass filter.

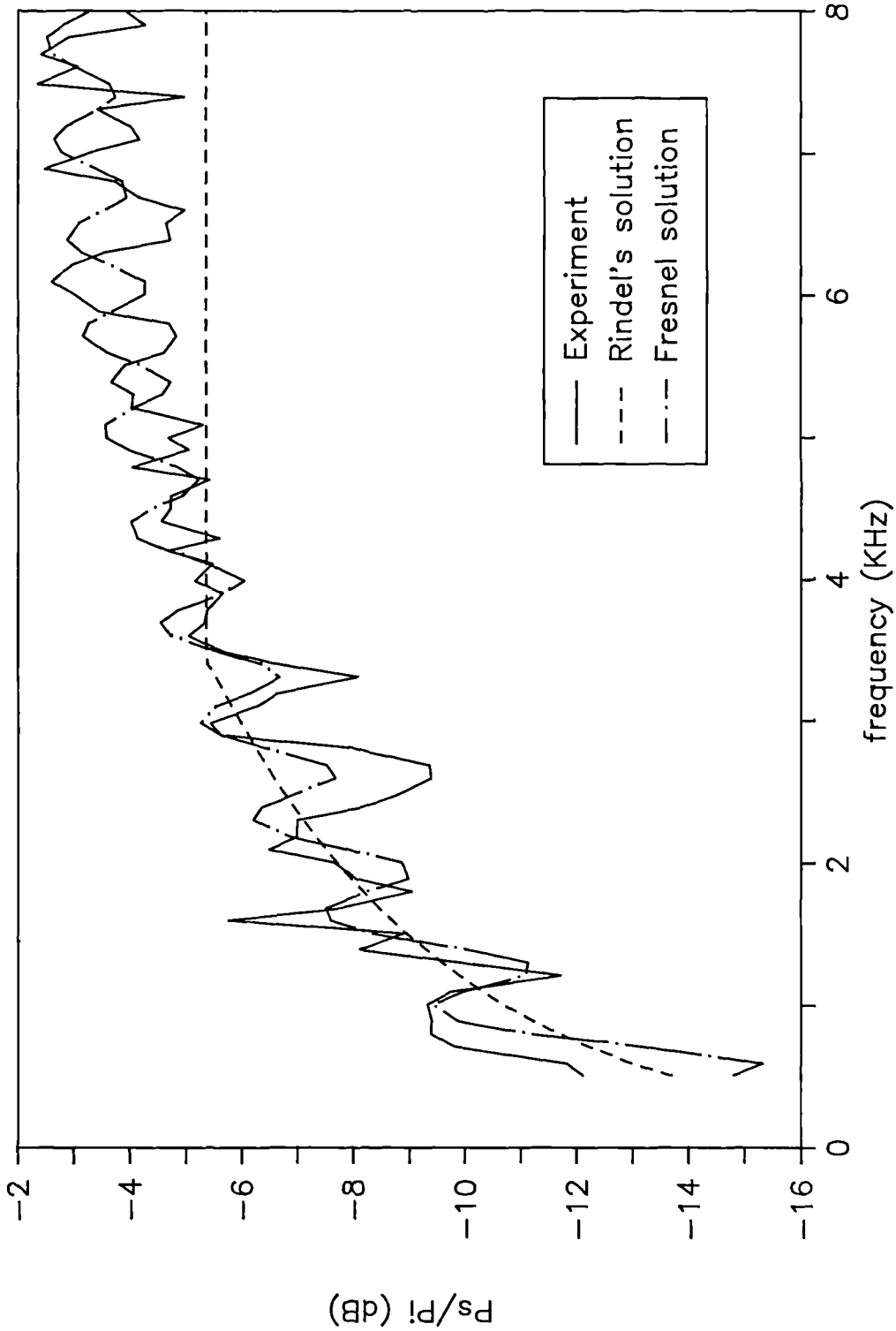

Figure 4.14 Scattered field from measured plane panel for on-axis receiver

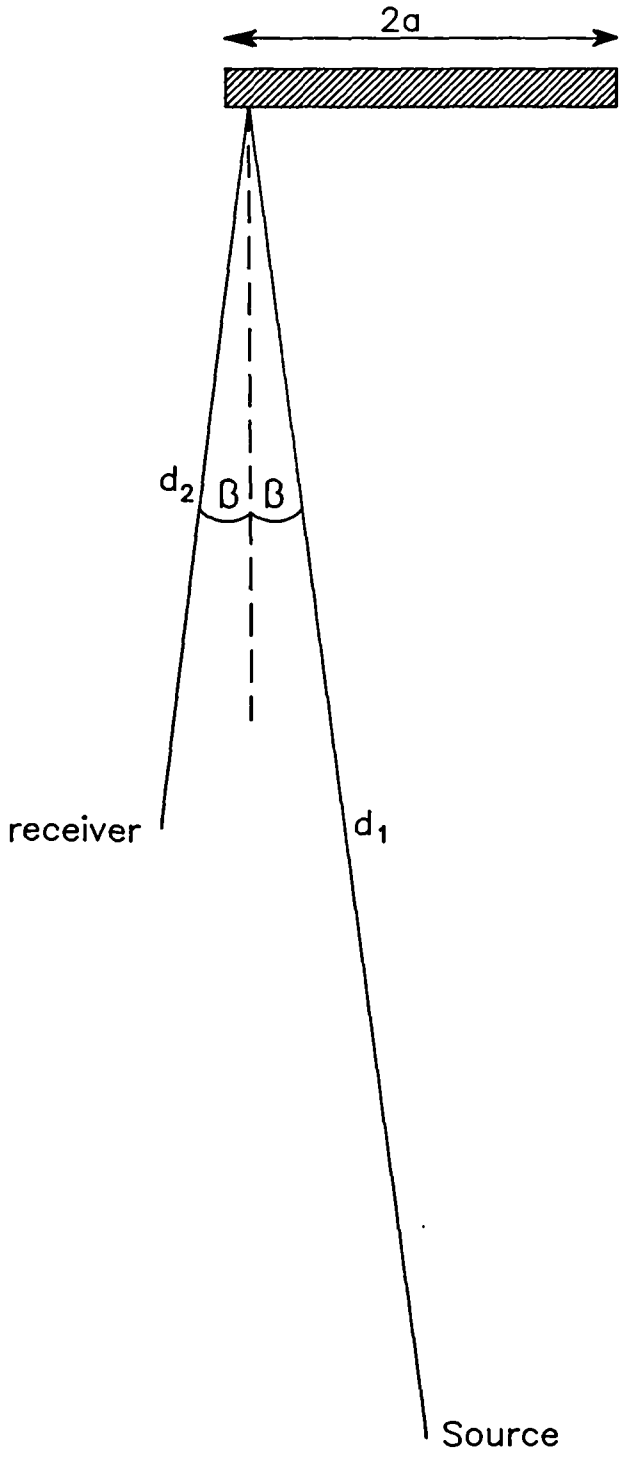

Figure 4.15. Definitions of distances and angles used in formulation of the cut–off frequency.

The use of a cut-off frequency becomes less valid as the receiver moves away from the geometric scattering angle. In Figure 4.16 theoretical predictions for the shorter simulated panel, at various angles of reflection for normal incidence sound, are given. It can be seen that representing the scattered pressure by a simple high pass filter does not work away from geometric scattering angle, where there is a complicated pattern of minima and maxima. When the point of reflection lies on the panel's surface, it is reasonable to assume that at high frequencies the scattered pressure is going to be roughly constant, as it will be dominated by specular type reflection. This is illustrated in Figure 4.17. When the point of reflection does not lie on the panel, however, the scattered pressure is entirely due to diffraction. As the frequency increases, the scattering will generally decrease. Consequently, a high-pass filter representation does not work there. A rough guide to the region over which the cut-off frequency representation works for the shorter simulated panel is therefore $\pm 8°$, the region over which the point of reflection lies on the panel. For a plane panel the case of scattering close to the geometric scattering angle is of most interest in auditoria, as this will have a large amount of the scattered energy. However, with significant energy scattered into other angles, the use of a cut-off frequency should be used with caution.

It was found that Rindel's formulation for Fresnel diffraction works well for reflection near to the geometric scattering angle, but breaks down as the receiver moves off axis.

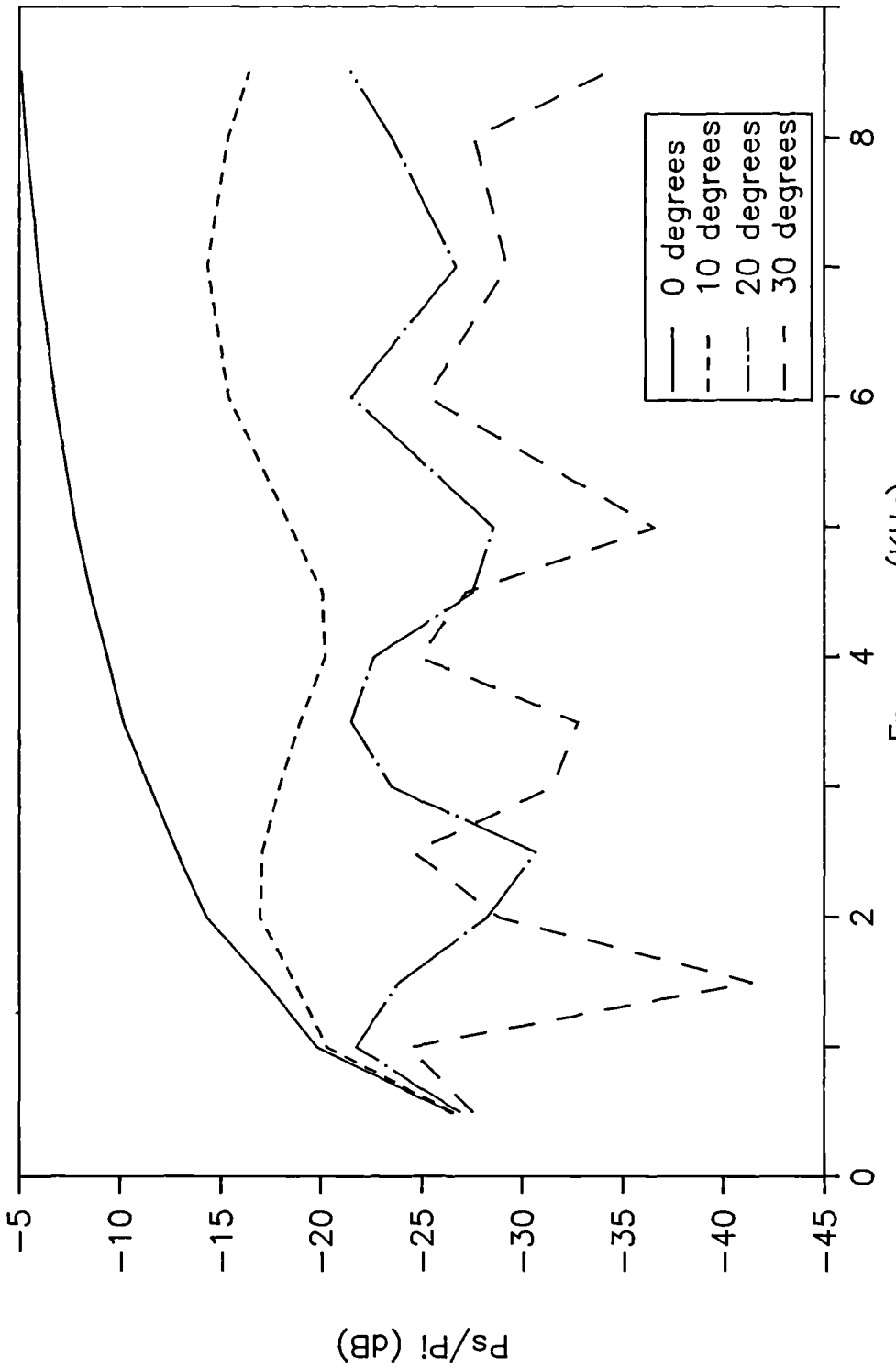

Figure 4.16. Scattering from short simulated plane panel at various scattering angles.

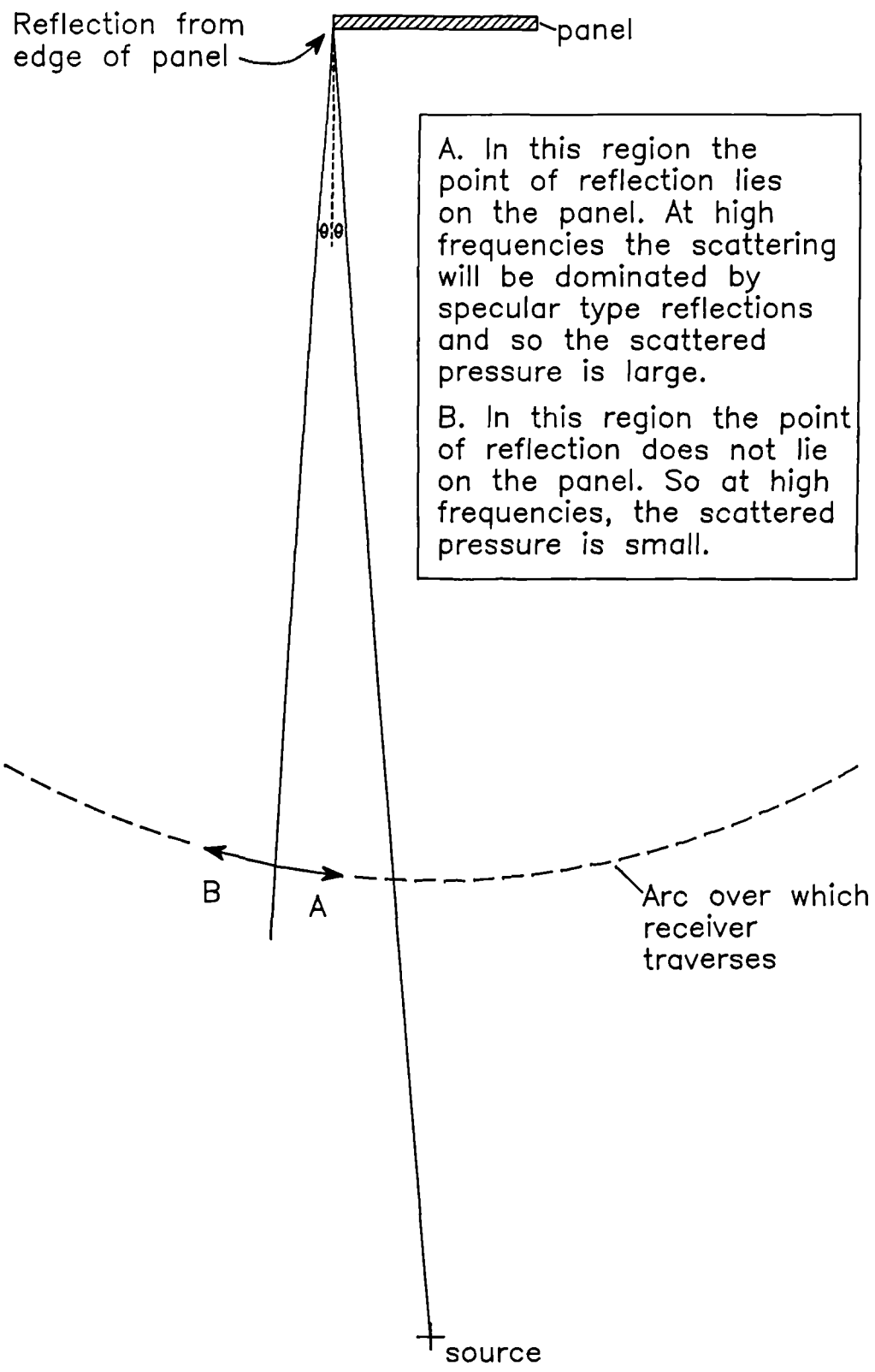

Figure 4.17. Explanation of reflection characteristics at high frequencies for plane panel for different receiver position regions.

4.6 Conclusions

The scattering produced by a thin rectangular rigid surface has been measured, and the results compared with various theoretical prediction methods. The methods can be ordered in terms of decreasing computation time and decreasing accuracy as:

1. 3D boundary integral method.
2. Thin panel limit solution method.
3. Kirchhoff approximate solution method.
4. Fresnel approximate solution method.
5. Fraunhofer approximate solution method.

The 3D boundary integral method is successful at all angles and all frequencies. The thin panel limit solution is also accurate except at large scattering angles above about 3 KHz. The Kirchhoff approximate theory and the Fresnel solution method are both accurate for small scattering angles and high frequency. The Fraunhofer solution method only works when the receiver is in the far field, and then solutions are only as good as the Kirchhoff approximate solution. Our results gave the far field as being for receiver distances greater than $.4kl^2$, where l is half the largest panel dimension.

The use of a cut-off frequency to describe the limits of diffraction in auditorium design is useful for scattering close to the geometric scattering angle.

The value of the cut-off frequency given by Rindel [1986] is approximately the -2.5 dB point of the panel, if the panel is modelled as behaving like a high pass filter. The further away from the geometric scattering angle the receiver moves, the less accurate the cut-off frequency representation becomes.

Chapter 5

Theoretical Predictions and Measurements of the Scattering from Curved Panels

5.1 Introduction

Curved reflecting panels are often used in auditoria. They provide far better diffusion than plane panels, avoiding the problem of strong specular reflections, while not being especially expensive to construct.

In this chapter various methods for predicting the sound scattering from curved surfaces will be examined. As with the plane panel, these encompass a range of approximations, accuracies and computation time. The use of a cut-off frequency to define the frequency above which diffraction effects become small will also be discussed. This chapter is only concerned with the success of the various prediction methods, the performance of the curved panel in scattering sound will be discussed in Chapter 7.

5.2 The Panels Tested and Measurement Technique

5.2.1 The curved panel measured

The cylindrical diffuser used was a piece of lead clad plywood of dimensions 1.92 x .30 x .01 metres. The panel was bent, with the use of wooden formers on the rear of the panel, into a curve of radius .341m about an axis along the panel length. The lead was 1.5 mm thick and on the front face only. The lead ensured a highly reflecting surface. The panel was a 1:5 scale model of reflectors typically found in auditoria.

5.2.2 The measurement system used

The single microphone cross correlation method was used for the measurements. The sound pressure field was measured at a radius of 1.27 m. The source was at a normal distance of 4 m from the panel centre. The temperature at the time of measurement was 19.5°c.

5.2.3 Other curved panels tested

The tests between theory and experiment were carried out up to 3 KHz. It would have been possible to test at higher frequencies, as was done for the plane panel, but it is expensive on computer time. Having shown that the 3D boundary integral method gives good agreement with experiment, the rest of the

investigation was done by prediction only using shorter panels. Both panels were again 1:5 scale models of reflectors typically found in auditoria. The two panels were used:

1. A short cylindrical diffuser of width .412m, radius .78m, length .24m and thickness .01m. The source was at a normal distance of 5m from the panel centre. The pressure field was predicted at a radius of 2m from the panel centre. The speed of sound was taken to be 346 ms^{-1}

2. A panel of .30m square bent into a radius of 34.1 cm about the width and length. The source was at a normal distance of 4m from the panel centre. The pressure field was calculated at a radius of 2m from the panel centre. The speed of sound was taken to be 346 ms^{-1}

5.3 Theoretical Prediction Methods Used

The theoretical prediction methods used were outlined in Chapter 3. Most of these involved solving the Helmholtz-Kirchhoff integral equation. The methods used were:

1. 3D boundary integral method.
2. Thin panel limit solution method.
3. Kirchhoff approximate solution method.
4. Geometric scattering theory methods.

5.4 Results and Discussions

The predictions of the first three theories listed above in Section 5.3 show similar trends to those for the plane panel. The results and discussions are outlined in brief below, greater detail can be found in Chapter 4.

5.4.1 3D boundary integral method

The rigorous numerical solution of the Helmholtz-Kirchhoff integral equation gives accurate predictions at all frequencies and scattering angles tested. Examples are shown in Figures 5.1 and 5.2 at 1.4 KHz.

5.4.2 Thin panel limit solution

The thin panel limit solution gives similar results to the 3D boundary integral method and experiment. The thin panel model is less accurate for large scattering angles and high frequencies. As for the plane panel, it can be shown that this is due to not representing the finite sized edges of the panel. Examples are shown in Figures 5.3 and 5.4 at 3 KHz. As the frequencies increase, the predictions at large angles become less accurate. The remaining errors are largely due to taking the finite distance between the front and rear of the panel as infinitely small.

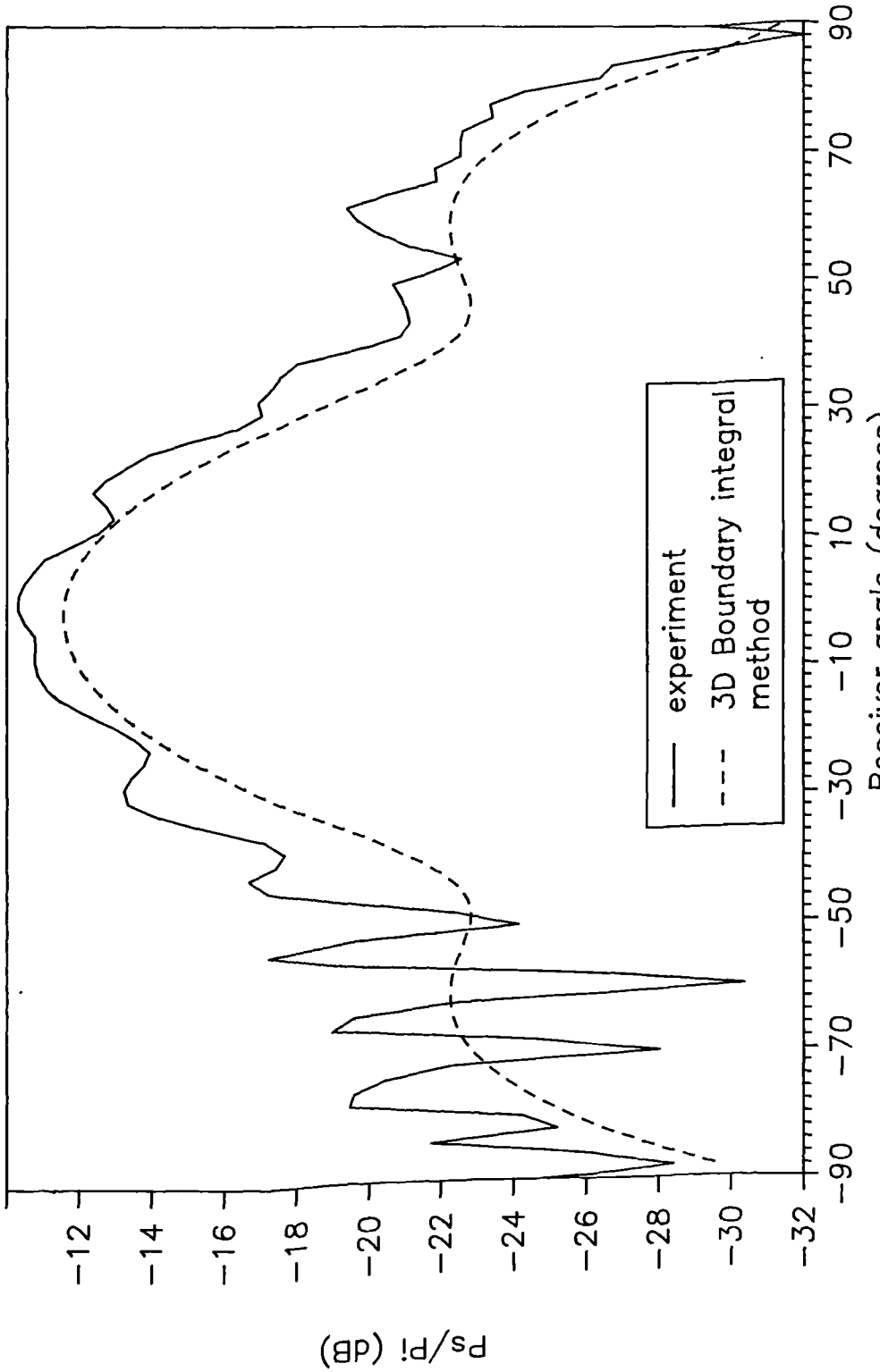

Figure 5.1. Comparison of 3D boundary integral method solution with experiment for curved panel. Scattered field at 1390 Hz.

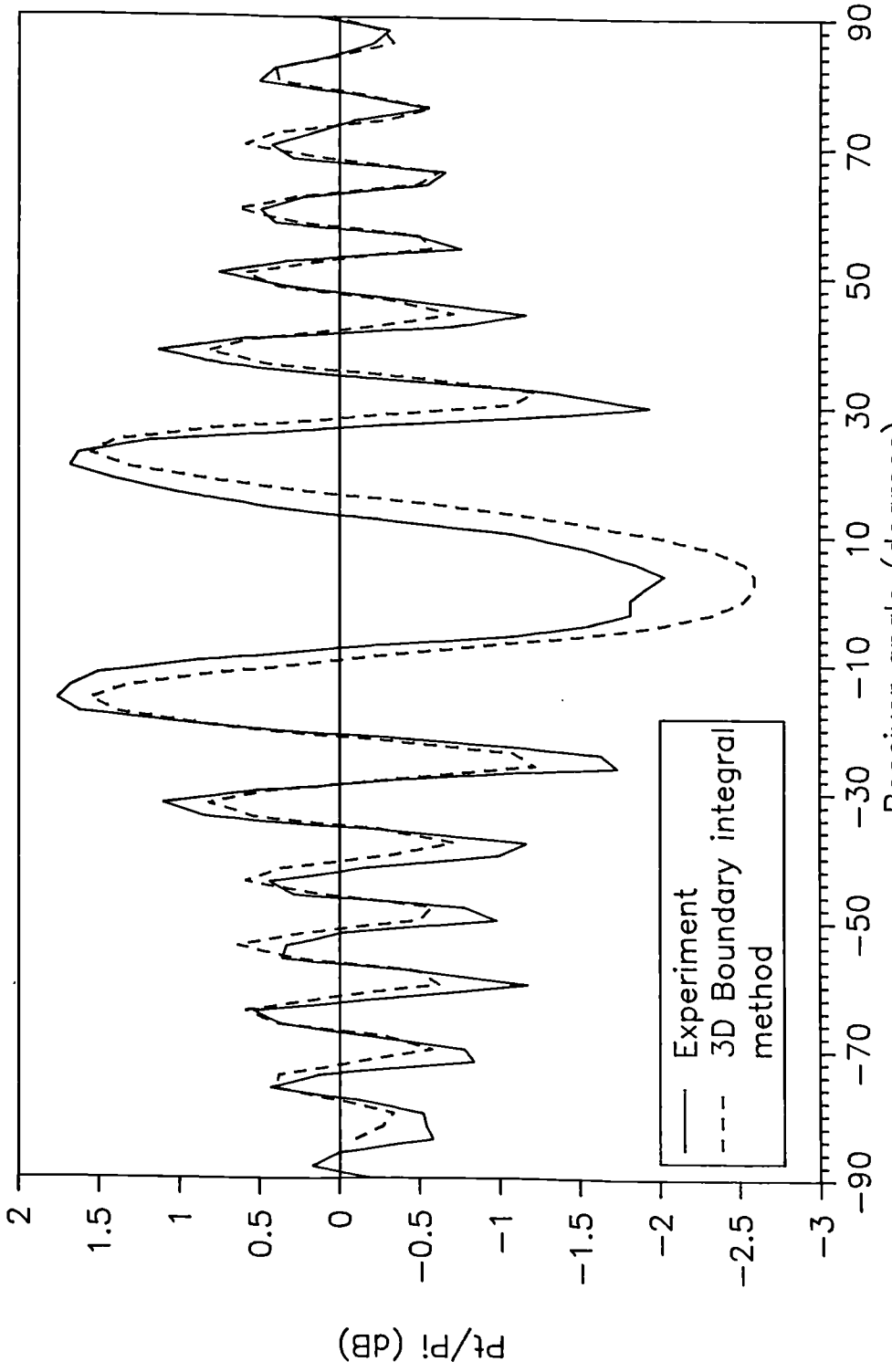

Figure 5.2. Comparison of 3D boundary integral method solution and experiment for curved panel. Total field at 1390 Hz.

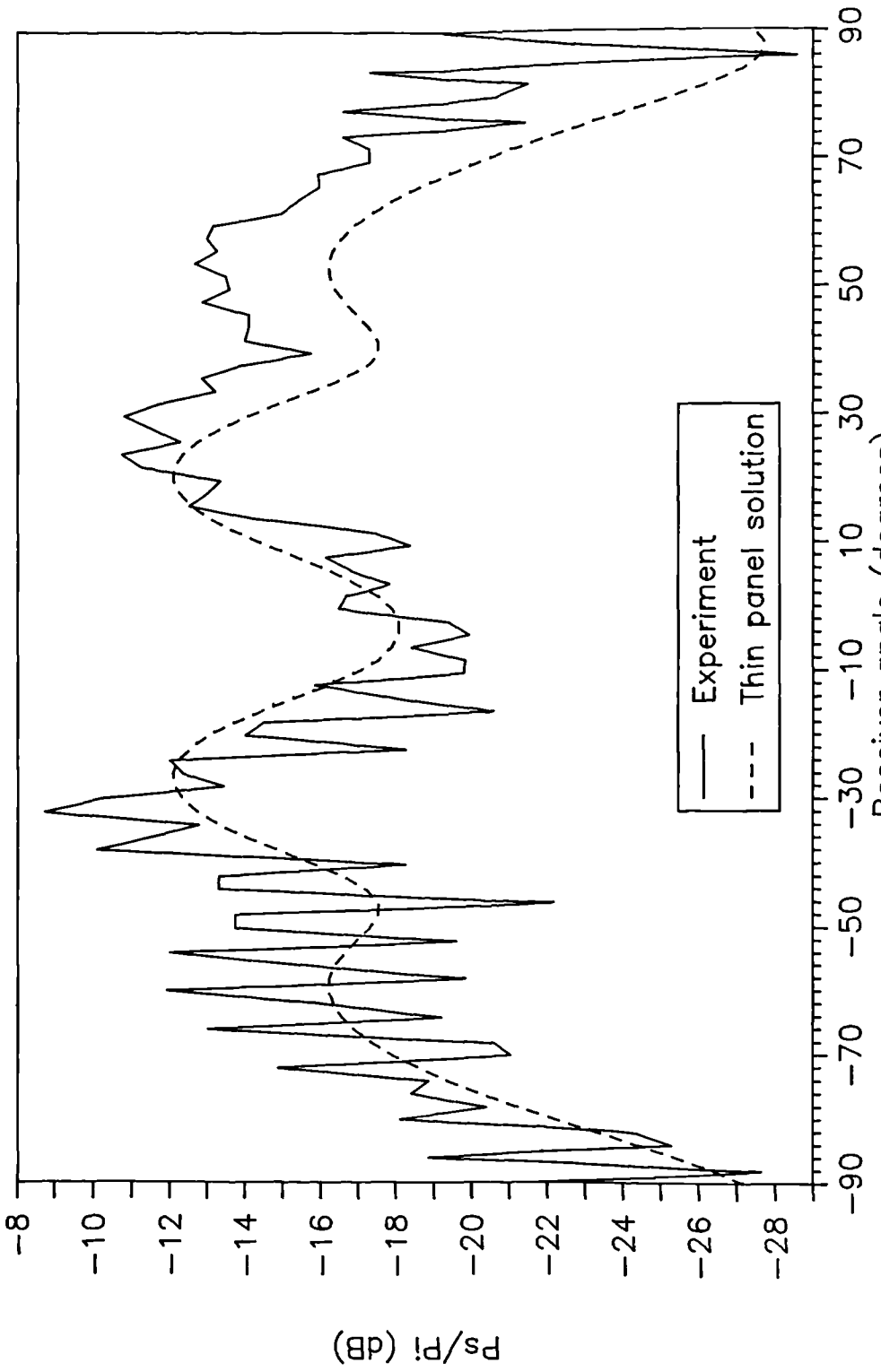

Figure 5.3. Comparison of thin panel limit solution and experiment for curved panel. Scattered field at 2998 KHz.

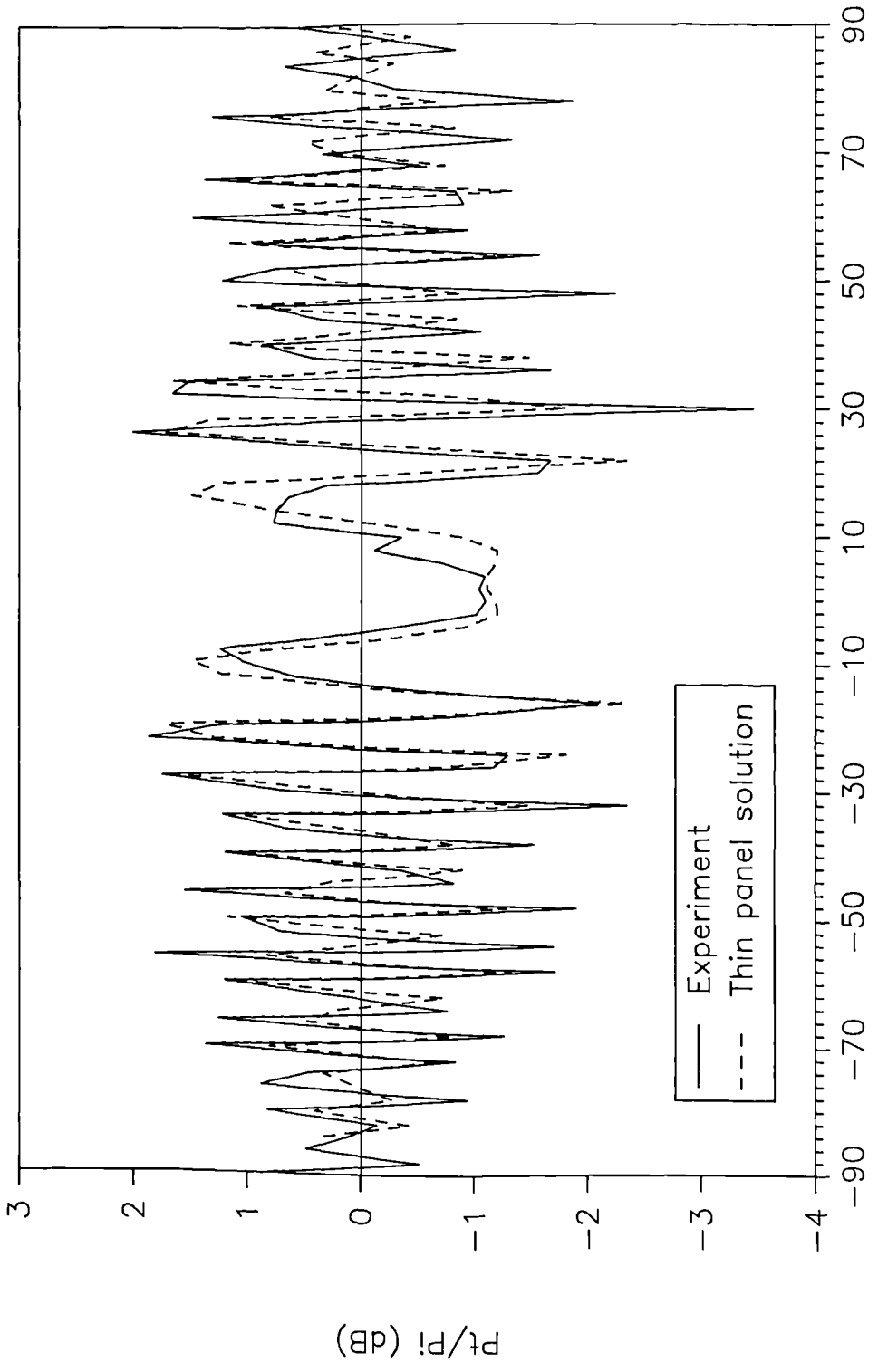

Figure 5.4. Comparison of thin panel limit solution and experiment for curved panel. Total field at 2989 Hz.

5.4.3 Kirchhoff approximate solution

The Kirchhoff approximate solution gives quite good agreement with experiment and the other more rigorous prediction methods. Typical examples are shown in Figures 5.5 and 5.6 at 2 KHz and 6 KHz respectively, these compare the Kirchhoff theory with the accurate 3D boundary integral method. In general the Kirchhoff approximate solution tends to smooth out the local minima and maxima in the scattered field, but the overall distribution is similar. As with the plane panel, the predictions are better for near on-axis receivers and at higher frequencies. The failure of the theory for off-axis receiver positions and at low frequencies is due to not representing the true pressure distribution on the surface, and the effects of not representing the edges and the back of the panel. The deviation between the Kirchhoff approximate solution and the accurate 3D boundary integral method solution is smaller for large scattering angles than for the plane panel. This is due to the curved panel producing more scattering to the sides, and so masking the effects of not representing the scattering from the back and sides.

5.4.4 Geometric scattering theories

The simple geometric scattering theories were tested against the accurate 3D boundary integral method solution using the shorter simulated panels. The geometric scattering theories split the diffraction into two processes: the diffraction from the finite sized panel, and the scattering due to the curvature.

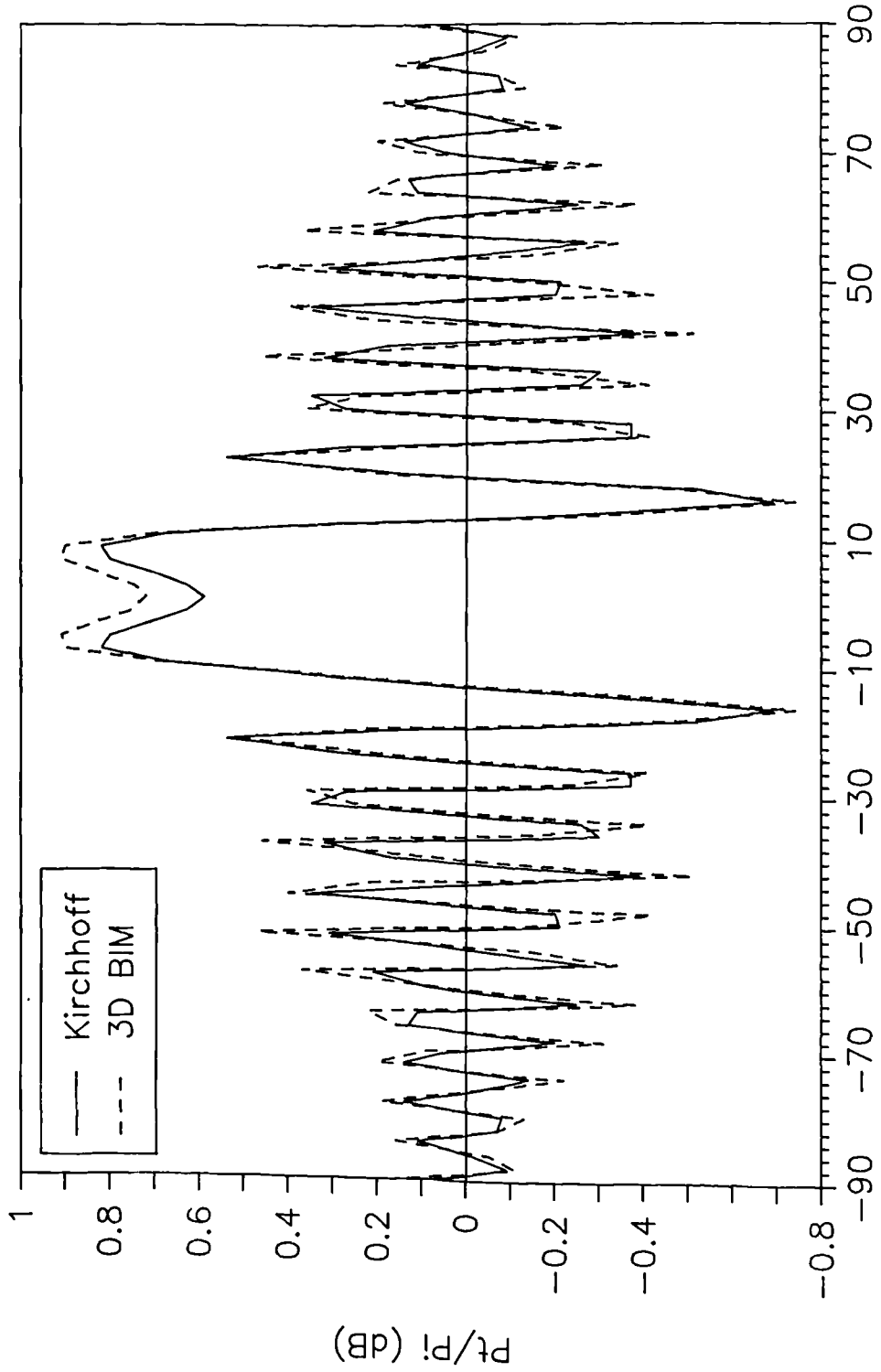

Figure 5.5 Comparison of Kirchhoff theory with accurate 3D boundary integral method for curved panel. Total field at 2012 Hz.

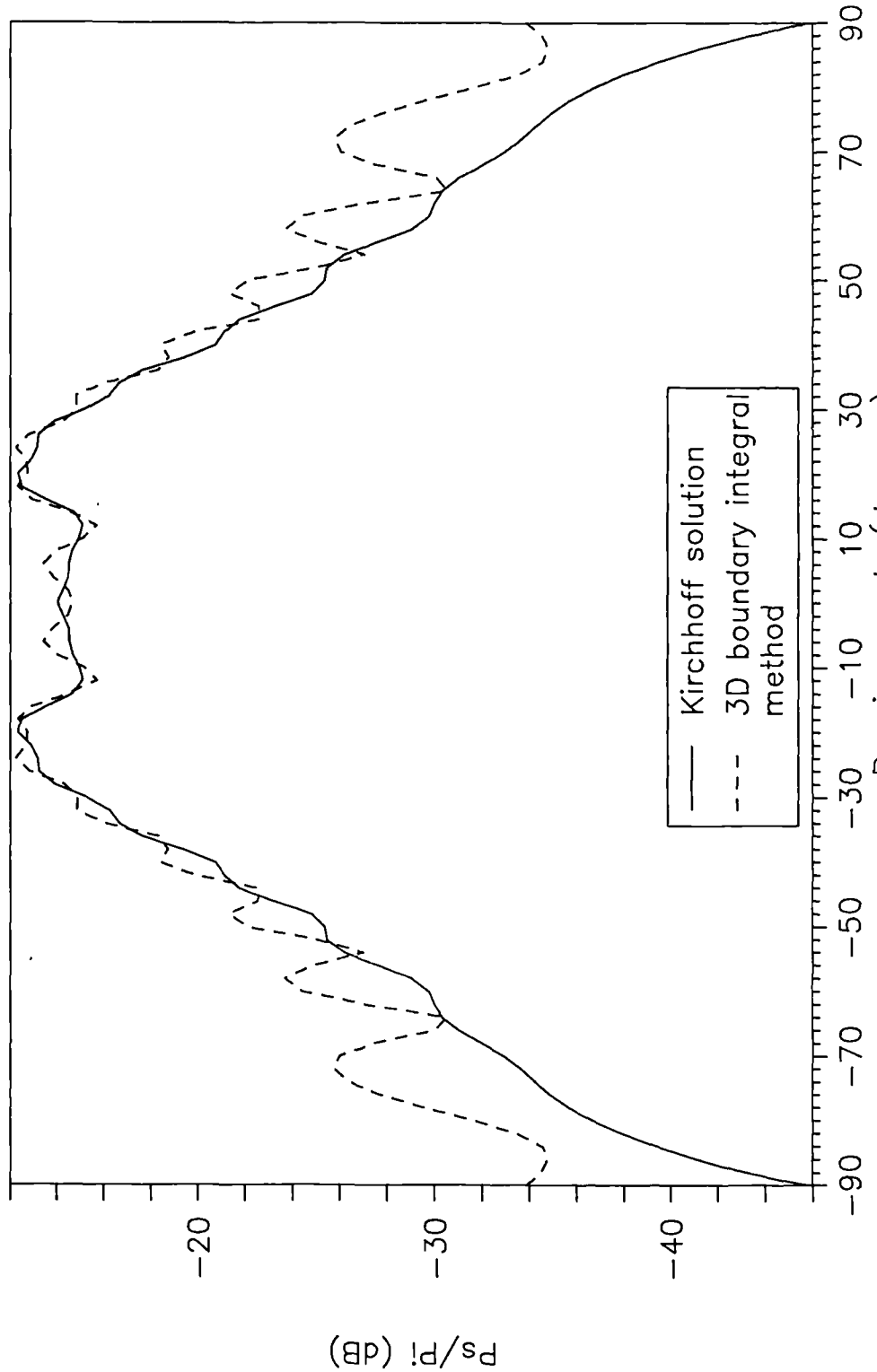

Figure 5.6. Comparison of Kirchhoff solution and accurate 3D boundary integral method solution for simulated curved panel. Scattered field at 6 KHz.

The first part is solved by Fresnel diffraction, the second by simple geometric considerations. Two forms of geometric scattering theory were used, one assumes incident plane waves [Rindel 1985], the other assumes incident spherical waves [Pierce 1981 page 413-417]. The theories has been described in Section 3.9.

In Figures 5.7 and 5.8 examples of the scattered pressure fields are shown. The first figure shows the scattered pressure as a function of frequency for the on-axis receiver case. The second gives the pressure field as a function of scattering angle at a fixed frequency of 6 KHz. At no frequency does either of the geometric theories predict the scattering for off-axis receivers particularly well. They do, however, have some success for receiver positions very close to on-axis. Although the plane wave and spherical wave predictions give slightly different results for the scattering, neither is particularly better or worse than the other.

The problem with the geometric scattering theories is that they assume some attenuation from the diffuser whatever the angle of reflection. This attenuation comes from the formulations of the effects of curvature - Equations 3.24 to 3.26. Consequently, even though the panel is non-absorbing, sound energy has been lost at all angles. The problem is illustrated in Figure 5.9. When the point of reflection lies on the surface of the panel, the reflection level from a plane surface will generally be large, and adopting some attenuation due to curvature seems reasonable. When the point of reflection lies beyond the edge of the panel, the reflection level from a plane panel will generally be small, and

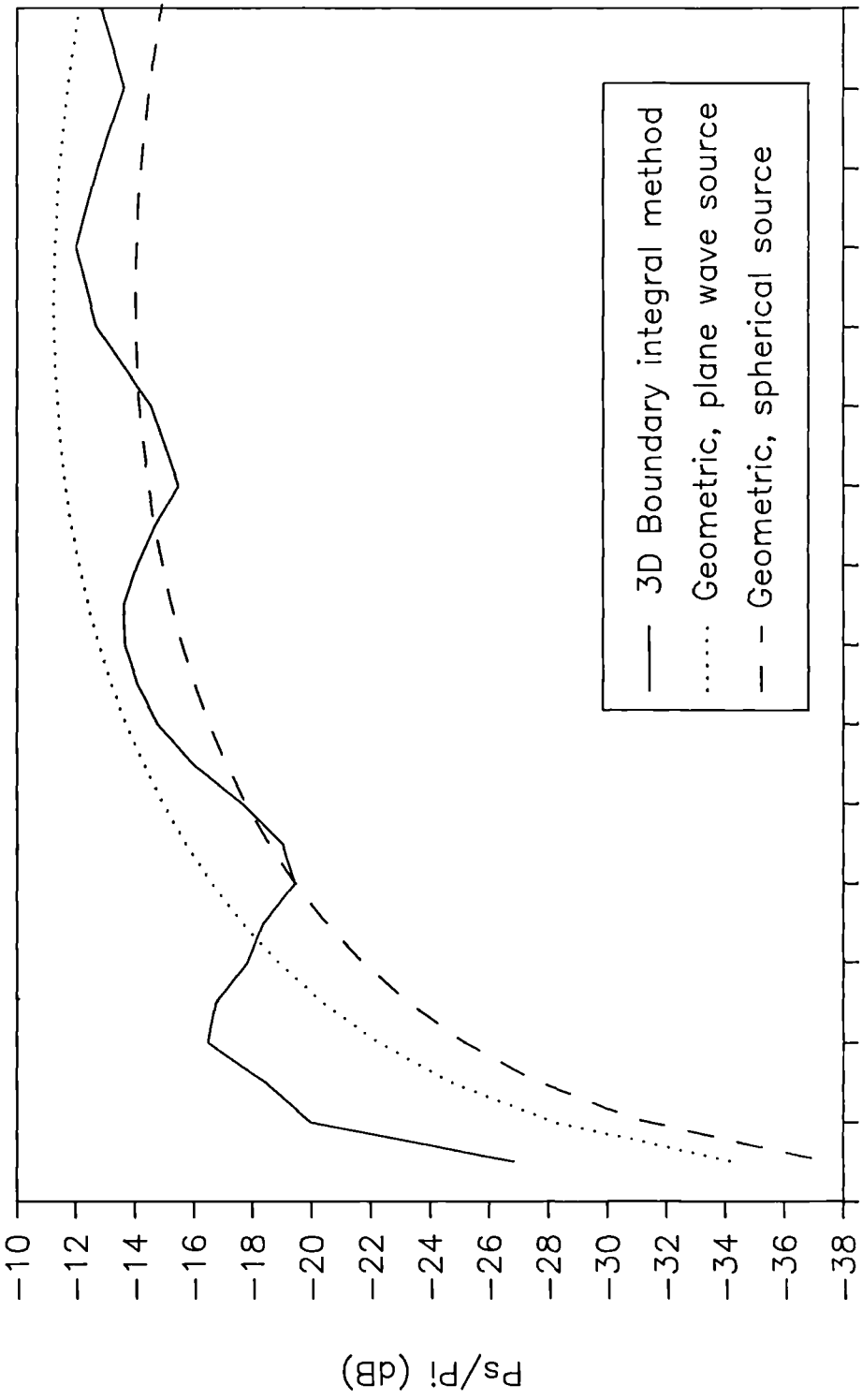

Figure 5.7. Comparison of geometric scattering theories with 3D boundary integral method predictions for a curved panel. Scattered field for on−axis receiver

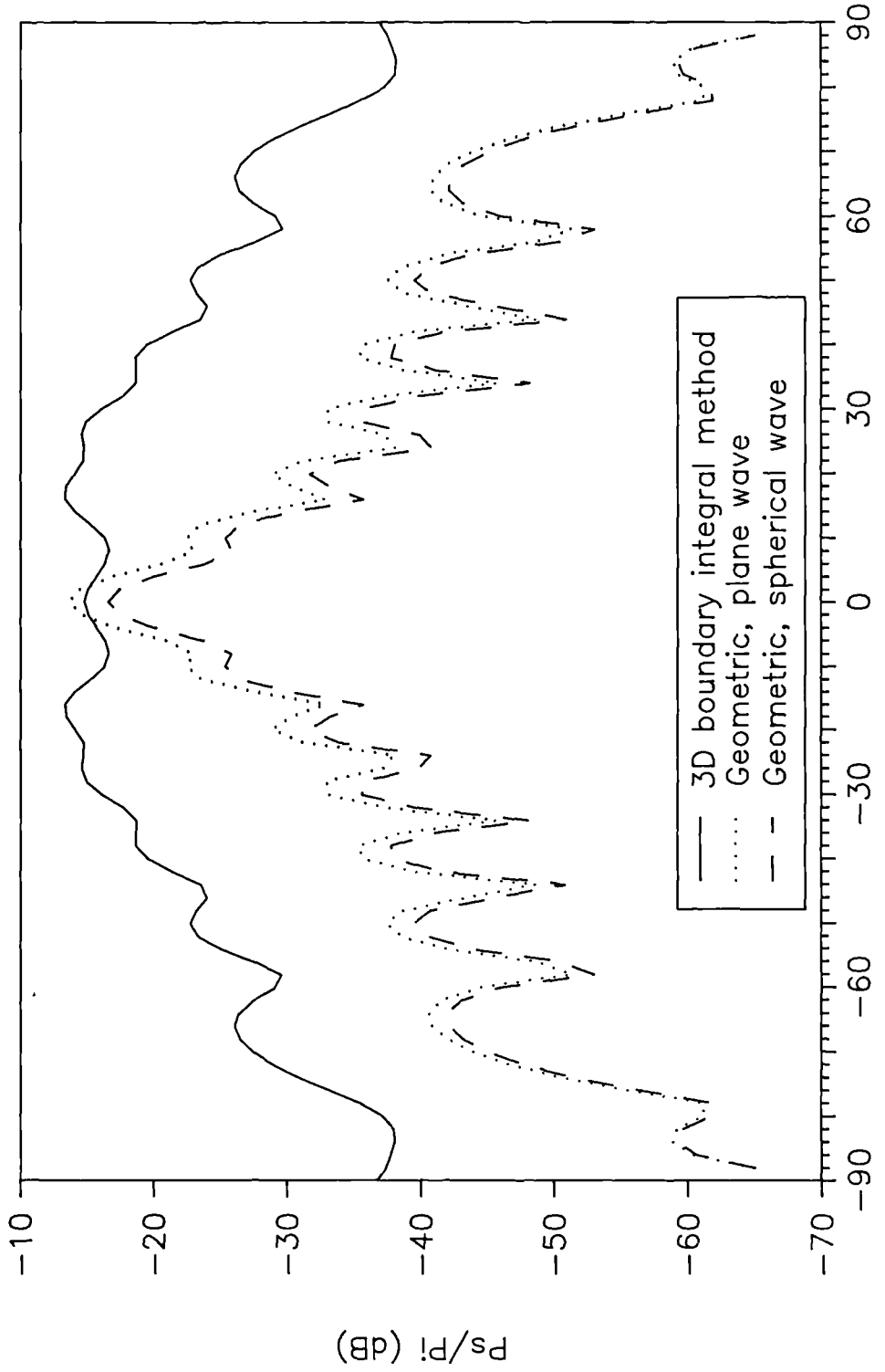

Figure 5.8. Comparison of scattering predicted by geometric scattering theories and 3D boundary integral method solution. Scattered field from curved panel at 6 KHz.

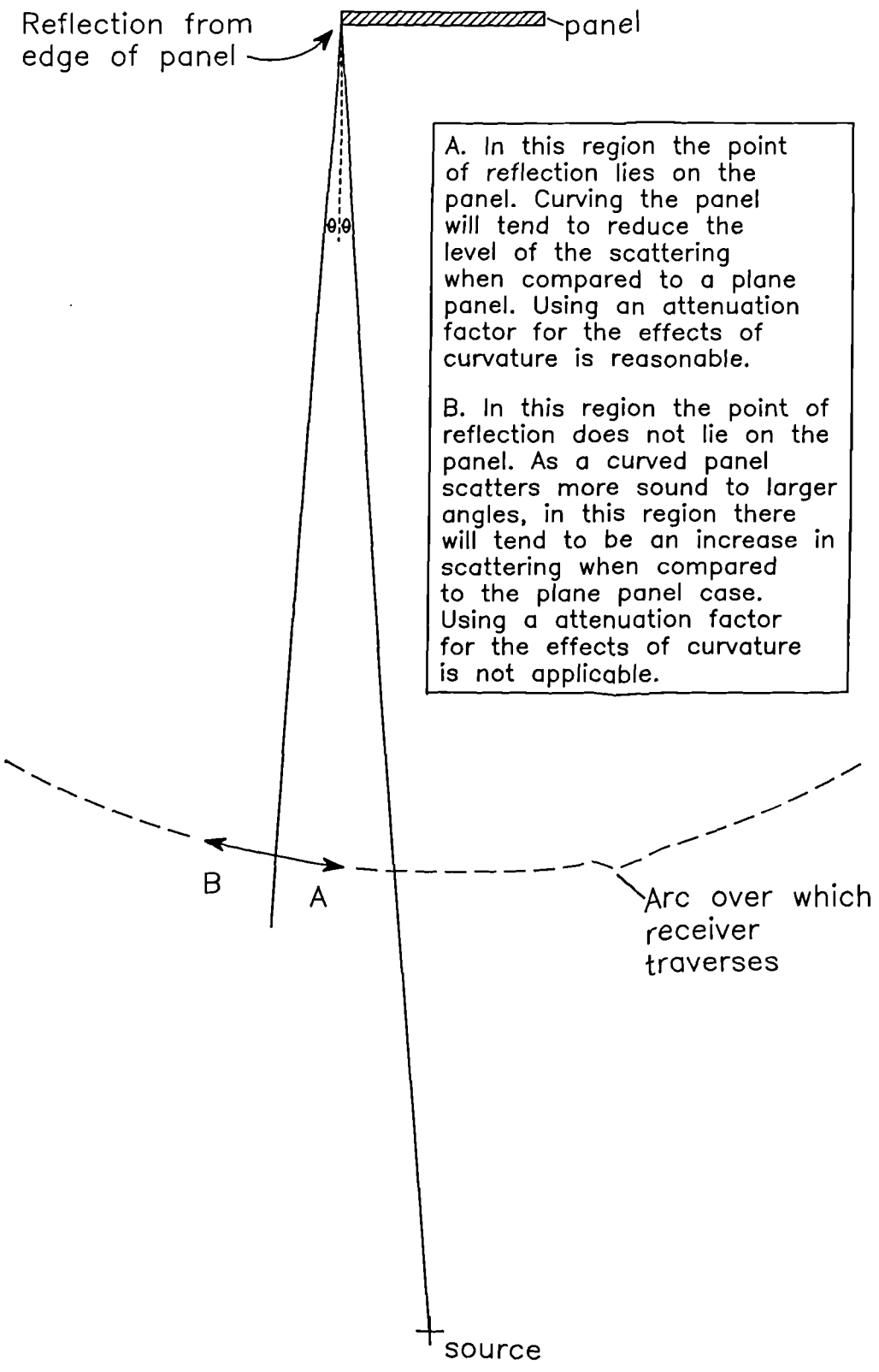

Figure 5.9. Explanation of reflection characteristics for curved panel for different receiver position regions.

the effect of the curvature will most likely increase the level. Consequently, a rough guide to the scattering angles over which the geometric theories work is the range over which the reflection point lies on the surface. For the size of panels tested here this meant a range of ± 8° (relative to the panel normal).

5.5 The Cut-off Frequency for Curved Panels

In Chapter 4, a cut-off frequency was used to describe the frequency above which diffraction effects for the plane panel become small. The scattered response from the plane panel looking something like a high pass filter. Rindel suggested that a cut-off frequency can also be applied to a curved panel [1985].

In Figure 5.10 the scattered pressure as a function of frequency for various receiver angles are shown (it can be compared to the plane panel responses shown in Figure 4.16). It can be seen that the use of a cut-off frequency to describe the scattered field works well for small receiver angles. It is not appropriate, however, for large receiver angles as the shape of the curve is no longer a simple high pass filter. The curves generally increase with frequency and no clear flattening out occurs. Describing the shape of the scattered pressure as a high pass filter with some cut-off frequency, however, is applicable over a larger range of angles than for the plane panel.

The formulation for the cut-off frequency is shown in Equations 4.1 and 4.2, and is the same as that used for the plane panel [Rindel 1986]. The cut-off

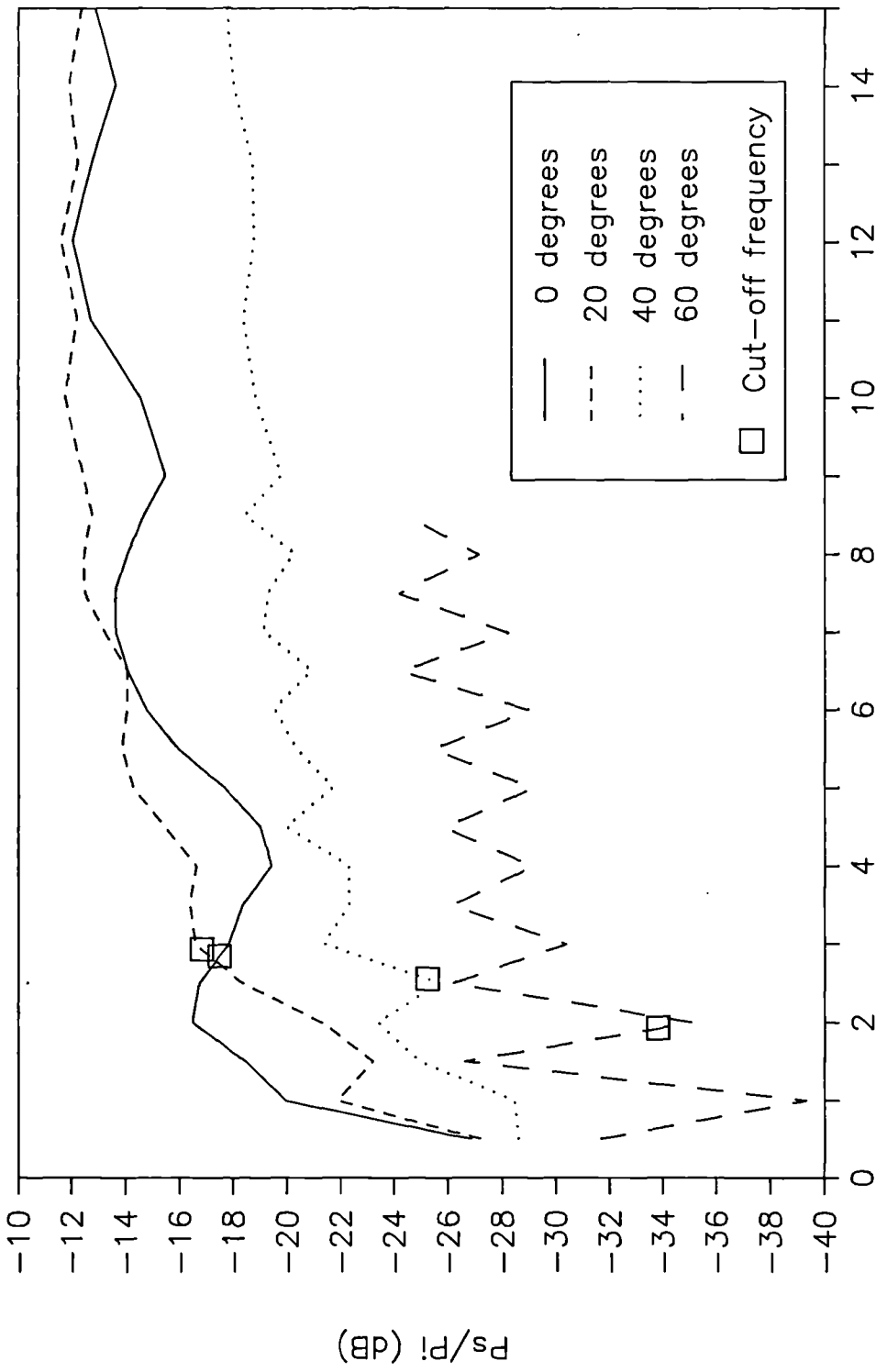

Figure 5.10 Scattering from curved panel for various scattering angles. Cut-off frequencies calculated by Rindel's method shown.

frequencies for various receiver angles are marked in Figure 5.10. The calculated cut-off frequencies work well for near normal receivers, but the calculated value underestimates the true value as the scattering angle increases.

5.6 Conclusions

The scattering from cylindrically curved panels has been successfully predicted by various theories based on the Helmholtz-Kirchhoff integral equation. There is little difference in the accuracy of the predictions from the simple plane panel case.

1. The 3D boundary integral method is the most accurate, but takes the longest to compute.

2. The thin panel limit solution only breaks down at large scattering angles and at high frequencies. This is because it does not representing the finite sized edge. It is considerably faster than the 3D boundary integral method.

3. The Kirchhoff approximate solution is much faster than the previous two methods as it eliminates the need to solve the simultaneous equations for the surface pressures. The accuracy is surprisingly good, being best for near on axis receivers and at high frequencies. The accuracy is better than achieved for the plane panel at large scattering angles.

4. The geometric scattering theories do not model the scattering from the panel well, except close to the geometric scattering angle.

Using a cut-off frequency to describe the scattered field from the curved panel works over a larger range of receiver angles than it did for the plane panel. The formulation used, however, underestimates the cut-off frequency value as the receiver angle increases.

Chapter 6

Theoretical Predictions and Measurements of the Scattering from Quadratic Residue Diffusers

6.1 Introduction

The Quadratic Residue Diffuser (QRD) was suggested in the 1970s by Schroeder as a surface which would produce 'optimum' diffusion [Schroeder 1979]. Since then this type of diffuser has been used in many concert halls, most recently in the Glasgow Royal Concert Hall. Its most popular use has probably been in monitor rooms in studios. The main part of the objective measurements and theoretical predictions in this project has been to test the performance of this type of diffuser. In Section 6.2, a brief introduction into the concept of the QRD is given. It is followed by detailed discussions of the measurements and theoretical predictions done. The predictions have covered a range of solutions of the Helmholtz-Kirchhoff integral equation with differing accuracies and computation times. These sections include descriptions of the tests which assessed the validity of the local reacting admittance assumption used in many of theoretical prediction methods. Discussions concerning the performance of the QRD as a diffuser, can be found in Chapter 7.

6.2 A Brief Introduction to Quadratic Residue Diffusers

The quadratic residue diffuser consists of a series of wells, of the same width, but of different depths. The depths are determined by a mathematical sequence called the quadratic residue sequence, which according to the theory described below, creates optimum diffusion. An example of a QRD can be seen in Figure 6.1, a picture is also shown in Plate 6.1.

The theory of the QRD is as follows. It is assumed, that over a certain frequency range, the acoustic waves travelling up and down the wells can be considered to be plane waves. This sound propagation up and down the wells induces a phase change, before the wave radiates from the well. The Fourier transform of the phase change, created by the quadratic residue sequence, is a constant. It is well established from optics that the Fourier transform of a 'surface' (the phase change due to the surface shape in this case) gives the far field diffraction pattern [Ghatak 1979]. From this it is expected that the scattering from the QRD should be independent of scattering angle.

The quadratic residue sequence is based on an odd prime number, N, and is given by:

$$n = k^2 \ MOD \ N \qquad k=0,1,2.... \qquad 6.1$$

For example two periods of the sequence for N=7 would be:

0 1 4 2 2 4 1 0 1 4 2 2 4 1

Plate 6.1. The Quadratic Residue Diffuser Measured.

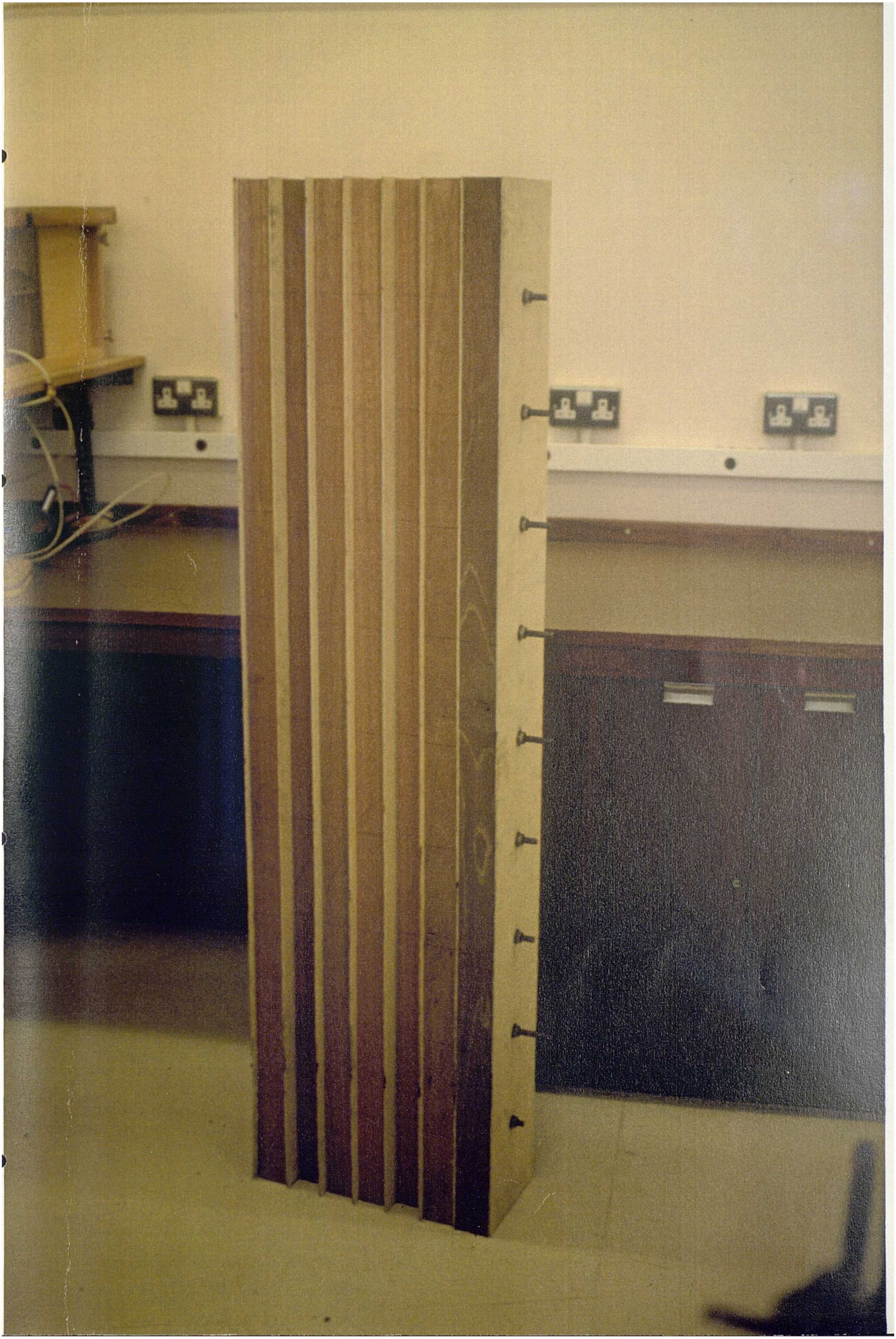

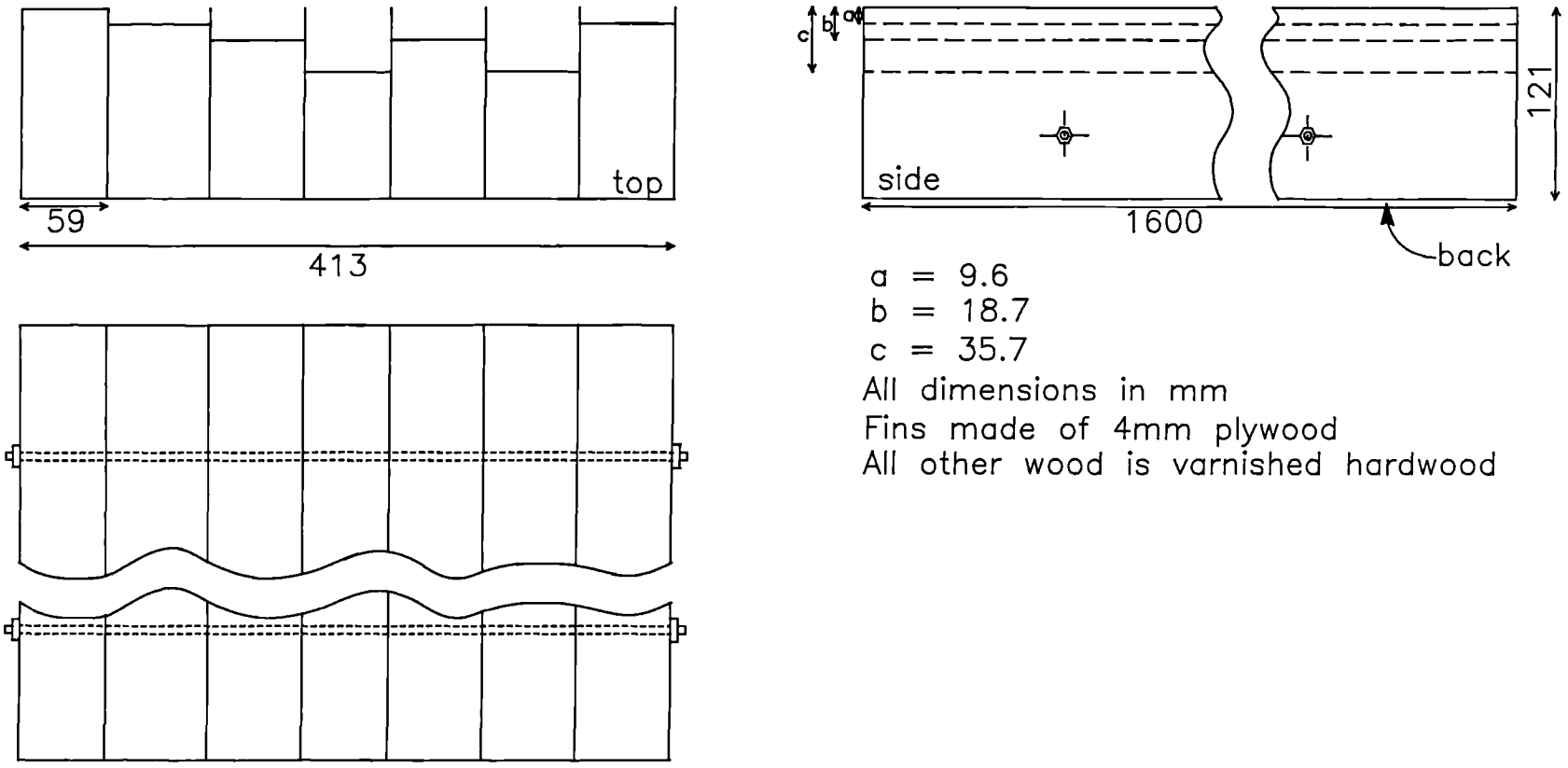

Figure 6.1. The quadratic residue diffuser measured.

The dimensions of the diffuser determine the bandwidth over which the optimum diffusion occurs. There will be a lower frequency limit below which the wells will be too shallow to affect the sound waves, and so the diffuser will behave as a plane panel. There will also be a higher frequency limit, above which the assumption of plane wave propagation within the wells, will not be valid. In terms of wavelengths, these limits are roughly [Schroeder 1979, D'Antonio 1984]:

$$\lambda_{max} \approx \frac{3Nd_{max}}{n_{max}} \qquad 6.2$$

$$\lambda_{min} \approx 2w \qquad 6.3$$

where w is the width of the well; d_{max} the maximum well depth; n_{max} the maximum number in the quadratic residue sequence; and N the odd prime number.

Using Equations 6.1 to 6.3, it is theoretically possible to design a diffuser of any desired bandwidth. The choice of prime number determines the number of minima and maxima in the diffraction pattern: the higher the prime number the greater the number of minima and maxima at a given frequency [D'Antonio 1984]. A one dimensional diffuser, like that shown in Plate 6.1, has the wells extending far along the full length. In that case most of the scattering is in one plane, dominated by the effects of the well depth sequence. It is also possible to make diffusers which work in two dimensions [Schroeder 1979], but that case has not been dealt with in this investigation.

Marshall was probably the first to use such diffusers in a concert hall, in the Michael Fowler Centre, Wellington, New Zealand. In concert halls reflectors generally should have the smallest possible absorption, and many deep wells in a diffuser would lead to large surface area, and potentially large absorption. In order to minimize the absorption, Marshall used diffusers with a small number of relatively shallow wells, and a quadratic residue sequence which has relatively small height variation. But this compromises the bandwidth over which the diffuser were most effective [Marshall 1978]. Example of the QRDs used in a recently built concert hall were shown in Plates 1.1 and 1.2. The QRD measured in this project was based on N=7, and followed the ideas of Marshall. This is the diffuser shown in Figure 6.1 and Plate 6.1. In contrast, the QRDs used in recording studios usually have many more much deeper wells, with narrower openings, giving them a larger bandwidth at the expense of greater absorption [D'Antonio 1985]. In recording studios additional absorption is not as critical as in concert halls, since the rooms are much smaller, and the source power can be easily increased. Therefore, the design of QRDs can have a large range of sizes and characteristics, depending on the application. Further details on QRD design can be found in [D'Antonio 1984].

6.3 The Diffusers Used for Measurements and Predictions.

6.3.1 The QRD used for measurements

The QRD used in the measurements was constructed mainly of varnished hard wood; the fins were made of plywood. A diagram of the panel is shown in

Figure 6.1 and a photo is shown in Plate 6.1. It was based on the prime number N=7. The overall dimensions were .412 by 1.6 by .12 m. The well width was 5.5 cm, the fin width 4 mm, and the maximum well depth 3.6 cm. It follows the designs found in auditoria and was a 1:5 scale model of the diffusers used in an actual concert hall[1].

Measurements were done using both the cross correlation measurement systems described in Chapter 2. The results presented here are for the single microphone cross correlation technique. The source was at a normal distance of 3.89m from the centre of the front face of the QRD. Measurements of the sound pressure were made at a radius of 1.4 m. The microphone at -90° was nearest the zero depth well. (To be slightly more precise, if the centre of panel front was at the origin, the source was at (0,0,3.89m), and the centre of the receiver's arc was at (-.06,0,-.03m). See Figure 3.3 for definitions of axes).

6.3.2 A simplified constant depth diffuser

A panel constructed of thin steel of seven wells of constant depth and width was also tested. A diagram is shown in Figure 6.2. This will be referred to as the Constant Depth Diffuser (CDD). Measurements on this panel was again done using the single microphone cross correlation technique. The source was at (0,0,3.94m). The sound pressures were measured at a radius of 1.41 m. The centre of the receiver's arc was at (0,0,-.01m).

---

[1]The name of the concert hall can not be used because of commercial confidentiality.

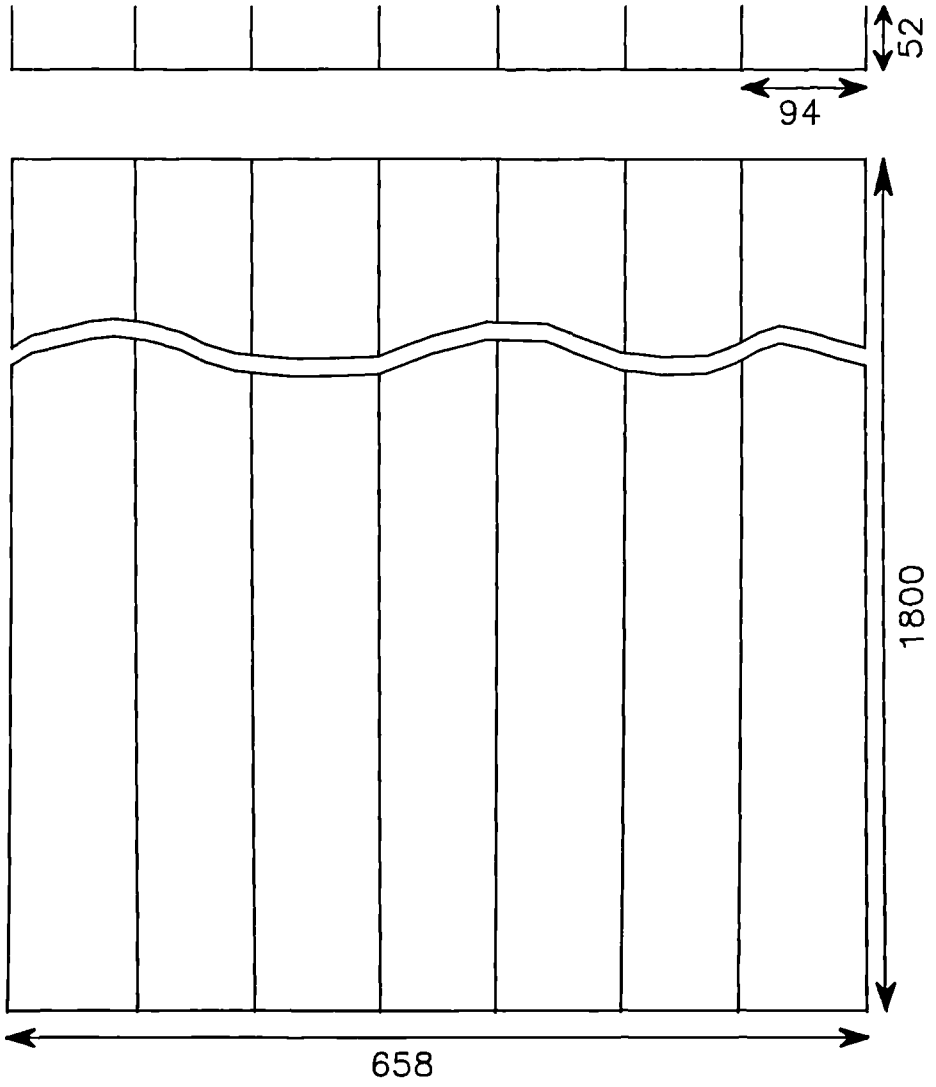

Outside fins 1.5 mm
All others 3mm.
Constructed from mild steel.
All dimensions in mm.

Figure 6.2. The constant depth diffuser (CDD).

Both the QRD and the CDD were constructed to ensure negligible absorption. Most importantly to make sure the vibration of the fins was small. Typical values of absorption for QRDs can be found in [Fujiwara 1992, Commins 1988].

6.3.3 Other diffuser models

Other QRD models were used to test the performance of the various theoretical methods by prediction only. For both models, short overall lengths were used to enable faster predictions at higher frequencies. The two models used were:

(1) A simulation of the type of QRD used in concert halls. This is similar to the measured QRD, the main difference being the reduced length and reduced overall depth. The design criteria were: one period; N=7; well width 59 mm; maximum well depth 35 mm; length .24m; depth 60mm. Pressures were calculated for radii of 2m and 10m, the source was at 5m or 20m.

(2) A QRD with a large number of deeper wells. The design criteria were: N=11; two periods; well width 59 mm; maximum well depth 59 mm; overall length .24m; overall depth 60mm. The pressures were calculated for radii of 2.5m or 20m, the source at 5m or 30m.

6.4 Theoretical Models used for the Quadratic Residue Diffusers and Constant Depth Diffuser.

The application of the theoretical prediction methods for the QRD and CDD are detailed in this section. More details of the theoretical prediction methods can be found in Chapter 3.

6.4.1 Thin panel limit solution

The thin panel limit solution of the Helmholtz-Kirchhoff integral equation allows explicit representation of the diffuser shape. The complete diffuser can be covered with thin panel elements, Figure 6.3 shows a typical example. The complete enclosure of the diffuser by thin panel elements, forces the interior to have zero pressure. Two problems could arise from this representation:

(1) A large number of thin panel elements with different sizes have to be sealed together. The technique is therefore more prone to modelling errors.

(2) The thin panel limit solutions for a plane panel, showed small inaccuracies for scattering parallel to the panel, particularly at high frequencies. This was due to not representing the finite sized edge. This could be a problem for the QRD, as the fins lie edge on to the source. For the frequencies tested, the fins were sufficiently thin compared to the well size and wavelength of sound, that there was not a problem.

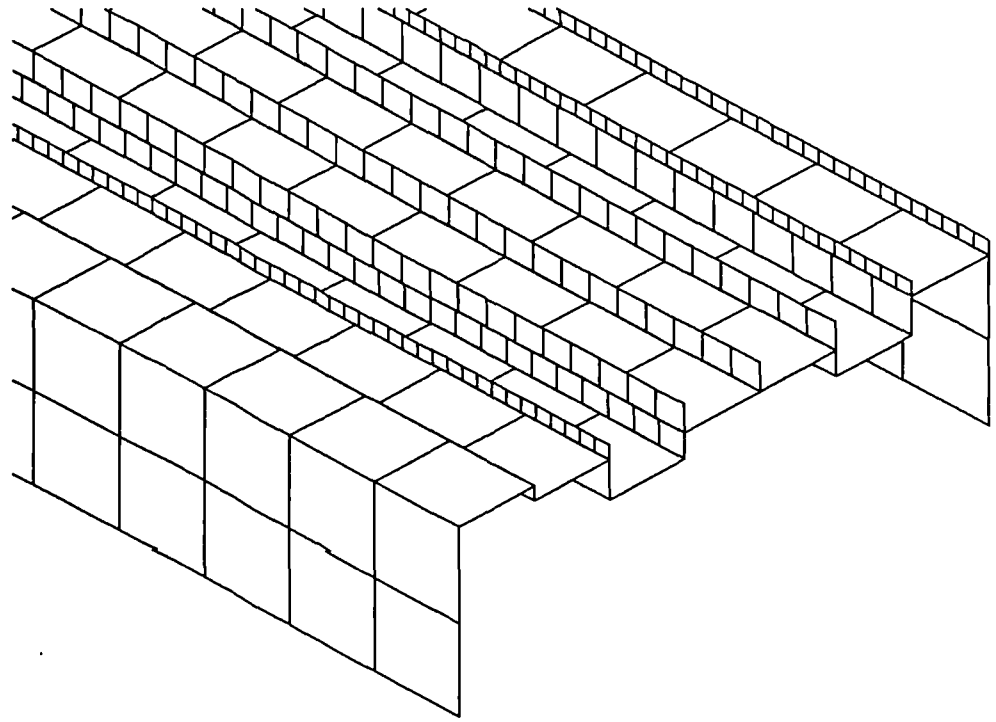

Figure 6.3. Coverage of QRD with elements in thin panel prediction method (back and top not shown for clarity).

The thin panel limit solution method used here involved a geometric mapping of each element to a square. This meant that the aspect ratio of the elements had to be close to one to achieve good accuracy. Unfortunately, this meant that the thin panel solution method requires a large number of elements to represent the diffusers.

6.4.2 Representation of the QRD by a box of variable admittance

It is not practical to model the shape of the QRD explicitly using the 3D boundary integral method. It would be necessary to cover all parts of the diffuser with elements, including both sides of the fins. Because these fins are narrow, the pressure discontinuity across the fins would be difficult to handle in the

numerical solution. Even if the fins were wide enough to allow explicit description of the diffuser's shape, the total number of elements required would be too large to allow computation at anything but the lowest frequencies.

Most authors who have solved the diffraction from the QRD have substituted the complicated shape of the diffuser by a simple box with a variable local reacting admittance on the top. The admittance at the entrance of each well is derived from the phase change of plane waves propagating up and down the wells [Schroeder 1979, Polack 1988, D'Antonio 1984, Strube 1980a]. This representation is expected to work under certain conditions:

(1) The frequency must be below the cut-off frequency of the well - see discussions of Equation 6.3.

(2) The impedance at the opening of the wells must not change from the simple phase change impedance.

There are two conditions necessary for assumption (2). First the radiation coupling between the wells has to be small, so that the impedance can be taken to be local reacting. Second the radiation impedance of each well must also be small. The validity of assumption (2), along with the importance of the cut-off frequency of assumption (1) have been tested. These tests will be discussed in detail in Sections 6.5.2, 6.6.2 and 6.7.1.

6.4.3 3D boundary integral method

The representation of the QRD as a box with a variable surface admittance has been used in the 3D boundary integral method. This involves a numerical solution of the Helmholtz-Kirchhoff integral equation by simultaneous equations.

6.4.4 Kirchhoff approximation

The simple 'box' representation of the QRD and CDD can also be used to solve the diffraction problem using Kirchhoff's approximate surface pressures. In this the surface pressures are taken to be $(1+R)P_{inc}$ where R is the reflection factor of the well entrance, given by the phase change of plane waves propagating up and down the well, and P_{inc} is the incident pressure at the top of the well. The Kirchhoff approximate solution is then given by numerical integration of the Helmholtz-Kirchhoff integral equation.

6.4.5 Simple Fraunhofer solution

Other authors have used Kirchhoff's approximate surface pressures, and solved the scattering problem in the far field by a method analogous to Fraunhofer diffraction in optics [Polack 1988, D'Antonio 1984]. The Fraunhofer solution for a surface of variable admittance was outlined in Chapter 3.

6.4.6 Other methods

A method used by Strube was based on a mode matching approach [Strube 1980b 1981]. In this case the theory ought to work above the cut-off frequency of the wells. However, it does not allow for mutual interactions between the wells. A method has been given by Ando to calculate the reflection from an arbitrary shaped periodic uneven profile [Ando 1976]. This could be adapted for QRDs. Both these methods were not tried in this project.

6.5 Results for the Constant Depth Diffuser

6.5.1 Thin panel solution and 3D boundary integral method

The constant depth diffuser has a simpler construction than the QRD. It was used to test out the assumptions and approximations associated with two of the prediction methods, the thin panel model and the 3D boundary integral method. Most important to test: (i) the assumption of a simple phase change local reacting admittance; and (ii) the cut-off frequency of the wells.

In Figures 6.4 and 6.5 typical examples of the total and scattered field are shown for 1.7 and 2.8 KHz respectively. It can be seen that both theories give accurate predictions: the minima and maxima are in similar locations, and the level of the pressure fields are generally within a few dB. It is possible, however, that a slight shift in the location of a minimum, can result in large differences between experiment and theoretical prediction at some microphone positions.

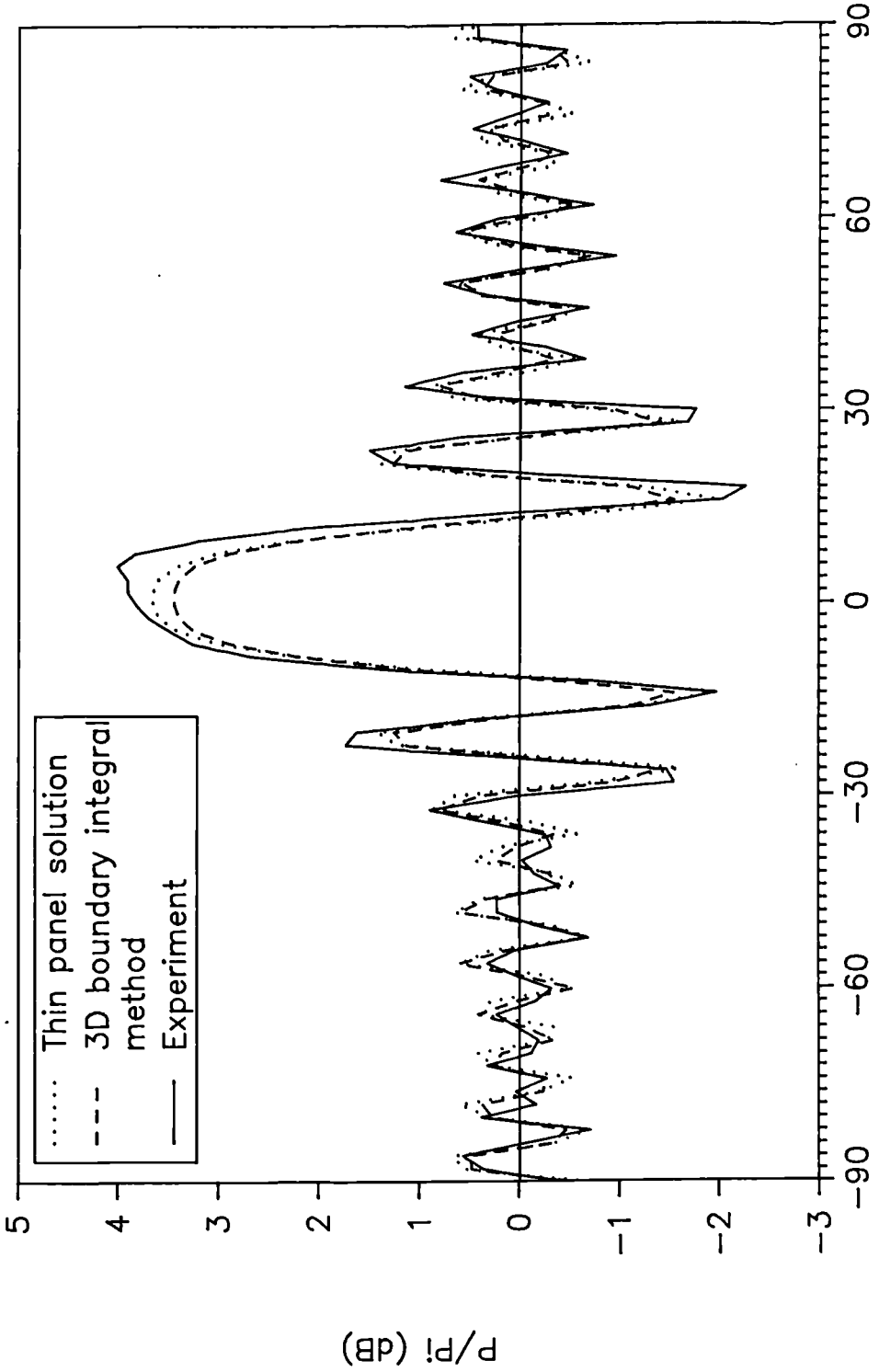

Figure 6.4. Total field for CDD. Comparison of experiment with thin panel solution and 3D boundary integral method. 1687 Hz.

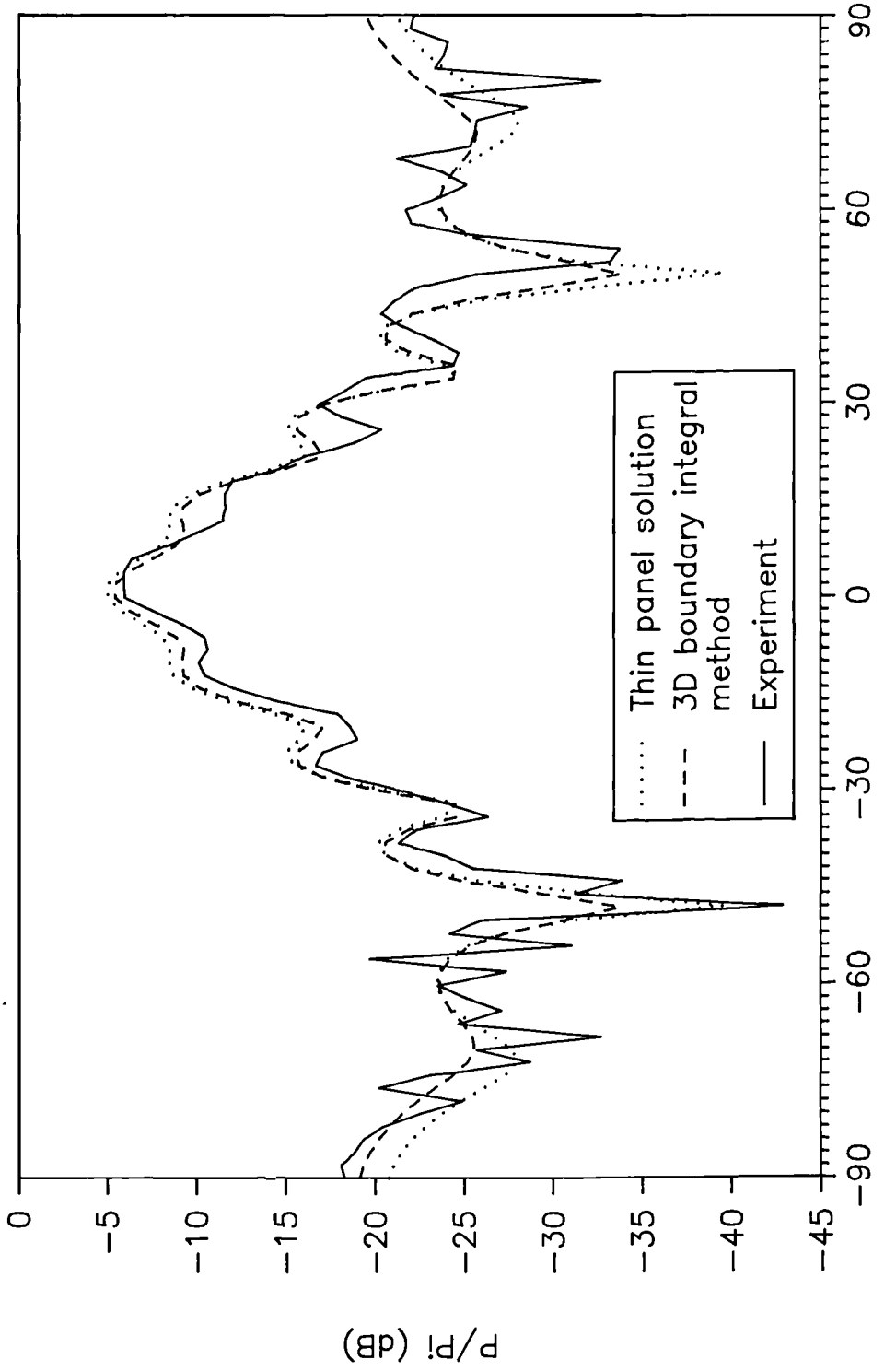

Figure 6.5. Scattered field for CDD. Comparison of experiment with predictions by boundary integral methods. 2811 Hz.

The theoretical predictions were accurate across the frequency range tested, which was up to 6.5 KHz.

6.5.2 Local reacting admittance assumption

The accuracy of the predictions by the 3D boundary integral method when compared to both experiment and the thin panel model shows, that in this case, the assumption of the simple phase change admittances does work well. So the assumptions of local reaction and negligible radiation impedance are good for the external point pressure calculation.

6.5.3 Cut-off frequency of the wells

Tests were carried out up to 6.5 KHz, above which computation limitations prevented further predictions. As noted in Section 6.5.1, at all frequencies tested, the 3D boundary integral method agreed with both the thin panel prediction model and experiment. Yet it was expected, that at high frequencies, plane waves would no longer dominate the sound propagating up and down the wells, and the phase change admittance approximation would no longer work. The wells of the diffuser are 9.4 cm wide, 6.5 KHz corresponds to a wavelength .6 times the well width. Others [Schroeder 1979, D'Antonio 1984] have expected the diffusers based on well structures to become less efficient when the wavelength of sound becomes less than twice the well width, which occurs at 1.8 KHz for this diffuser. It appears that the breakdown of the plane wave propagation assumption is more gradual than previously expected. So these

results show that diffusers made of wells based on a simple phase change admittance, work at higher frequencies than previously expected. Figure 6.6 shows that the cut-off limit is not apparent even at 6.5 KHz, 3.6 times the expected cut-off frequency.

6.5.4 High frequency prediction techniques

When predictions were done at higher frequencies, above about 3 KHz, computation limitations on the number of elements meant that full representation of the diffuser shape was difficult. Two compromises were made: (1) the back of the diffuser was not always represented in the 3D boundary integral method; (2) the predictions were done using half the panel length.

The first compromise creates no significant error at these high frequencies. For the second compromise, Figures 6.7 and 6.8 show typical examples of the predictions for full length and half length panels. Halving the length of the panel does reduce the accuracy of the predictions, up to a few decibels in the scattered field. However, the effects of the removed portions does not prevent comparison, as the locations and relative magnitudes of the minima and maxima are very similar. The error in the amplitude can be reduced to an acceptable level by a correction factor discussed in the following paragraphs.

It is possible to apply an approximate correction to the predicted value for the shortened diffuser, to allow for the change in length. The diffraction in the length direction can be estimated using simple rigid plane panels. A

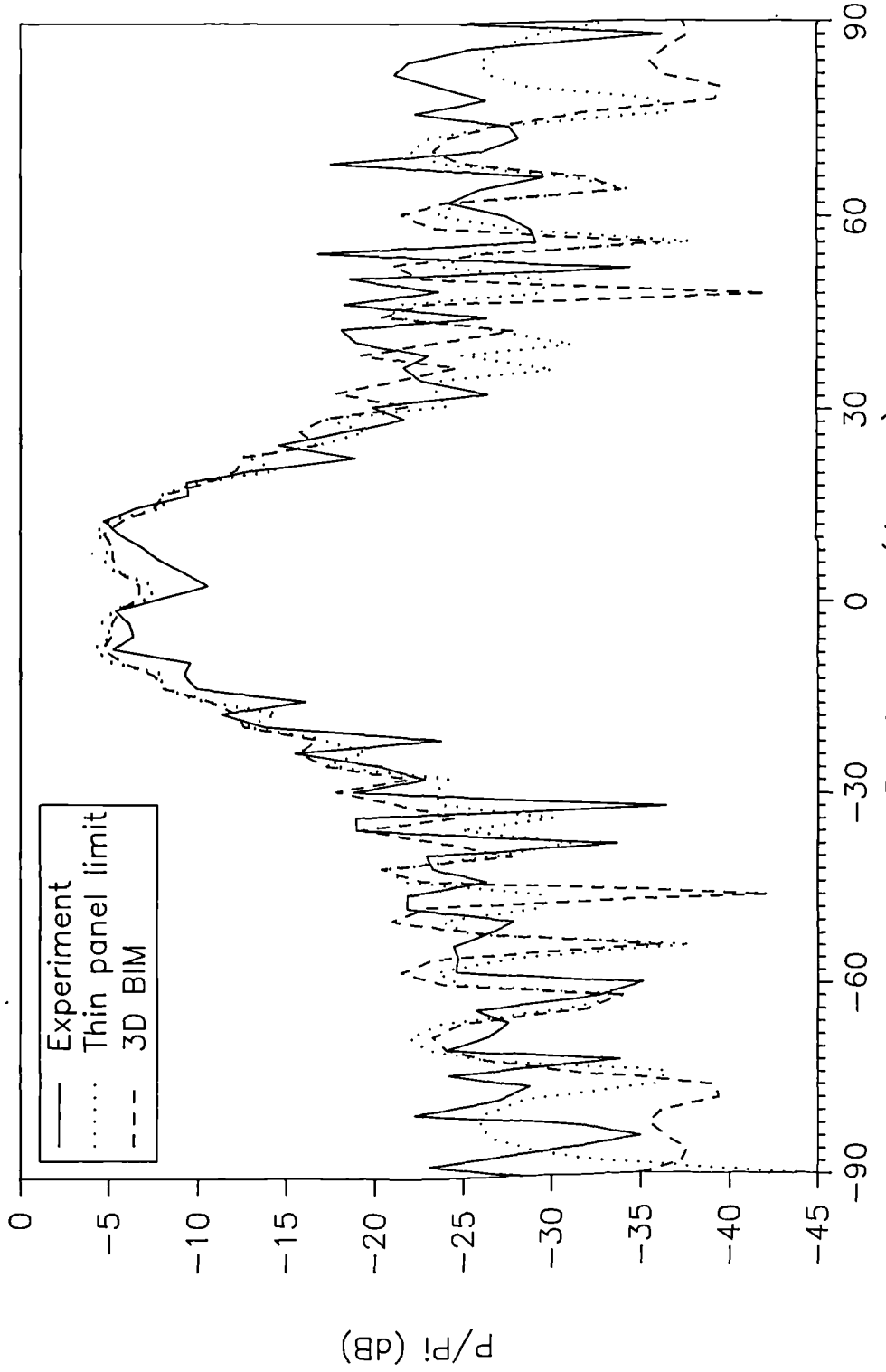

Figure 6.6. Scattered field from CDD at 6 KHz. Comparison of experiment with thin panel solution and 3D boundary integral method solution.

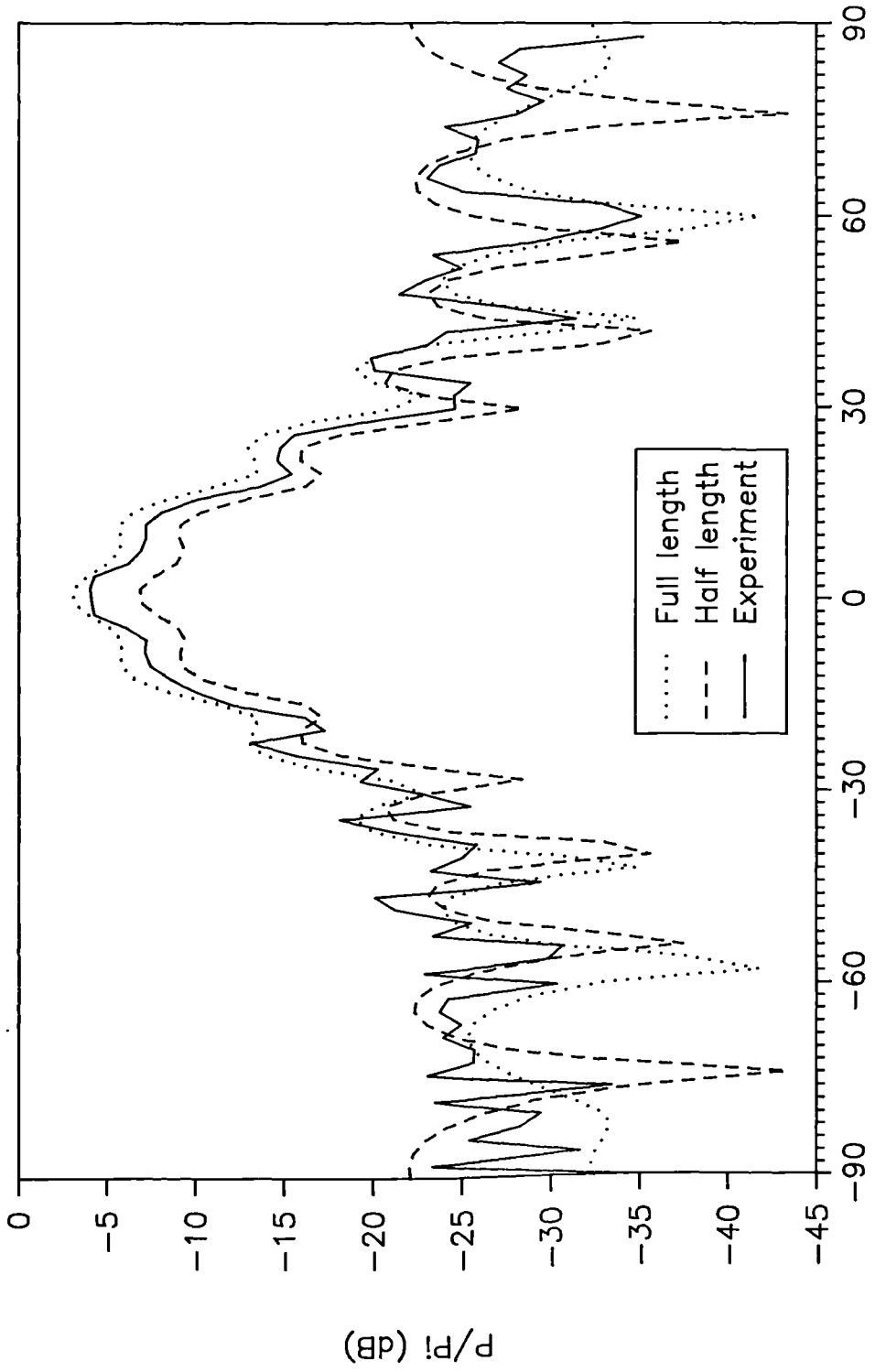

Figure 6.7. Effects of halving length of CDD on predictions by thin panel model. Scattered field 3.2 KHz.

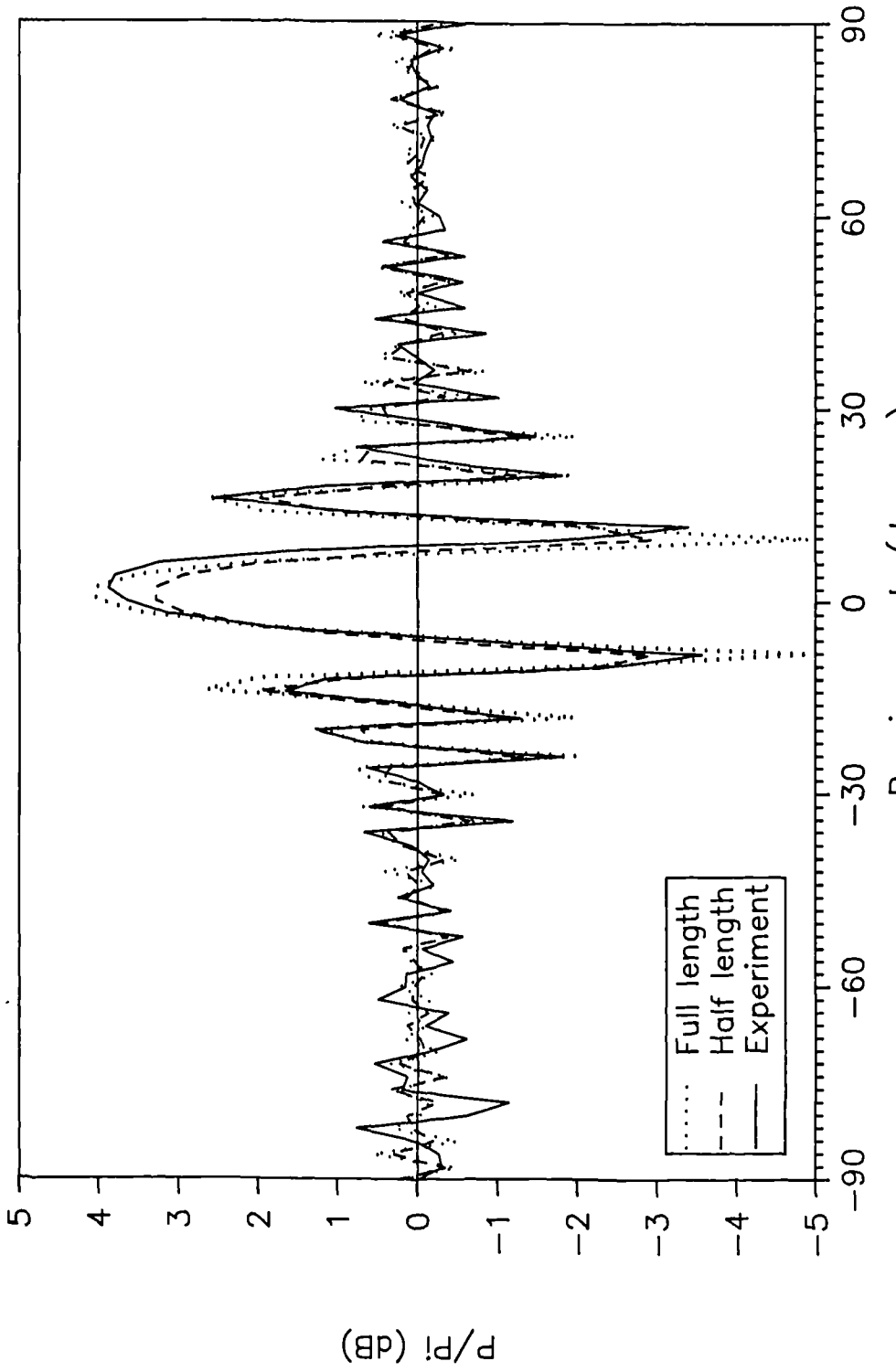

Figure 6.8. Effects of halving length of CDD on accuracy of thin panel prediction method. Total field 3 KHz.

correction factor can then be calculated from the ratio of the predicted on-axis scattered pressures, for the correct length plane panel, over the half length plane panel. Orthogonality of the diffraction along the panel width and panel length has to be assumed; this in line with the assumptions of Fresnel diffraction discussed in Chapter 3. True orthogonality, however, can only be achieved when the panel is infinitely long in one direction. Therefore, the true correction factor can only be determined with infinitely wide panels and for the on-axis scattered pressure. This is then only an approximate correction factor for other angles.

The scattered pressures for the full length and half length CDD will be represented as $P_1(f,\theta)$ and $p_{1/2}(f,\theta)$. The predictions for the full length and half length plane panels are $P'_1(f,0°)$ and $P'_{1/2}(f,0°)$. The correction formula is then:

$$P_1(f,\theta) = P_{1/2}(f,\theta)\frac{P'_1(f,0°)}{P'_{1/2}(f,0°)} \qquad 6.4$$

where θ is the scattering angle.

As these corrections are at high frequencies, the correction factors can be calculated very fast and accurately using Fresnel diffraction. It was shown in Chapter 4, that for on-axis scattering and high frequencies, Fresnel diffraction gives accurate predictions. Figure 6.9 shows a typical result of applying a correction to the scattered field at 3.2 KHz. It shows that the correction works very well close to on-axis, although the accuracy of the correction decreases as the scattering angle increases. As the frequency at which this correction is used increases, the size of the correction factor generally decreases, and consequently so does the error involved in applying it.

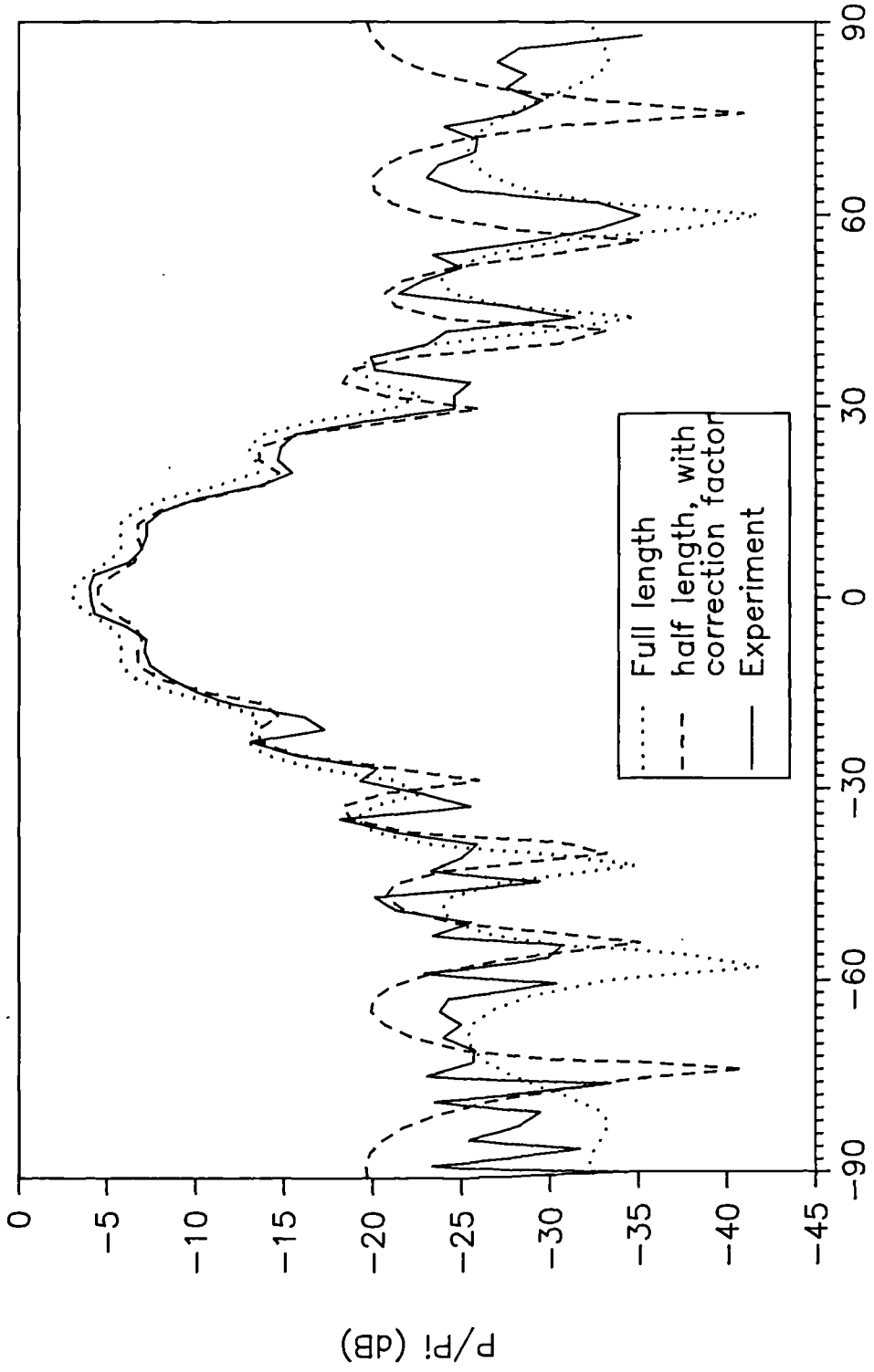

Figure 6.9. Demonstration of use of corection factor to improve accuracy of thin panel predictions when only half the panel length is modelled. Scattered field 3.2 KHz.

6.6 Measurements and Predictions of a Quadratic Residue Diffuser

6.6.1 Thin panel limit solution

The thin panel predictions of the QRD scattering performance agrees very well with experiment at all frequencies tested. It was tested to 3 KHz. In Figures 6.10 and 6.11 examples can be seen at 1213 Hz and 2012 Hz.

Because of the complicated nature of the diffuser, approximate representation of the QRD shape was necessary, similar to those made for the CDD. This was discussed in Section 6.5.4. For the QRD the back might be removed, the top might also be removed, and the panel shortened in length[2]. The effects of the removing back and top were small. An example can be seen in Figure 6.12 at 1213 Hz. 1213 Hz was the lowest frequency at which the approximation was used and where such an approximation should be at its worst. The effects of shortening the panel length are very similar to that for the CDD. An example for the CDD has been given in Figures 6.7 and 6.8. The correction factor for panel length discussed in Section 6.5.4 which was used for the CDD predictions was also applied here. In fact the predictions for Figure 6.11 were done with half the panel length and then the correction for panel length applied.

---

[2]Definitions of the 'top', 'sides' and 'back' of the QRD were given in Figure 6.1.

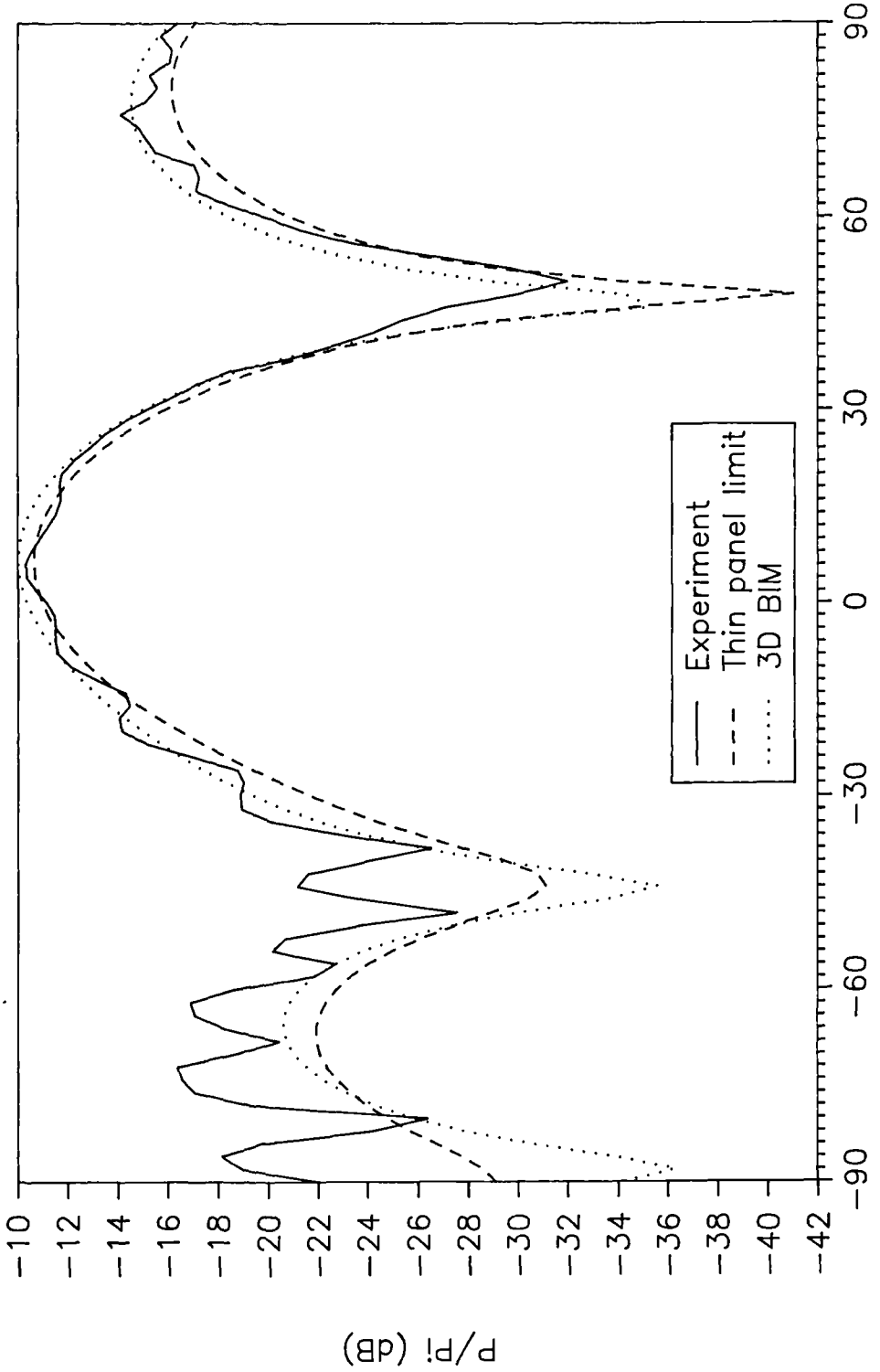

Figure 6.10. Scattered field from N=7 QRD at 1213 Hz. Comparison of experiment with thin panel limit solution and 3D boundary integral method.

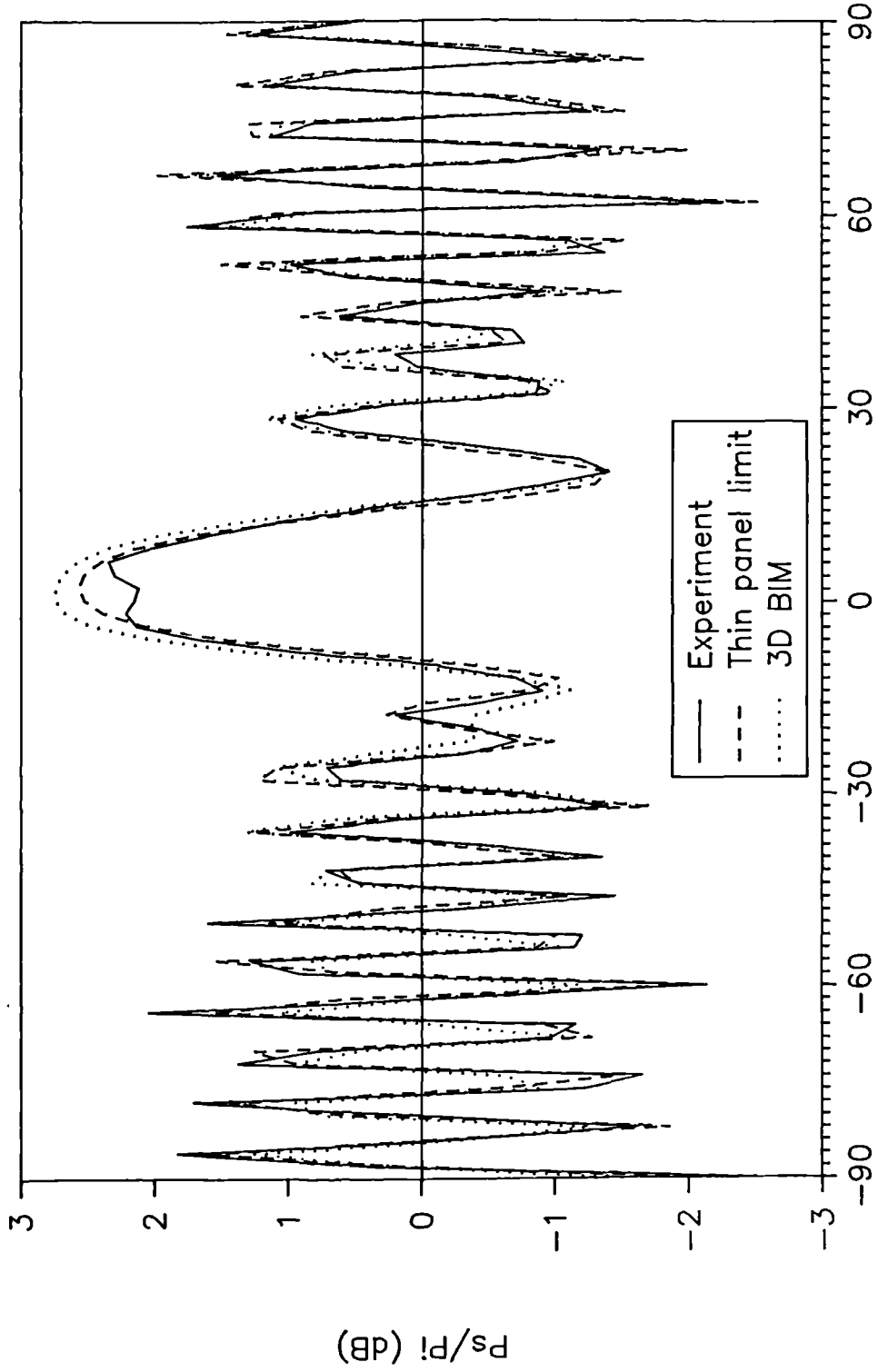

Figure 6.11. Scattered field from N=7 QRD at 2012 Hz. Comparison of experiment with thin panel limit solution and 3D boundary integral method.

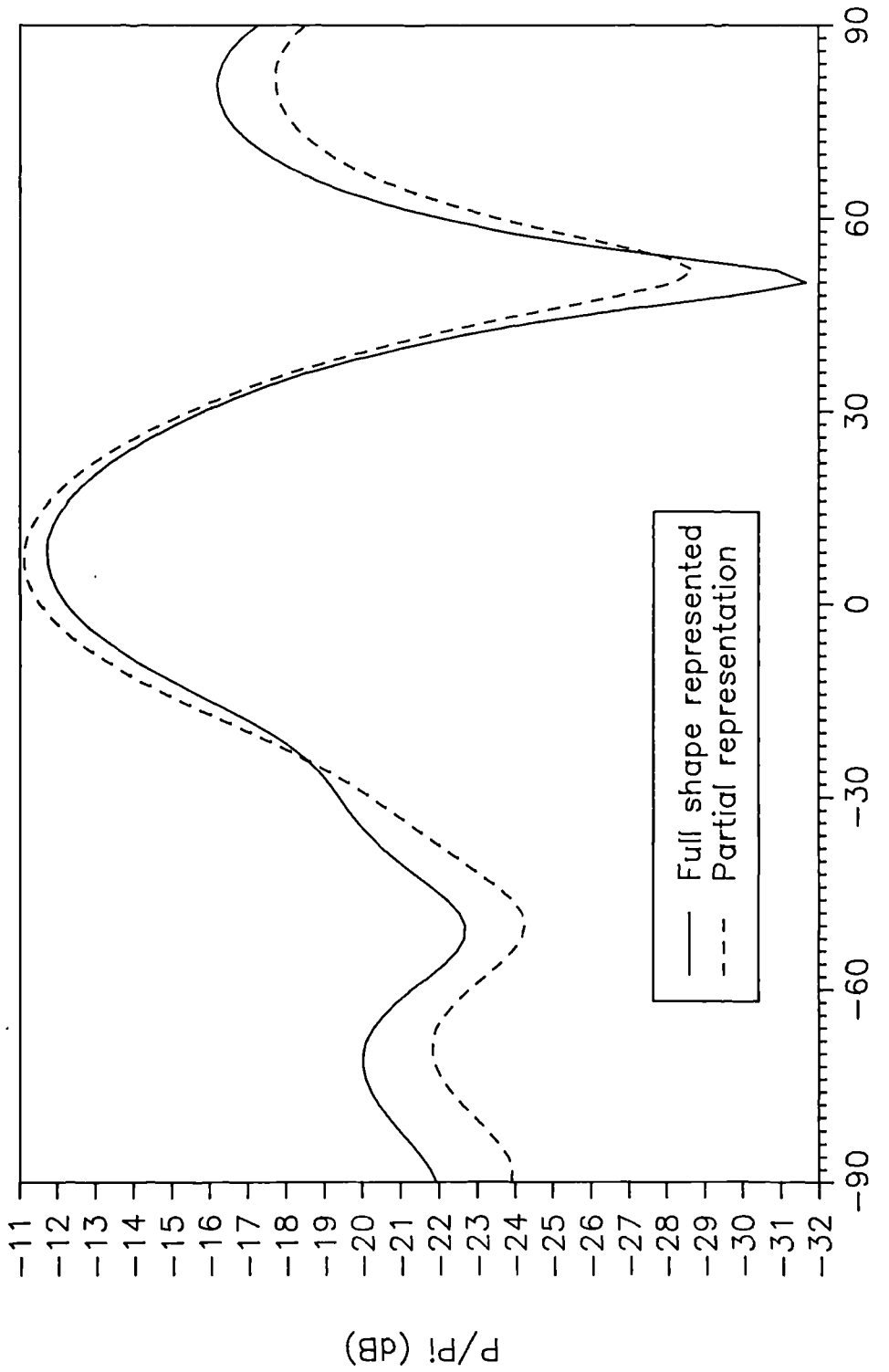

Figure 6.12. Effects of removing back and top on accuracy of QRD predictions by boundary integral methods. 1213 Hz.

6.6.2 3D boundary integral method

The 3D boundary integral method also gives accurate predictions, as shown in Figures 6.10 and 6.11. This shows the success of the simple phase change local reacting admittance assumption for the QRD. To look at this assumption in more detail, the admittances across the surface of the panel were compared with the expected value from the simple phase change calculations. The admittances were calculated by finding the external point pressures at the well entrance and just above the well entrance, using the thin panel prediction model. The velocity was derived from the pressure gradient between the two points. The admittance was then given by the ratio of the velocity over pressure.

In Figures 6.13 and 6.14, the variation of the normalized admittance, along the width and the length of the diffuser, are compared to the expected value by the simple phase change calculation. The admittance on the surface of the zero depth well is zero, and so not calculated.

The imaginary part of the admittance varies along the length of the panel, but only very near the end of the panel does it radically deviate from the value at the diffusers centre. This is due to the scattering from the panel end. This does not greatly affect the external point calculation as the deviation occurs only for a small portion of the panel, which is furthest from the receiver. It was found that for the variation in admittance across the panel width, the imaginary part of the simple phase change admittance is similar to that produced by the thin panel model. This demonstrates why the local reacting admittance approximation

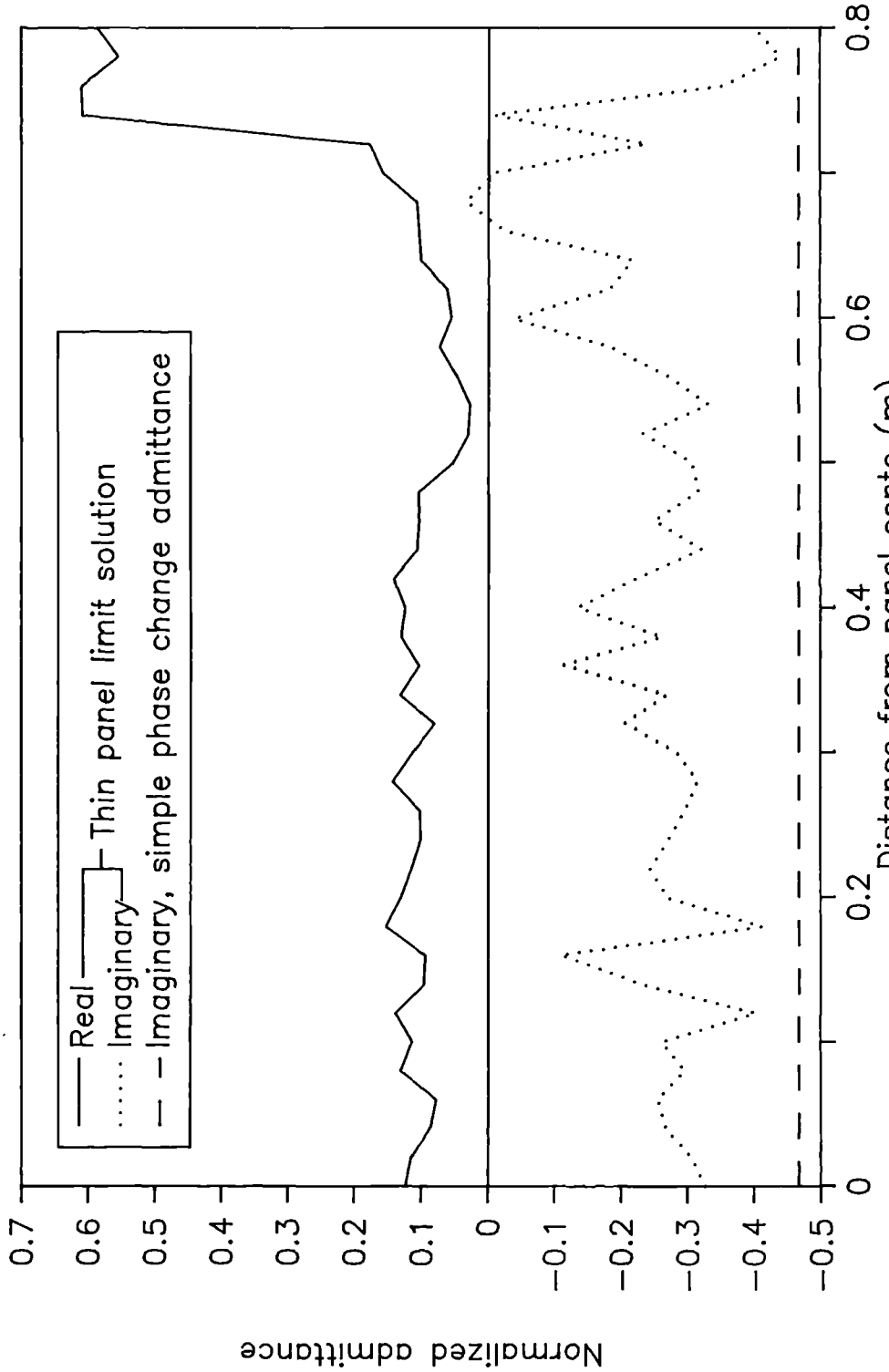

Figure 6.13. Admittance along length of centre well of N=7 QRD at 1390 Hz. Comparison of thin panel limit solution with simple phase change admittance values.

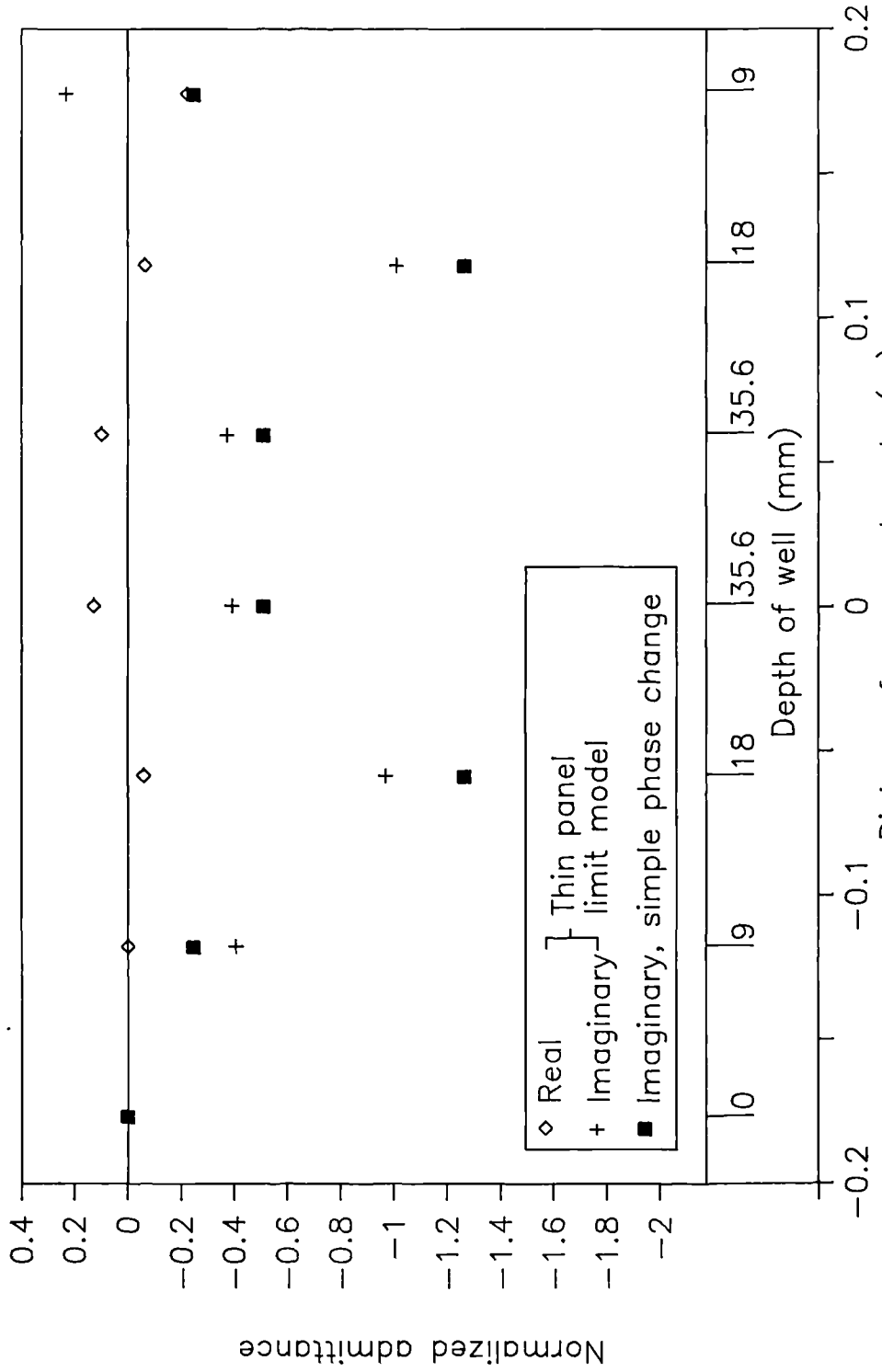

Figure 6.14. Variation of admittance across width of N=7 QRD. Comparison of thin panel predicted value and simple phase change admittance. 1390 Hz.

works. The example shown is at 1390 Hz, which is a relatively low frequency. At higher frequencies, the mutual interactions across the panel should decrease, and so the approximation should work even better.

The real part of the thin panel predicted admittance is not zero, which is not as expected for the simple phase change admittance of a completely non-absorbing well. This is caused by interactions between the wells. The real part represents energy absorption or emission. Since the system is completely non-absorbing and passive, the absorption and emission must cancel out over the whole diffuser. Consequently, non-zero real part should not significantly affect the far field external point pressure. The cancellation can be seen in Figure 6.14, the real part of the admittances of the wells vary taking both positive (absorptive) and negative (emissive) values.

The large number of elements needed to represent the whole diffuser meant that the theoretical prediction methods could only be tested at low to mid frequencies. The maximum frequency tested was 3 KHz, corresponding to a wavelength roughly twice the well width.

6.7 Simulated Quadratic Residue Diffusers

As the thin panel prediction model has been shown to be accurate, and should work both below and above the cut-off frequency of the wells, it was decided to do further tests with prediction models only. The performances of two

more QRDs were tested. The first was an N=7 single period QRD similar to those found in concert halls - this will be referred to as the simulated concert hall QRD. The second diffuser had more wells and deeper wells. It was based on two periods of N=11. Section 6.3.3 gave more details about the designs of these diffusers.

To enable computation to higher frequencies for the N=11 diffuser, the fact that the quadratic residue sequence is always symmetric for all but a single zero depth well was exploited. From Equation 6.1, it can be shown that two periods of an N=11 quadratic residue sequence is:

0 1 4 9 5 3 3 5 9 4 1 0 1 4 9 5 3 3 5 9 4 1

By removing the first zero depth well, symmetry could be exploited and so reduce the number of elements needed to represent the diffuser by half. In Figure 6.15 an example of the scattered field for the diffuser with and without the zero depth well is shown at 2 KHz. It can be seen there is little loss of accuracy, and then only at large scattering angles at which the accuracy is still acceptable.

6.7.1 Cut-off frequency

The simulated concert hall diffuser was tested up to 8.5 KHz. At this frequency, the wavelength is .7 times the width of the wells. Again little divergence between the thin panel model and 3D boundary integral method was seen. A typical example can be seen in Figure 6.16. The similarity of the

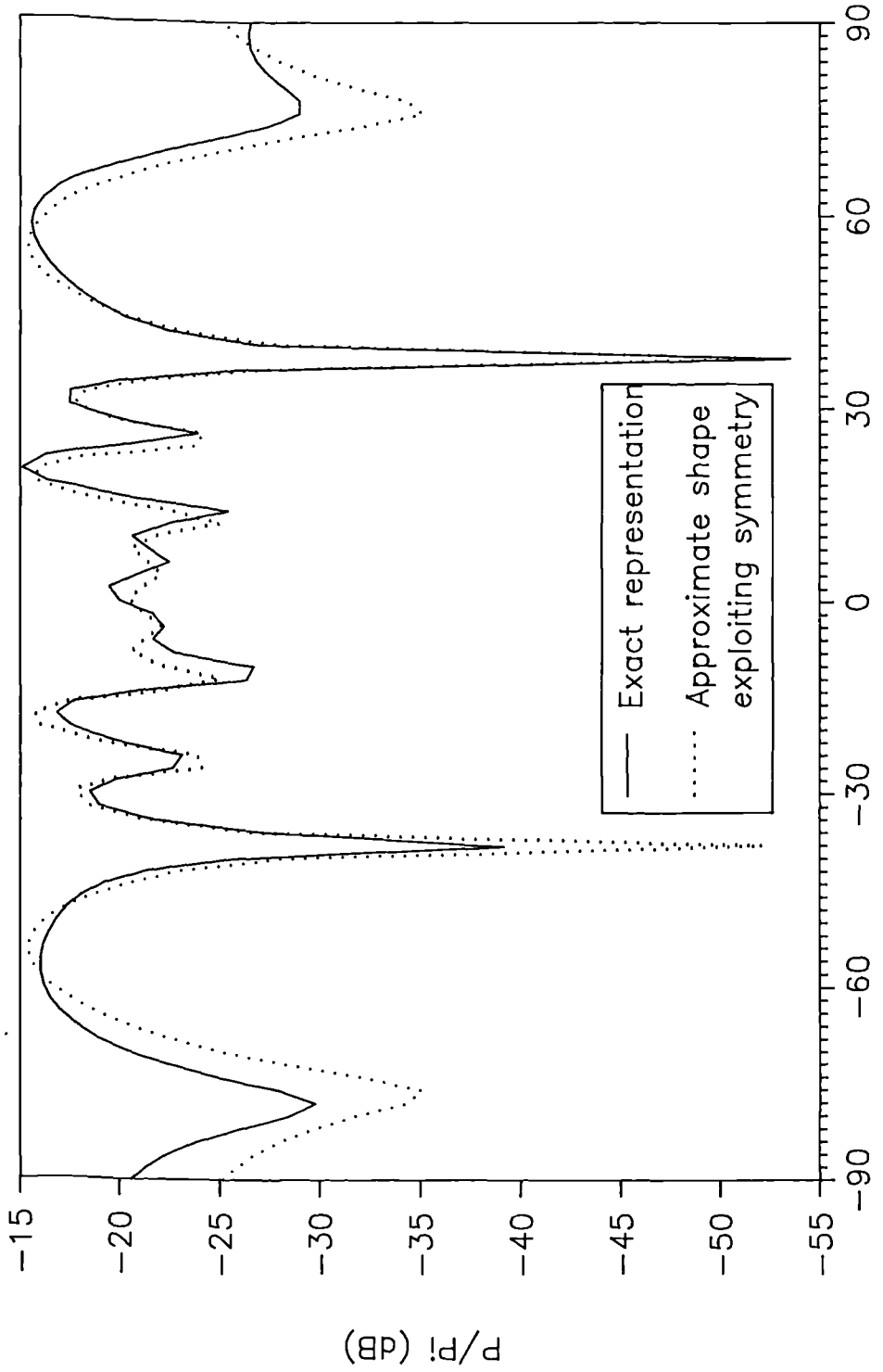

Figure 6.15. Prediction of scattered field from N=11 QRD at 2 KHz. Comparison of solution with exact QRD shape with a more approximate representation which allows exploitation of symmetry.

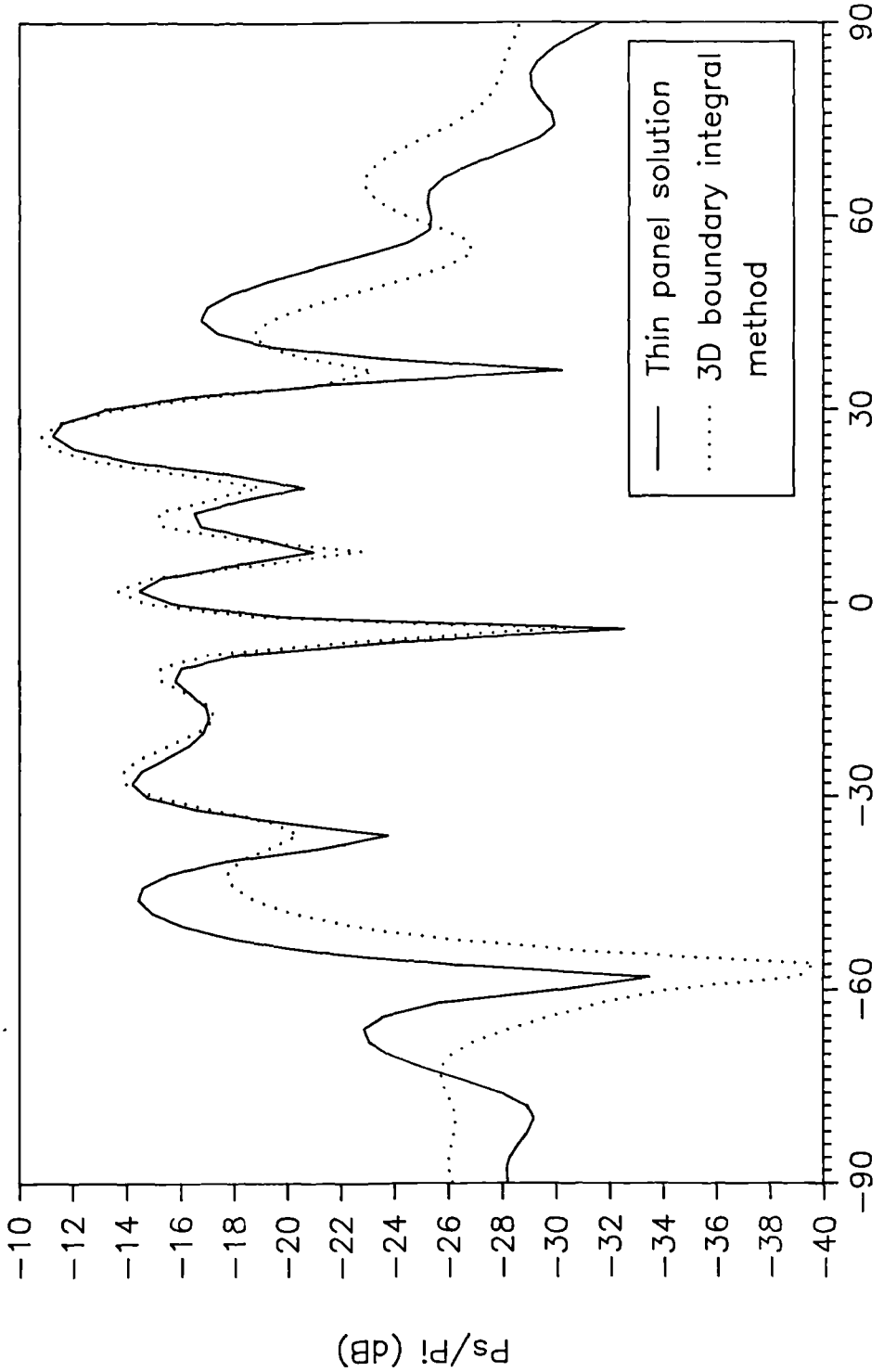

Figure 6.16. N=7 simulated QRD. Scattered field at 5 KHz.
Thin panel limit solution and 3D boundary integral method solution.

predicted pressures, shows that the phase change local reacting admittance assumption works well, at least till this frequency for normal incidence. This is not surprising as the CDD worked beyond this ratio of well width to wavelength. The on-axis 3D boundary integral method predictions are accurate, there is a slight decrease in the accuracy for larger scattering angles.

So far the local reacting admittance approximation has only been tested for the normal incidence case. It has been suggested [Polack 1988], that the further away from normal incidence the source is, the greater the interaction between the wells, resulting in the local reacting approximation breaking down at lower frequencies. This was tested using the N=7, simulated concert hall diffuser, at an incident angle of 60°. This is an extreme value for incident angles occurring in concert halls. At the frequencies tested - up to 8.5 KHz - the predictions produced by the 3D boundary integral method are not as accurate as for the normal incidence case. An example is shown in Figure 6.17 at 8.5 KHz. As noted in the normal incidence case, the 3D boundary integral method is most accurate close to the geometric scattering angle, and this is again true for the 60° incident case. The data shows no evidence that the cut-off frequency has been lowered by the non-normal incidence. It does show, however, that if predictions for the scattering from -90° to +90° in front of the panel is required, the 3D boundary integral method is less accurate away from normal incidence.

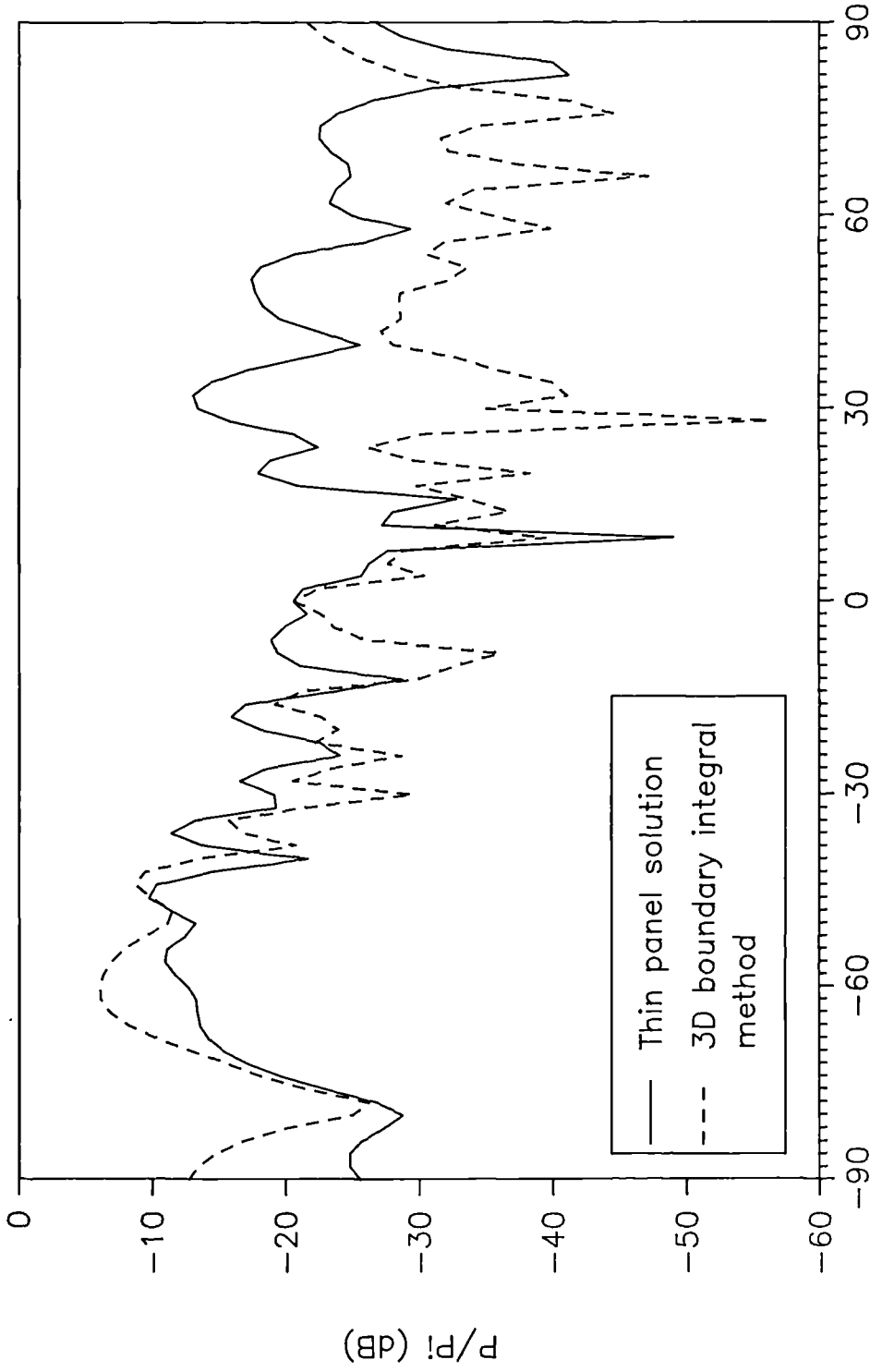

Figure 6.17. Scattering from N=7 QRD at 8.5 KHz for off-axis source. Thin panel prediction compared to 3D boundary integral method solution.

6.7.2 Lower frequency limit

As discussed above in 6.2, there is a low frequency limit below which the wavelength of sound is so long compared to the well depths, that the QRD effectively behaves as a plane panel. The low frequency limit was tested by doing predictions on a rigid square box with the same outside dimensions as the QRD and comparing the results. This was done for the N=7 simulated concert hall diffuser. Examples are shown in Figure 6.18 and 6.19 at 700 Hz and 900 Hz. For very low frequencies the plane box and QRD give very similar results as expected. The predictions for 900 Hz and above, however, showed distinct differences between the two predictions. Therefore, 900 Hz is taken as the low frequency limit of the diffuser. This limit is lower than that found using Equation 6.2 which gives a value of 1900 Hz for a N=7 diffuser of maximum depth 36mm. So our results have shown that the low frequency limit was about an octave lower than that expected by Schroeder, although he was not that specific in defining the limit.

6.7.3 Kirchhoff approximate solution

The Kirchhoff approximate solutions assumes both the simple phase change admittance and also Kirchhoff's approximate surface pressures. It behaves in a similar way to that found for the curved panels and plane panels. Theoretical prediction examples are shown in Figures 6.20 and 6.21 at 1.5 KHz and 6.5 KHz respectively. The prediction model does not fully take into account the mutual interactions between different parts of the diffuser, and so is not

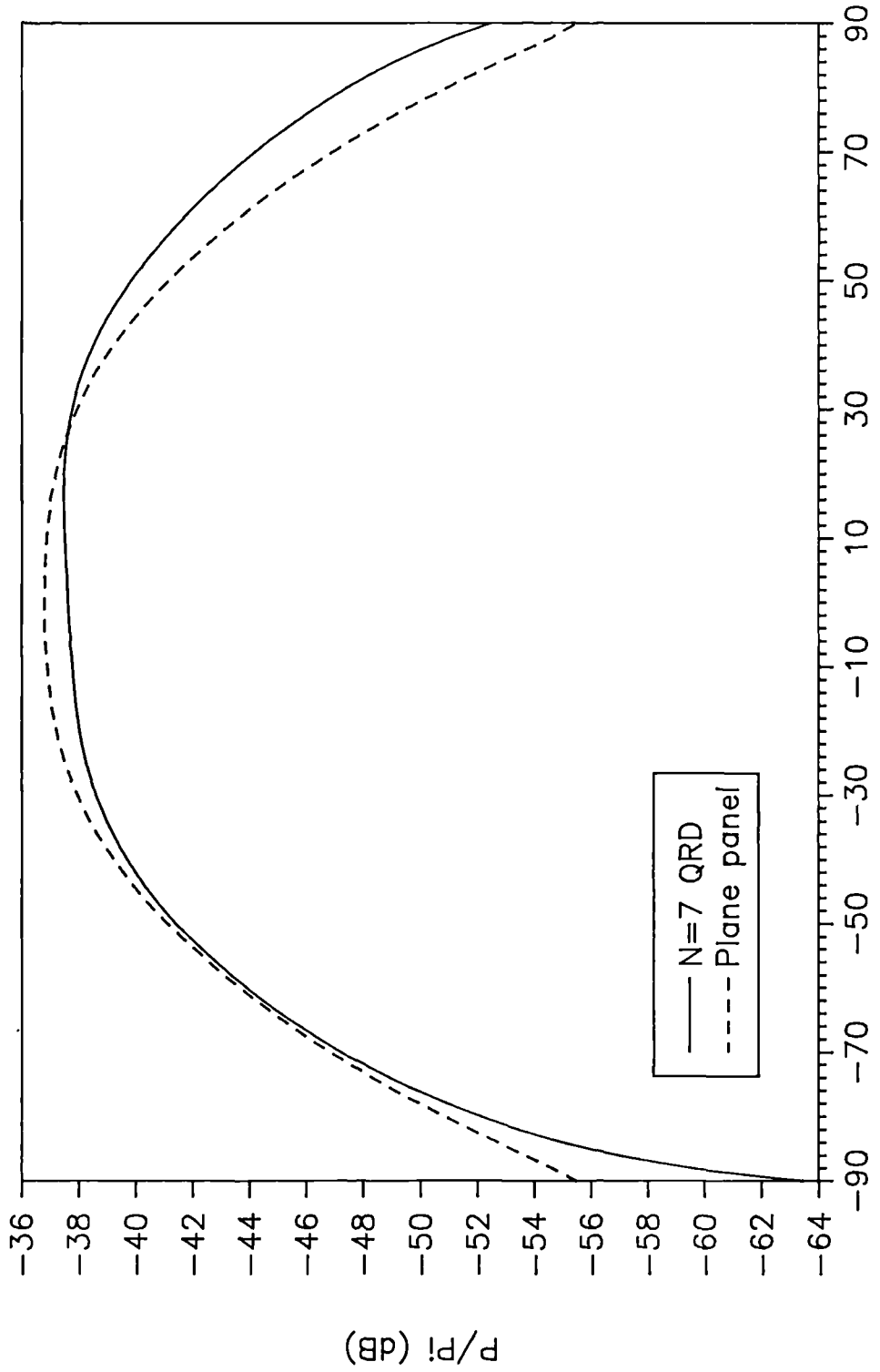

Figure 6.18. Scattering from the N=7 QRD compared with scattering from a plane panel with the same overall dimensions. 700 Hz.

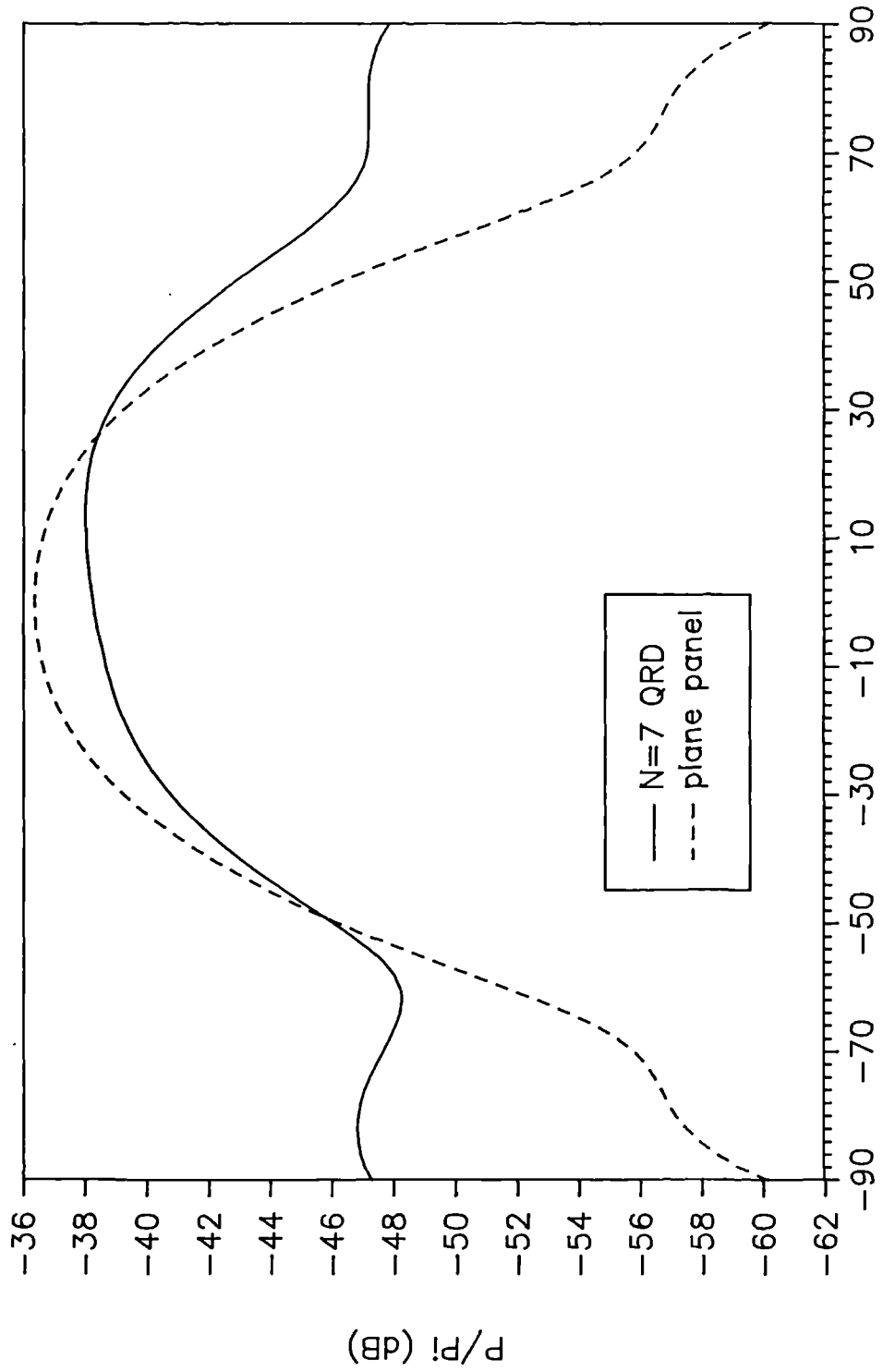

Figure 6.19. Comaprison of scattering from N=7 QRD and plane panel of same overall dimensions. 900 Hz

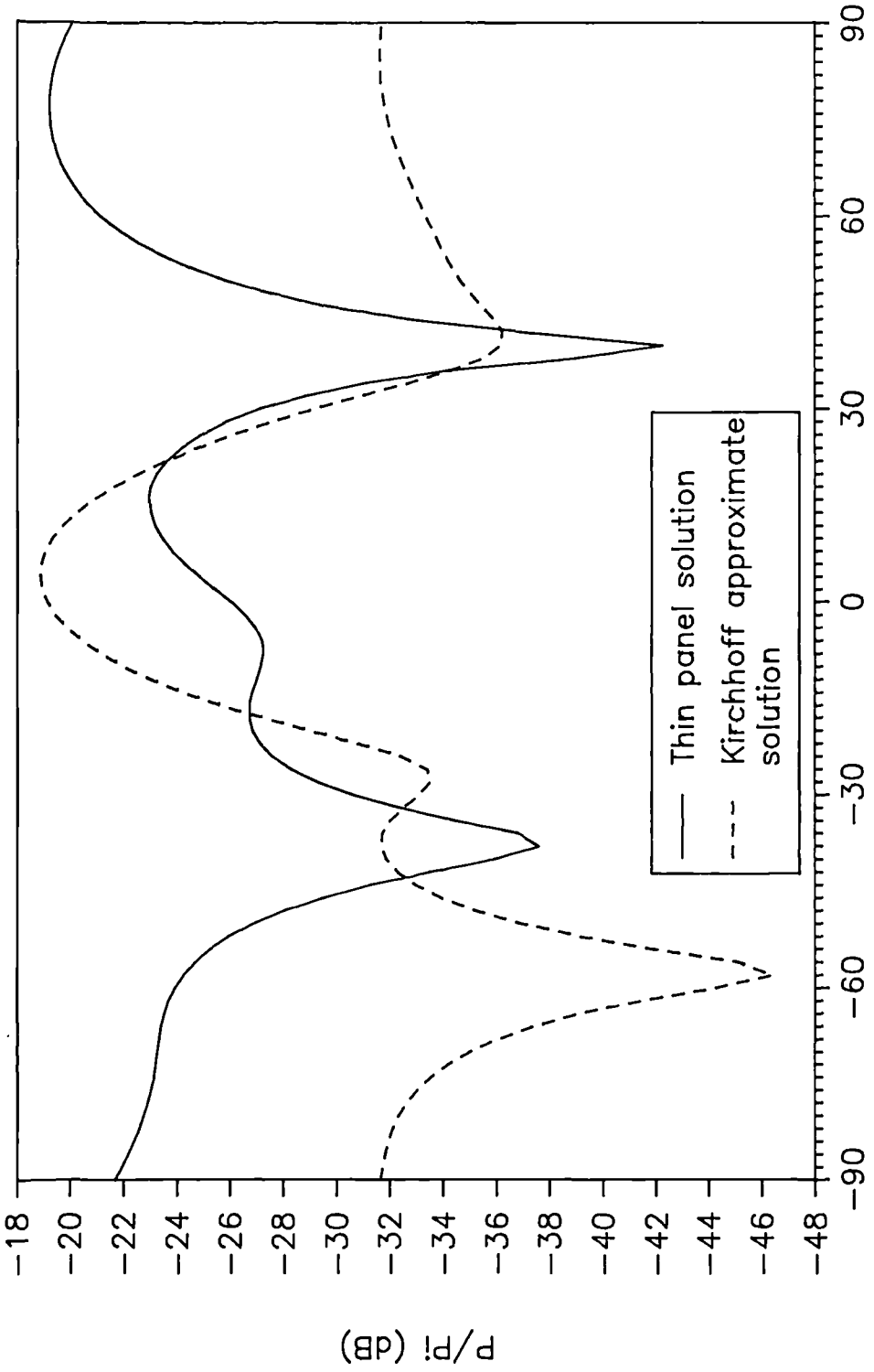

Figure 6.20. Kirchhoff approximate solution compared to accurate thin panel solution for N=7 QRD at 1.5 KHz.

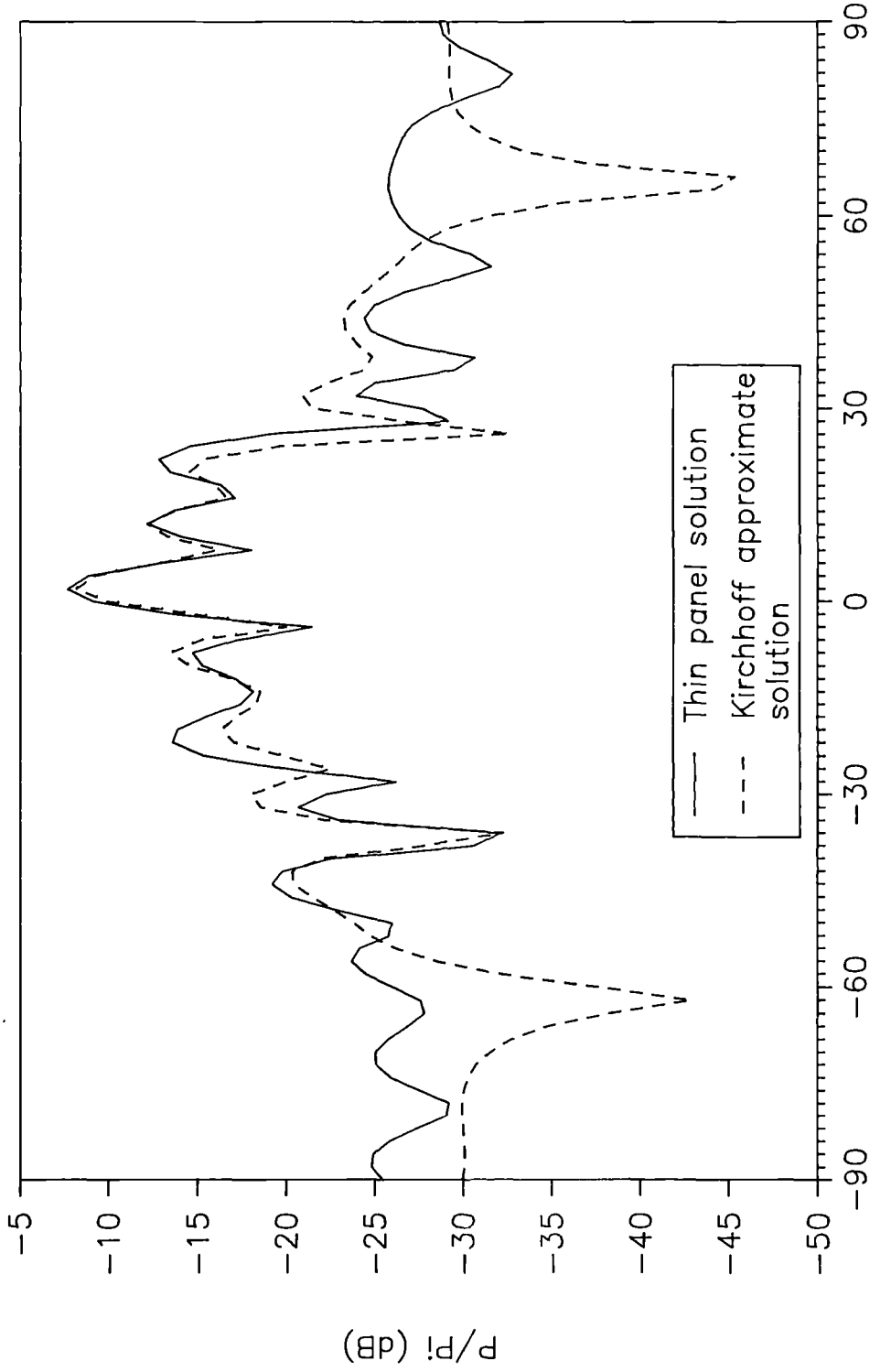

Figure 6.21. Kirchhoff approximate solution for the scattering from N=7 QRD compared to accurate thin panel solution. 6.5 KHz.

completely successful in predicting the sound field. This is most noticeable at low frequencies, below about 2.5 KHz, where the interactions across the surfaces are most important. As the frequency increases the accuracy of the predictions increase as the mutual interactions become less important. The accuracy is about the same for both the N=7 and N=11 diffusers. One feature which was clearly seen for the plane panel in Chapter 4, was the failure of the Kirchhoff theory as the scattering angle increases. For the QRD predictions, however, such effects are less obvious. The Kirchhoff theory is certainly more accurate for an on-axis receiver than it is for a receiver at a large angle, but the deviation is not as large as for the plane panel. The difference is due to the variation of the surface admittances on the QRD. The quadratic residue well depth sequence is used to scatter more sound to the sides than happens with a plane panel. This leads to a greater masking of the error due to inadequate representation of scattering from the sides and back of the diffuser and inadequate representation of the surface pressure distribution.

The Kirchhoff theory behaves similarly to the 3D boundary integral method for oblique incident sound. An example is shown in Figure 6.22 at 5 KHz. It is less accurate than for the normal incident case, particularly away from the geometric scattering angle. When the predictions deviate from the thin panel model they tend to follow the 3D boundary integral method solution. This shows the breakdown is mainly due to the simple phase change admittance approximation.

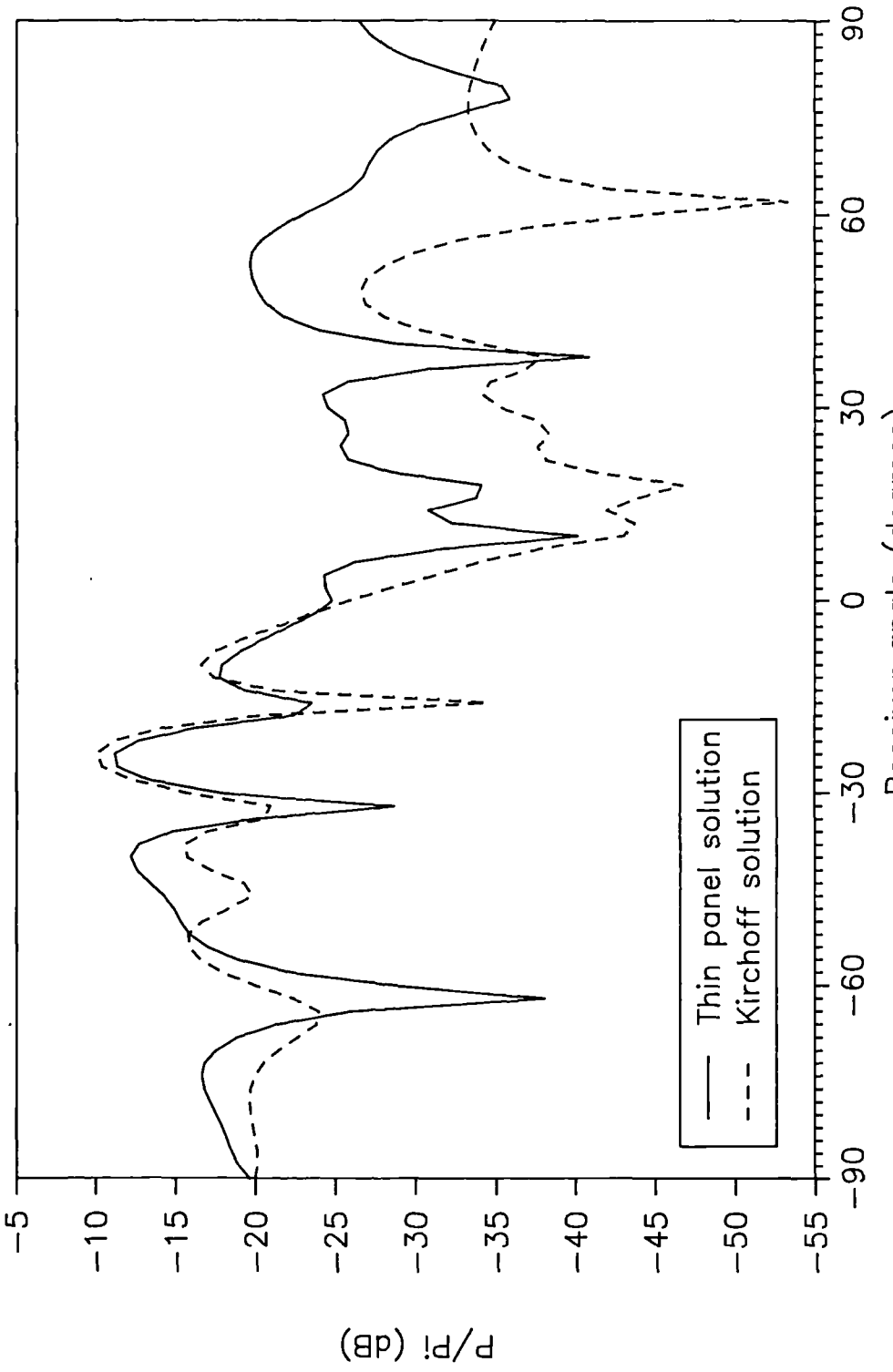

Figure 6.22. Scattered field from simulated N=7 QRD for off-axis source at 5 KHz. Comparison of Kirchhoff solution with accurate thin panel solution.

6.7.4 Simple Fraunhofer theory

The Fraunhofer theory, like the Kirchhoff theory, fails to take into account the mutual interactions on the surface of the diffuser. This is a problem at the lowest frequencies, below 2.5 KHz, where the interactions are at their most significant. The Fraunhofer solution follows the Kirchhoff solution at these frequencies.

Above the lowest frequencies, unlike the other theories tested, the success of the Fraunhofer theory varies between the N=7 diffuser and N=11 diffuser. Examples can be seen in Figures 6.23 and 6.24 for both diffusers at 3 KHz. For the N=7 simulated concert hall diffuser the predictions are very satisfactory up to the highest frequency tested (8.5 KHz). For the N=11 diffuser, however, although the overall shape of the diffracted pressure field is similar to the 3D boundary integral method solution, the fine detail of minima and maxima are not well predicted. As discussed in Chapter 3, the Fraunhofer solution requires the receiver to be in the far field. So there is an assumption of large receiver distance compared to panel width. The N=11 diffuser is much wider than the N=7 diffuser. As shall be shown below, for the N=11 diffuser the receiver is effectively in the near field. Consequently, the Fraunhofer solution is not as successful.

It can be demonstrated that the reason that the Fraunhofer theory breaks down is due to the receiver being in the near field. If the receiver is moved a

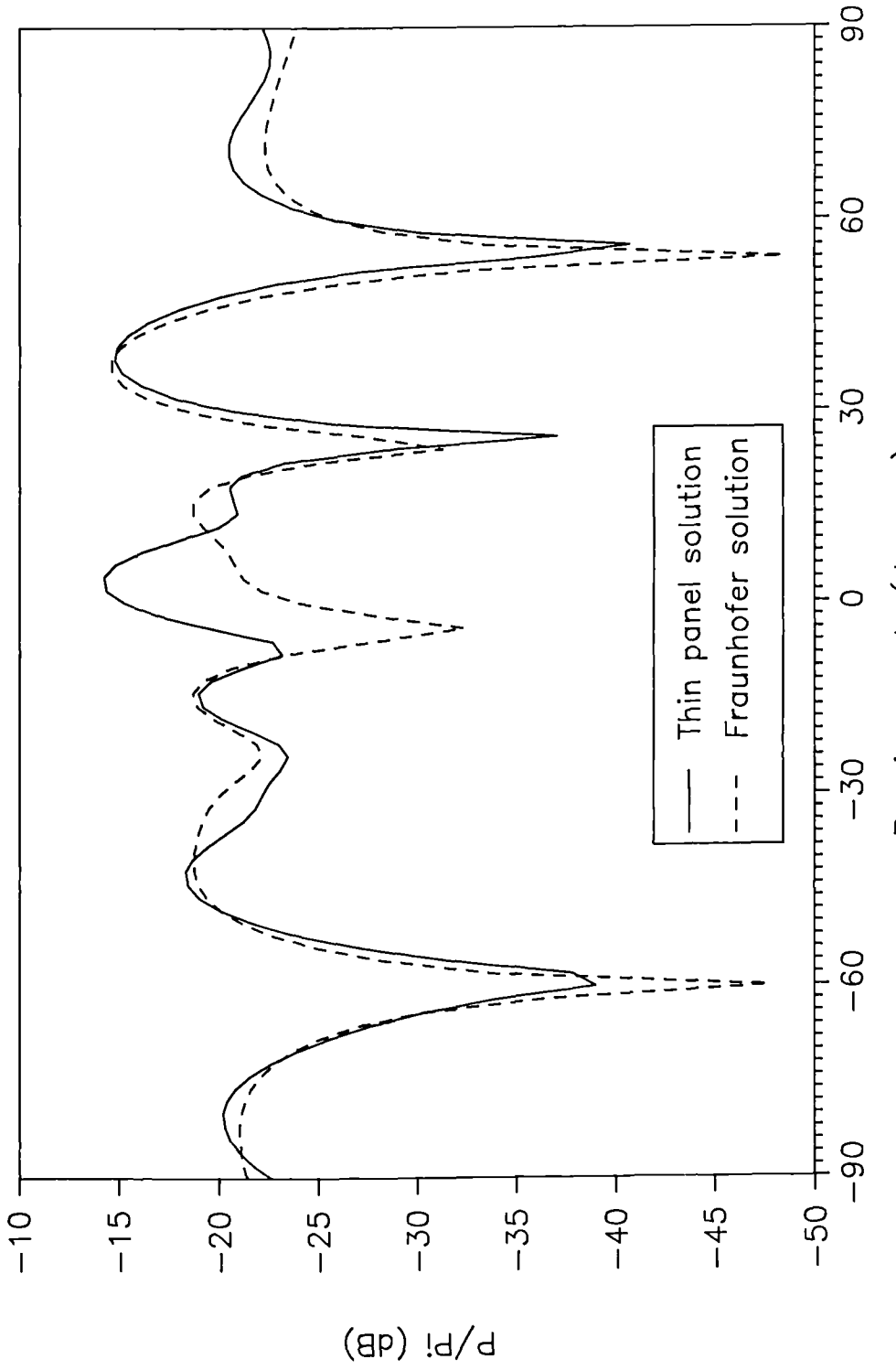

Figure 6.23. Fraunhofer solution for the scattering from the N=7 QRD compared to the thin panel limit solution. 3.5 KHz.

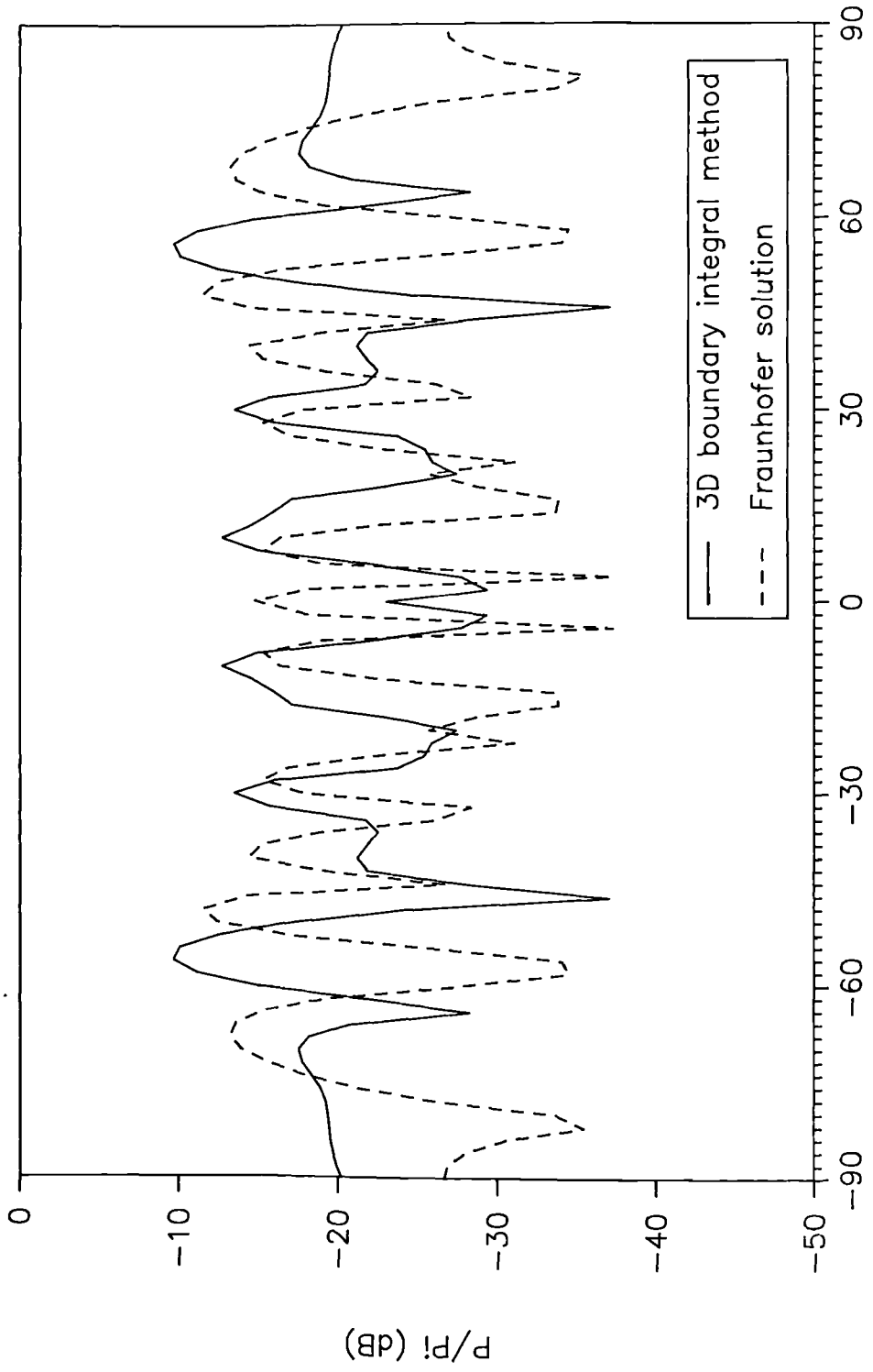

Figure 6.24. Fraunhofer solution for scattering from N=11 QRD compared to 3D boundary integral method solution. 3.5 KHz.

long way from the panel, it is found that the Kirchhoff approximate solution and the Fraunhofer solution converge. This is shown in Figure 6.25.

The far field is generally taken to be for receiver distances larger than l and kl^2, l being half the largest dimension of the panel [Pierce 1981 page 225]. In this case the later constraint is the limiting factor. According to this formulation the frequency limit of the far field should be about 2.6 KHz for the N=7 diffuser and 400 Hz for the N=11 diffuser. Yet the N=7 diffuser works up till 8.5 KHz. From our results it is possible to estimate that the Fraunhofer theory becomes inaccurate due to the near field effects for receiver distances between 1/5 to 1/3 kl^2. As the near field extends further at higher frequencies, this is can be translated to an upper limiting frequency for the Fraunhofer solution method. The limit is slightly stricter than the $.4kl^2$ found for the plane panel in Chapter 4.

When solving the simple Fraunhofer solution method for long panels, the length direction is crucial in determining whether the receiver is in the near or far field. An improvement in the accuracy of the simple theory predictions can be brought about by using Fraunhofer diffraction along the width direction, and Fresnel diffraction along the length direction.

6.7.5 Comparison of computation time for theories

The computation time for the various theories varies with frequency. As the frequency increases the element size needed to ensure good representation

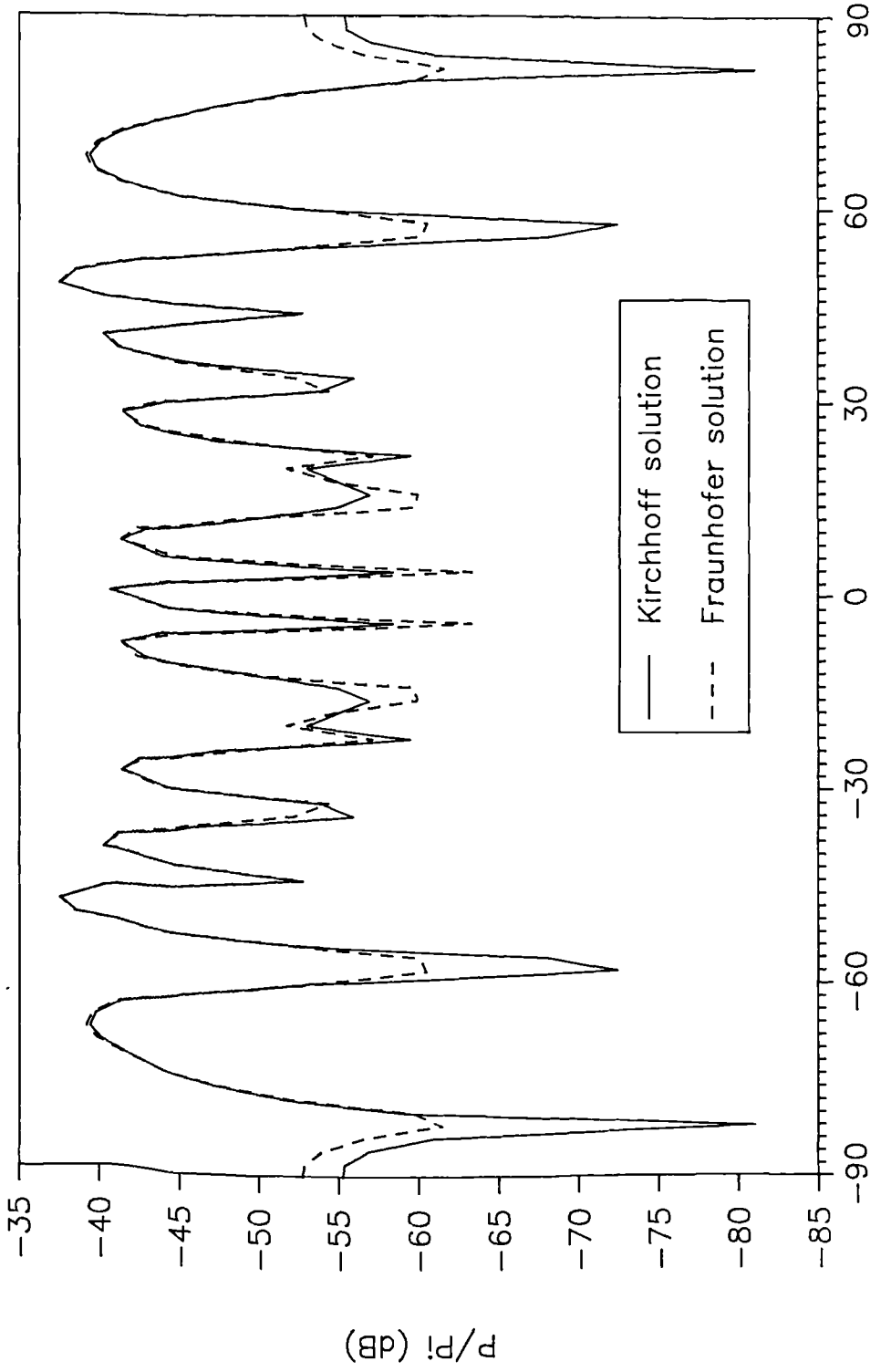

Figure 6.25. Fraunhofer solution and Kirchhoff solution for receiver positions in the far field. Receiver radius 50 m. 3.5 KHz.

of the surface pressure distribution decreases, hence the number of elements increases and so does the computation time. A guide as to the typical prediction time on a IBM 486 compatible PC for the N=7 simulated concert hall diffuser is given below in Table 6.1.

6.8 Conclusions

The performance of quadratic residue diffusers has been predicted successfully with a range of theoretical prediction methods encompassing a range of approximations and computation times. The cross correlation measurement systems provided accurate measurements of the scattering from both the CDD and QRD.

The **thin panel limit** solution allows exact representation of the panel shape. It is accurate and works both above and below the cut-off frequency of the wells. Computation time is long and so this theory can not be used above the middle frequency range (3 KHz).

The **3D boundary integral method** uses the simple phase change local reacting admittance approximation. It provides good accurate predictions faster than the thin panel limit solution. Accuracy decreases as the receiver position moves away from the geometric scattering angle. For applications in auditoria the accuracy should be perfectly satisfactory. The cut-off frequency, above which the local reacting admittance assumptions breaks down, was higher than expected

Table 6.1 Comparative computation times per frequency for different frequency ranges and theoretical prediction methods. Times shown for N=7 QRD.

Frequency range (KHz)	Solution method	Number of elements	Approximate computation time
<2.9	Thin panel limit	432	1 hour
	3D Boundary integral method	200	15 minutes
	Kirchhoff approximate	-	2 minutes
	Fraunhofer	-	a few seconds
<5.6	Thin panel limit solution	565[1]	2 hours
	3D Boundary integral method	336[1]	1 hour
	3D Boundary integral method	756	9½
	Kirchhoff approximate	-	15 minutes
	Fraunhofer	-	a few seconds
<8.7	Thin panel limit	767[2]	4 hours
	3D Boundary integral method	768[1]	10 hours
	Kirchhoff approximate	-	15 minutes
	Fraunhofer	-	a few seconds

[1] Back and top of diffuser not represented
[2] Back, top and sides of diffuser not represented

($\lambda_{min} < .6w$, where w is the well width); this indicates that the quadratic residue diffuser works to a higher frequency than commonly quoted [Schroeder 1979, D'Antonio 1984].

The **Kirchhoff approximation solution** also works well, except at low frequencies, below about 2.5 KHz. Above 2.5 KHz, the accuracy is generally as good as that found for the 3D boundary integral method solution. Below about 2.5 KHz, the failure to account for the mutual interactions across the surface reduces the accuracy of the predictions. The accuracy of this Kirchhoff approximate solution is better than for the plane panel at large scattering angles due to the influence of the surface admittances. This theory is much quicker than either of the two previous more exact theories.

The **Fraunhofer solution** method does not work at low frequencies, below about 2.5 KHz, due to the failure of Kirchhoff's approximate surface pressures. Above 2.5 KHz, however, the method does give accurate predictions of the scattering from the narrow diffuser even when the receiver is only a couple of metres from the panel. It is less successful with the wider diffuser of those tested due to inaccuracies caused by the far field approximation. Even so, although the local minima and maxima are not well predicted, the overall shape of the scattered field is. This is by far the fasted prediction method taking only a few seconds to predict the scattering at any one frequency.

The lower frequency limit for QRDs was found to be lower than expected. The limit is defined as the frequency below which the wells are shallow

compared to wavelength, and the diffuser behaves like a plane panel. For the N=7 simulated concert hall diffuser the wavelength of the limit was about 11 times the maximum well depth. This compares to the 5 times the maximum well depth expected [D'Antonio 1984, Schroeder 1979].

Chapter 7

The Scattering Performance of Diffusing and Reflecting Surfaces

7.1 Introduction

So far this thesis has been concerned with methods to measure and predict the sound scattered from surfaces, without discussing the merits of the scattering produced. In this chapter the performances of plane panels, curved panels and quadratic residue diffusers will be compared. First the merits of the QRD when compared to the original design concept of Schroeder will be considered.

The graphs in this chapter have had the scattering at all receiver positions, normalized to the incident sound at a single receiver position. This is done so the line of constant scattering with receiver angle, is of constant magnitude. More details on the displaying of graphs can be found in Section 2.6.

7.2 The Scattering Performance of Quadratic Residue Diffusers

7.2.1 'Optimum' Diffusion

The design principle of the QRD was that the Fourier transform of the exponentiated quadratic residue sequence is a constant. As this Fourier transform of the 'surface profile', represents the scattering field at infinity (a standard result of Fourier optics [Ghatak 1979]), such a surface should produce 'optimum' diffusion [Schroeder 1979]. As Schroeder shows, this is only achieved under several approximations:

1. No radiation coupling between the wells.
2. No radiation impedance for each individual well.
3. Orthogonality of the diffraction along the length and across the width of the diffuser.
4. Source and receiver in the far field.
5. Perpendicular receiver.

In Chapter 3, under approximations 1 to 4 above, the expression for the scattered pressure, $P_s(\underline{r})$, from a surface with a variable admittance was derived. If the surface admittance is characterized by a space dependant reflection factor $R(\underline{r}_s)$, it was shown that the scattered pressure is given by:

$$P_s(r) = \frac{-ikP_i}{4\pi}\frac{e^{-ik(r+r_0)}}{rr_0}(COS(\theta)+1)\int_S\int R(\underline{r}_s)e^{-ikr_sSIN(\theta)}ds \qquad 7.1$$

Figure 3.1 gave definitions of the vectors and angles. The two quantities of most interest here are θ which is the receiver angle and $\underline{r}_s$ which is the vector along the surface. Using the orthogonality approximation (3) Equation 7.1 can be simplified as:

$$P_s(r) = \frac{-ikP_i h}{2\pi}\frac{e^{-ik(r+r_0)}}{rr_0}(COS(\theta)+1)\int_{-a}^{a} R(\underline{x}_s)e^{-ikx_sSIN(\theta)}dx_s \qquad 7.2$$

where x_s is the surface vector in the x direction.

Using the representation of the QRD discussed in Section 6.4.2, $R(\underline{r}_s)$ is the phase change due to plane waves propagating up and down each well. In other words, the exponentiated quadratic residue sequence. It can be seen that Equation 7.1 only matches the Fourier transform of the exponentiated quadratic residue sequence under the condition $kx_sSIN(\theta) \rightarrow kx_s$. This is approximation (5) above, the requirement for a perpendicular receiver. Therefore, when looking at the scattering from a QRD as a function of receiver angle, the scattering will not be uniform. This is because the approximations behind Schroeder's design are ideals which are never achieved, a point Schroeder made himself.

When attempting to assess the performance of the QRD, two criteria will be considered:

1. The Fraunhofer diffraction solution, given by Equation 7.1 above. This will be taken as a first approximation to best uniform scattering achievable by a diffuser constructed of wells.
2. True optimum diffusion, i.e. scattering independent of receiver angle.

Two diffusers will be considered here. The first is a narrow diffuser based on a single period N=7 sequence. The second was wider, had many more deeper wells, and was based on two periods of N=11. Both are roughly 1:5 scale models. Section 6.3.3 gave more details about these diffusers.

7.2.2 QRD performance compared to Fraunhofer solution

For the N=7 diffuser it was found that there was a good match between the accurate thin panel limit solution and the Fraunhofer solution for most frequencies. The only exception was at low frequencies, below about 2.5 KHz. Here the mutual interactions on the surface of the diffuser reduced the accuracy of the predictions. At these low frequencies, however, the degree of diffusion produced by the accurate thin panel solution is not particularly worse than for the Fraunhofer solutions. This is illustrated in Figure 7.1 at 2 KHz. So at all frequencies tested, up to 8.5 KHz, altering the diffuser shape of the N=7 diffuser is not needed to improve the diffusion produced when compared to the Fraunhofer solution.

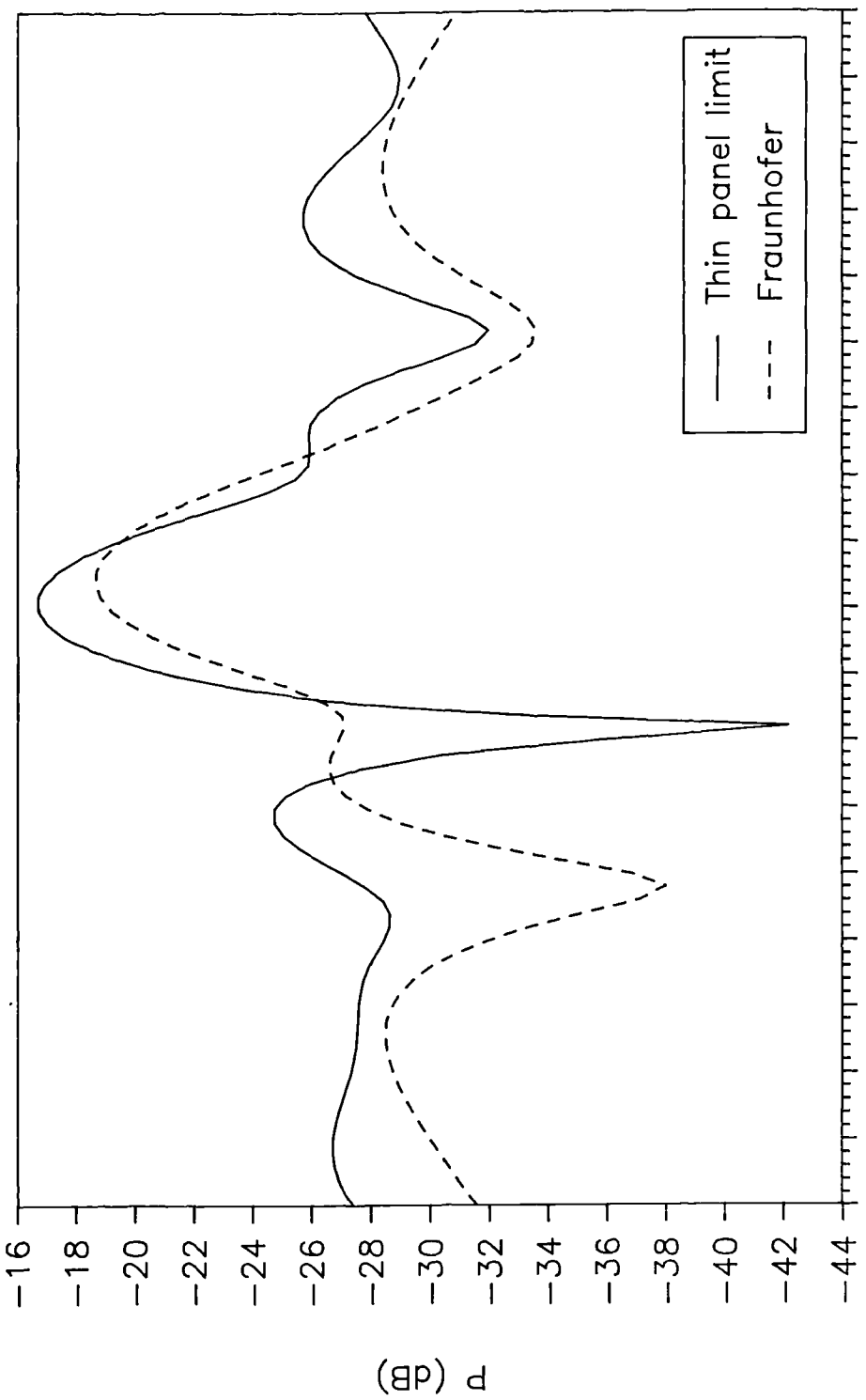

Figure 7.1. Comparison of degree of 'diffusion' produced by accurate thin panel limit solution and Fraunhofer solution methods. N=7 QRD at 2 KHz.

For the N=11 diffuser the Fraunhofer solution method was much less satisfactory. As discussed in Chapter 6, the reason for the break down in the Fraunhofer prediction method was the larger width of the diffuser. This resulted in the receiver not being in the far field. It was suggested by Schroeder [Orlowski 1989] that by bending the diffuser into a concave shape, it would be possible to focus the far field Fraunhofer image at a near receiver. This is analogous to the use of lenses or mirrors in telescopes and other optical equipment to focus images. This is illustrated in Figure 7.2a. When attempting this approach, instead of bending the diffuser we modulated the well depths by the shape of a concave parabolic mirror. This is illustrated in Figure 7.2b. It was felt that bending a QRD would be prohibitively expensive for manufacture, and so this well modulation would be much more useful to acousticians. It was found that the far field picture could be reproduced at a 'close' receiver position (2.5m) with the well modulated QRD. An example is given for 3.5 KHz in Figure 7.3. Unfortunately, this approach is not necessarily of great use in practical auditorium design. Consider the near field and simple theory pressure distributions as shown in Figure 7.3a. It can be seen that although there is not a great match between the two theories for the detailed 'local' maxima and minima, the overall shape is very similar. As one set of maxima and minima are not to be preferred over another set; the bending of the diffuser does not necessarily represent an improvement on the amount of diffusion produced by the original design. The only advantage is that it improves the predictability of the diffracted pressure distribution.

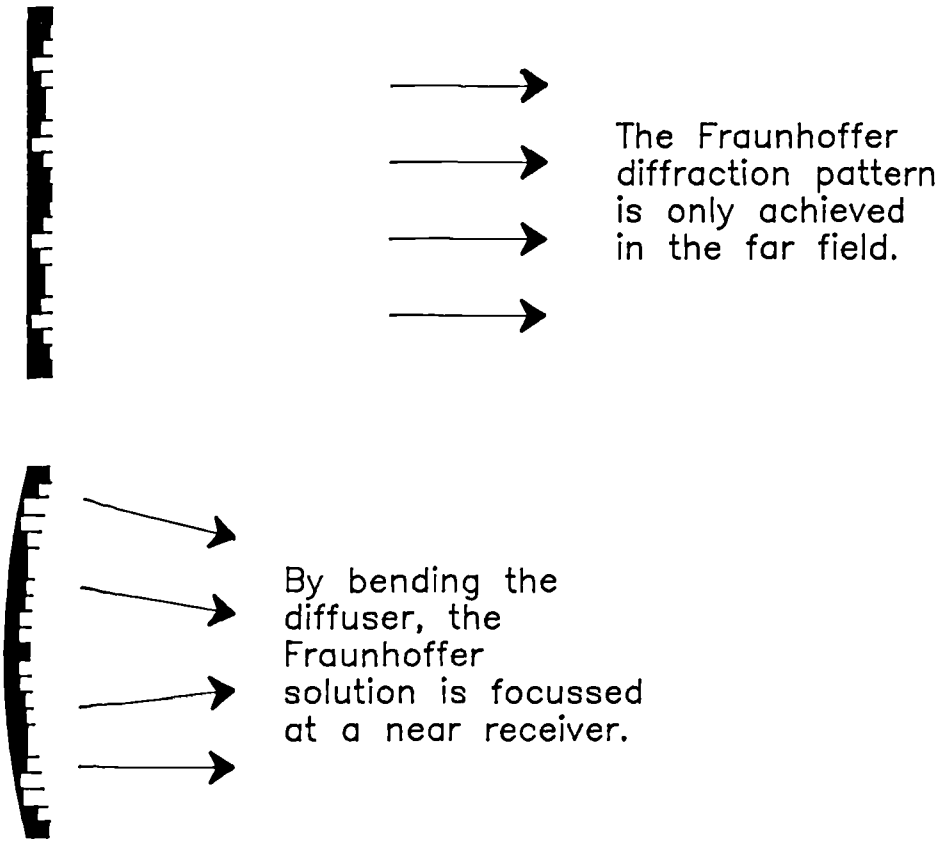

Figure 7.2b. Focussing the Fraunhoffer diffraction field at a near field receiver by bending diffuser.

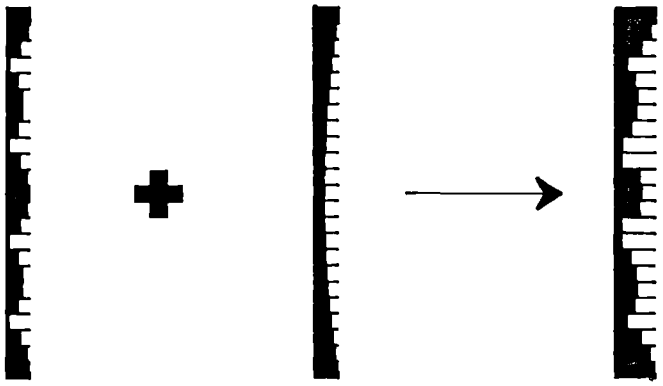

Figure 7.2b. Instead of bending the diffuser, modulating the QRD depth sequence with a curved surface has a similar effect.

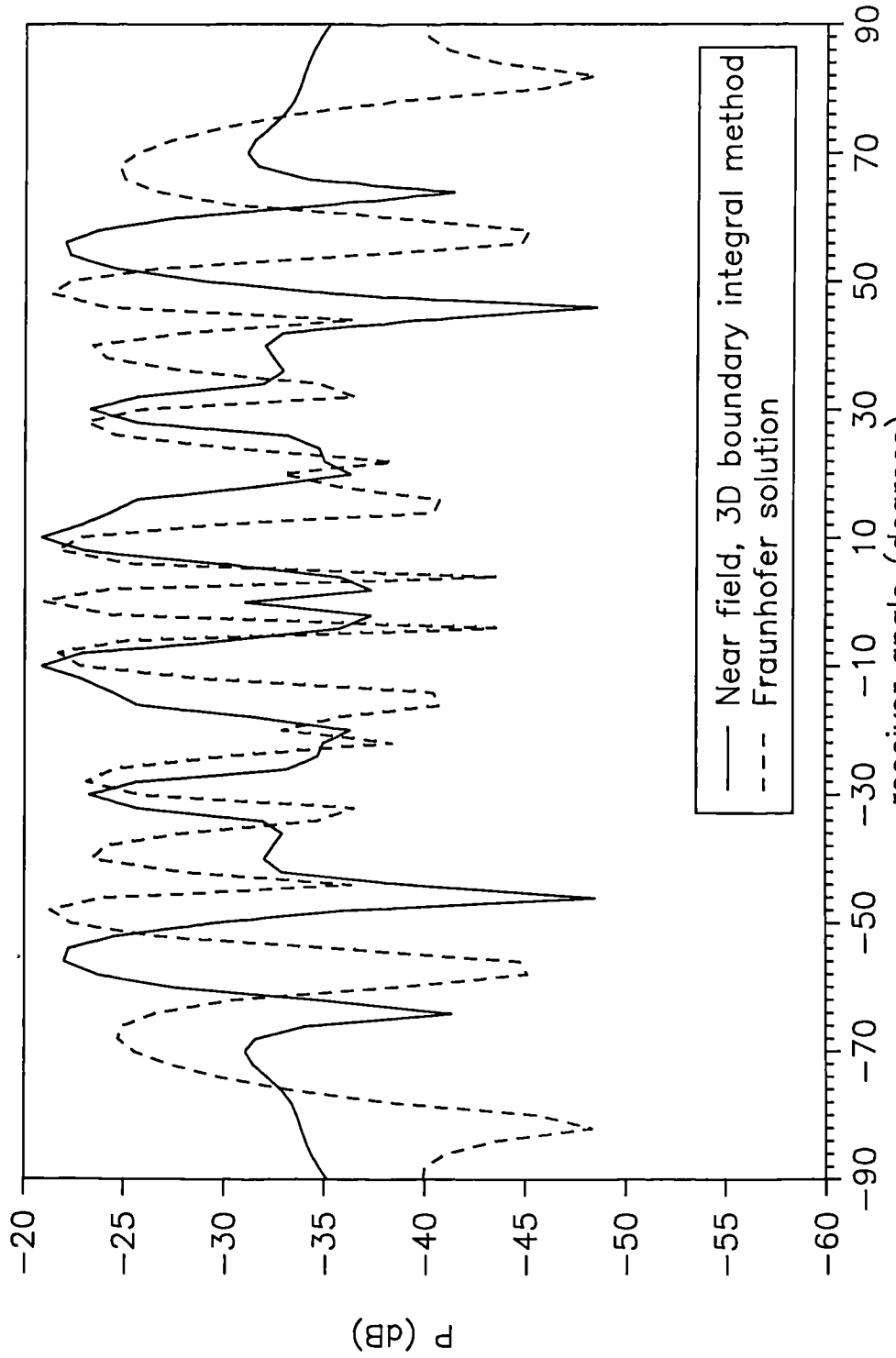

Figure 7.3a. Comparison of near field scattering from N=11 QRD with Fraunhofer solution. 3.5 KHz.

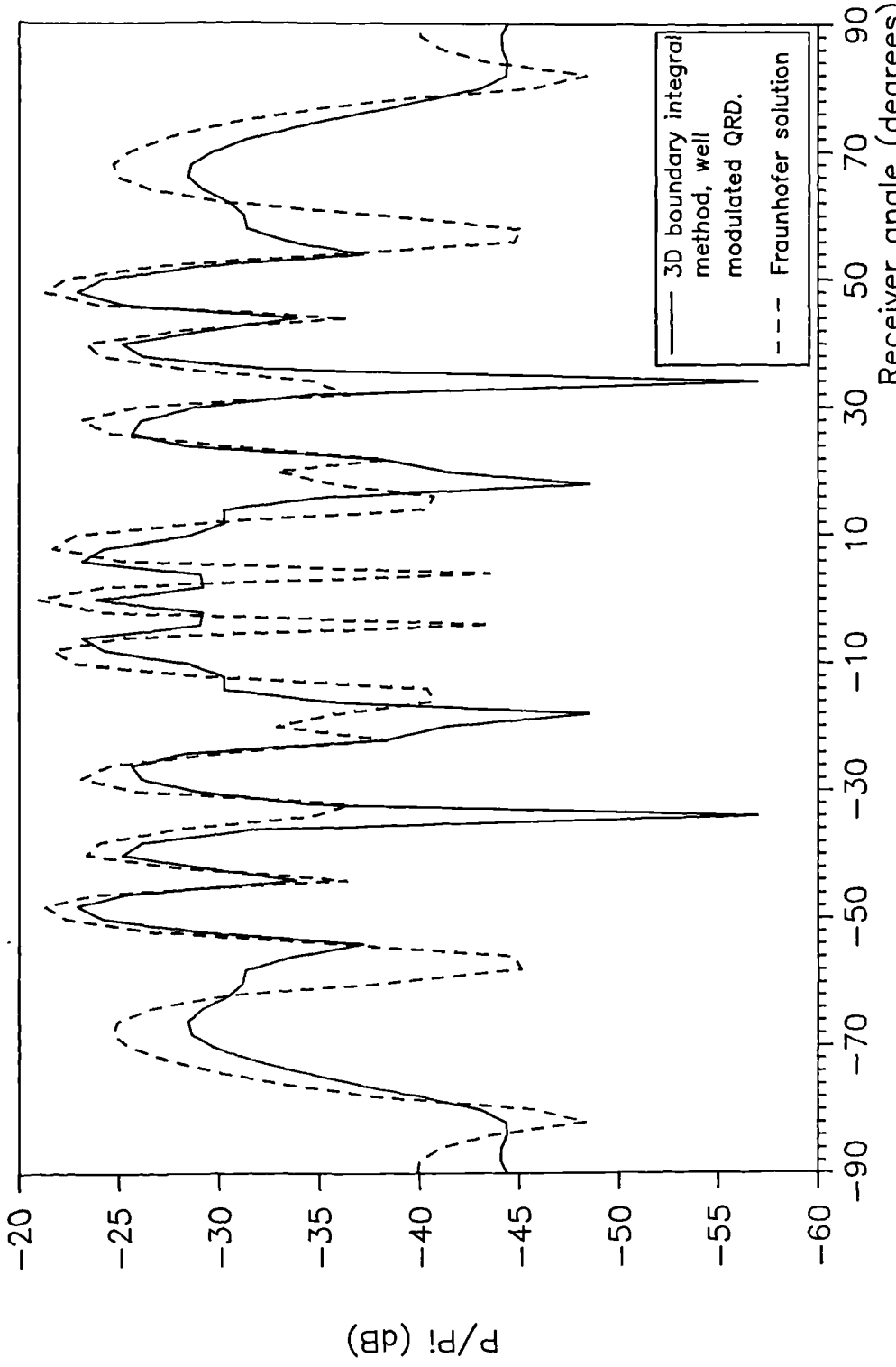

Figure 7.3b. Scattering from well modulated N=11 QRD, compared with Fraunhofer far field solution. 3.5 KHz

7.2.3 QRD performance compared to uniform scattering

The scattering performance of the QRD was also tested against scattering independent of scattering angle. In Figures 7.4 and 7.5 comparative examples are shown for both the N=11 and N=7 diffusers at 2 KHz and 6.5 KHz. As the diffusers were different sizes the magnitude of their scattering was different. Consequently these graphs have been rescaled to allow direct comparison of the overall shapes. Superimposed is the line of scattering independent of angle. At low frequencies, below about 4 KHz, the diffusers conform best to the uniform diffusion producing reasonable scattering to the sides. An example is shown in Figure 7.4. As the frequency increases the amount of scattering to large angles decreases. This can be seen in Figure 7.5. The N=11 diffuser tends to scatter more sound to the sides than the N=7 diffuser. It is noted, however, that N=11 diffuser is three times as wide as the N=7 diffuser and this is a likely cause of the difference.

7.2.4 Performance of a QRD for an oblique source

Predictions were also done for one oblique source position (60°). For frequencies below about 5 KHz the overall scattering pattern is very similar to that for the on-axis source, although the minima and maxima are not always in the same position. An example is shown in Figure 7.6 at 2.5 KHz. Above 5 KHz, however, the amount of diffusion is different to the normal incident case. The scattering is less uniform. An example is shown in Figure 7.7 at 8.5 KHz.

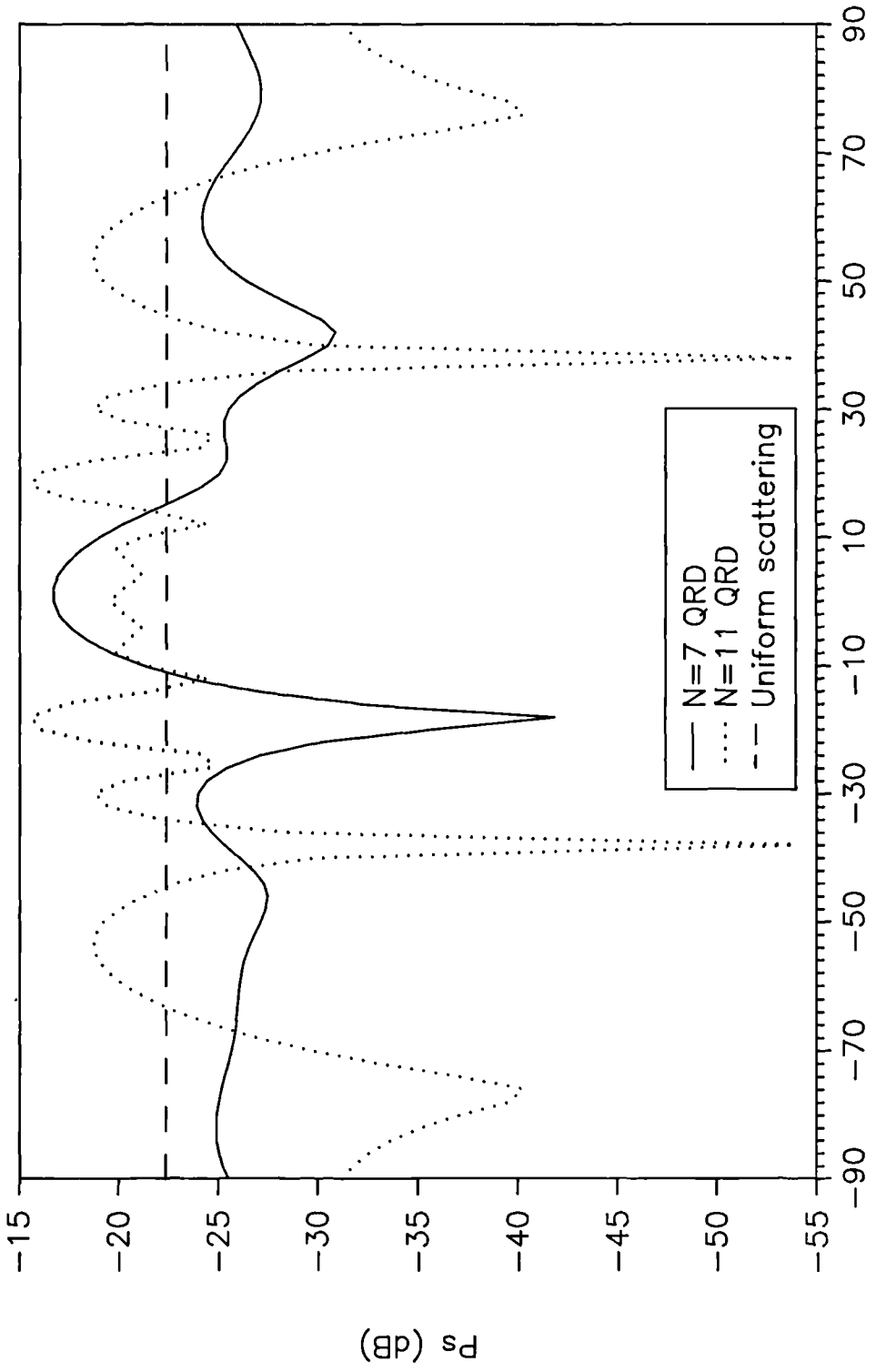

Figure 7.4. Performance of two QRDs compared to uniform scattering. Scattered field at 2 KHz.

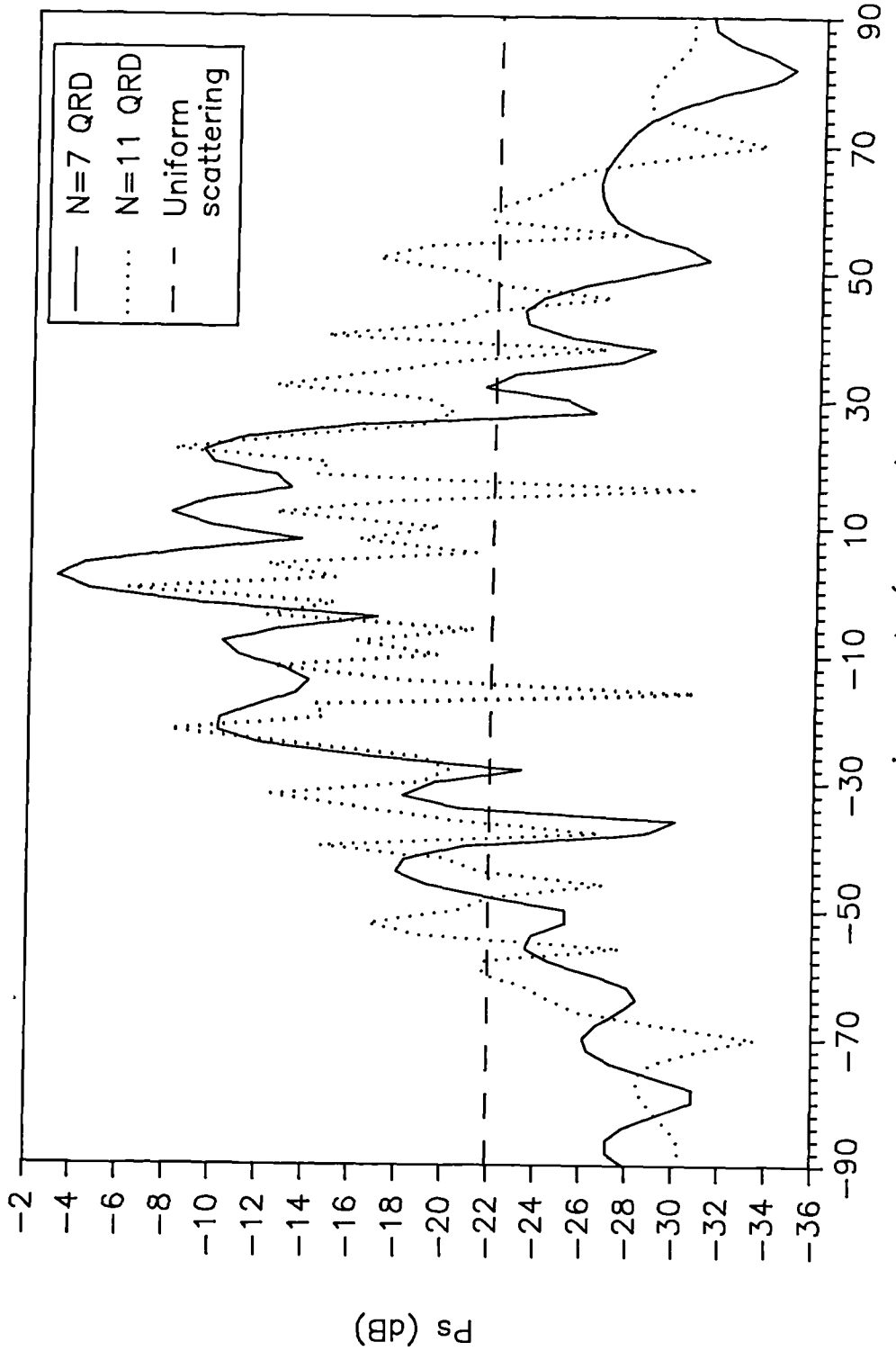

Figure 7.5. Performance of two QRDs compared to uniform scattering. Scattered field at 6.5 KHz.

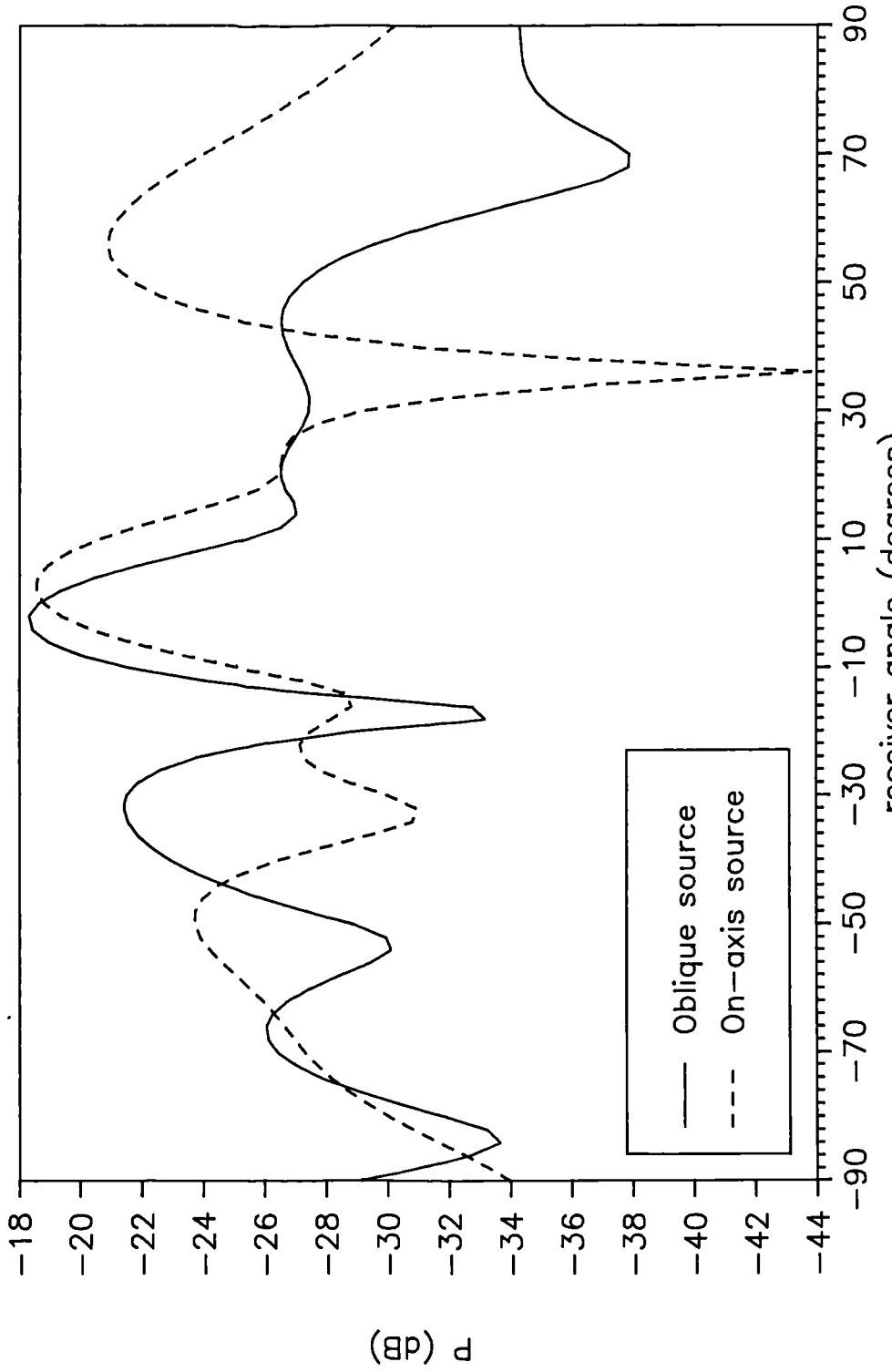

Figure 7.6. Comparison of scattering from N=7 QRD for normal incidence sound and oblique incidence sound. 2.5 KHz.

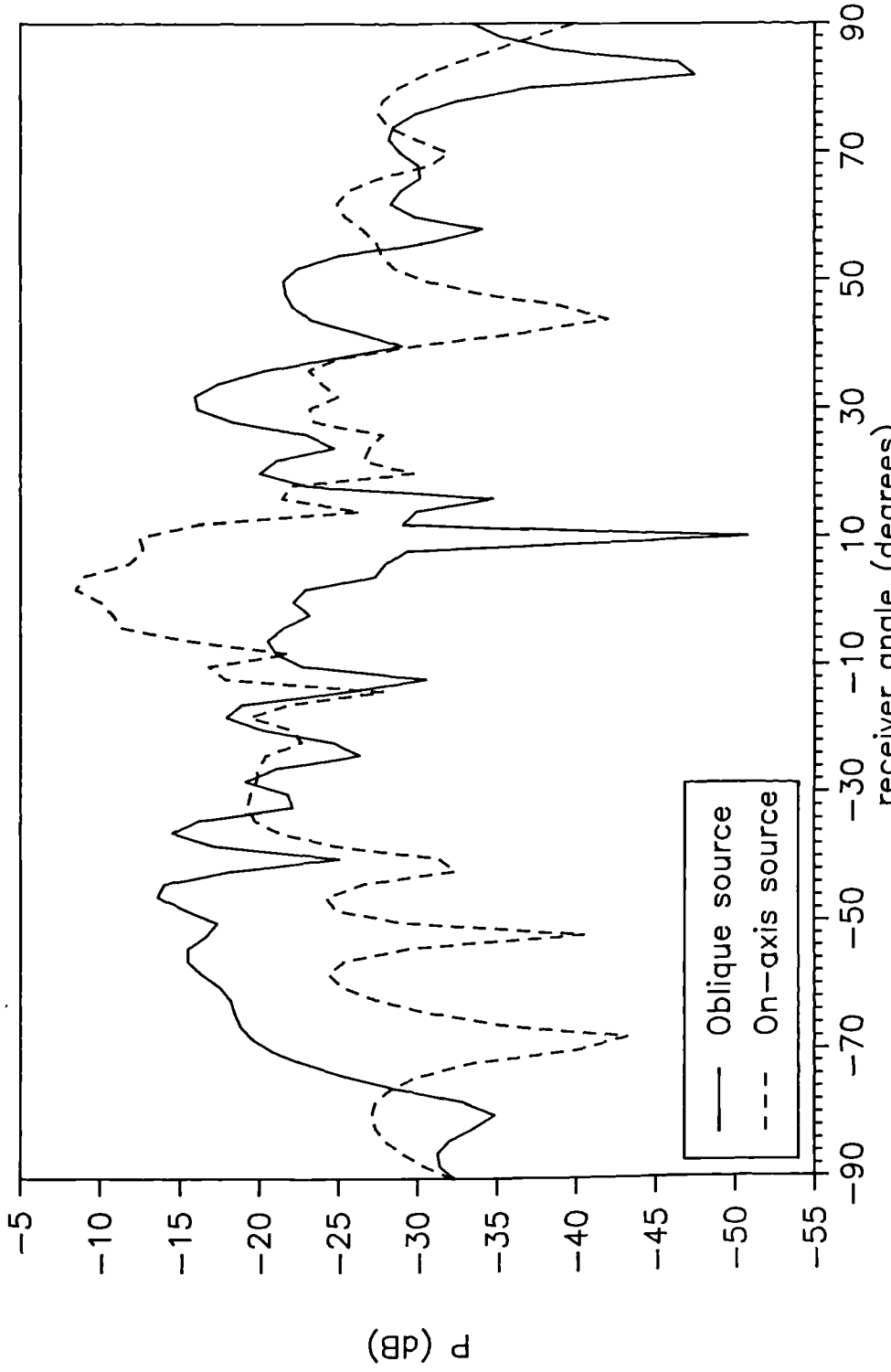

Figure 7.7. Scattered pressures from N=7 QRD for normal incidence source, and oblique incidence source. 8.5 KHz.

7.3 The Relative Performance of Diffusers and Reflectors

7.3.1 Scenario for comparing diffusers and reflectors

As shown in Chapters 4 to 6, this study has developed methods which can accurately predict the scattering from surfaces. So to test the relative merits of the diffusing and reflecting surfaces comparisons could be done using theoretical predictions only.

The problem was considered where an acoustician wants a fixed size of diffuser or reflector, but needs to know the correct surface treatment to use. The surface could be:

1. A quadratic residue diffuser.
2. A plane reflector.
3. A cylindrically curved reflector.

The simulated concert hall diffuser is a single period quadratic residue diffuser based on N=7 as described previously in Section 6.3.3. The plane panel and cylindrical curved panel were of the same overall size as the QRD. A diagram of sections through the panels can be seen in Figure 7.8. The curved panel had a radius of .78m, about twice the panel width of .412m and was described in Section 5.2.1. A survey carried out by the author of sections through various concert halls, showed that this radius to width ratio lies within the range

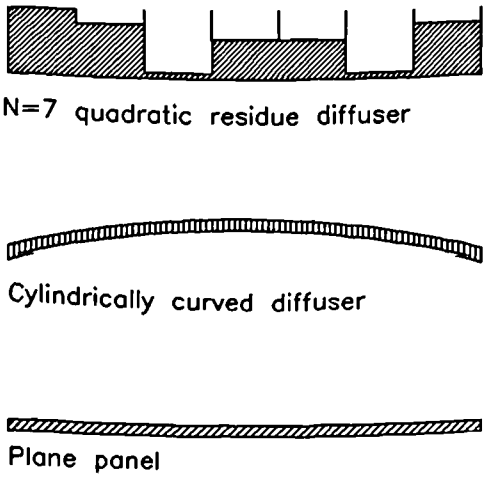

Figure 7.8. Sections through the three surfaces tested.

typically found in auditoria. The plane panel was described in 4.2.3. With the size of panels tested, these were approximately 1:5 scale models. Computational time limitations when doing predictions for the QRD determined the frequency range tested. The panels were tested to 8.5 KHz or 1.7 KHz full scale.

7.3.2 Normal incidence case

In Figures 7.9 and 7.10 two examples are given of the scattered field from the three surfaces at 1.5 KHz and 7.5 KHz. The plane panel gives less uniform scattering than either of the other two panels at all frequencies. The scattered field also has much more pronounced minima and maxima, particularly the central maxima at high frequencies. The result is hardly new; acousticians tend to avoid plane reflectors in concert halls as these can produce strong specular reflections which can lead to echoes. This is particularly true from highly directional instruments such as trumpets.

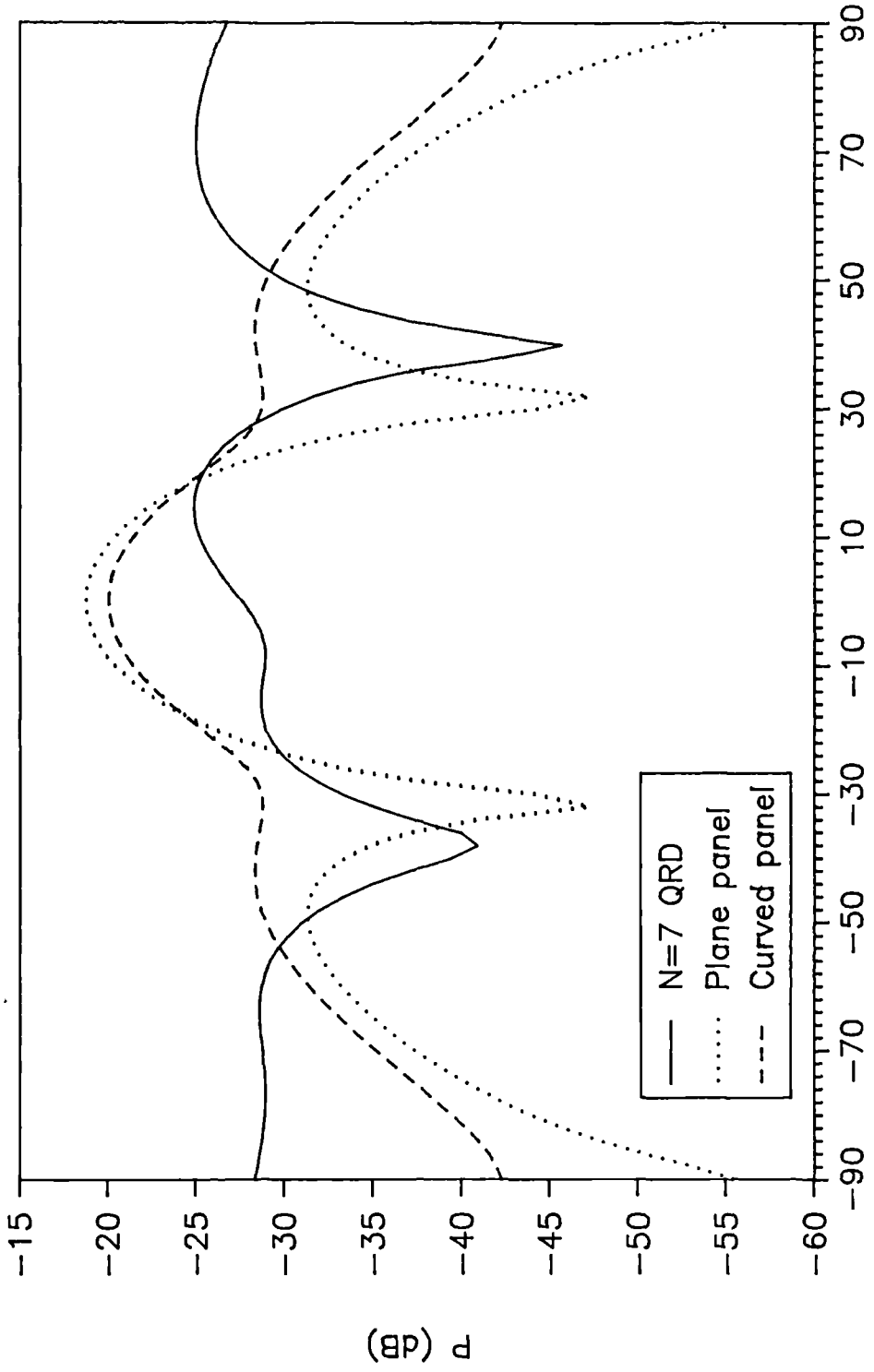

Figure 7.9. Comparison of scattering performance of three surfaces at 1.5 KHz

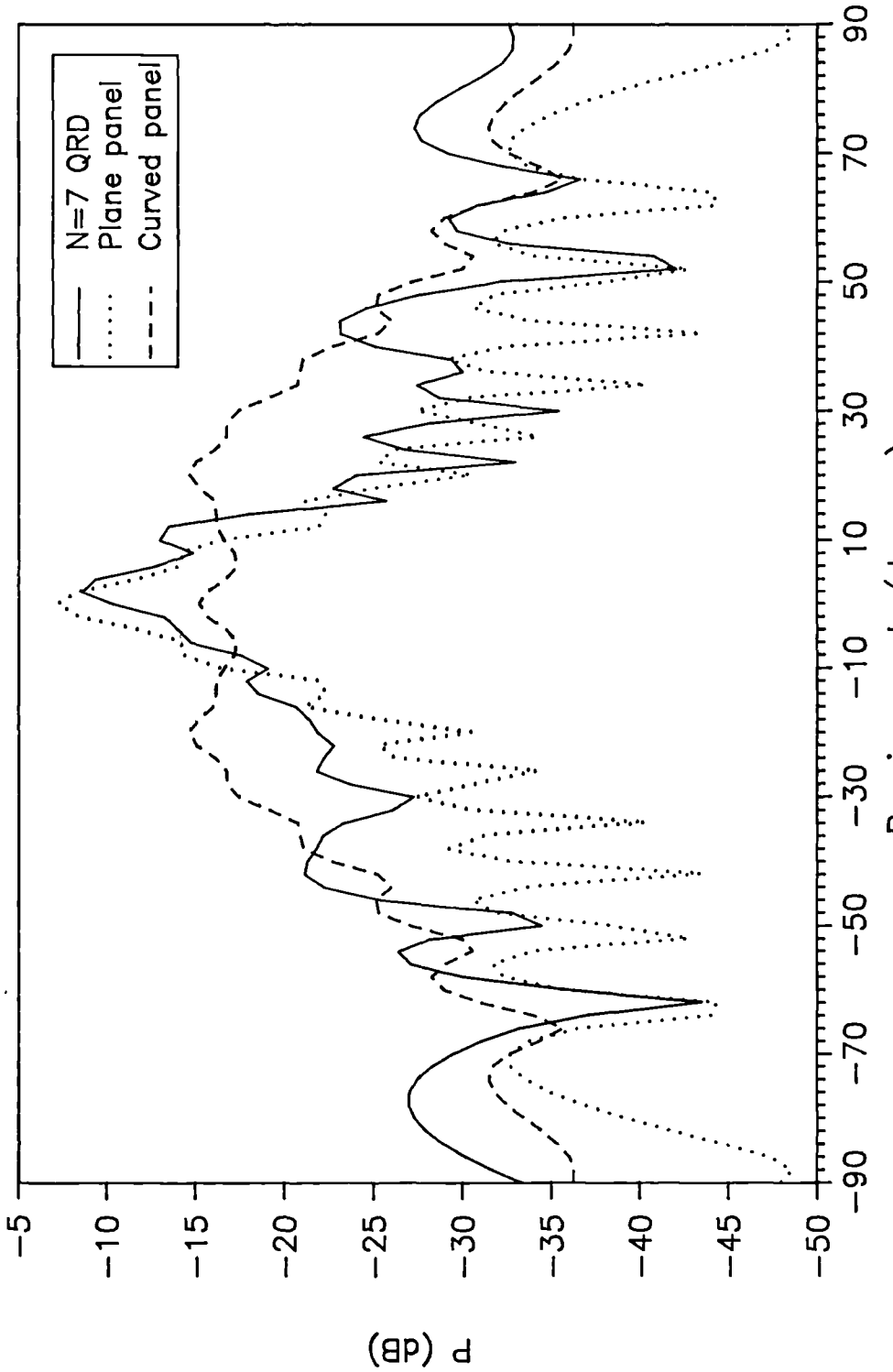

Figure 7.10. Comparative scattering performance of three surfaces at 7.5 KHz. On-axis source.

Overall there seems to be little to distinguish the relative performances of the curved panel and the Quadratic Residue Diffuser. Below about 3.5 KHz the QRD does produce more scattering to large angles, but at the expense of having large minima at some receiver positions. Above 3.5 KHz the amount of scattering away from the normal direction is similar for both panels. However, the QRD again has many more, well defined minima and maxima. Although these minima and maxima will be less pronounced if the ⅓ octave spectrum is considered. As illustrated in Figure 7.9, a particular problem for the QRD at high frequencies is that the central maximum is large and similar to the central lobe for the plane panel. Hence, there seems to be a risk of strong specular reflections from QRDs at high frequencies, which might lead to echo problems. If the construction of the QRD and curved panel are compared, Figure 7.8, it can be seen that the maximum 'depth' of the curved panel (28 cm) is of similar order to the maximum depth of the QRD wells (35 cm). So for the same overall size in all dimensions, and for on-axis incidence, it is possible to achieve better diffusion with the curved panel above 3.5 KHz or 700 Hz full scale.

7.3.3 Oblique incidence

The case of an oblique source at an incident angle of 60° was also tested. Here the relative performances of the diffusers were much different to the on-axis receiver case. Examples are shown in Figures 7.11 and 7.12 at 3 KHz and 5 KHz respectively. At low frequencies, below about 3 KHz, the curved panel does not perform a great deal better than the plane panel, although it does have

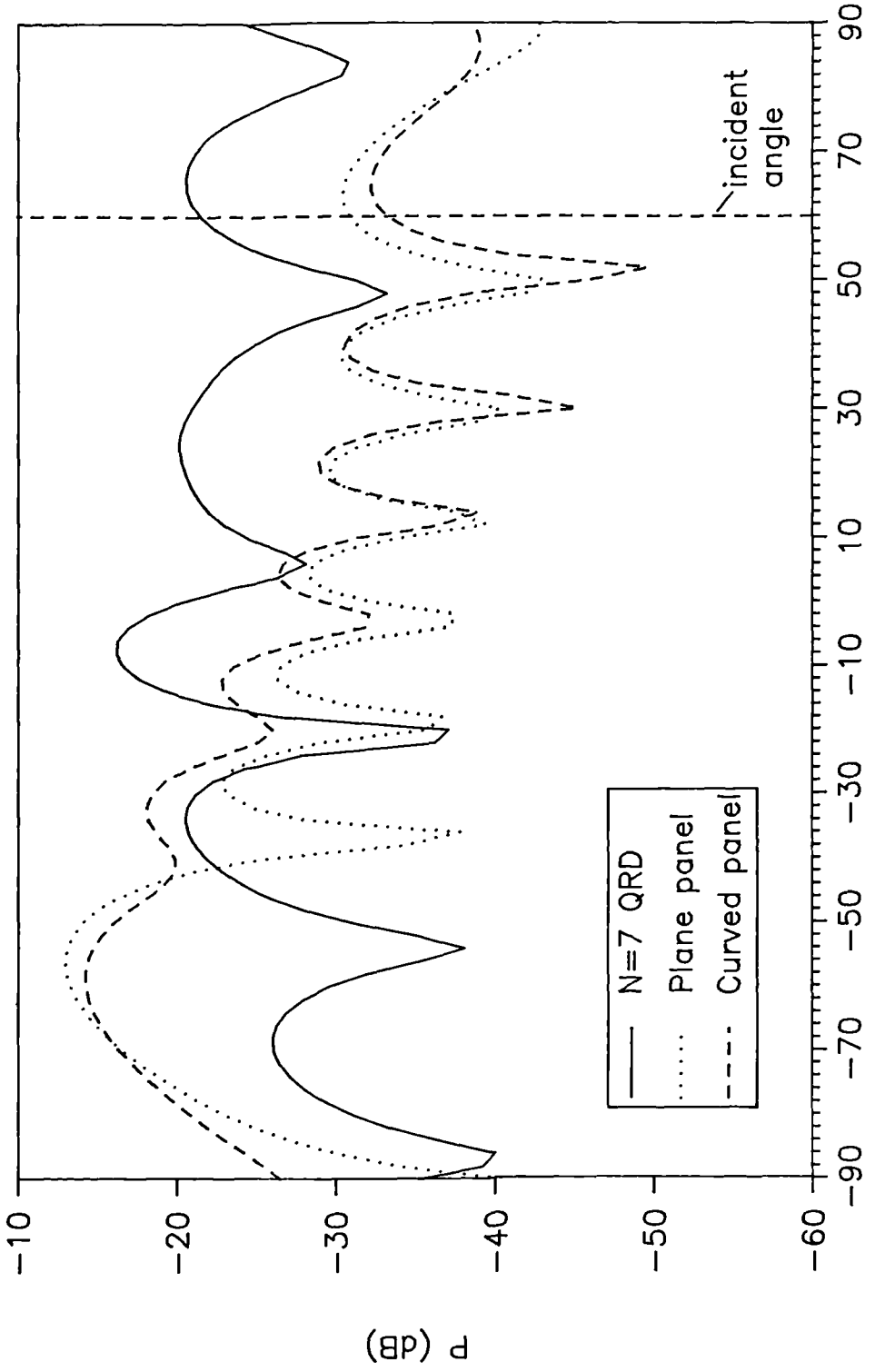

Figure 7.11. Scattering performance of three panels for off-axis source. 3 KHz.

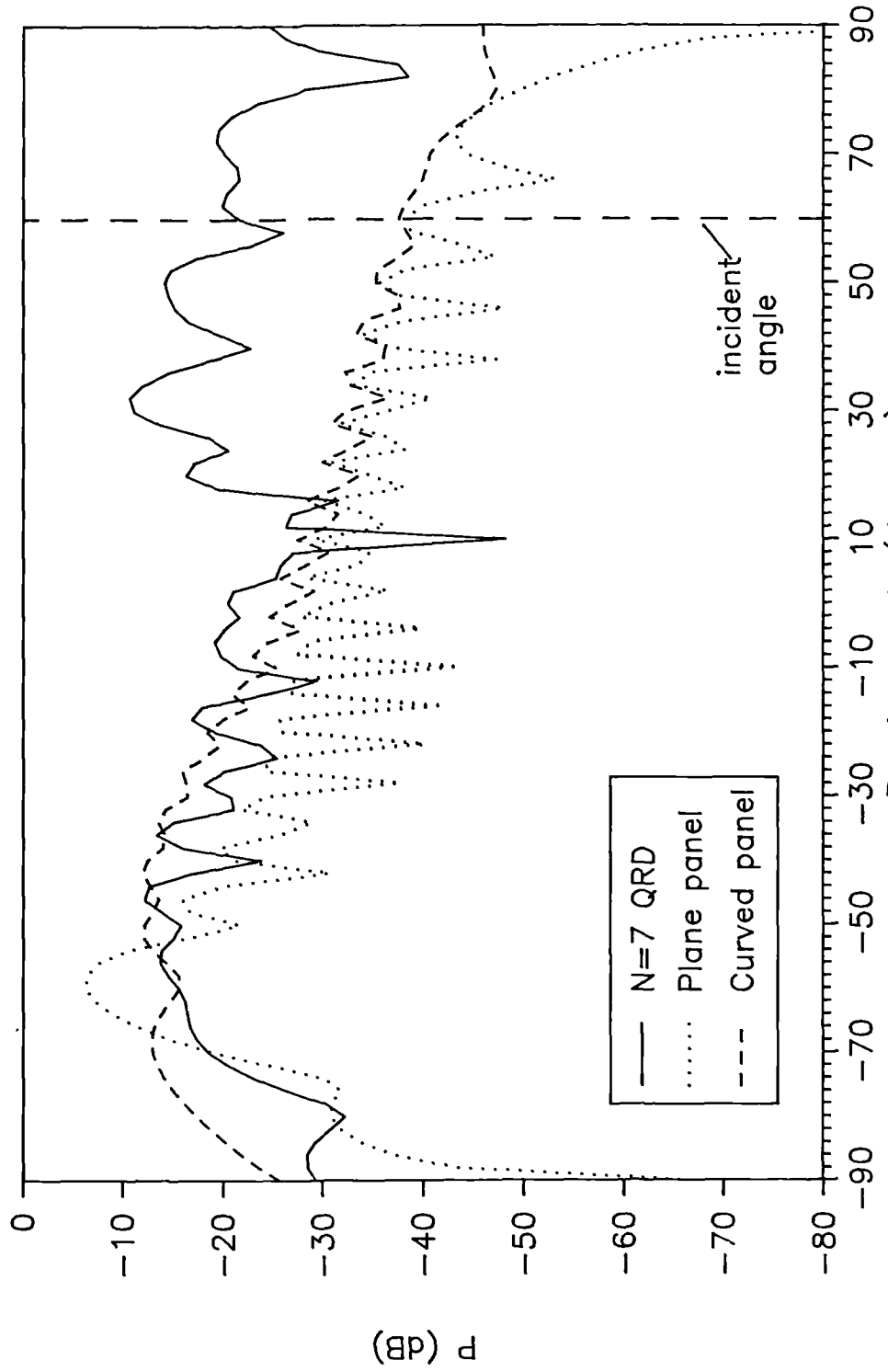

Figure 7.12. Scattering performance of three surfaces for an off-axis source. 5 KHz

a slightly smoother scattered field pattern. At higher frequencies the curved panel does produce more diffusion than the plane panel, but the scattering is far from uniform. At all frequencies tested, the QRD out performs both the other panels producing much more uniform scattering. This is even true at high frequencies where the QRD's scattering becomes less uniform. At high frequencies the scattering from the QRD avoids the large central lobe which occurred with a on-axis source. In this respect the scattering performance from the QRD is improved.

7.4 Conclusions

The scattering performance of the QRD was tested. The degree of diffusion is roughly the same as predicted by the simple Fraunhofer theory. The Fraunhofer theory was the basis behind Schroeder's design [1979]. However, this scattering is far from optimum diffusion as defined by uniform scattering into all angles. Better diffusion is produced at lower frequencies, below about 3.5 KHz whatever the angle of incidence. For normal incidence and at high frequency, the QRD produces a large central lobe which might lead to echo problems. This large central lobe is not seen for oblique incidence.

The relative performances of reflectors and diffusers were tested. The plane panel produced the worst diffusion. There is little difference in performance between the QRD and the cylindrical diffuser for an on-axis source. At low frequencies, below about 3.5 KHz, the QRD produces more uniform

scattering. At high frequencies the cylindrical diffuser has fewer, less prominent, minima and maxima in the scattered pressure field and the amount of diffusion is comparable to the QRD. Therefore, when a near on-axis source can be guaranteed, as might be the case for reflectors over the stage area, the curved diffuser is a better solution than the QRD. This is true because of the higher construction costs of the QRD.

In contrast, For an off-axis source, the QRD produces much more uniform diffusion at all frequencies.

Chapter 8

The Subjective Measurement System

8.1 Introduction

The subjective tests measured the smallest change in the early sound field which could be perceived by listeners. The early sound field is the section of the impulse response most influenced by the positions and orientations of diffusers and reflectors. (The early sound field is defined as the first 80 ms after the arrival of the sound direct from the source).

In this chapter the system used for the subjective testing is described. Care was taken so that not only did the simulated field sound natural subjectively, but also that standard objective parameters were all within reasonable ranges. The reverberation time; early decay time; centre time; early lateral energy fraction; and the A-weighted sound pressure level of the simulated sound field were sensible values when compared to measurements in actual halls and to subjective measurements done by others to determine preferred values.

Our test system used a completely artificial sound field created as follows. An anechoic music source from a compact disc was split into a number of signal

channels. These were fed through various delay units, reverberation units and attenuators before being reproduced by an array of loudspeakers in an anechoic chamber. Altogether, this arrangement generated a direct sound, nine early reflections whose delay and level could be altered, plus reverberation whose decay time, delay and level could also be altered. The impulse response is shown in Figure 8.1. This simulation technique was not new, it has been used by many investigators for example [Reichardt 1966 1967 1975 1981, Barron 1974, Blauert 1986a-c, Ando 1977 1979]. The various merits and drawbacks of different types of simulation system are discussed in Section 8.2. The rest of the chapter is devoted to describing our simulation system in detail.

8.2 Experimental Systems for Subjective Testing

There are many experimental methods for determining subjective preference in auditorium acoustics. These range from tests carried out in real concert halls with full orchestras, to laboratory tests using artificially simulated sound fields created in an anechoic chamber. This investigation used the later approach. The range of techniques used by previous experimenters reflects the differing advantages and disadvantages offered by the methods.

The advantages and disadvantages of using an artificial simulation system can be summarized as:

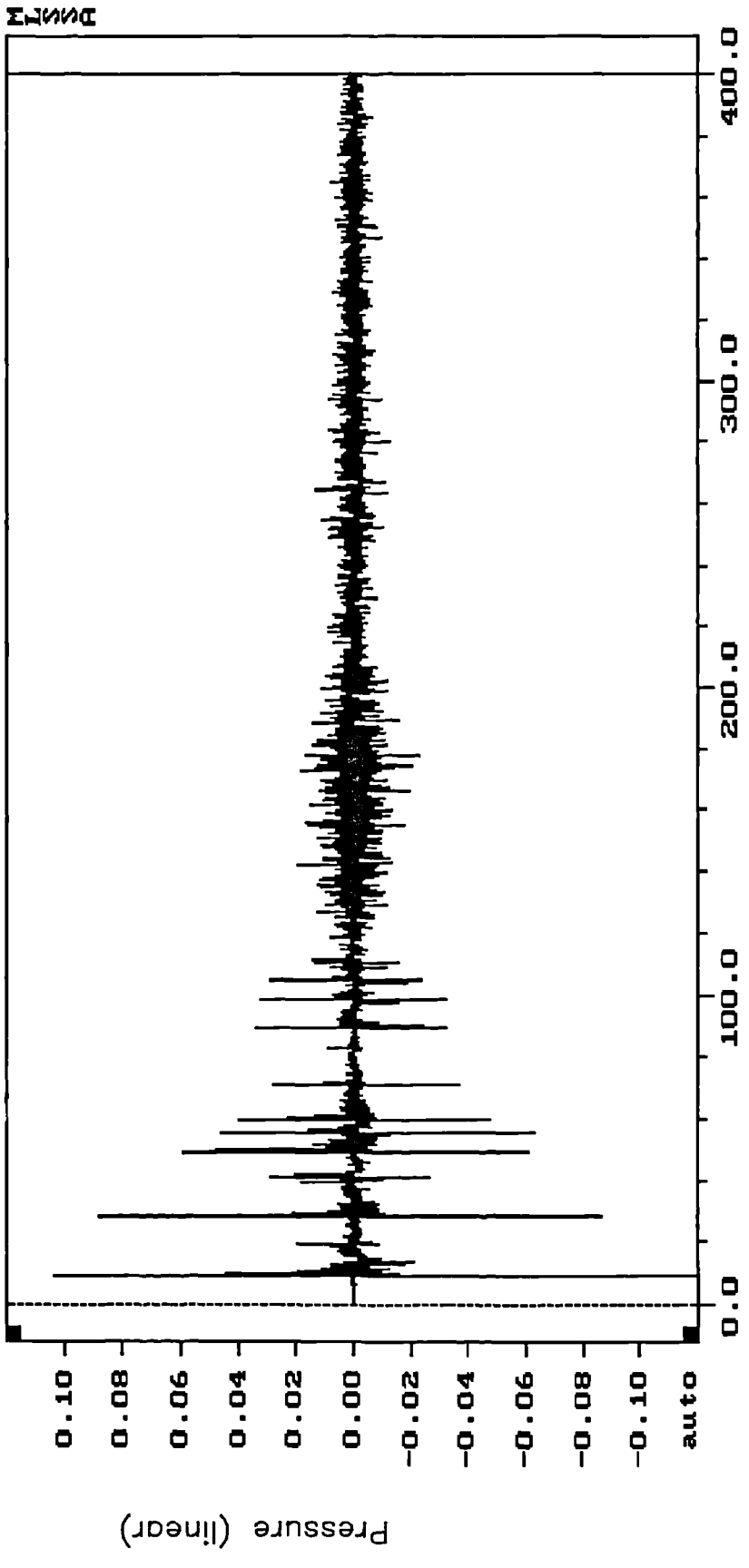

Figure 8.1 The simulator impulse response.

Advantages:

1. Complete control over the sound field.

2. Subjects can make immediate comparison of sound fields.

Disadvantages:

3. Too few reflections in the early sound field.

4. The orchestra being represented by a single loudspeaker.

5. No visual clues of the distance to the stage.

6. No orchestra for listeners to empathise with.

7. The visual clues given by location of the loudspeakers.

These advantages and disadvantages are all discussed in detail in the next few paragraphs.

1. The complete control over the simulated room's impulse response is the system's main merit. In particular, it allows a single subjective effect to be changed on its own. In contrast are the experiments carried out using existing concert halls [Gottlob 1973, Schroeder 1974, Barron 1988, Berlin group (see Cremer 1982 pages 593-605)]. These have many subjective effects varying simultaneously. Consequently, factors of lesser significance are difficult to evaluate as their effects will be swamped by other more obvious factors. For example, nearly all subjective tests where the operators can alter the overall volume level, are done with sound pairs of equal loudness. Otherwise it is found

that subjects judge almost solely on loudness and not on other factors [Cremer 1982 page 584].

2. The ease with which our system can be changed allows immediate direct comparisons between different sound fields. This is an advantage as judgements are not dependent on the memory of the subjects over more than a few seconds. Adjacent comparison of pairs has been used in many subjective experiments in auditorium acoustics. Among the exceptions are Barron [1988] and the Berlin group [Cremer 1982 pages 593-605]. In these examples, subjects visited a variety of halls completing questions about each concert such as marking the degree of reverberation on a scale. The results were then derived from the responses to these questionnaires. This method relies on the consistent judgements of subjects over many weeks, leading to larger statistical variations, which makes it harder to extract significant results. Despite this, the realism of using of a full orchestra as the sound source, during a real concert, in actual auditoria is what makes such tests worthwhile.

3. To achieve a reasonable balance of early and late sound in the simulator with only nine reflections in the early sound field, requires the level of the individual reflections to be relatively high. This problem has been recognized by others, for example [Naylor 1986]. However, listening tests with our simulator found that subjects did not perceive individual reflections. There were no discontinuities in the decay of the sound, no echoes from individual

reflections, or any other subjective effect which might hint that the relatively spartan early sound field was a problem.

4. With only a single loudspeaker reproducing the direct sound, our simulation lacks the extended nature of the orchestra. This has been true of many similar testing systems [Barron 1981, Reichardt 1966 1967 1975 1981]. Some researchers [Barron 1988, Berlin group see Cremer 1982 pages 593-605] have used the ideal sound source of a full orchestra. The problem with using real orchestras is that the sound source will not be consistent but varies from test to test. Gottlob [1973] and Williamson [1989] used music recorded in anechoic conditions reproduced by two loudspeakers on the stage of real auditoria. Although this is an improvement on our simulation system, it still fails to reproduce the varied directionality and distribution produced by a full orchestra. Such a system has also been criticized as sounding unreverberant when compared to a full orchestra [Barron 1988].

5-7. In a real concert hall visual clues can play a minor role in determining the quality of the sound perceived by the audience. For example, Barron [1988] found that seats at the back of auditoria with low absolute sound levels were not necessarily perceived to be quiet. He suggested that this was due to the distance to the stage making the listener anticipate low volume levels anyway. There is also a factor in the whole ambience of watching an orchestra playing and an empathy produced between the listener and the orchestra. Both these effects are secondary compared to the other effects (1-4), however, and did

not prevent the production of a very realistic sounding simulation. The visual clues provided by the loudspeakers in the anechoic are worthy of note, but not thought to be a problem.

All the available systems have their advantages and disadvantages and no-one has yet produced a test method which overcomes all the problems. Possible improvements to simulations systems will be discussed in Chapter 14. Using an artificial simulation system seemed to provide the simplest and quickest method for measuring the smallest perceivable change in the early sound field, while not compromising too much the realism of the sound field.

8.3 The Simulator

A diagram of the experimental set up is shown in Figure 8.2. An anechoic music source was reproduced from the compact disc player. The signal was then split: one signal went direct to the mixing desk to simulate the direct sound; two signals went to the two digital delay units; and two signals to the reverberation units. The delay units produced a total of nine simulated early reflections with variable delays. The stereo reverberation output signals from the Boss SE50 (A and B) were mixed to produce a further two reverberation signals by the A+B, A-B function box. These four signals then provided the reverberation. All these signals were fed to the mixing desk, some of the signals going through a pre-mixer first to allow the maximum number of early reflections to be used. The mixing desk allowed all the signals to be mixed and sent down to the eight

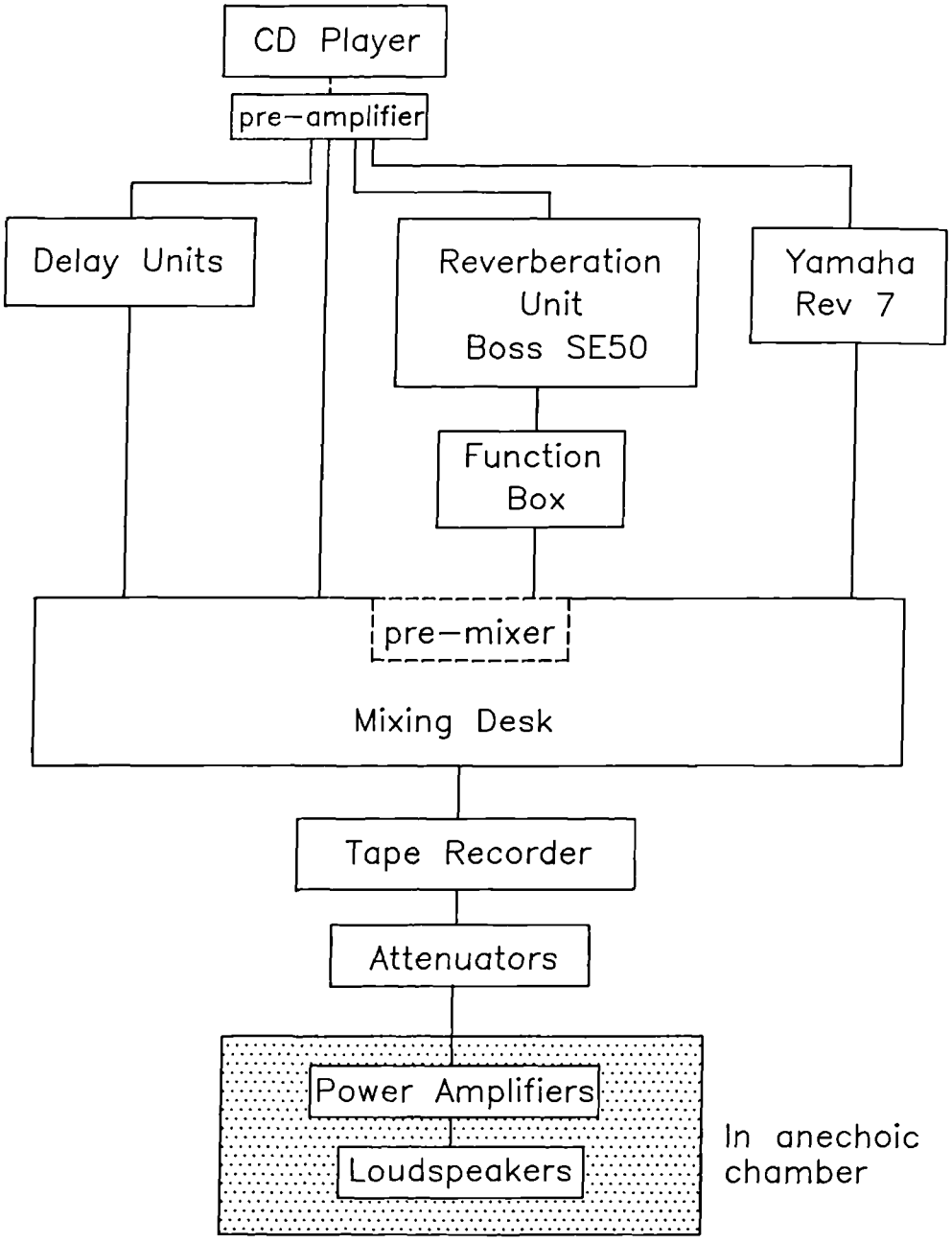

Figure 8.2. Schematic diagram of subjective measurement system.

loudspeaker channels available with the correct relative levels. A tape recorder was available to record the output signals from the mixing desk for the centre time tests. The outputs from the tape recorder or mixing desk were fed through attenuators to power amplifiers and then the loudspeakers, the later two being within the anechoic chamber. The use of attenuators improved the signal to noise ratio as it allowed higher levels to be used in the mixing-desk and tape recorder systems.

The signal to noise ratio was good, overall being 56 dBA. A very small amount of hum could be heard when no music was being played, but this was very much lower than the music level and could not be heard during the tests.

8.4 Reflection Sequence Used in the Tests.

In this section a detailed description of the reflection sequence is given along with the reasons why the particular field was chosen. A range of information was used when designing the sound field: (i) measurements in real concert halls giving reflection angles, levels and delays; (ii) measurements in auditoria for the objective parameters used to characterize impulse responses - e.g. reverberation time; (iii) subjective measurements for preferred values of objective parameters; and (iv) predictions by ray tracing and image source computer model simulations.

8.4.1 Loudspeaker positions and reflection directions

A Japanese survey of European concert halls [Tachibana 1986] gave information about arrival directions of reflections in several halls. The reflection directions were measured by Tachibana et al using a four microphone array [Tachibana 1989]. This information was used to decide reflection directions along with a simple computer image source model of the Boston Symphony Hall [Kirszenstein 1984]. An image source model is a standard method for predicting the impulse response within a room by constructing a large number of image sources in substitution for the reflections off the walls [Stephenson 1990, Kuttruff 1991a pages 282-287]. Other factors such as the need for all round reverberation and hence the need for rear loudspeakers, the restrictions imposed by the size of the anechoic chamber, and the number of loudspeakers available were also important.

The Japanese survey gave a wealth of information about arrival directions. A distribution of the major reflections averaged over several of the concert halls was used. It became clear that several reflection directions predominated:

1. Direct sound.
2. Lateral reflections from both sides.
3. Ceiling reflections from above.
4. Reflections from the stage area.
5. Reflections from below off seating.

The image source model of the Boston Symphony Hall confirmed the existence of reflections of 1-4 above. Also significant were reflections which come off both the ceiling and side walls involving two or more reflections; these will be referred to as corner reflections. The modelling of reflections off seating in computer models is not satisfactory, due to the seating being modelled as a plain surface where in fact the seating is a very complicated shape. This meant that the presence of seating reflection, type 5 above, could not be confirmed or denied from the computer models. These seating reflections certainly exist and are significant as they are known to cause the 'seat dip' effect [Schultz 1964, Sessler 1964], but the size and frequency response of these reflections in an occupied auditoria are not well known at the moment. As there were only eight loudspeakers available, it was felt better to simulate the corner reflections rather than the seat reflections. The loudspeaker positions are shown in Table 8.1. Figure 8.3 shows a diagram of the loudspeaker placement. Plate 8.1 shows a photograph of the loudspeakers in the anechoic chamber.

8.4.2 Early reflection order, arrival times and levels

A computer model of the Royal Festival Hall using the Odeon program was used [Naylor 1991a-b, Rindel 1991], along with the image source model of the Boston Symphony Hall to determine reflection order, arrival times and levels. Odeon is another program used to predict the sound field within enclosures. It uses a hybrid of the ray tracing and image source techniques.

Table 8.1 The loudspeaker positions for the simulation system.

Loud-speaker	Description	Angle (azimuth,vertical)	Distance to subject (m)
1	Direct sound	(0°,-10°)	2.9
2	Lateral reflection right	(45°,0°)	2.0
3	Rear right	(135°,0°)	2.0
4	Rear left	(-135°,0°)	2.0
5	Lateral reflection left	(-45°,0°)	2.0
6	Stage area reflection	(-12°,-5°)	2.9
7	Ceiling reflection	(-1°,27°)	3.1
8	Corner reflection	(21°,23°)	3.3

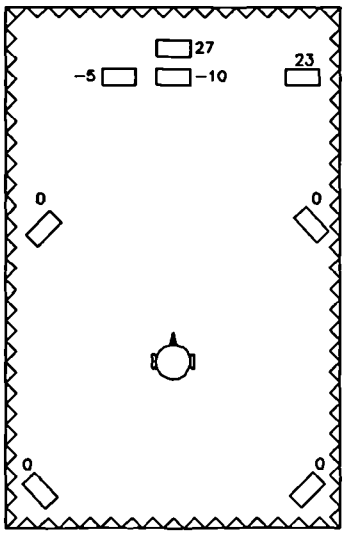

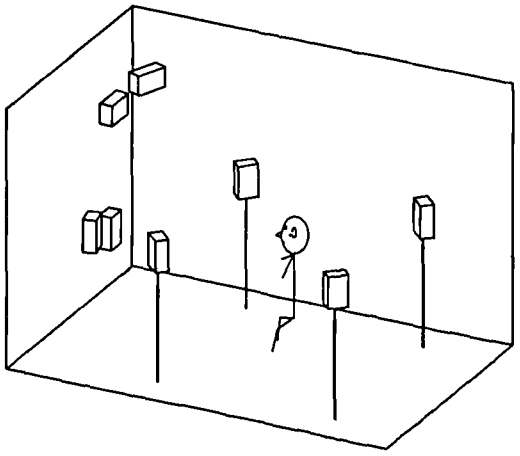

Figure 8.2. Placement of loudspeakers in anechoic chamber for subjective tests. The elevation of the loudspeakers given in degrees.

Plate 8.1. View of the simulation system set up in the anechoic chamber.

The simulations were done for a listener half way back from the stage and a quarter of the way from the side wall. Care had to be taken with the computer model results, especially with reflections off the seating area and reflections from finite sized surfaces. This is because these are both not well simulated in either ray tracing or image source models. Because of this an exponential decay rather than the predicted levels was used as the main guide to reflection levels.

8.4.3 Balancing Lateral to Non-lateral Energy

It was important to get a balance between the amount of lateral and non-lateral sound to get a degree of spatial impression which might be expected in a real auditoria. Spatial impression is the sensation of being enveloped in the sound and is created by sound arriving laterally [Barron 1974 1981]. It is well established that spatial impression plays a key role in determining preference in auditoria [Barron 1974, Gottlob 1973, Blauert 1986a-c 1983, Williamson 1989]. In the simulator, the degree of spatial impression was tested using the two standard objective parameters: *early lateral energy fraction (ELEF)* [Barron 1981] and *inter aural cross correlation coefficient (IACC)* [Ando 1985 pages 35-41]. Early lateral energy fraction measurements on the subjective system were made using a standard technique which utilizes a switchable figure of eight, omnidirectional microphone [Barron 1983]. IACC was derived using a method given by Ando [1985 pages 35-41]. Both methods are detailed in Chapter 9. Figure 8.4 shows a graph of ELEF verses frequency.

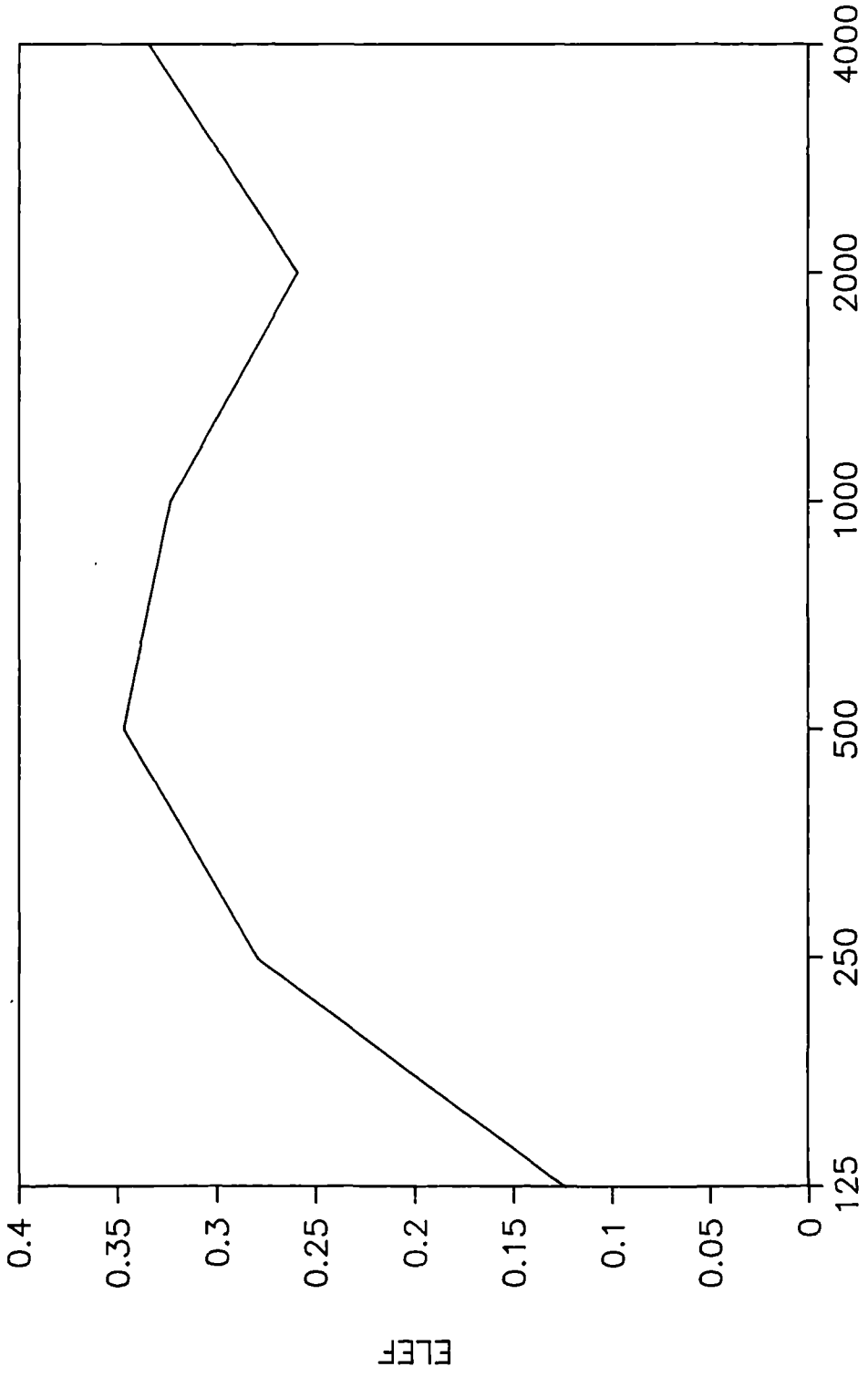

Figure 8.4. Early lateral energy fraction (ELEF) in the simulator.

A problem with comparing the simulator's parameter values with those measured in actual halls, is that we were trying to simulate an occupied hall, whereas objective measurements in halls are generally done in the unoccupied state. However, in the case of ELEF, an assumption will be made that the parameter is little changed between the occupied and unoccupied case. Any early reflections which interact with the seating will be greatly attenuated and so will have a much smaller effect on ELEF than reflections from the side walls and other hard surfaces. When the change between the unoccupied case to occupied case is considered, it might be expected, therefore, that the difference in ELEF would be small. The assumption was tested using the Odeon model of the Royal Festival Hall. This model was run twice, once with the seating absorption set to values typical for an occupied state and once for values typical for an unoccupied state. It was found that there was virtually no change in ELEF between the two predictions.

There are few measurements in halls to compare our simulator's ELEF value with. An added complication is that there is no standard measurement technique. A measurement by Bradley [1989a] gives values of ELEF for a fan shaped hall with orchestral shell as .25. This value has been averaged over the octave bands 125 Hz to 2000 Hz and using a factor of 1.5 to correct for the figure of eight microphone response [Barron 1983]. This compares to our 5 octave averaged value of .27. Other measurements by Bradley [1989b] have measured ELEF in a range from .12 to .19 in ten concert halls. Unfortunately, the exact measurement technique is not known, and as noted above the method

of extracting the amount of lateral sound can greatly influence the ELEF value. Assuming that Bradley used the figure of eight microphone system again, the correction factor of 1.5 ought to be applied, this makes the true range really lies between .18 and .29. Our simulator values lie within this measured range.

There is not thought to be a preferred range of ELEF within the values normally achievable in concert halls, the higher the value of ELEF obtained, the more preferred the sound field [Barron 1981, Williamson 1989]. (This is true as long as problems such as image shift are avoided). So it was not possible to compare our ELEF value to a preferred range from subjective tests. Consequently, values produced in real halls gave guidelines for the simulator.

Another measure of the spatial distribution of reflections is the Inter Aural Cross-Correlation Coefficient (IACC). This measures the degree of incoherence between the two ears of a dummy head. As the dissimilarity of the signal between the two ears is created by diffraction around the head, the more lateral sound there is the greater the incoherence, and the lower the cross correlation coefficient. The maximum value for cross correlation coefficient is the single value normally quoted [Ando 1985 pages 35-41]. The values for the simulator have been derived from a calculation method and dummy head data given in [Ando 1985 pages 121-132]. Chapter 9 has more details on the calculation method.

In Table 8.2 two published set of values are given alongside the simulator's performance. Unfortunately, the actual value of IACC is highly dependant on the noise source used, the time over which the correlation coefficient is calculated and the dummy head used. Bradley calculated his values over 50 ms, it was band limited by a low-pass 4 KHz filter and A-weighted. All three of these factors would change the value of IACC and not all in the same direction. The values for inter aural cross correlation coefficient measured by a group of Japanese researchers [Tachibana 1986] have values in a similar range to those given by Bradley. Unfortunately, the nature of the source signals for these measurement are not known. Our results lie within the range of both sets of measurements.

Table 8.2. Values of inter aural cross correlation coefficient measured by various researchers compared to simulator's performance.

	Value or range of inter aural cross correlation coefficient (IACC)
Simulator	.33
Japanese Survey of European Concert Halls [Tachibana 1986]. Data for 6 halls.	.22 - .43
Bradley [1983]	.17 - .41

To summarize: both our values for ELEF and IACC fall within ranges measured in actual halls, although comparison is hampered by differing measurement techniques.

8.4.4 Reverberation simulation

A modern artificial reverberation unit enabled a good natural sounding simulation of a reverberant decay, and was much better than the metallic-sounding reverberation plates. The stereo outputs, A and B, of the reverberation unit were mixed by simple A+B and A-B operations to obtain four signals. Two of the signals A and B were fed to the two rear loudspeakers (3) and (4) respectively; and three frontal loudspeakers (6),(7) and (8) were fed with A-B, A+B and A+B respectively. Figure 8.3 showed the loudspeaker layout, and Table 8.1 the exact positions. Using five loudspeakers with different arrival times and directions decreased the coherence between the reverberation signals achieving a balanced sound; it also had the added advantage of producing a good quantity of reverberation in the vertical plane. The reverberation was balanced front and back as well as left and right.

During preliminary testing, it was found that the discontinuity between the discrete early reflections and the dense reverberation was disconcerting to listeners. A second reverberation unit, the Yamaha rev7, set on a special 'early reflections' setting, created a short burst of early reflections slowly increasing in density just before the main reverberation. With these extra early reflections, no discontinuity could be heard and the problem was solved.

The levels of the reverberation units were set to obtain a smooth transition, following a rough exponential decay, from the early reflections to the

reverberation. It was also set to produce the values for various objective parameters which would be expected in real concert halls. The reverberation time was set to be about 2.1 s, just above the average found in British halls which are generally un-reverberant, but within the preferred range [Cremer 1982 page 620]. The Early Decay Time (EDT) was shorter than the reverberation time at 1.8s (mid frequencies). A graph of reverberation time and EDT verses frequency can be seen in Figure 8.5.

8.4.5 Clarity index, centre time and deutlichkeit

It was important to balance the amount of sound arriving early to that arriving late in the impulse response. This balance determines the clarity of the sound in the hall [Cremer 1982 pages 430-435]. There are three commonly used measures; *centre time* (T_c), *clarity* (C_{80}) and *deutlichkeit* (D). Chapter 10 gives more details on these measures. All three measures represent the distribution of the sound energy along the impulse response by a single value. The centre time measures the centre of gravity of the energy impulse response; the clarity and Deutlichkeit give a ratio of early to late sound in dB and in % respectively.

There have been a few measurements to determine the preferred range for clarity measures. Reichardt and Lehmann [Reichardt 1981] did subjective measurements with synthetic sound fields to find preferred values of clarity. They found the range from 3 to 8 dB was preferred for one impulse response and 0

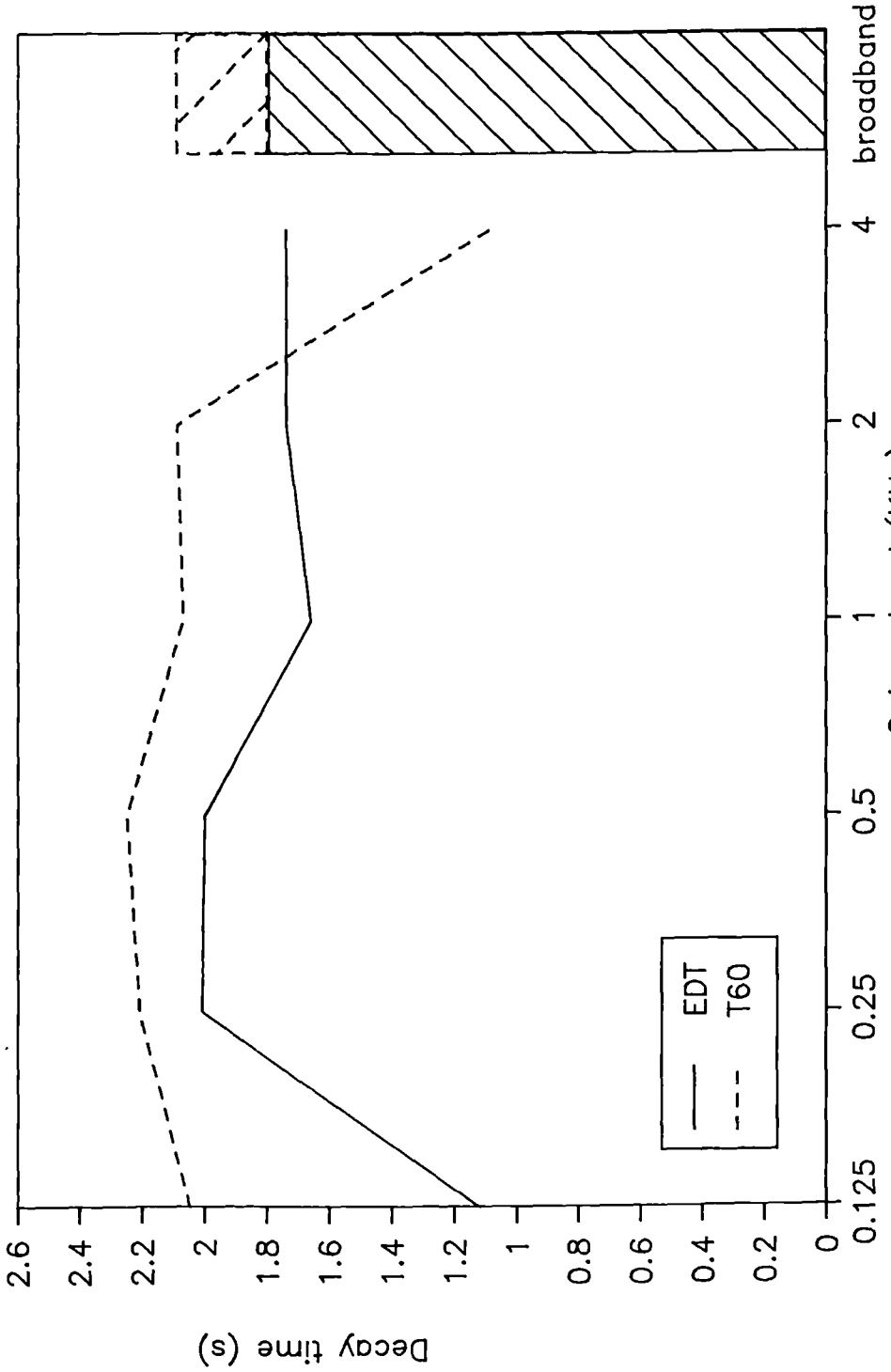

Figure 8.5. Early decay time (EDT) and reverberation time (T60) in the simulator.

to 5 dB for another. From this it seems that values of clarity between 0 and 8 dB are good, preferably near the middle of the range. This compares very favourably with the value given by our simulator of about 3.0 dB. Figure 8.6 shows the simulator's clarity response with frequency.

Subjective measurements by Lehmann [Cremer 1982 page 605] recommended that the centre time should not exceed 140 ms; our simulator has a centre time of 80 ms at mid frequencies.

The values of the clarity measures can not be easily compared to measurements in real concert halls. The problem is that the values for the parameters change considerably between the unoccupied case when people measure the objective parameters, and the occupied case, which is what we are trying to simulate. The presence of an audience increases the absorption of the seating area, and this will have great influence on the later arriving reflections which will be attenuated more by the seating area. This leads to less energy arriving later in the sound field which increases the clarity of the hall. This can be illustrated by the use of the Odeon model of the Royal Festival Hall. In Table 8.3 the change in the various parameters between the unoccupied and occupied case are shown. These values can not be taken as absolutes due to the fact that the accuracy of parameters produced by computer models have not, as yet, been fully verified. They do, however, give guide lines to what changes could occur between occupied and unoccupied measurements.

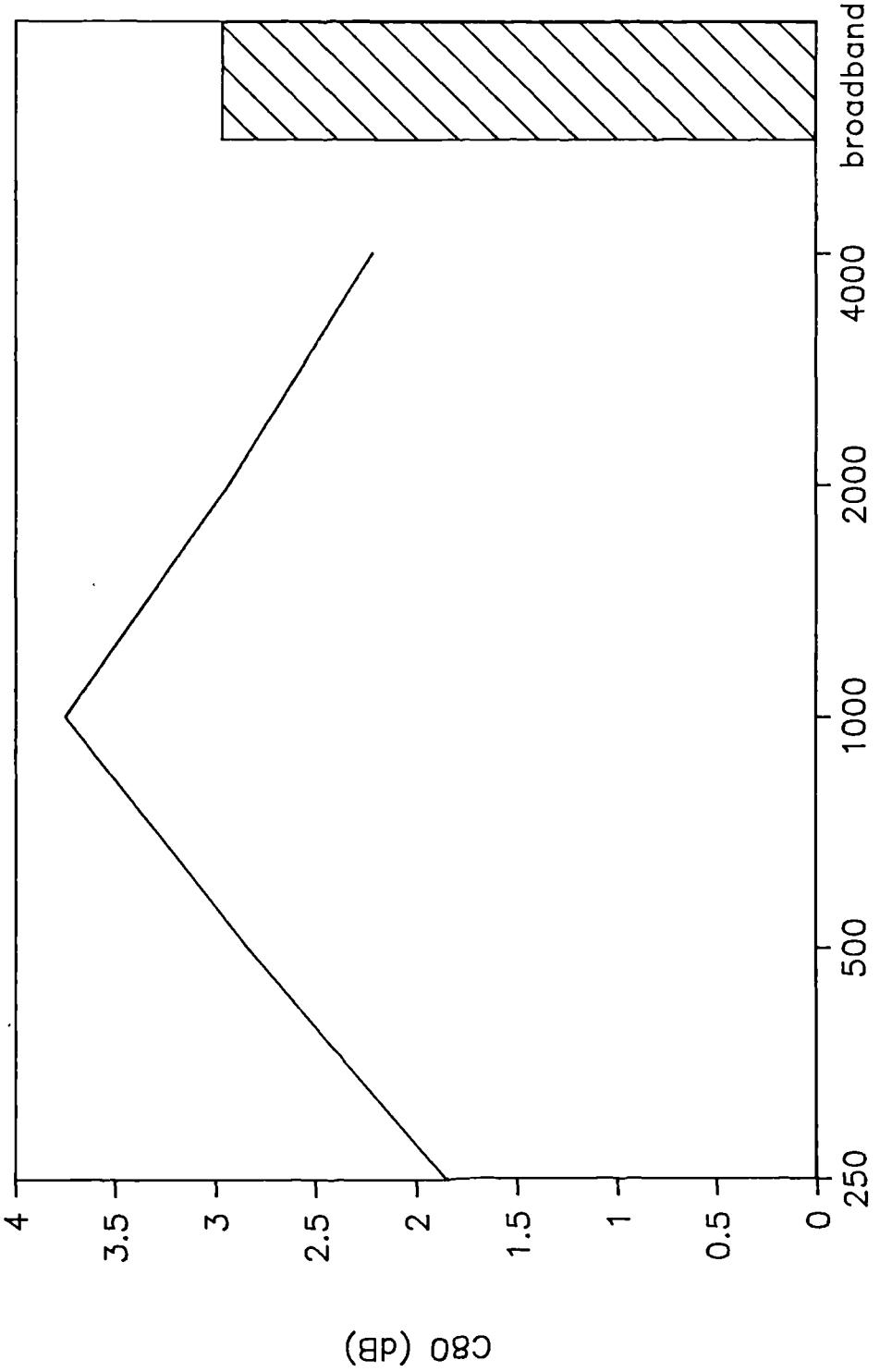

Figure 8.6. Variation of clarity index (C80) with frequency in simulator.

Table 8.3. Variation in Centre time, clarity index and Deutlichkeit between occupied and unoccupied halls. Values calculated using ray tracing model of Royal Festival Hall.

	Occupied		
Octave band Hz	Centre time T_c	Clarity C_{80}	Deutlichkeit D in %
500	84	2.9	52
1000	70	3.4	57
2000	66	3.7	57
	Unoccupied		
500	133	.4	38
1000	104	1.6	43
2000	83	2.7	48

The values for mid frequency clarity index measured in the Japanese survey of European concert halls [Tachibana 1989] ranged from -2.9 to 2.7 dB for unoccupied halls. Table 8.3 indicates that a change of about 2 dB from the unoccupied to the occupied case might be expected, so the range of occupied clarity is estimated to be -.9 to 4.7 dB. Our simulation, where C_{80} equalled 3.0 dB at mid frequencies, falls well within this range. A similar analysis for the Japanese measured centre times and deutlichkeit have produced similar results.

Bradley [1983] measured clarity ranging from -2 to +7 dB with an average value of 1.5 dB in four halls. A similar analysis to the previous paragraph leads to an estimated range of 0 to 9 dB and average value 3.5 dB for the occupied case. Our simulation value of 3.0 dB is similar to the average value.

Beranek and Schultz [Beranek 1965] measured Reverberant to early sound energy - yet another objective measure - in four unoccupied concert halls. To compare these values with our simulator it is simplest to convert these to Deutlichkeit. The reverberant to early energy ratio R is given by :

$$R = 10\ LOG_{10} \frac{\int_{50ms}^{\infty} P^2(t)dt}{\int_{0}^{50ms} P^2(t)dt} \qquad 9.1$$

The Deutlichkeit D is given by :

$$D = 100 \frac{\int_{0}^{50ms} P^2(t)dt}{\int_{0}^{\infty} P^2(t)dt} \qquad 9.2$$

From these definitions it can be shown that :

$$D = \frac{100}{1 + 10^{R/10}} \qquad 9.3$$

Beranek and Schultz measured values ranging from 0.5 to 7.5 dB for reverberant to early energy ratio at mid frequency. These convert to a range of 15 to 47% for Deutlichkeit in the unoccupied case. An estimated range of 30 to 60% for the occupied case can be made based on our previous analysis. Our deutlichkeit value for the simulator was 63%, just beyond the top end of the range.

The above evidence shows that the balance of energy in terms of arrival times was well within subjectively preferred ranges and also within the limits normally found in concert halls.

8.4.6 Overall sound level

The mean level of the simulator was set to be 79 dBA for both pieces of music when averaged over the full motifs used. This was set to sound subjectively natural.

Ando measured preferred listening level and found this to be motif dependant [Ando 1985 page 67]. Taking the results for both the motifs tested, he found that an overall level between about 77 and 80 dBA was preferred. This compares well with our value of 79 dBA.

Our simulator level of 79 dBA for the mean level and 75 dB for the direct sound only also compares well to that set by other subjective experimenters. Barron [1974] set a mean level of 77 dB, Blauert [1986a-c] used 77 dB for the direct sound level, and Ando [1977 1979] used 80 dB for the direct sound level

8.4.7 The impulse response

In Figure 8.1, the impulse response used was shown. Table 8.4 gives the full details of reflection directions, delays and levels.

Table 8.4. Details of the impulse response used.

	Level (dB) re direct	delay (ms) re direct	Angle of incidence (azimuth,elevation)
direct sound	0	0	(0,-10)
First lateral reflection	-3	19	(45,0)
Ceiling reflection	-6	41	(-1,27)
Corner reflection	-7.5	46.5	(21,25)
lateral reflection left	-10	50.5	(-45,0)
stage reflection	-12	81	(-12,-5)
ceiling reflection	-12	90	(-1,27)
rear right	-12	61	(-135,0)
rear left	-12	32	(135,0)
rear left	-14	95	(135,0)
Early reflections from rev 7	-8.4[1]	100	(0,-10)
reverberation	-2.2[1]	110	(±135,0) (-12,-5) (-1,27) (21,25)

[1]Steady state levels

8.5 Motifs Used in the Tests

Anechoic music recorded on compact disc was used as the music source (Denon PG-6006) [Hidaka 1988]. The two motifs were chosen to be varied in style and tempo. The first was the first five bars from Handel's Water Music Suite, lasting about 8 seconds. This is a fairly fast moving piece, with precisely placed notes and with instruments across the whole frequency range being

played. The second motif was from the fourth movement of Mendelssohn's symphony no.3 in A minor, opus 56 "The Scottish". This lasted a little over 5 seconds. The Mendelssohn motif has a slower tempo, the notes are more sustained and longer. Both pieces had very similar spectral content, as shown in Figure 8.7. Although the Water Music Suite was originally written for a relatively small orchestra, on this recording it was played by quite a full orchestra and hence the fairly high listening level of 79 dBA.

8.6 Setting Up Procedure

A photograph of the simulation system can be seen in plate 8.1. The impulse responses were measured on an omnidirectional microphone placed where the centre of the listener's head would be. The MLSSA measurement system was used to measure the impulse response. MLSSA is an implementation of a pseudo-random white noise source measurement system which allows impulse responses to be measured quickly, to high accuracy, and room parameters to be calculated on the resulting impulse response [Rife 1991]. The setting up procedure was:

1. The delays of the reflections were set on the delay units and checked by measurements using MLSSA.
2. The phase of all loudspeakers were set to check that there were no negative reflections. (This was possible for all but one of the later reflections).

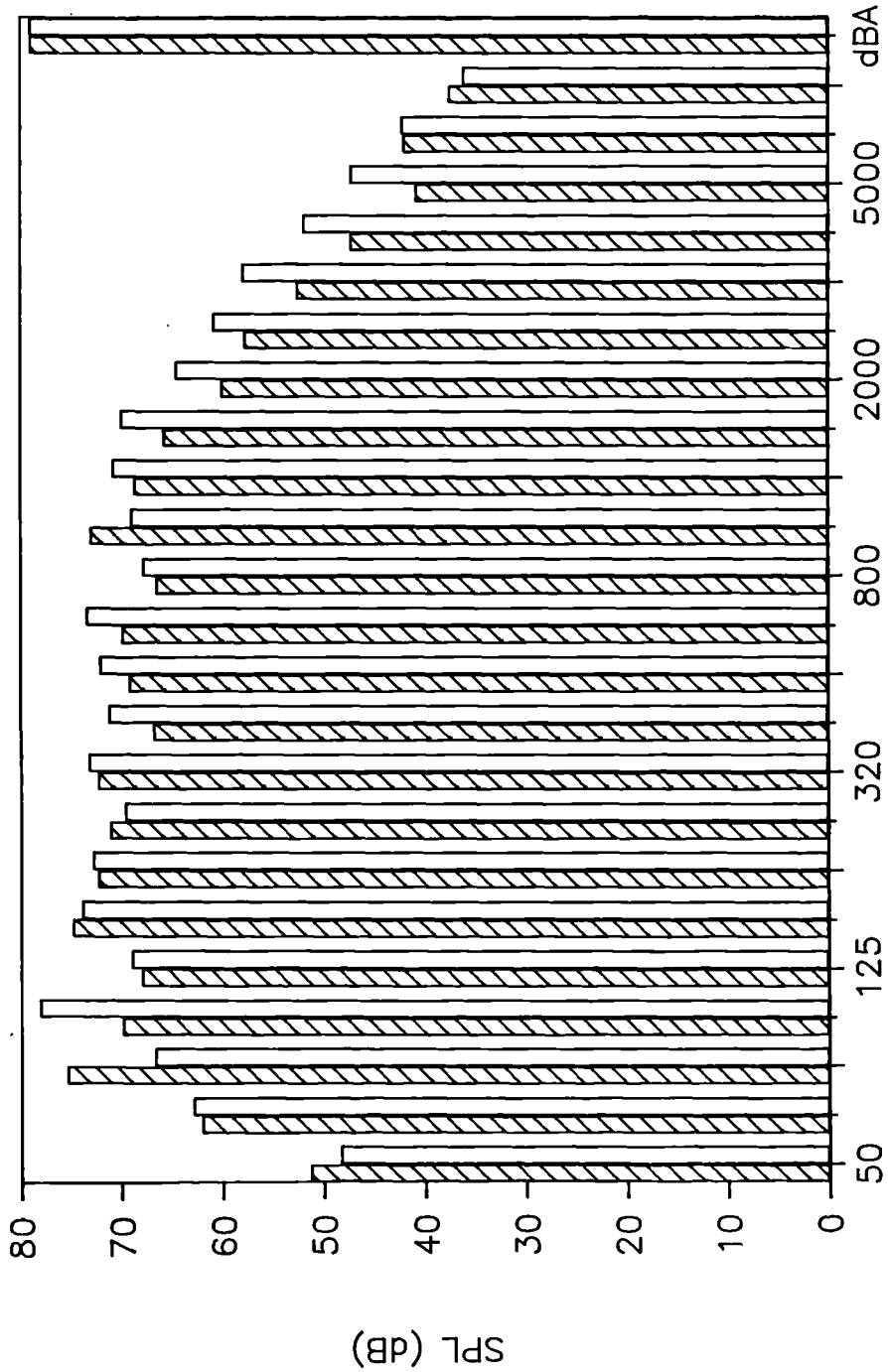

Figure 8.7. 1/3 Octave spectra for the two motifs.

3. The level of the direct sound was set to be 75 dBA with music playing averaged over the whole motif.
4. The level of all reflections were set relative to the direct sound using MLSSA with a 2 octave filter about 1 KHz.
5. The setting of reverberation units, e.g. reverberation time, was done.
6. The reverberation levels, and the level of the early reflection sequence from the Yamaha rev7 were set with steady state white noise.
7. Small adjustments were made to the reverberation levels until the correct centre time was achieved - as measured by MLSSA.

8.7 Test Subjects

The number of subjects ranged from 7 to 10 for the tests. All had musical experience either in playing an instrument or were regular concert goers. All test subjects had normal hearing.

8.8 Test Method

8.8.1 Overview of Method Available

There are a whole range of psychological test techniques applicable to measuring the smallest perceivable changes in the objective parameters [Guilford 1954, Torgerson 1958]. (The smallest perceivable change is known as the difference limen). Using the nomenclature used by Guildford, the possible

procedures are discussed below. The measurement of the difference limen for decreasing level for a lateral reflection is given as an example:

1. **Method of constant stimulus differences.**

   Pairs are constructed of a reference sound field and sound fields with a reduced level for the side reflection. These pairs are presented in a random order and the subject required to say whether the sound fields are different or the same.

2. **Method of average error.**

   The observer is presented with two fields, one is a fixed reference field the other has a variable lateral reflection level adjustable by the observer. The observers job is to adjust the stimuli until both are equal.

3. **Method of minimal changes.**

   The observer is presented with pairs as in the method of constant stimulus differences and has to judge whether the pairs are different or the same. This time the pairs are presented in an order known to the subject, either starting from a noticeable difference and going to no-noticeable difference or vice versa. The difference in the pairs decreases (or increases) until the observer changes his judgement from the sound fields being different to the same (or from same to different).

The method of average error could not be used for the tests for measuring the difference limen for centre time. In those tests many reflection levels and delays had to be changed simultaneously and this could not be controlled by the subject.

In the method of constant stimuli differences the uncertainty caused by the randomized order of the pairs means that the pairs have to be presented many times to the observer to average out observer error. Guildford suggests 50 to 200 times. Consequently, the labour of this method is large. It was for this reason that the method of constant stimuli differences was rejected.

The method of minimal changes overcomes some of the uncertainty in the observer's judgement by giving them some knowledge about the order of the pairs, either proceeding from a noticeable difference to no difference or vice versa. Consequently, the observer's judgement is more certain and less repetition is needed. For this reason the method of minimal changes was used. Giving the observer knowledge about the order of the pairs obviously affects the judgements made. But by the use of the procedures outlined in Section 8.8.2 this should not be a problem.

Of the three test techniques it is expected that: the method of average error would give the lowest limen as the observer has control over the stimuli; the method of constant stimuli would give the largest limen because of the

uncertainty in the judgement; and the method of minimal changes would give a limen somewhere between the two.

8.8.2 Method of minimal changes

For the method of minimal changes, the difference limen measured with the test starting from a noticeable difference and going to no noticeable difference will quite often be different from that measured with the test starting with no noticeable difference and going to a noticeable difference (for simplicity the two type of tests will be said to have different 'run' directions). There are two errors in the observers judgement which lead to the run direction affecting the limen. Habituation is when the observer waits until one or more pairs after the limen before acknowledging it. Expectation is when the observer anticipates the limen by one or more pairs. The actual difference limen is taken to be an average of the two opposite run direction results. So it is assumed that the errors of habituation and expectation are the same for both run directions and will average out.

As with all psychological testing, care has to be taken to avoid effects of training and fatigue. To avoid fatigue tests were kept short, to be less than 20 minutes. To avoid training the first pairs presented at the start of each test session were always with a large difference to allow the subject to get used to hearing the differences. In addition all subjects took two trial runs before the actual testing to familiarize themselves with the testing method.

The test pairs were presented in the order A B A B where A and B are reference and modified impulse responses respectively. Whether the reference field was presented first or second was randomized. The first playing of A had a tendency to sound more reverberant because it was being played just after silence and complete anechoic conditions. Subjects were warned to be careful when listening to the first note, and this randomized presentation order was used so that errors could average out. Subjects could ask for pairs to be repeated if they wished.

The starting point for any run had to be chosen with care. If a set number of pairs, x, above the approximate limen was used regularly, subjects who did many tests could fall into the trap of expecting the limen because x pairs had been presented. Consequently, the starting point of each run was varied to eliminate this error.

8.9 Analysis Techniques

8.9.1 Testing for training and fatigue, the F test.

The first step when analyzing the difference limen data was to test whether training or fatigue had any influence on the results. If the subjects were still getting used to the measurements when results were taken a decrease in limen each time a subject took a test would be seen until they were properly

trained. Conversely, too many tests in one sitting can lead to an increased limen due to fatigue effects.

As detailed in Section 8.8.2, care was taken to avoid training and fatigue effects. Despite this, such effects have to be tested for in the final data. The standard statistical technique is an analysis of variance and an F test [Guilford 1954 page 105].

To test for training effects the data is split into two sets, one for the first two tests taken by each subject, one for the final two tests taken by each subject. Then the hypothesis that both data sets came from the same normal distribution could be tested using the F test [Moroney 1968]. This involves calculating the inter and intra set variance. If the inter set variance is much smaller than the intra set variance it implies that the variation between the sets was much smaller than the variation within the two sets, and so it could be said that the two data sets were statistically the same. So there were no training or fatigue effects in that case.

The actual mechanics of the tests were only slightly more involved. The F ratio was calculated, it was the ratio of the inter and intra set variance. The F ratio was compared to different F-distribution tables to find at what 'level' of the F distribution it was significant. If the ratio was significant at a level greater than 5%, then there was significant probability that the two data sets originated from the same normal distribution. It is standard to take this level to mean that

within statistical error the data sets were the same. If the significance level was less than 5% it could be said that the two data sets originated from two different normal distributions.

8.9.2 Calculating the Limen

Once it has been shown that the data showed no sign of training and fatigue effects, a difference limen could be obtained by simply averaging all the limens measured. The difference limen quoted are the smallest perceivable changes in the parameter that 50% of the listeners could hear.

8.10 Conclusions

An artificial simulation system was used to produce a natural sounding simulation of a concert hall sound field. The standard objective parameters - such as: the reverberation time (2.1s); early decay time (1.8s); clarity index (3.0 dB); and early lateral energy fraction (.27) - were all reasonable values when compared to real measurements in halls, and subjective preference measurements by others. The measurement methods used in the tests have been detailed in this chapter.

Chapter 9

The Difference Limen for Spatial Impression

9.1 Introduction

It has long been established that reflections arriving laterally to listeners in auditoria cause a subjective effect called spatial impression. The listener perceives that they are enveloped in the sound because the sound field at the two ears is different due to diffraction around the head [Barron 1974, Blauert 1983, Ando 1985, Williamson 1989]. The relative importance of this effect has been established in several subjective surveys. For example Gottlob [1973] showed that a high correlation existed between preference and the inter aural coherence, an objective parameter related to spatial impression.

9.2 Experimental Method

It has been shown [Barron 1974] that the degree of spatial impression is proportional to the ratio of early arriving lateral to non lateral energy, the *Early Lateral Energy Fraction (ELEF)*. Therefore, in our experiments the amount of early lateral energy was altered by changing the level of the first lateral reflection. This achieved a change in spatial impression without changing other

subjective perceptions. These subjective perceptions can be monitored by the following objective measures: clarity index, reverberation time, early decay time and overall A-weighted sound pressure level. The changes in clarity index were below a difference limen, the value of which was established by the measurements described in Chapter 10. Changes in loudness were negligible. The reverberation and early decay times were kept constant.

The isolation of spatial impression from other subjective perceptions was obviously important so that a true difference limen for ELEF could be found. Indeed during the tests subjects noted a change in spatial impression only and no other effects. The primary effect perceived was a change in source width. Also noticed were changes in source depth - i.e. a receding of the source. The fact that spatial impression encompasses such a range of perceptions has been found by many researchers [Barron 1974, Morimoto 1989, Blauert 1983].

The test method used was the method of minimal changes which has been described in Chapter 8. A measure of the difference limen for the sound pressure level of the first lateral reflection was made. From this it was possible to derive a difference limen for the early lateral energy fraction. A difference limen for the inter aural cross correlation coefficient was also calculated - this is an alternative measure favoured by some researchers [Ando 1977 1979, Morimoto 1988]. The limen was measured with two contrasting music pieces, namely the Handel and the Mendelssohn motifs.

9.3 Results for the Handel Motif

The difference limen for the first lateral reflection, for the Handel Motif, was determined for 10 subjects. Each subject repeated the test four times. The statistical F test was carried out to determine whether training or fatigue had any significant effect on the limen. The F test showed there to be no effects of training or fatigue. The F ratio was significant at a level greater than 5%. It is standard in an F test to take a greater than 5% significance level to mean that the two data sets are the same within statistical error [Moroney]. Table 9.1 summarizes the results of the F test.

Table 9.1. Summary of F test for effects of training and fatigue on the difference limen of side reflection level for the Handel motif.

Source of variation	Sums of the squares	Degrees of freedom	Variance	F ratio	Significance
Between samples	0.016	1	.016	.0091	>5%
Within samples	66.7	38	1.75		
Total	66.7	39			

Care was taken to ensure that the subjects had sufficient practice with the test method and had familiarized themselves with listening for the particular changes heard in the tests. This explains the lack of a training effect. A contributory factor to the lack of training was that most subjects found listening

to changes in spatial impression quite easy, and made judgements with confidence most of the time.

Analysis of the results to obtain the difference limen was simple as there were no training or fatigue effects. To obtain the difference limen all the results were averaged. The difference limen and the standard error (95% confidence limits) for decreasing level of the first lateral reflection for the Handel motif was:

$$(2.6 \pm .4) \text{ dB}$$

9.4 Results for Mendelssohn Motif

Identical tests to that used for the Handel motif were carried out using the Mendelssohn motif. In this case there were nine subjects. Eight subjects undertook 4 tests and one subject undertook 2 tests. Training effects, as tested through an F test, was again negligible. The results of the F-test are shown in Table 9.2.

The difference limen for decreasing level of the first lateral reflection and the standard error (95% confidence limits) for the Mendelssohn motif was:

$$(2.1 \pm .4) \text{ dB}$$

Table 9.2. Summary of F test for effects of training and fatigue on the difference limen of the first lateral reflection for Mendelssohn motif.

Source of variation	Sums of the squares	Degrees of freedom	Variance	F ratio	Significance
Between samples	0.281	1	.281	.227	>5%
Within samples	37.1	30	1.24		
Total	37.4	31			

9.5 Effects of motif

The effects of motif on the limen was tested. For this, the two data sets consisting of the limen results from each motif were compared to see if they came from the same normal distribution. This could be done with an F test. As the results in Table 9.3 show, there was no significant difference between the limen for the two motifs, the significance being greater than 5%.

Table 9.3. Summary of F test for effects of motif on difference limen of the first lateral reflection.

Source of variation	Sums of the squares	Degrees of freedom	Variance	F ratio	Significance
Between samples	3.24	1	3.24	2.43	>5%
Within samples	82.5	62	1.33		
Total	85.7	63			

In the tests, the impulse responses for both motifs were the same, the overall volume was the same, and the ⅓ octave spectra of the two motifs were

very similar. The motifs were chosen only to have contrasting style and tempo. These results show no evidence that the style and tempo of the music affects the listeners perception of spatial impression.

The results for the two motifs were averaged to get the best estimate of the limen with the smallest standard error. It was found that the difference limen and it's standard deviation (95% confidence limits) for decreasing the level of the first lateral reflection is:

$$(2.4 \pm .3)\ \text{dB}$$

9.6 Difference Limen for Early Lateral Energy Fraction

The results for the difference limen of level change for the first lateral reflection, and objective measurements in the simulation system, were combined to derive a difference limen for early lateral energy fraction (ELEF). The definition of early lateral energy fraction is:

$$ELEF = \frac{\int_{5mS}^{80mS} P^2(t)COS(\theta)dt}{\int_{0}^{80mS} P^2(t)dt} \qquad 9.1$$

where p(t) is the pressure arriving at the listener at time t, and θ the horizontal angle of incidence of p(t) relative to an axis drawn through the ears of the listener.

Values for early lateral energy fraction were derived in two different ways. The first method is the one most commonly used by acousticians, the second is a slightly more rigorous approach.

9.6.1 Figure of eight microphone measurement

Impulse responses were measured using a microphone switchable between a figure of eight response and a omnidirectional response. For the figure of eight microphone measurement the direction of least microphone sensitivity was pointed at the direct sound loudspeaker. The microphone therefore measured mostly lateral sound, and this was used on the numerator of Equation 9.1. The measurement using the omnidirectional microphone setting was used for the denominator of Equation 9.1. The impulse responses were measured using the MLSSA system. The draw back of this system was that the response of the figure of eight microphone was COS(θ) for pressure, while the formulation for ELEF requires a response of COS(θ) for pressure squared. Therefore, following the method of Barron [1983], a correction factor of 1.5 was applied. If the pressure measured with the figure of eight microphone is represented by $P_8(t)$, and the pressure measured on the omnidirectional microphone by P(t), then the formulation for ELEF becomes:

$$ELEF = 1{\cdot}5\frac{\int_{5}^{80mS} P_8^2(t)dt}{\int_{0}^{80mS} P^2(t)dt} \qquad 9.2$$

This method can be criticised as the factor 1.5 depends very much on the decay time of the hall and the directional distribution of the reflections. In addition, the directional cancellation produced by the figure of eight microphone would not have been perfect. Although accurate methods for measuring ELEF in concert halls exist [Kliener 1989], the figure of eight microphone method is simple and most widely used, and so to most acousticians it is the most useful method.

9.6.2 Direct calculation

As the directions of the reflections were known from the loudspeaker positions in the simulator, Equation 9.1 could be applied directly to an impulse response measured on an omnidirectional microphone. This method assumed that all the sound came straight from the various loudspeakers. In the simulator there were also reflections from the equipment within the anechoic chamber, such as the supports for the loudspeakers and the loudspeakers themselves. As the angular distribution of these reflections was fairly random and the reflections were relatively small in magnitude, these effects were neglected when calculating ELEF. This method could not be used to calculate the ELEF value in low

frequency octave bands. The reflections overlapped each other after the octave band filter had been applied, making it impossible to separate the different reflections. This happened in the 125 Hz band and below.

9.6.3 Results

The values for ELEF were calculated by averaging the results for the five octave bands from 125 Hz to 2 KHz for the figure of eight microphone method, and for the four octave bands from 250 Hz to 2 KHz for the direct calculation method. This reflected the fact that spatial impression effects occur at all frequencies, with the low frequencies being most important [Morimoto 1988]. It was in line with the ideas of Barron [1983]. The results are tabulated in Table 9.4. The standard errors have been calculated by assuming that the errors were dominated by the variance in the subjective responses and not by the variances in the objective measurements of ELEF.

Table 9.4. The Difference limen for early lateral energy fraction. Results for different motifs and different measurement techniques.

	Difference limen for Early lateral energy fraction	
	Method 1, figure of eight microphone	Method 2, direct calculation
Handel motif	·061 ± ·006	·051 ± ·007
Mendelssohn motif	·053 ± ·006	·043 ± ·007
Both motifs	·058 ± ·005	·048 ± ·005

9.7 The Difference Limen for Inter Aural Cross Correlation Coefficient.

9.7.1 Definition of IACC

The parameter *Inter Aural Cross correlation Coefficient (IACC)* measures the degree of incoherence of the signals at the two ears. As spatial impression is created by the signals at the two ears being different, inter aural cross correlation is directly related to the degree of spatial impression produced [Cremer 1982 Page 444]. The lower the value of IACC, the greater the incoherence between the signals at the two ears, and the greater the degree of spatial impression. This parameter has been used by several researchers such as [Gottlob 1973, Ando 1985, Bradley 1983]. If the two signals at the left and right ears are $P_l(t)$ and $P_r(t)$ respectively, then IACC is defined as:

$$k(\tau) = \frac{\int_0^T P_l(t)P_r(t+\tau)dt}{\sqrt{\int_0^T P_l^2(t)dt \int_0^T P_r^2(t)dt}} \qquad 9.3$$

The cross correlation integral was carried out over 70 ms in this project, a range similar to that used for early lateral energy fraction. IACC was calculated over the maximum difference in inter aural arrival times ($\tau \leq 1$ ms). The single value quoted is then the maximum value of the IACC. For a completely symmetric sound field this should be at $\tau = 0$. In Figure 9.1 a typical result for our simulator is shown. The single value for IACC in that case is .33.

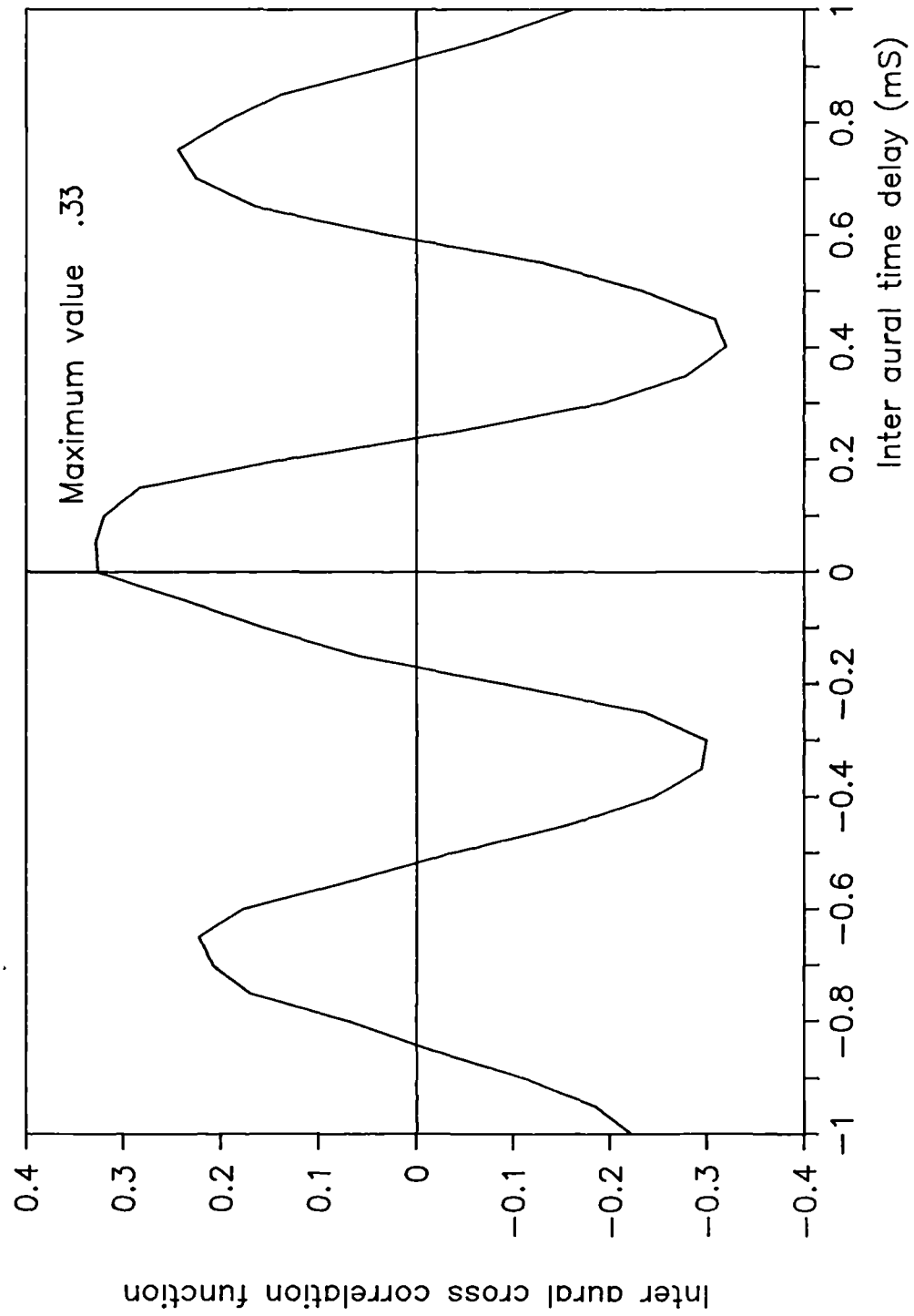

Figure 9.1. Inter aural cross correlation in the simulator.
Band pass noise.25 Hz to 2 KHz.

9.7.2 Calculation of IACC

To get a true value for IACC it is necessary to measure the signals in the ear canals of a dummy head. Alternatively, Ando [1985 pages 35-41] gave a method for calculating the IACC from the arrival directions and levels of the reflections. Ando showed that Equation 9.3 can be rewritten as:

$$k(\tau) = \frac{\sum_{n=0}^{N} P_n^2 \Phi_{lr}(\tau,\theta)}{\sqrt{\sum_{n=0}^{N} P_n^2 \Phi_{ll}(0,\theta) \sum_{n=0}^{N} P_n^2 \Phi_{rr}(o,\theta)}} \qquad 9.4$$

where P_n is the discretized impulse response components; Φ_{ll}, Φ_{rr} are the auto correlation coefficients for the left and right ears respectively; Φ_{lr} is the cross correlation coefficient between the left and right ear; θ is the horizontal angle of incidence; and N is taken to give an integration over 70 ms.

Ando has published experimental data for the cross correlation and auto correlation functions of the ears of a dummy head as a function of inter aural delay and angle [Ando 1985 pages 121-132]. With this data, Equation 9.4 can be combined with our impulse response and knowledge of reflection angles, to calculate the value of IACC. Ando has shown that this calculation has quite high accuracy [Ando 1979].

The values of IACC are highly source dependant, and this is reflected in the fact that the values for the auto correlation and cross correlation coefficients

are also source dependant. The IACC difference limen was obtained by averaging the calculated results for the 4 octave bands 250 Hz to 2 KHz. The results are tabulated in Table 9.5.

Table 9.5. Difference limen for inter aural cross correlation.

	Difference limen for Inter Aural Cross correlation Coefficient.
Handel Motif	·080 ± ·011
Mendelssohn motif	·067 ± ·011
Average result for both motifs	·075 ± ·008

9.8 Comparison with Previous Measurements

The commonly quoted result was obtained by Reichardt and Schmidt in the 1960's [Reichardt 1966 1967; see Cremer 1982, Kuttruff 1991a and Barron 1974 for a brief English translation of results]. The impulse response used in that experiment is shown in Figure 9.2.

A direct comparison of our difference limen and that of Reichardt and Schmidt's is not easy because of the different volume levels used. The amount of spatial impression depends on the volume levels [Keet 1968]. Barron [1974] estimated the level of Reichardt and Schmidt's experiment to be about 70 dBA, but our experiment had a level of 79 dBA. Reichardt and Schmidt's results showed that the difference limen for early lateral energy fraction varies with the

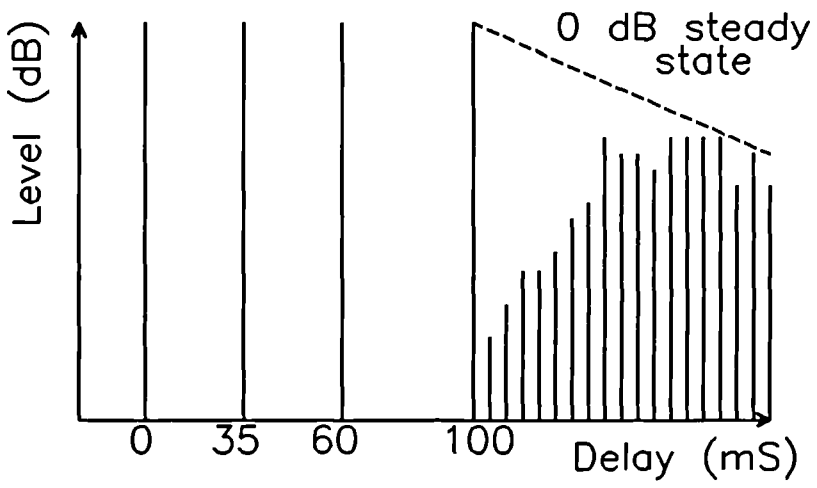

Figure 9.2. Impulse response for Reichardt and Schmidt's experiments. Direct sound; lateral reflection at 35 ms; ceiling reflection at 60 ms; and reverberation.

early lateral energy fraction value. To allow a comparison of results, Barron's equation for perceived degree of spatial impression was used. Barron tentatively forwarded the following equation for degree of spatial impression, SI [Barron 1981]:

$$S.I. = 14{\cdot}5(ELEF - 05) + \frac{(L - L_0)}{4{\cdot}5} \qquad 9.5$$

where L is the sound pressure level. In this case L_0 can be taken to be 70 dBA to allow a simple comparison with Reichardt and Schmidt's results.

Equation 9.5 shows that the level difference of 9 dB between our's and Reichardt and Schmidt's experiment is equivalent to two degrees of spatial impression. From Equation 9.5 it can be shown that a system playing at 70 dB would have to produce an early lateral energy fraction of .42 to create an equal degree of perceived spatial impression to our system playing at 79 dBA with an

early lateral energy fraction of .28. In Figure 9.3 a graph of difference limen for decreasing early lateral energy fraction against value of early lateral energy fraction is shown. This was derived from Figure 3 of Reichardt and Schmidt's paper [Reichardt 1967] using the impulse response shown in Figure 9.2. At an ELEF value of .42 the limen expected from Reichardt and Schmidt's results is .065 ± .010. This is similar to our result of .048 ± .005 shown above in Table 9.5. In this case the results using the direct calculation method was used, as this represented the better measurement of the difference limen. Figure 9.3 also shows that at these levels of early lateral energy fraction, the difference limen does not vary much with ELEF. Therefore, even though Equation 9.3 is only a tentative result of Barron's, the comparison between our results and Reichardt and Schmidt's should be quite robust.

Our experiment was an improvement on Reichardt and Schmidt's due to greatly improved equipment quality. Reichardt and Schmidt's reverberation would have sounded metallic because of the use of a reverberation plate, and their early reflections, both in level and number, are only a very basic simulation of reality. Reichardt and Schmidt used only two early reflections while our simulator had nine early reflections plus the early reflection sequence created by the Yamaha Rev7. Consequently, our difference limen for spatial impression is a improvement on the most commonly quoted value.

One other quoted value for the difference limen was been published by Collados [1980]. There is however insufficient information in terms of the exact

lateral energy values produced in his experiment to allow a comparison like that done with Reichardt and Schmidt's results. It is noted that Callados quotes a value of 2.1 dB for a limen which he compares to the 1.5 dB measured by Reichardt and Schmidt.

9.9 Conclusions

The difference limen for early lateral energy fraction and inter aural cross correlation have been measured in a realistic artificial simulation of a concert hall sound field. The method of minimal changes worked well for the production of such limen. It has been found that the difference limen does not vary significantly for contrasting motifs with similar spectra and the same overall volume levels. The measured limen is smaller than a previously measured value, although the difference between the two results is small.

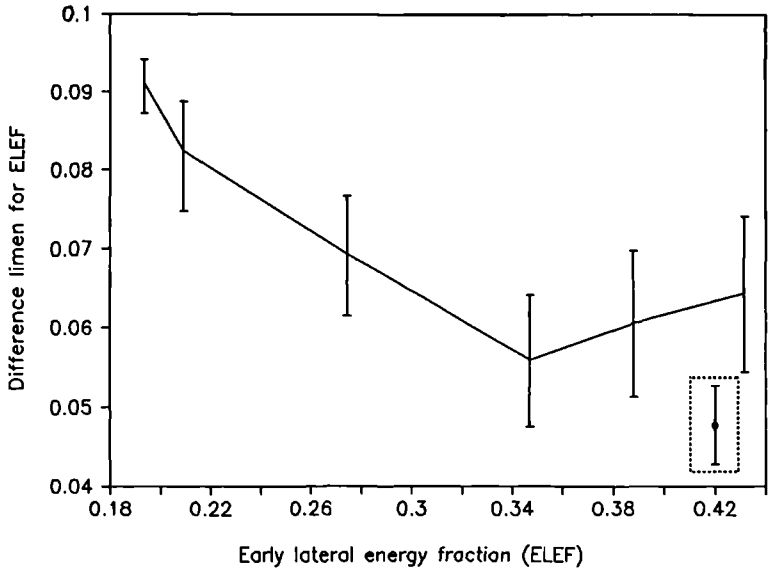

Figure 9.3. Difference limen for early lateral energy fraction verses early lateral energy fraction as measured by Reichardt et al. Our result is also shown highlighted in box.

Chapter 10

The Difference Limen for Clarity

10.1 Introduction

The distribution of sound energy with respect to time is important to the perception of sound in auditoria. The related subjective effect can be described as clarity. With plenty of reflected energy arriving soon after the direct sound a clear distinctive sound can be heard, whereas more reflected energy arriving late will give a more reverberant feel [Thiele 1953, Cremer 1982 page 430-435]. In an auditorium, a balance between clarity and reverberation has to be made. The audience wants to be able to distinguish individual notes as well as having sufficient reverberation to 'support' the music. In Britain there is a tendency for concert halls to be less reverberant and have a clearer sound than on the continent [Barron 1988].

There have been several studies which have confirmed the importance of clarity to audiences. A summary of the most important results can be found in Cremer and Müller [Cremer 1982 pages 493-605]. The author of this thesis has not seen published results for the difference limens for the objective parameters associated with clarity. When designing a concert hall it is important to know how much of a difference changes, such as those created by adding reflectors,

will have on the perceived sound. The measure of the difference limen will solve this problem.

10.2 Experimental Method

Changes in clarity were made by altering the distribution of reflection arrival times. The characteristics of the early sound field were mainly changed. This was because our interest was in the use of reflectors and diffusers which affect mostly the early sound field.

It was important that other subjective effects were kept constant so that judgements solely on clarity would be made. The other subjective effect most likely to change would be spatial impression. From Barron's measurements [Barron 1974 1981], it is known that the degree of spatial impression is largely independent of delay over the limits used in this experiment. From Blauert's measurements [Blauert 1986c], it is known that the effects of reverberation on spatial impression are small when compared to changes in the early sound field. So from these results, if the delay of the early reflections as well as the delay and level of the reverberation were altered, a change in clarity could be produced without a change, or with only a small change, in spatial impression.

It was not surprising to find that the combined effects of changing many reflection delays and the reverberation produced a slight change in the degree of spatial impression for some of the pairs (this occurred for about 50% of the pairs). In such cases listeners were asked to check the pairs for equal source

width and minor adjustments were made. This was done by switching a single reflection to a different loudspeaker. This changed the incident angle and so changed the degree of spatial impression. The adjustments needed were small.

According to some researchers [Ando 1977 1979, Beranek 1962] there is a preference associated with the arrival time of the first reflection. As will be shown in Chapter 12, no such effect was found within the delays used for this experiment and with this simulated sound field. Consequently, there was no restriction in moving the delay of the first reflection.

Both the reverberation time and early decay time (EDT) were kept constant within .1 second. Seraphim [1958] measured a difference limen of .06s for reverberation time, but this was with band pass noise. With continuous running music it seems reasonable that the limen would increase as comparing pairs with non steady state signals is harder. Certainly, Cremer does not think that a change of a few tenths of a second in the reverberation time will be noticed [Cremer 1982 page 507].

The listeners confirmed that there were no changes to other subjective effects, only changes to clarity. The effect was described by most subjects as sounding like a different sized room. As more reflections arrived early it sounded 'boxy'. The sound field with the highest clarity did sound a little less reverberant due to the reduced reverberation level. But as this was not near the limen it should not have affected the results.

The test technique used was similar to that used for the determination of the difference limen for spatial impression. The only difference was that the pairs had to be recorded on tape in advance; for the spatial impression tests real time alterations could be made. Although using the tape resulted in a slight reduction in signal to noise ratio, the noise level was still much smaller than the music level and should not have affected the judgements. The tests were done with the two motifs detailed in Chapter 8.

10.3 Objective Parameters used for Clarity

There exists a variety of objective measures which are related to clarity. All of them are similar in that they try and characterize the distribution of energy along the impulse response by a single value. The two which we shall be using most are the *clarity index*, C_{80} [Reichardt 1975], and *centre time*, T_c [Cremer 1982 page 434]. For a pressure impulse response p(t), these are defined as:

$$C_{80} = 10LOG_{10}\frac{\int_{0}^{80ms} P^2(t)dt}{\int_{80ms}^{\infty} P^2(t)dt} \qquad 10.1$$

$$T_c = \frac{\int_{0}^{\infty} tP^2(t)dt}{\int_{0}^{\infty} p^2(t)dt} \qquad 10.2$$

The centre time gives the centre of mass of the energy impulse response. The clarity index gives the proportion of energy arriving in the first 80 ms relative to the energy arriving after 80 ms.

There are other measures, such as *deutlichkeit*, *reverberant to early sound ratio*, *rise time*, and *signal to noise ratio* [Cremer 1982 pages 430-335] which are variations or precursors to the clarity index. Deutlichkeit is the appropriate measure for speech sources, and is similar to the clarity index but integrated over 50 ms instead of 80 ms. The reverberant to early sound ratio is the reciprocal of the deutlichkeit.

The rise time, signal to noise ratio and centre time, were all suggested to overcome the problem caused by the sharp cut-off at 80 ms in the definition of the clarity index. A large reflection arriving at a delay of about 80 ms could make quite a difference to the clarity index depending on which side of the boundary it falls. In the case of our simulator this was a significant problem as the early sound field comprises a series of large discrete reflections. In the case of auditoria where there are many more weaker reflections in the early sound field, it is much rarer for this to be a problem. For this reason, in our tests centre time has been used to monitor the change in perceived clarity as this avoids the problems of the sharp cut-off. As many acousticians use the clarity index, the difference limen results were also converted to this.

10.4 Results

10.4.1 Results for Handel Motif

The difference limen for centre time was measured using 8 subjects each taking 4 tests. F tests were carried out to see whether either training or fatigue affected judgements. Results for the F tests are shown in Table 10.1. It was found that overall neither training or fatigue had an effect on the listeners judgements. The difference limen and its standard deviation (95% confidence limits) for centre time for the Handel motif was:

$$(5.7 \pm .9) \text{ ms}$$

Table 10.1. Summary of F test for effects of training and fatigue on the difference limen for centre time for the Handel motif.

Source of variation	Sums of the squares	Degrees of freedom	Variance	F ratio	Signif icance
Between samples	6.04	1	6.04	1.25	>5%
Within samples	145	30	4.84		
Total	151	31			

10.4.2 Results for Mendelssohn motif

The difference limen for centre time was measured using 7 subjects each taking 4 tests each. There was no training or fatigue effects. The results of the F tests are shown in Table 10.2. The difference limen and its standard error (95% confidence limits) for centre time for the Mendelssohn motif was found to be:

$$(11.4 \pm 2.7) \text{ ms}$$

Table 10.2. Summary of F test for effects of training and fatigue on the difference limen for centre time for Mendelssohn motif.

Source of variation	Sums of the squares	Degrees of freedom	Variance	F ratio	Signif icance
Between samples	.0129	1	.0129	2.4e-4	>5%
Within samples	1405	26	54.0		
Total	1405	27			

10.4.3 Comparison of results for the two motifs

The two motifs gave different results for centre time. This can be confirmed by the use of another F test, the results of which are shown in Table 10.3. The difference limens for the two motifs have a less than .1% chance of being from the same data set.

Table 10.3 Summary of F test for effects of motif on difference limen for centre time.

Source of variation	Sums of the squares	Degrees of freedom	Variance	F ratio within samples to between samples	Signif icance
Between samples	434	1	434	14.9	<.1%
Within samples	1573	54	29.1		
Total	2007	55			

The results showed that listeners were much less sensitive to clarity changes in the Mendelssohn motif which was more legato and slower moving. The result was hardly surprising, even though the doubling of difference limen between the two motifs was quite dramatic.

As the two motifs have contrasting tempo and style, the average of the two results should give a better estimate of a typical average limen for music, than either motif on its own. The average difference limen for centre time for both motifs is:

$$(8.6 \pm 1.6) \text{ ms}$$

10.5 Comparison With Previous Results

Reichardt et al's measurements [1967] have given data for the difference limen for varying the delays of lateral and ceiling reflections. Our simulation of

the impulse response used in their experiments is shown in Figure 10.1. If it is assumed that in their experiments the changing sensation with reflection delay was purely a change in clarity, which seems reasonable, then these values can be converted to a difference limen for centre time.

Reichardt found that the difference limen for lateral reflection delay for decreasing delay was (7.0 ± 0.6) ms and for increasing delay 9 ms. This was true for reverberation levels starting at 0 dB and -5 dB. For the ceiling reflection the difference limen for 0 dB reverberation level and increasing delay was 12 ms, and 14 ms for decreasing delay. For -5 dB reverberation level the limen were 12 ms and 11 ms respectively. Kuttruff [1991a] pointed out, however, that there was some uncertainty in their measured values for the difference limen.

Given details of the impulse response, it is possible to estimate a change in centre time from these values. The reflection sequence was simulated using the appropriate early reflection impulses plus reverberation created by the "reverberation plate" setting on the Boss SE50. This simulated Reichardt's reverberation plate. The impulse response was then convoluted with a typical loudspeaker impulse response. The simulated field is shown in Figure 10.1. Averaging all eight results, it is found that Reichardt measured a difference limen of 3.2 ± .5 ms

Our results showed that the difference limen is motif dependant. Reichardt used Handel's Firework music, which has a similar rhythm to our first

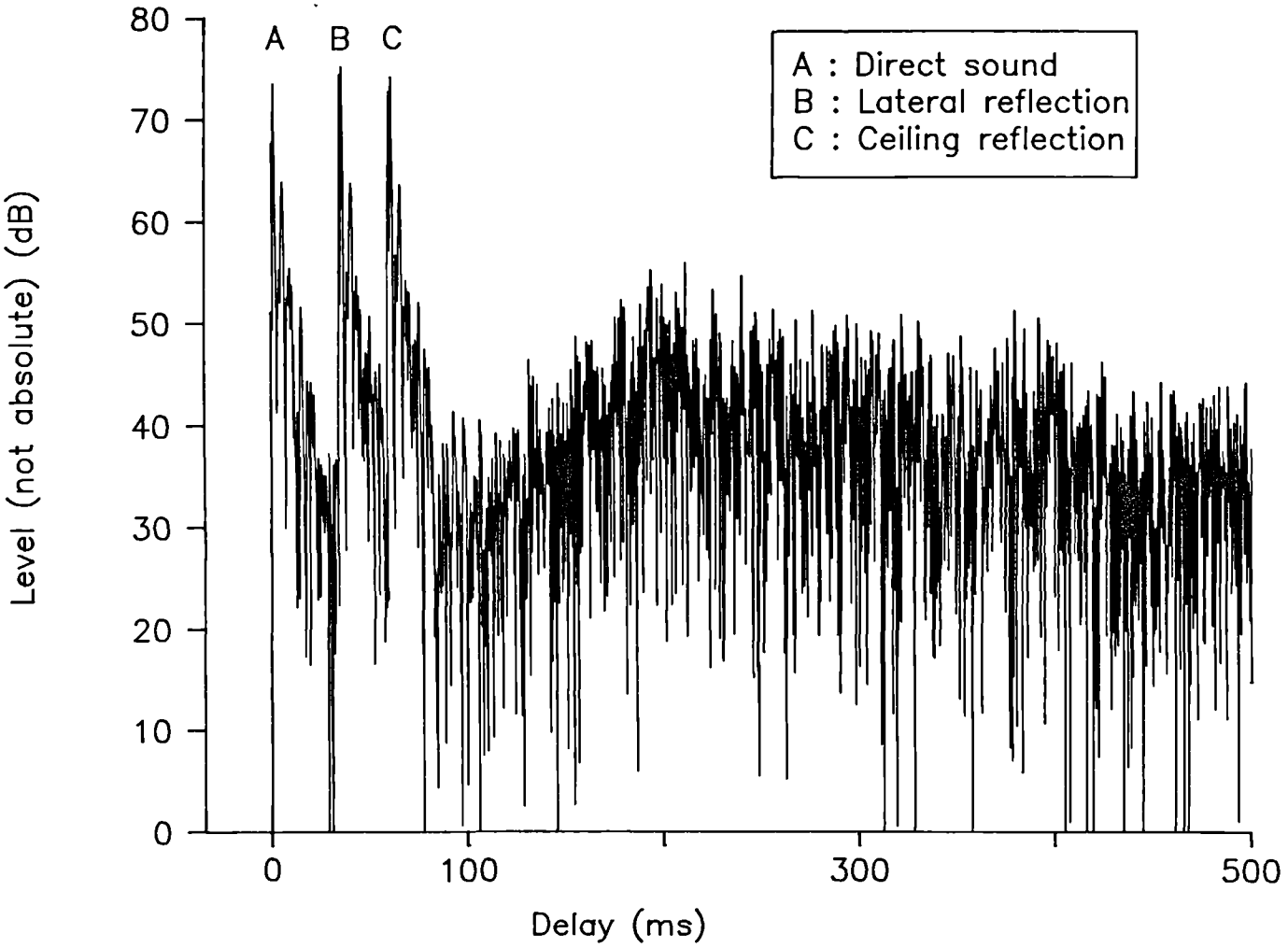

Figure 10.1. Impulse reponse used by Reichardt and Schmidt.

motif, Handel's Water music. Comparing our difference limen for this motif of 5.7 ± .9 ms, it can be seen that our value is significantly higher than the equivalent values measured by Reichardt.

Reichardt [1967] showed that the difference limen for the delay of a reflection increases with the bandwidth of the reflection. This implies that the difference limen for centre time should also increase with bandwidth. However, this is not likely to be the cause of the discrepancy between the two results as our larger valued difference limen came from tests where the bandwidth of the motifs were not restricted. Unfortunately, this can not be confirmed as full details of the spectrum of Reichardt's experiment is not known.

A more likely cause for the disparity between the two results is the difference in the impulse responses used. Our more realistic sound field had many more reflections and therefore this may have masked the changes in clarity. In that respect, our measurement should represent an improvement on that done by Reichardt because of the more realistic simulation of a concert hall sound field.

Warusdfel [1989] quoted a difference limen for early centre time, measured over the first 80 ms only, as 20 ms. Unfortunately, there was insufficient information to convert this value to a difference limen for centre time.

10.6 The Difference Limen for Clarity Index

So far for reasons explained in Section 10.2, only centre time has been used as a measure of clarity. Although there are many other measures available, the only other parameter widely used to assess clarity quality with music, is the clarity index. Therefore, the difference limen for clarity index has also been derived from the results for centre time. To do this it is assumed that the difference limen for an exponential decay will not differ much from that for our simulator's decay, which was close to but not exactly exponential. With an exponential decay the following standard equation can be used to describe the energy decay, E(t), verses time [Kuttruff 1991a page 94]:

$$E(t) = E_0 \exp\left[\frac{-ct(4mv - s\ln(1-\alpha)}{4v}\right] \qquad 10.3$$

$$= E_0\, EXP\left(\frac{-13.9t}{T_{60}}\right) \qquad 10.4$$

where (4mv-s.LN(1-a)) gives the air and surface absorption of the room; v is the volume of the room; c is the speed of sound; T_{60} is the reverberation time of the room; and E_0 the initial energy.

An equation relating centre time and clarity index can be derived by applying Equation 10.4 to the definitions of centre time and clarity Equations 10.1 and 10.2. It can be shown that:

$$C_{80} = 10\ LOG_{10}\ [\exp(\frac{1}{12.5T_c})-1] \qquad 10.5$$

The derivative of Equation 10.5 with respect to time is needed for calculation of the difference limen. If Δ is used to signify the change in a parameter, then:

$$\Delta C_{80} = \frac{10\ \Delta T_c}{LN(10)[1-EXP(-\frac{1}{12.5T_c})]12.5\ T_c^2} \qquad 10.6$$

Using Equation 10.6 the difference limen for clarity index and their errors were derived. These are shown in Table 10.4.

Table 10.4. Difference limen for clarity

	Clarity, C_{80} (dB)
Handel motif	.44 ± .07
Mendelssohn motif	.92 ± .22
Both motifs	.67 ± .13

10.7 Discussion of Difference Limen Results for Clarity and Spatial Impression

The relative importance of clarity and spatial impression to the perception of the sound within a concert hall was examined. To do this three hypothetical cases where the early reflections of a hall were changed was considered: (i) changes in lateral reflection levels; (ii) changes in non-lateral reflection levels; and (iii) changes in reflection delays. These can be considered as cases where the orientation and position of diffusers and reflectors were changed.

(i) If the levels of the lateral reflections were altered, a greater change in spatial impression rather than clarity would be produced. For example, in our simulator a change in the lateral energy of the first reflection of one difference limen (2.4 dB) for spatial impression produced a change of 4.6ms in centre time. This was significantly less than the average difference limen of 8.6ms.

(ii) Changes in the levels of reflections arriving in the listeners median plane could be brought about by altering overhead reflectors above the stage area. For our simulated field, a large change in the level of the first ceiling reflection was made by completely removing the reflection. It was found that this produces a change of .031 in spatial impression (65% of the difference limen) and 3.7ms in centre time (43% of the difference limen). As in case one, more difference was made to spatial impression than to centre time.

(iii) Large changes in individual reflection delays produce only small changes in centre time while spatial impression changes are negligible. For example if the first lateral reflection was moved from 19 ms to 4 ms only a 2.2 ms change in centre time is produced. This is only 26% of the difference limen.

From this it was concluded that:

(i) When the position and orientations of diffusers and reflectors are changed, the audience are more likely to perceive the changes as ones of spatial impression rather than clarity.

(ii) Acousticians can gain the most from a hall by paying attention to lateral sound levels (Turning the ceiling reflection off did not produce a significant change in spatial impression, it only takes a 2.4 dB reduction in the lateral reflection level to produce a significant change). This is particularly true for British and Australian concert halls, as others have found that they tend to be a long way short of the subjectively measured optimum spatial impression [Williamson 1989]. While British concert halls already tend to have sufficient clarity [Barron 1988].

10.8 Conclusions

The difference limen for centre time (8.6 ± 1.6ms) has been measured with two contrasting motifs in a realistic simulation of a concert hall sound field. From this result, the difference limen for clarity index has also been derived (.67 ± .13 dB). The results have been found to be motif dependant with the listener being less perceptive to changes in the slower moving more legato piece. The difference limen results were significantly higher than those derived by this author from measurements by Reichardt (3.2 ± .5ms) [1967]. This was probably due to the more complicated but realistic nature of our simulation field.

Chapter 11.

The Perception of Diffuse Reflections in the Early Sound Field.

11.1 Introduction

When compared to a large plane surface, diffusing panels in auditoria, such as quadratic residue diffusers, change the distribution of energy versus angle arriving at the listener. They also produce reflections with a different frequency response. In the late reverberant sound field such effects are not noticeable because of the large number of reflections present [Barron 1980]. In the early sound field, where there are relatively few reflections, listeners maybe able to perceive differences between diffuse and specular type reflections. This chapter details experiments used to test this hypothesis. This will determine whether it is necessary to treat surfaces with diffusers beyond what might be needed to achieve adequate 'coverage' over the audience area and also to prevent echoes.

11.2 Simulation of Diffuse Reflections

The subjective measurement system described in Chapter 8 simulates specular reflections at various angles and delays. In most auditoria, such reflections occur for the first lateral and ceiling reflections for all but the lowest

frequencies. This is because the side wall and ceiling are large compared to wavelength. However, such strong specular reflections may not occur in many other cases such as for reflections off finite sized diffusers and balcony fronts.

To test whether diffuse reflections are perceived differently from more specular reflections, the 'side wall surface' of the simulator was replaced by a simulated 'diffusing surface'. To simulate the spatial spreading from the diffusing surface, the side loudspeaker was replaced by a wide column loudspeaker placed horizontally. This had five separate drivers as shown in Plate 11.1. The reflection signal over the full frequency range was either fed to all five drivers, or just to the central driver. With a finite sized diffusing surface the change in sound field depends very much on the wavelength of the sound and the size of the diffuser. As all frequencies were altered in our tests, the results therefore represented the largest difference case for the effects of diffusion.

The relative phases of the five drivers determined the type and orientation of diffuser being simulated:

Test 1: All speakers radiating in phase. This represented a simplification of the case of diffusion from a finite sized plane panel at normal incidence and reflection. The size of the panel was such that it subtended an angle of 24° to the observer.

Plate 11.1 The column loudspeaker used to simulate diffuse reflections.

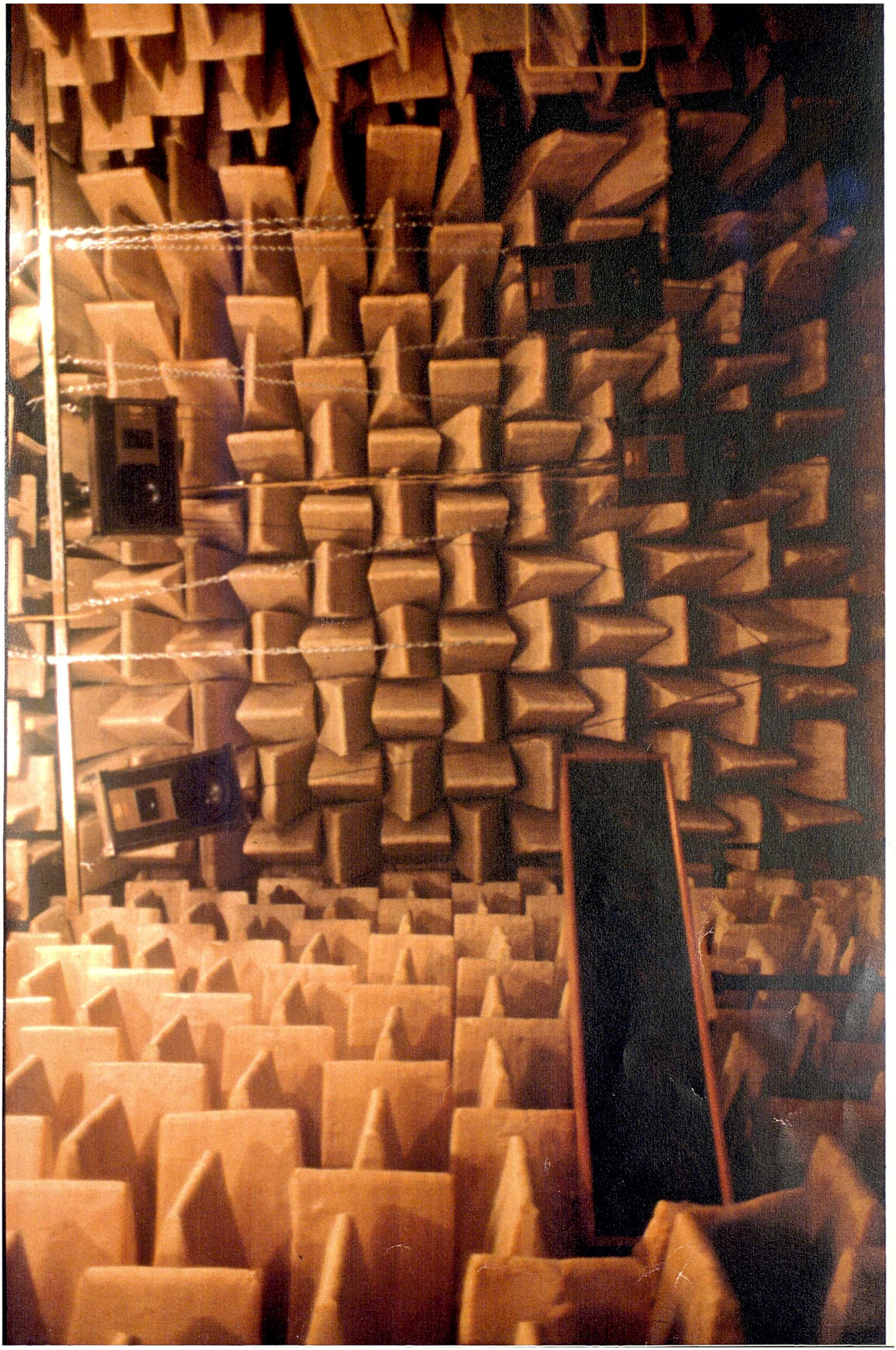

11.3 Measurement Technique

First the appropriate delays were set in the drivers and each driver set to radiate with equal power while the other four drivers were shorted. The mutual interaction between drivers when all five were radiating was assumed to be small. In the case of the QRD simulation, pairs of drivers with equal delay were set simultaneously.

Subjects compared the altered 'diffuse' field with the standard field and asked if they could hear a difference. Subjects undertook the tests for several different situations:

A. Listening monaurally to side reflection only with far ear blocked.

B. Listening binaurally to side reflection only.

C. Listening binaurally to simplified full field (direct sound, first lateral reflection, ceiling reflection and reverberation).

D. Listening binaurally to full field.

E. As D except using white noise instead of the motif.

The tests were designed so that by situation D, the most important test, subjects were used to listening to small differences produced in this type of experiment. Four subjects who were experienced at listening to small frequency and spatial changes in sound fields were used. The Handel motif was used.

11.4 Results and Discussions

11.4.1 Spatial effects

The spatial effects noted are given in Table 11.1. They were the same for all tests 1-4 whatever panel was being simulated.

Situations A and B. When listening to the side reflection on it's own binaurally, the increased sense of spatial spreading when compared to monaural listening was not surprising.

Situation C. It appeared that once the sound field became complicated - even by just the addition of direct sound, ceiling reflection and reverberation - spatial effects due to diffusion became either completely masked or were extremely small. There was a slight filling between the direct sound and lateral reflection noted by two of the subjects. These subjects emphasized that the differences were extremely small.

Situation D. When the full field was used, no difference between the reference field and the 'diffuse' field could be heard by any subject. The chances of perceiving the effect in an actual auditorium will be even less than that for the simulator. In an auditorium, there would be many more early reflections and often the source is not a simple point source. These conditions would further mask 'diffuse' reflection effects.

Table 11.1. Spatial effects caused by diffuse reflections. The results are identical for tests 1-4.

Test situation		Effects noted by all subjects	Effects noted by only two subjects
A.	Monaural, single reflection.	No effect.	Very slight spatial spreading.
B.	Binaural, single reflection.	5 drivers gave a wider source.	-
C.	Simplified full field.	No effect.	Very slight filling in of sound between direct and side reflection.
D.	Full field.	No effect.	No effect.
E.	Full field, white noise.	No effect.	No effect.

11.4.2 Frequency differences

Frequency content differences between the cases of a single driver radiating and all five drivers radiating were only noted in test 3. Test 3 had a frequency response with the largest number and most defined minima and maxima of all the tests. The frequency of one of the maxima coincided with a particular mid frequency note in the motif. With only the side reflection on, situations A or B, this notch filter could clearly be heard. However, once more reflections were added, situations C to E, the effect disappeared. As noted in Section 11.4.1, in a real auditorium such effects would be further suppressed.

11.5 Conclusions

Tests have been carried out to see if the creation of a more diffuse early sound field will affect the perceptions of listeners. This was done using an artificial simulation system. The introduction of a diffuser changed the distribution of sound energy verses angle arriving at the listener, as well as introducing a frequency response with many well defined minima and maxima. The frequency responses of the standard field and 'diffuse' field were only normalized in ⅓ octave bands. No effects could be heard by the listeners when a complicated sound field simulating an auditoria was present. This study indicates that the presence of diffusers to provide reflections in the early sound field in auditoria does not improve the quality of the hall to the listeners, beyond providing reasonable sound 'coverage' over the audience and eliminating echoes.

Chapter 12

The Initial Time Delay Gap

12.1 Introduction

Beranek's [1962] well known survey of concert halls produced a rating system for auditoria based on many parameters including the *Initial Time Delay Gap*. The initial time delay measures the time delay between the direct sound and first major reflection. Beranek found that this was one of the most important objective parameters in determining the acoustics of concert halls. Unfortunately, his methods and rating scheme followed a linear additive system which is different to modern psychological methods now known to be correct. For example, in Beranek's scheme bad background noise levels in a hall could be compensated for by very good reverberation time. Despite the overall rating scheme being shown to be flawed, the specific parameter of the initial time delay gap has remained and has been used by a few researchers, notably Ando. Ando has found a correlation between initial time delay gap and preference for concert hall music [Ando 1977 1979].

If the arrival time of the first reflection was crucial to preference it would have importance consequences for the position of walls, reflectors and diffusers

in auditoria. It was therefore decided to construct an experiment to test the significance of the delay of the first reflection to preference.

Of secondary importance, it was necessary to show whether the initial time delay gap was important for the measurement of the difference limen for centre time. The measurement of the difference limen for centre time has been discussed in Chapter 10.

12.2 Experimental Method

The delay of the first reflection was changed between 5 ms and 40 ms. These values are typical of those found in a shoe box shaped hall. For seats in the centre of the very front rows of the stalls values as high as 50 ms can be obtained, but producing such a delay in our simulator would not have been possible without altering other objective parameters simultaneously. This is particularly true of the clarity measures. Consequently, these few extreme values were excluded. To allow this variation in the first reflection delay, the reflection arriving at 32 ms had to be removed. (Details of the impulse response can be found in Table 8.4). This reflection was of minor importance anyway, and values of the objective parameters were not significantly altered as a result. Over the entire range of first reflection delays used, no other objective parameter was significantly changed.

The test was carried out separately for the first lateral reflection and for the ceiling reflection. In the later case the impulse response was changed by swapping the first lateral reflection and ceiling reflections arrival times. The tests were carried out using the Handel motif.

The impulse response with the changed first reflection delay was compared with the normal reference field and the subject asked to say whether they were different or not. The only changes heard were perceived as ones of source width. To quantify the changes in source widths, the new source width was normalized against a change in width caused by the attenuation of the first lateral reflection. The attenuation was applied to whichever field had the largest source width. The method was to measure the difference limen of the lateral reflection level at each delay using the method of minimal changes, provided the subject could hear a difference when comparing the two sound fields with no attenuation. The difference limen then measured was the attenuation required to give the same source width as the delay.

12.3 Results and Discussions

12.3.1 Lateral reflection results

If any differences were heard by subjects, they were only small differences in source width. These source widths were quantified against the width change caused by attenuating the first lateral side reflection. In Figure 12.1 the results

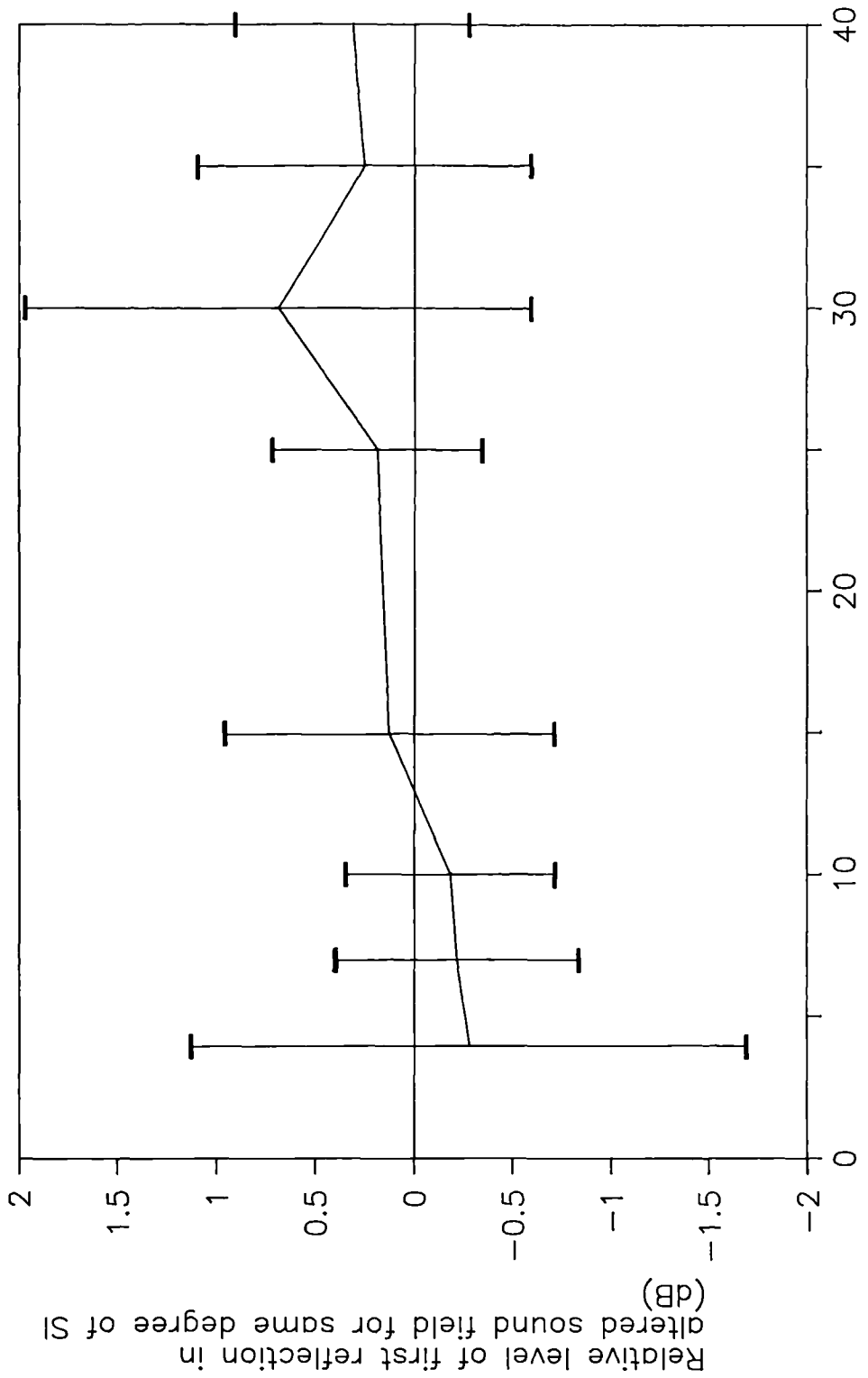

Figure 12.1. Relative level of first reflection in altered sound field to achieve same degree of spatial impression as reference field.

are displayed along with the 95% confidence limit errors. It can be seen that none of the delayed fields had an equivalent attenuated reflection level significantly different from zero - i.e. the pair with the delayed reflection had the same width as the standard pair. The general trend of the data is for a decrease in spatial impression with the delay of the first reflection. The data was modelled as a straight line using a standard least squares fit. It was found that the gradient of .02 ± .01 dB/ms was significantly different from zero. If the difference limen for the first lateral reflection level (2.4 dB) is considered, however, it can be estimated that a change in the delay of the first reflection of 120 ms would be required to get a perceivable difference. Consequently, there is no significant change in source width with the delay of the first reflection.

In these tests little or no difference could be perceived by the subjects for many delays. Any judgements made by the subjects were usually made with a large degree of uncertainty. Because of this, it would have been better if the measurements had been repeated many times for each subject. But the measurements were laborious and time consuming and extra tests were difficult. Judging from the small significance of the results it was thought not worthwhile.

12.3.2 Ceiling reflection

None of the subjects tested could hear a difference with the delayed ceiling reflection when the ceiling reflection was the first to arrive. Four subjects were tested.

12.3.3 Discussion

Both these results show that there is very little subjective preference difference associated with a changing initial time delay gap. The tests on the ceiling reflection show that there is nothing fundamentally important about the arrival time of the first reflection which can influence the perception of the sound field. The tests with the lateral reflection show that individual subjects can occasionally hear a slight difference in width associated with the delay of the first reflection, but the difference is small and averaged over all subjects the differences are negligible.

12.4 Comparison with Previous Measurements

12.4.1 Measurements by Barron

Our results can be compared with those done by Barron on the influence of reflection delay on spatial impression [Barron 1974 1981]. Figure 12.2 shows Barron's experimental results. Barron similarly compared the changes in source width for a delayed first reflection with an equivalent attenuation of the reflection. He found that the degree of spatial impression created was independent of the delay between 8 and 60 ms. Below 8 ms the spatial impression decreased sharply with shorter delays. He found that this decrease in spatial impression at small delays was slightly motif dependant.

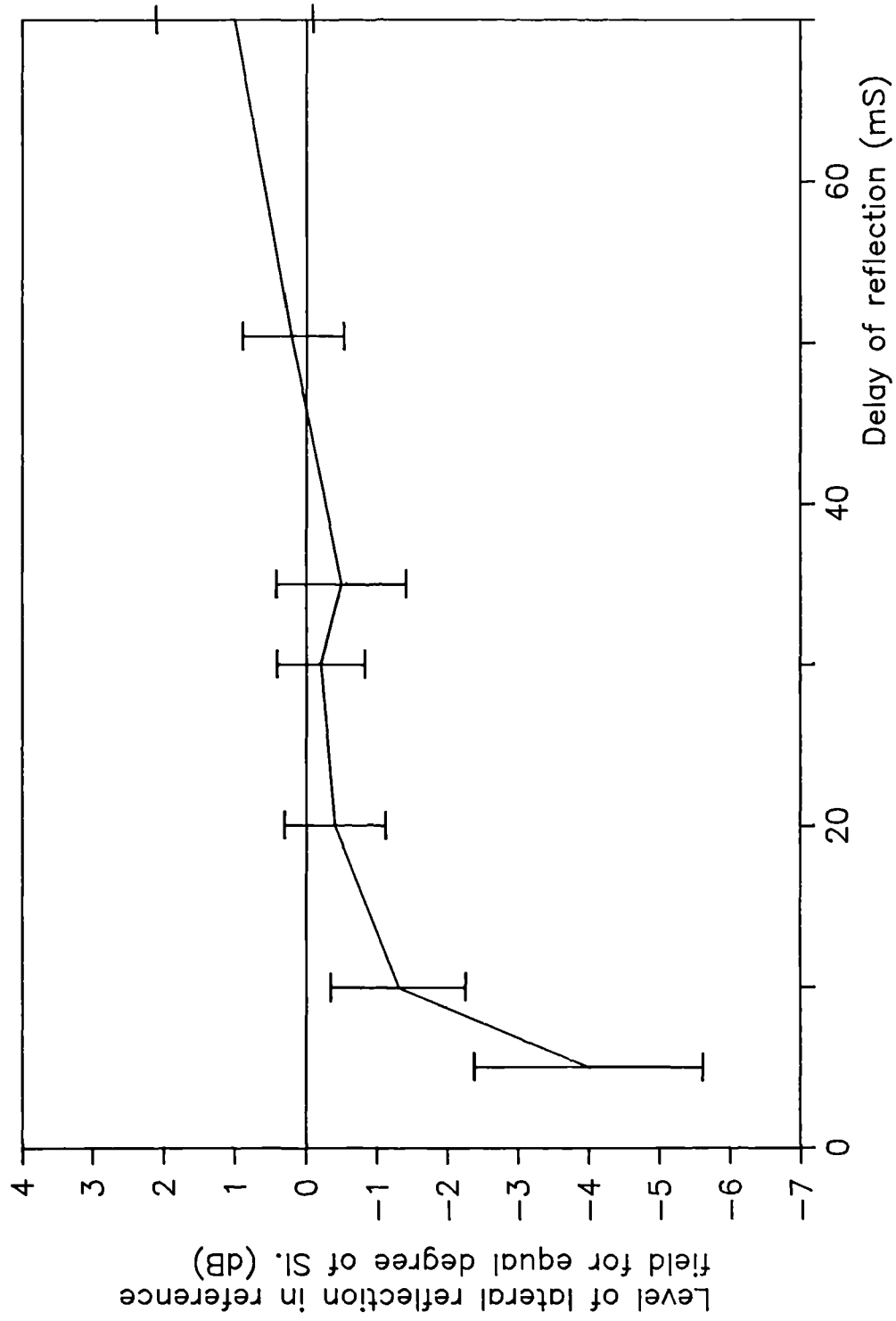

Figure 12.2. Barron's results for change in spatial impression with delay of lateral reflection.

Our results agree well with Barron's findings, except that we found no tail off in spatial impression for small delays. It is possible that the discrepancy is due to interference between the direct sound and first reflections at short delays being perceived differently in the two experiments. This interference pattern could exaggerate or suppress certain frequency ranges, particularly at low frequencies, so causing changes in the perceived source widths. With the much simpler sound field used by Barron such effects would be more obvious than in our experiment, where the much more complicated and realistic sound field could mask such effects.

12.4.2 Measurements by Ando

Ando has done many measurements on subjective effects in auditoria and has found a preferred value for initial time delay gap [Ando 1977 1979]. Unfortunately, no detail is given as to how the sound was perceived, in terms of width, clarity etc, with varying initial time delay gap. Some of the preference he found for initial time delay gap could be explained in terms of centre time changes. Impulse responses with short initial time delay gaps will tend to have short centre times. Ando found an optimum initial time delay gap and there are known to be optimum values for centre time [Reichardt 1981]. Such an argument, however, can not explain all the preferences in Ando's measurement. Figure 12.3 shows two impulse responses used by Ando [1979]. He found a clear preference difference between the two, yet the only difference between the two reflection sequences were the levels of the first two reflections. The changes in

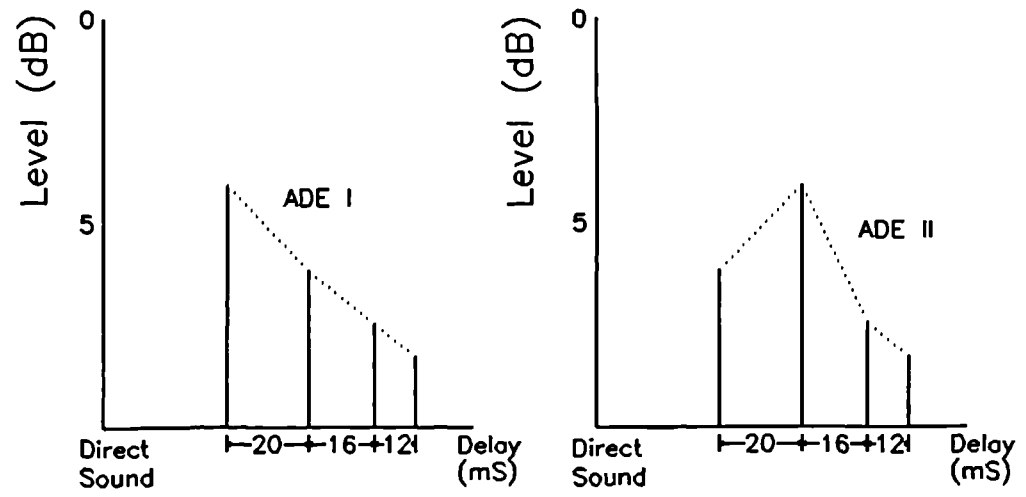

Figure 12.3 The impulse responses used by Ando.

centre time created by the two reflection sequences are smaller than the difference limen for centre time found in Chapter 10. There is no obvious explanation for the contradiction in our results and Ando's results.

12.5 Conclusions

No evidence was found that the arrival time of the first reflection influences the listener's preference over a range of initial time delay gap realizable in normal concert halls. With a ceiling reflection arriving first no difference could be heard for a wide range of delays. With a side reflection arriving first some small changes in widths could be heard, but when averaged over all subjects the effects were negligible. No evidence of a sharp decrease in

spatial impression for reflections of very short delay was found. This is different to the results of Barron. It is suggested that this was not noticed in our experiments because the more complicated but realistic sound field we used could have masked interference effects between the direct sound and the first reflection.

Chapter 13

Conclusions

13.1 Introduction

This project has evaluated the performance of diffusers and reflectors used in auditoria. This has been done with: (i) objective measurements and theoretical predictions to determine the scattering from such surfaces; (ii) subjective work to evaluate the smallest perceivable change in the early sound field. This part of the impulse response is most influenced by reflectors and diffusers.

13.2 Objective Measurements

Measurement systems have been developed which allow accurate measurement of the scattering from finite sized surfaces by cross correlation methods. The first system was based on a white noise source. Although it provided accurate predictions, the system was slow due to the large number of averages needed to reduce the random error endemic to white noise. The introduction of a deterministic pseudo-random noise source greatly reduced the measurement time with no loss of accuracy.

The cross correlation methods enabled us to accurately measure a range of surfaces commonly found in auditoria: rigid plane panels, curved panels, and quadratic residue diffusers. These measurements were then used to gauge the success of various theoretical prediction methods.

13.3 A General Result from Theoretical Predictions

Accurate prediction methods were found for all surfaces tested. As many surfaces in auditoria are either combinations or hybrids of the three types of surfaces tested, this then gives us a set of prediction methods for most of the surfaces found in auditoria.

13.4 Results for Plane Panels and Curved Panels

13.4.1 Results common to both panels

Tests were carried out on rigid plane panels and rigid cylindrically curved panels, of typical width .4 m, curvature .78 m. These were rough 1:5 scale models of the typical surfaces found in auditoria. It was found that a rigorous numerical solution of the Helmholtz-Kirchhoff integral equation, the **3D boundary integral method,** gave accurate predictions of the scattering at all angles and frequencies tested. A solution of the integral equation in the **thin panel limit** produced very similar results with much reduced computation time. The only deviations for the thin panel limit model occurred at large scattering angles, becoming significant

at about 3 KHz, and increasing with frequency. This was due to not representing the finite sized edge in the thin panel model.

The **Kirchhoff approximate** solution greatly decreased computation time by assuming Kirchhoff's approximate surface pressures. This method provided accurate predictions at most frequencies. The theory is most accurate at high frequencies and small scattering angles. The inaccuracies at low frequencies and large scattering angles was due to misrepresenting both the panel's true surface pressure distribution and the pressures on the back and sides of the panel. At large scattering angles, the Kirchhoff theory is more successful for the curved panel than for the plane panel as the scattering of the sound to the sides with the curved panel masks errors due to the incorrect surface pressure distribution.

13.4.2 Results applicable to plane panel only

The **Fresnel** and **Fraunhofer** solutions were applied to the plane panel. Both solutions assume the Kirchhoff approximation for the surface pressures. Fresnel diffraction gives very similar results to the Kirchhoff approximate solution and only requires a few seconds of computing time.

Fraunhofer diffraction is also successful in predicting the scattering for the plane panel provided that the receiver is in the far field. The position of the near field extends further at high frequencies and for oblique receivers. For the plane panel tested the near field extended to a receiver distance of about $.4kl^2$, where

l is half the longest panel dimension. The Fraunhofer predictions significantly deviated from experiment in the near field.

13.4.2.1 Guidelines to predicting scattering from plane panels

When predicting the scattering from plane panels, Fraunhofer theory is only satisfactory in the far field. In auditoria the receiver is frequently not in the far field of reflecting surfaces. Fresnel diffraction is quick and accurate close to the geometric scattering angle, and as this angle is where most of the energy is reflected from the panel, the method is very satisfactory. If the receiver is very close to a large reflector, the assumptions behind Fresnel diffraction will breakdown, and there the Kirchhoff approximate solution should be used. Only when dealing with large scattering angles away from the geometric scattering angle, large angles of incidence, or at low frequencies is it necessary to use either the more exact thin panel limit solution or the 3D boundary integral method.

13.4.3 Results applicable to curved panel only

It was found that the geometric scattering theories are only really applicable at very high frequencies and close to the geometric scattering angle. For the panel tested the range was roughly $\pm$ 8°. This is the range over which the point of reflection lies on the panel. At larger angles the theory greatly underestimates the scattered pressure.

13.4.3.1 Guidelines to predicting scattering from curved panels

When predicting the scattering for the curved surface, the Kirchhoff approximate theory is more accurate at large scattering angles than for the plane panels. Unless the prediction of scattering at very large receiver angles, at grazing incidence, or at low frequencies is required, the use of the more rigorous solutions may not be necessary.

13.4.4 The use of a cut-off frequency

The use of a cut-off frequency to represent the point where diffraction effects due to the finite size of the diffuser become small, was examined. It was found that the formulation of Rindel [1986] works well close to the geometric scattering angle for both the plane and curved panel. For the plane panel, away from the geometric scattering angle ($>8^{\circ}$), the formulation quickly breaks down as the frequency distribution of the pressure is no longer like a high pass filter. As most of the energy of the plane panel is reflected around the geometric scattering angle this breakdown is not necessarily a problem. For the curved panel, approximating the scattered pressure to a high-pass filter works better over a larger range of angles ($\pm 50^{\circ}$). However, the accuracy of the formulation of Rindel for the cut-off frequency reduces as the scattering angle increases.

13.5 Results and Discussions for Quadratic residue diffusers

The **thin panel limit solution** provides accurate predictions of the scattering from Quadratic Residue Diffusers. This is a model which can work both below and above the cut-off frequency of the wells.

With the other theoretical prediction methods, the QRD was approximately represented as a box with a variable admittance on the surface. The surface admittance was approximated by that given by the phase change due to plane waves propagating up and down the wells. The admittance was assumed to be local reacting and the radiation impedance of each well was assumed to be negligible. It was found that this approximation works very well at least down to $\lambda_{min} \approx 0.6w$, where w is the width of the wells.

It was also found that the QRD worked to lower frequencies than previously thought. The lower limit was found to be $\lambda_{max} \approx 11 d_{max}$ where d_{max} is the deepest well depth. This implies that diffusers based on simple wells will work over a larger range of frequencies than previously expected.

The **3D boundary integral method** has very similar accuracy to the thin panel limit solution; although the accuracy decreases slightly with increasing angle.

The **Kirchhoff approximate** solution has similar accuracy as the 3D boundary integral method but requires much less computation time. The theory fails at low frequencies, below 2.5 KHz (.5 KHz full concert hall scale), as it does not account for the mutual interactions on the surface of the diffuser. The accuracy also decreases with increasing scattering angle. It was found that the decrease in accuracy with scattering angle, is much smaller than it was for the plane panel due to the influence of the surface admittances.

The simple **Fraunhofer** solution gives good accurate predictions of the scattering, provided that the receiver is in the far field. The only exceptions being below about 2.5 KHz (.5 KHz full scale) where the failure to account for the interactions across the surface significantly decreases the accuracy of the predictions. The limit of the near field was found to be somewhere between 1/5 and 1/3 kl^2 - a slightly stricter limit than that for the plane panel. Although the local minima and maxima are not well predicted by the Fraunhofer solution method in the near field, the overall shape is still similar to the accurate predictions. It is possible, however, by bending the diffuser in the shape of a parabolic mirror, to focus the far field pressure distribution in the near field.

13.5.1 Guidelines to predicting the scattering from QRDs

When predicting the far field scattering from the quadratic residue diffuser, the Fraunhofer solution will be satisfactory in many cases. If the QRD is long, better accuracy can be achieved by using the Fresnel solution to predict

the scattering in the length direction. When the receiver is in the near field for both the width and length direction, more accurate predictions can be done with the Kirchhoff approximate solution. Only at low frequencies below 2.5 KHz (.5 KHz full scale), at large scattering angles, or at large angles of incidence, do the more rigorous prediction methods have significant advantage over the Kirchhoff approximate method. The thin panel limit solution is the only method which will go above the cut-off frequency of the wells where the local reacting admittance assumption breaks down.

13.6 Performance of Diffusers and Reflectors

Comparing the scattering performance of QRDs to 'optimum' uniform diffusion, it was found that this ideal is never achieved. Below 3.5 KHz (.7 KHz full scale) but above the lower cut-off frequency, however, the amount of scattering away from the geometric scattering angle is similar to that produced at the geometric scattering angle. At high frequencies the scattering is less uniform.

When testing the relative performances of the three types of surfaces, it was found that the angle of incidence made a crucial difference. If near normal incidence can be guaranteed, the curved panel is as good, if not better than the QRD. This would be the case for reflectors over the stage area in auditoria. Although the QRD produces more 'diffusion' than the curved panel below about 2.5 KHz (.5 KHz full scale), at high frequencies the QRD diffraction pattern has

a large number of well defined minima and maxima, with the central lobe being as strong as for the plane panel. There seems to be a risk of strong specular type reflections from QRDs at high frequencies. At these high frequencies the curved panel produces as much scattering away from the geometric scattering angle as for the QRD with a smoother diffracted pressure field.

For situations with oblique incidence the QRD produces much more scattering to the sides and out performs both the plane panel and the curved panel. The strong central lobe seen for the QRD at normal incidence is not present for oblique incidence.

13.7 Subjective measurements

A subjective measurement system was developed to test how small a difference people can perceive in the early sound field. This is the part of impulse response most influenced by reflectors and diffusers. It was an artificial system based in an anechoic chamber. It sounded natural. The key objective criteria; reverberation time (2s), early decay time (1.8s), early lateral energy fraction (.27), clarity index (3.0 dB), and overall level (79 dBA), were all reasonable values. All the values compared well to measurements in real halls and preferred values measured by others in subjective measurements.

13.7.1 Difference limen for spatial impression

The difference limen for early lateral energy fraction was measured as (.048 ± .005). This value was averaged over all experiments and it was found that the limen was independent of motif. The measured limen was slightly smaller than that measured by Reichardt et al [Reichardt 1966 1967] (.065 ± .010). The difference limen for inter aural cross correlation was also derived. This was (.075 ± .008).

13.7.2 Difference limen for clarity

The difference limen for centre time was found to be motif dependant. The slower more legato motif had a limen twice the size of the other motif. For the slower motif, the limen was (11.4 ± 2.7) ms. The faster motif limen had a limen of (5.7 ± .9) ms. The average limen for the two was (8.6 ± 1.6) ms.

These values were converted to difference limen value for clarity index. For the slow motif, fast motif, and averaged over both motifs the limen were: (.92 ± .22) dB, (.44 ± .07) dB and (.67 ± .13) dB respectively.

13.7.3 Discussion of difference limen results

It was found that when the position and orientations of diffusers and reflectors are changed, the audience are most likely to perceive the changes as

ones of spatial impression rather than clarity. Acousticians can gain the most from a hall by paying attention to lateral sound levels. This is particularly true for British and Australian concert halls, as they are usually a long way short of the subjectively measured optimum spatial impression [Williamson 1989]. While these halls already tend to have sufficient clarity [Barron 1988].

13.7.4 Diffuse reflection tests

It was found that changing the spatial distribution of reflections in the early sound field in a way similar to that produced by diffusers could not be heard by listeners in a full concert hall simulation. There was no evidence that providing diffuse reflections in the early sound field plays an important part in subjective preference beyond what is needed to get good 'coverage' of sound over the audience and eliminate echoes.

13.7.5 The initial time delay gap

The initial time delay gap over the range 4 to 40 ms was found to be not significant in determining the preference of listeners in concert halls. This also confirmed the results of others [Barron 1974 1981], that the degree of spatial impression is independent of delay over a large range. In our experiments, a range of 4 to 40 ms was tested. Unlike Barron, no decrease in spatial impression for very short delays was found in these measurements. It was suggested that the more complicated but realistic sound field in our experiments has masked

interference effects. Consequently, acousticians should not be concerned about listeners being too close to walls as far as the degree of spatial impression is concerned. Obviously image shift could still be a problem if the first lateral reflection is particularly large. The insignificance of initial time delay gap contradicts the results of Ando.

13.8 Conclusions

The author believes that the following points are the main achievements of this research project:

1. Development of accurate measurement systems for measuring the scattering from diffusers and reflectors.
2. Development of accurate prediction methods for the scattering from all surfaces tested.
3. Defining the limitations of more approximate prediction methods.
4. Testing the performance of QRDs, particularly the assumptions behind Schroeder's original design.
5. Testing the relative performance of plane panels, curved panels and QRDs.
6. Evaluating the smallest perceivable change in two key objective parameters: i.e. early lateral energy fraction and clarity index.
7. Finding that: (i) providing diffuse reflections in the early sound field; and (ii) the value of the initial time delay gap, do not affect preference.

Chapter 14

Further Work

14.1 Development of Theoretical Prediction Methods

It would be possible to develop both the thin panel limit method and the 3D boundary integral method to radically decrease computation time. This would be done by using the two dimensional form of the Helmholtz-Kirchhoff integral equation. Such methods have been used to predict the attenuation of traffic noise by barriers [Hottersall 1991]. In the two dimensional theory, the panel is taken to be infinitely long and the sound source a line source. To get a measure of the absolute scattered pressure, corrections for the panel length and for the non-point source would then have to be made. For this to work the diffraction in the length and width direction would have to be orthogonal. The success of the Fraunhofer solutions in predicting the scattering from the quadratic residue diffusers shows that a good degree of orthogonality exists for all but the lowest frequencies. Ultimately, this would allow testing to high frequency, to cover the whole frequency range of the QRD both above and below the cut-off frequency.

14.2 Optimization of the Quadratic Residue Diffuser

As was shown in Chapter 7, the quadratic residue diffuser does not perform as an 'optimum' diffusor - the scattering is not independent of scattering angle. This project has developed accurate methods for predicting the scattering from diffusers. Using these methods it would be possible to try a variety of diffusor shapes, calculate the external point pressure, then evaluate the diffusion. By this method an optimum diffusor shape can be found. Such a method has been tried by others [de Jong 1980], but only at single frequencies. There are two problems in developing an optimization method: (i) the method for evaluating the diffusion; and (ii) the long computation time.

(i) A method would have to be found to quantify the diffusion produced by the QRD. A quantity similar to the directivity index used for sources might be possible. The index would give the ratio of the pressure at a particular angle, to the pressure at the centre. But the diffraction pattern will always contain a set of minima and maxima, so some form of averaging over a range of microphone positions would be need. The real problem lies in the fact that the scattering is likely never to be uniform, and so how strict a criteria should be used to monitor the optimization process?

(ii) The computation time would be particularly long because predictions would have to be done at many frequencies, and possibly many incident angles. The thin panel limit solution is accurate at all frequencies but would be far too slow to use for optimisation. At the mid frequency ranges - for the N=7 diffuser this

would be above 2.5 KHz and below the cut-off frequency of the wells - the Kirchhoff theory has been found to be perfectly satisfactory. This prediction method is fast enough for this trial and error optimisation process. Below 2.5 KHz, one of the boundary integral method would be needed, and fortunately at these low frequencies these methods are at their fastest. Above the cut-off frequencies of the wells, the 2D boundary integral method discussed in Section 14.1 would be necessary.

14.3 Further Subjective Work

14.3.1 Improving the subjective measurement system

The subjective measurement system used for these measurements was a good example of artificial simulation in an anechoic chamber. It produced a natural sound, but as outlined in Chapter 8, there are several problems. The advantages and disadvantages were listed as:

Advantages:

1. Complete control over the sound field.
2. Subjects can make immediate comparison of sound fields.

Disadvantages:

3. Too few reflections in the early sound field.
4. The orchestra being represented by a single loudspeaker.
5. No visual clues of the distance to the stage.

6. No orchestra for listeners to empathise with.

7. The visual clues given by location of loudspeakers.

A possible method to overcome many of the disadvantages of the system, would be to carry out tests in a real concert hall which contained an artificial enhancement system. Artificial enhancement systems add extra reflections and reverberation to existing halls to improve the acoustics [Kuttruff 1991a page 289-]. These added reflections are given different delays and frequency characteristics.

With such a system we still keep the advantages 1 and 2, although the control of the sound field would be limited by the acoustics of the existing hall. Many of the disadvantages of the old simulation system would be eliminated or altered. Most importantly, the early sound field would have sufficient density of reflections. How the other disadvantages would change would depend on the exact set up of the measurement system.

14.3.2 Further subjective measurements

There is still much not known about subjective effects in auditoria, and almost any additional measurement of subjective effects would be useful. Logistics mean that most subjective studies can not have a very large number of subjects, and so it takes many studies to confirm or deny the importance of parameters. Consequently, doing measurements to determine the relative

importance of the various objective parameters would be of use, even though such tests have been done by many - including Gottlob [1973], the Berlin group [Cremer 1992 pages 403-] and Barron [1988].

The difference limen tests for spatial impression and clarity carried out in this project need to be repeated for more impulse responses and more motifs. Although this project only tested two motifs and one impulse response, it still usefully adds to the knowledge of subjective criteria. As noted in the previous paragraph, the nature of subjective testing means that no one test is likely to be complete and definitive.

Appendix 1

Error Calculation for Two Microphone Measurement System

This appendix outlines the error calculation used for the two microphone white noise source measurement system. Bendat and Piersol [1980 1986] have derived formulae for the variance of mathematical functions associated with white noise. If n samples are taken of the functions, the variance, σ^2, associated with the magnitude of the auto spectrum is:

$$\sigma^2(|S_{xx}(\omega)|) = \frac{|S_{xx}(\omega)|^2}{n} \qquad \text{A.1}$$

If the cross spectrum is written as:

$$S_{xy}(\omega) = C_{xy}(\omega) + iQ_{xy}(\omega) \qquad \text{A.2}$$

Then the errors in the real and imaginary part of the cross spectrum are [Bendat 1980 1986]:

$$\sigma^2(C_{xy}(\omega)) = \frac{S_{xx}(\omega)S_{yy}(\omega) + C_{xy}^2(\omega) - Q_{xy}^2(\omega)}{n} \qquad \text{A.3}$$

$$\sigma^2(Q_{xy}(\omega)) = \frac{S_{xx}(\omega)S_{yy}(\omega) + Q_{xy}^2(\omega) - C_{xy}^2(\omega)}{n} \qquad \text{A.4}$$

These errors shown in the above equations will be combined with the standard formulations for the combination of variances [Topping 1961 page 82]. To do

this it is assumed that the errors are independent. To aid clarity the following nomenclature will be introduced. The cross spectrum for the with diffuser measurement will be written as:

$$S_{xy1}(\omega) = S_1(\omega) = C_1(\omega) + iQ_1(\omega) \qquad \text{A.5}$$

The cross spectrum for the measurement without the diffuser will be given as:

$$S_{xy2}(\omega) = S_2(\omega) = C_2(\omega) + iQ_2(\omega) \qquad \text{A.6}$$

The processed cross spectrum will be given as:

$$S'_{xy}(\omega) = S'(\omega) = C'(\omega) + iQ'(\omega) \qquad \text{A.7}$$

It can then be shown that the error in the cross spectrum magnitude is given by:

$$\sigma^2(|S'(\omega)|) = \frac{C'^2(\omega)\sigma^2(C'(\omega)) + Q'^2(\omega)\sigma^2(Q'(\omega))}{|S'(\omega)|^2} \qquad \text{A.8}$$

where

$$\begin{aligned} \sigma^2(C'(\omega)) &= \sigma^2(C_1(\omega)) + \sigma^2(C_2(\omega)) \\ \sigma^2(Q'(\omega)) &= \sigma^2(Q_1(\omega)) + \sigma^2(Q_2(\omega)) \end{aligned} \qquad \text{A.9}$$

If negligible error in the microphone calibration transfer function H_{mic}, is assumed, then the error in the magnitude of the measured transfer function given in Equation 2.2 is:

$$\sigma^2(|H(\omega)|) = \frac{|S'(\omega)|^2}{|H_{mic}(\omega)|^2|S_{xx}(\omega)|^2}\left[\frac{\sigma^2(|S'(\omega)|)}{|S'(\omega)|^2} + \frac{\sigma^2(|S_{xx}(\omega)|)}{|S_{xx}(\omega)|^2}\right] \qquad \text{A.10}$$

where $S_{xx}(\omega)$ is the auto spectrum for the measurement without the diffuser.

References

Abramowitz, M. and Stegun, I.A. 'Handbook of Mathematical Functions' (1965) Dover publications inc, New York.

Ando, Y. and Kato, K. 'Calculations on the Sound Reflection from Periodically Uneven Surfaces of Arbitrary Profile' (1976) Acustica **35** 322-329.

Ando, Y. 'Subjective Preference in Relation to Objective Parameters of Music Sounds Fields with a Single Echo' (1977) J.Acoust.Soc.Am. **62** 1436-1441.

Ando, Y. and Gottlob, D. 'Effects of Early Multiple Reflections on Subjective Preference Judgements on Music Sound Fields' (1979) Letters to the editor: J.Acoust.Soc.Am. **65** 524-527.

Ando, Y. 'Concert Hall Acoustics' (1985) Springer Series in Electrophysics 17. ISBN 3-540-13505-7 (Berlin).

Aoshima, N. 'Computer Generated Pulse Signal Applied for Sound Measurement' (1981) **67** 1484-1488.

Barron, M. 'The Effects of Early Reflections on Subjective Acoustical Quality in Concert Halls' (1974) PhD Thesis, University of Southampton.

Barron, M. 'Diffusion in Auditoria and Auditorium Models' (1980) Proc. Institute of Acoustics (UK).

Barron, M. 'Spatial Impression due to Early Lateral Reflections in Concert Halls: The Derivation of a Physical Measure' (1981) J.Sound.Vib. **77**(2) 211-232.

Barron, M. 'Objective Measures of Spatial Impression in Concert Halls' (1983a) Proc. 11th ICA 105-108.

Barron, M. 'Auditorium Acoustic Modelling Now' (1983b) Applied Acoustics **16** 279-290.

Barron, M. 'Impulse Testing Techniques for Auditoria' (1984) Applied Acoustics **17** 165-181.

Barron, M. 'Acoustics Scale Modelling for Enclosed Spaces' (1987) Building Technical File **18** 51-56.

Barron, M. 'Subjective Study of British Symphony Concert Halls' (1988) Acustica **66** 1-14.

Bendat, J. and Piersol, A. 'Random data, analysis and measurement procedures' (1986) 2nd edition, John Wiley inc, New York.

Bendat, J. and Piersol, A. 'Engineering applications of correlation and spectral analysis' (1980) John Wiley inc, New York.

Beranek, L. L. 'Music, Acoustics, and Architecture' (1962) John Wiley, New York.

Beranek, L.L. and Schultz, T.J. 'Some Recent Experiences in the Design and Testing of Concert Halls with Suspended Panel Arrays' (1965) Acustica **15** 307-318.

Blauert, J. 'Spatial Hearing' (1983) 2nd edition. ISBN 0-262-02190-0.

Blauert, J. and Lindemann, W. 'Explorative studies on Auditory Spaciousness' (1986a) 12th ICA Toronto.

Blauert, J. et al. 'Supplementary Psychoacoustical Results on Auditory Spaciousness' (1986b) Acustica **59** 292-293.

Blauert, J. and Lindemann, W. 'Auditory Spaciousness: Some Further Psychoacoustical Analyses' (1986c) J.Acoust.Soc.Am. **80** 533-542.

Borish, J. and Angell, J.B. 'An effective Algorithm for Measuring the impulse Response using Pseudo-random Noise' (1983) J.Audio.Eng.Soc. **31** 478-487.

Bradley, J.S. 'Experience with New Auditorium Acoustic Measures' (1983) J.Acoust.Soc.Am. **73** 2051-2058.

Bradley, J.S. and Halliwel, R.E. 'Making Auditorium Acoustics More Quantitative' (1989a) Sound and Vibration **23**(2) 16-23

Bradley, J.S. 'Hall Average Characteristics of 10 Halls' (1989b) proc. 13_{th} ICA 199-202.

Burton, A.J. 'The Solution of Helmholtz Equation in Exterior Domains Using Integral Equations' (1973) National Physical Laboratory Report NAC 30.

Cable, R.C. and Hilliard, J.K. 'The Practical Application of Time-Delay Spectrometry in the Field' (1980) J.Audio.Eng.Soc. **28** 302-309.

Collados, E. 'Subjective Response of Early Reflections in Auditoria' (1980) proc.IOA (UK) 1.5 17-20.

Commins, D.E. et al. 'Diffusion and Absorption of Quadratic Residue Diffusers' (1988) proc.IOA(UK) **10.**

Cremer, L.L. 'The Different Distributions of the Audience' (1975) Applied Acoustics **8** 173-

Cremer, L. and Müller, H.A. 'Principles and Applications of Room Acoustics', translated by T.J. Schultz. (1982) Applied Science, London. Volume 1.

Cremer, L. 'Early Reflections in Some Modern Concert Halls' (1989) J.Acoust.Soc.Am. **85** 1213-1225.

Cremer, L. 'Fresnel's Methods of Calculating Diffraction Fields', (1990) Acustica **72** 1-

D'Antonio, P. and Konnert, J. 'The Reflection Phase Grating: Design, Theory, and Application' (1984) J.Audio.Eng.Soc. **32** 228-238.

D'Antonio, P. and Konnert, J. 'The Acoustical Properties of Sound Diffusing Surfaces: The Time, Frequency, and Directivity Energy Response.' (1985) Proc.Audio.Eng.Soc. 79th Convention.

D'Antonio, P. and Konnert, J. 'Complex Time-Response Measurements Using Time-Delay Spectrometry' (1989) J.Audio.Eng.Soc. **37** 674-690.

de Jong, B.A. and van den Berg, P.M. 'Theoretical Design of Optimum Planar Sound Diffusers' (1980) J.Acoust.Soc.Am. **68**(4) 1154-1159.

Dodd, G. Personal communication. (1988) Acoustics Research Centre, University of Auckland, New Zealand.

Friedman, M.B. and Shaw, R. 'Diffraction of Pulses by Cylindrical Obstacles of Arbitrary Cross Section' (1962) Transactions of the ASME 40-46.

Fujiwara and Miyajima. 'Absorption Characteristic of a Practically Constructed Schroeder Diffuser of Quadratic Residue Type' (1992) Applied Acoustics Technical note. **35**(2) 147-150.

Ghatak, A.K. and Thyagarajan, K. 'Contemporary Optics' (1978) Plenum Press, New York.

Gilford, J.P 'Psychometric Methods' (1954) McGraw-Hill, New York.

Gottlob, D. 'Comparison of Objective Acoustic Parameters in Concert Halls with Results of Subjective Experiments' (1973) Dissertation. Building Research Establishment translation, 1985, M.Barron.

Guilford, J.P. 'Psychometric Methods' (1954) McGraw-Hill, Inc.

Herbert, A. and Schroeder, M.R. 'A Fast Hadamard Transform Method for the Evaluation of Measurements Using Pseudo-random Noise Signals' (1983) proc.ICA 235-238.

Heyser, R.C. 'Acoustical Measurements by Time Delay Spectroscopy' (1967) J.Audio.Eng.Soc. **15** 370-382.

Hidaka, Y. et al. 'Recording of Anechoic Orchestral Music and Measurement of its Physical Characteristics Based on the Auto Correlation Function' (1988) Letters to the editor. Acustica 68-70.

Hothersall, D.C. personal communication. (1991) Department of Civil Engineering, University of Bradford, West Yorkshire.

Kawai, Y. and Terai, T. 'A Numerical Method for the Calculation of Transient Acoustic Scattering from Thin Rigid Plates' (1990) J.Sound.Vib. **141** 83-96.

Keet, W de V. 'The Influence of Early Lateral Reflections on the Spatial Impression' (1968) 6th ICA Tokyo, Japan. E-2-4. 53-56.

Kinsler, L.E, Frey A.R, Coppens A.B, Sanders, J.V. 'Fundamentals of Acoustics' (1982) 3rd edition. John Wiley and Sons, Inc.

Kirszenstein, J. 'An Image Source Computer Model for Room Acoustics Analysis and Electroacoustic Simulation' (1984) Applied Acoustics 275-290.

Kliener, M. 'A New Way of Measuring the Lateral Energy Fraction' (1989) Applied Acoustics Technical note **27** 321-327.

Kuttruff, H. 'Room Acoustics' 3rd edition (1991a), Elsevier Applied Science.

Kuttruff, H. Personal communication. (1991b) Institut für Techniscne Akustik, Technische Hochschuie Aachen, Aachen, Germany.

Lam, Y.M. and Hodgson, D.C. 'The Prediction of the Sound Field due to an Arbitrary Vibrating Body in a Rectangular Enclosure' (1990) J.Acoust.Soc.Am. **88**(4) 1993-2000.

Leizer, I.G. 'Applicability of the Methods of Geometric Acoustics for the Calculation of Sound Reflection from Plane Surfaces' (1966) Soviet Physics-Acoustics **12** 180-184.

Marshall, A.H. and Hyde J.R. 'Evolution of a concert hall: lateral reflections and the acoustical design for Wellington Town Hall' (1978) J.Acoust.Soc.Am. **63** S36.

Mitzer, K.M. 'Numerical Solution for Transient Scattering from a Hard Surface of Arbitrary Shape - Retarded Potential Technique' (1967) J.Acoust.Soc.Am. 391-397.

Morimoto, M. and Maekawa, Z. 'Effects of Low Frequency Components on Auditory Spaciousness' (1988) Acustica **66** 190-196.

Morimoto, M. and Maekawa, Z. 'Auditory Spaciousness and Envelopment' (1989) proc. 13th ICA 215-218.

Morse, P.M. and Ingard, R.U. 'Theoretical Acoustics' (1968) McGraw-Hill, New York.

Moroney, M.J. 'Facts From Figure' (1971) Penguin books ltd., England.

Naylor, G.M. Ph.D. Thesis. (1986) Heriot Watt University.

Naylor, G.M. 'Odeon Room Acoustics Program' Version 1.0 user manual. (1991a) The Acoustics Laboratory, Technical University of Denmark, Building 352, DK-2800 lyngby.

Naylor, G.M. 'Odeon - Another Hybrid Room Acoustical Model' (August 1991b) International Symposium Denmark

Orlowski, R.J. Personal communication. (1989) Arup Acoustics, St. Giles Hall, Pound Hill, Cambridge, UK.

Ortega, J.C. 'Measurement of Panel Reflection using Acoustical Scale Modelling Techniques' (1991) J.Audio.Eng.Soc. **39** 752-760.

Pierce, A.D. 'Acoustics, An Introduction to its Physical Principles and Applications' (1981) McGraw-Hill, Inc.

Polack, J. and Dodd, G. 'About Schroeder's Reflection Phase Grating Diffusers' (1988) unpublished.

Reichardt, von W. and Schmidt, W. 'The Audible Steps of Spatial Impression in Music Performances' (1966) Acustica **17** 175-179.

Reichardt, von W. and Schmidt, W. 'The Detectability of Changes in Sound Field Parameters for Music' (1967) Acustica **18** 275-282.

Reichardt, von W. et al. 'Definition and Basis of Making an Objective Evaluation to Distinguish Between Useful and Useless Clarity Defining Musical Performances' (1975) Acustica **32** 126-137.

Reichardt, von W. and Lehmann, U. 'Optimisation of Room-Impression and Transparency of Musical Performances by Evaluation Through Sound-Impulse Tests' (1981) Acustica **48** 174-185.

Rife, D.D. and Vanderkooy, J. 'Transfer-Function Measurement with Maximum-Length Sequences' (1989) J.Audio.Eng.Soc. **37** 419-444.

Rife, D.D. 'MLSSA Maximum-Length Sequence System Analyzer' (1991) Reference Manual version 7.0. DRA laboratories

Rindel, J.H. 'Attenuation of Sound Reflections From Curved Surfaces' (1985) 25th Conference on Acoustics.

Rindel, J.H. 'Attenuation of Sound Reflections due to Diffraction' (1986) Nordic Acoustical Meeting. 257-260.

Rindel, J.H. and Haylor, G.M. 'Odeon - Another Hybrid Room Acoustical Model' (November 1991) Western Pacific Regional Acoustics Conference iv Brisbane.

Schenck, H.A. 'Improved Integral Formulation for Acoustic Radiation Problems' (1968) J.Acoust.Soc.Am. **44** 41-58.

Schroeder, M.R, Gottlob, D. and Siebrasse, K.F. 'Comparative Study of European Concert Halls: Correlation of Subjective Preference with Geometric and Acoustic Parameters' (1974) J.Acoust.Soc.Am. **56** 1195-1201.

Schroeder, M.R. 'Binaural Dissimilarity and Optimum Ceilings for Concert Halls: More Lateral Sound Diffusion' (1979) J.Acoust.Soc.Am. **65** 958-963.

Schultz, T.J. and Watters, B.G. 'Propagation of Sound Across Audience Seating' (1964) J.Acoust.Soc.Am. **36** 885-

Seraphim, H.P. (1958) Acustica **8** 280-

Sessler, G.M. and West, J.E. 'Sound Transmission over Theatre Seats' (1964) J.Acoust.Soc.Am. **36** 1725-

Skudrzyk, E. 'The foundations of Acoustics' (1971) Springer-Verlag, Wien.

Stephenson, U. 'Comparison of the Mirror Image Source Method and the Sound Particle Simulation Method' (1990) Applied Acoustics **99** 35-72.

Strube, H.W. 'Diffraction by a Planar, Locally Reacting, Scattering Surface' (1980a) J.Acoust.Soc.Am. **67** 460-469.

Strube, H.W. 'Scattering of a Plane Wave by a Schroeder Diffusor: A Mode Matching Approach' (1980b) J.Acoust.Soc.Am. **67** 453-459.

Strube, H.W. 'More on the Diffraction Theory of Schroeder Diffusers' (1981) J.Acoust.Soc.Am. **70** 633-635.

Tachibana, H. et al. 'The Acoustical Data of European Concert Halls Obtained by Survey with New Methods' (1986) (Unpublished)

Tachibana, H. et al. 'Acoustic Survey of Auditoriums in Europe and Japan' (1989) J.Acoust.Soc.Jpn (in English) **10** 73-85.

Terai, T. 'On the Calculation of Fields around Three-Dimensional Objects by Integral Equation Methods' (1980) J.Sound.Vib. **68** 71-100.

Thiele, R. 'Richtungsverteilung und Zeitfolge der Schallruckwurfe in Räumen' (1953) Acustica 291-302.

Topping, J. 'Errors of Observation and Their Treatment' (1961) 3rd edition Chapman and Hall, Ltd, London.

Torgerson, W.S. 'Theory and Methods of Scaling' (1958) John Wiley.

Vanderkooy, J. 'Another Approach to Time-Delay Spectrometry' (1986) J.Audio.Eng.Soc. **34** 523-538.

Warusfel, O. et al. 'Perception of Coloration and Spatial Effects in Room Acoustics' (1989) proc. 13th ICA 173-176.

Williamson, R.P. 'Optimisation of Variable Lateral Energy for Spatial Impression in a Hall' (1989) Applied Acoustics **26** 113-134.